WESTERN SYDNEY UNIVERSITY

Synthesis and Characterisation of New Schiff-Base Metallo-Supramolecular Assemblies

Kyle Howard-Smith

Master of Research Thesis 2017

Presented to Western Sydney University in Fulfillment of the Requirements for the Degree of Master of Research

Supervisor: Dr Feng Li

For Laura

Foreword

The present dissertation is the result of nine months of research conducted from January 2017 to September 2017, as part of the Masters of Research degree at Western Sydney University. The Masters of Research program is a two-year full-time degree that involves a one-year course work component followed by a nine-month research period. This thesis has been presented in the style of a thesis by publication.

Contents

Abstract

This thesis reports the design, synthesis and structural characterisations of new metallo-supramolecular assemblies, all incorporating a Schiff-base type ligand. The Schiff-base moiety was employed as it is widely documented in supramolecular architectures due to its ease of synthesis, interesting properties and its strong binding affinities to various metal ions. Small changes to the ligand, such as the addition of electron withdrawing or electron donating functional moieties were explored, as well as, shortening the ligand backbone in order to promote different rigidity of the ligand. The synthesis and characterisation have been communicated in each chapter and where possible physical properties have also been studied.

In chapter two, a flexible N_4O_2-donor Schiff-base ligand incorporating an electron donating functional moiety (diethylamine) was employed. Four new complexes are presented containing metal centres (Fe^{III}, Co^{III}, Ni^{II} and Cu^{II}). It was demonstrated that all complexes, except Cu^{II}, formed in a 1:1 ligand-to-metal (L:M) ratios, while the Cu^{II} complex exhibited an unexpected 3:2 (L:M) ratio due to the flexibility of the N_4O_2-donor Schiff-base ligand and Cu^{II} having the flexibility to form 4 or 5 coordinate bonds.

In chapter three, adopting a similar flexible N_4O_2-donor Schiff-base as described in chapter two. The ligand utilised incorporated an electron withdrawing functional moiety (bromine) rather than an electron withdrawing functional moiety. Three new complexes ([Fe**L**]$(BF_4)_2$, [Mn**L**](PF_6) and [Co**L**]PF_6) were reported and structural characterisation revealed all complexes exhibit a 1:1 (L:M) stoichiometric ratio in both the solid and liquid phase.

In chapter four, a flexible N_6-donor Schiff-base ligand incorporating thiazolyimine functional groups was synthesised, complexation resulted in the formation of a mononuclear complex ([Fe**L**]$(BF_4)_2$) that displayed a high-temperature spin transition. Structural characterisation revealed the complex exists in a 1:1 stoichiometric ratio in both the solid and liquid state.

In chapter five, the backbone of the previous Schiff-base ligand (from chapter 4) was shortened and replaced by a hydrazine moiety in order to create a semi-flexible N_3-donor Schiff-base ligand. Five new Fe^{II} complexes [Fe$\mathbf{L_2}$]$(A)_2$ (A = BF_4^-, BPh_4^-, Cl^-, Br^- & I^-) were

reported. Structural characterisation was successful on four complexes and revealed that they exist in a 2:1 (L:M) stoichiometric ratio in both solid and liquid state.

Acknowledgments

I would like to thank my primary supervisor Dr Feng Li for his continued guidance and support throughout my Master's degree. Thank you for believing in me and giving me the opportunity to be a part of your team. Your expert knowledge and determination are second to none. I would also like to thank my co-supervisor Dr Patrice Castignolles for your continued support.

To Feng Li's research team, a big thank you to all of you for your help and continued support over the course of this degree, thank you to Daniel Fanna for teaching me UV-Vis and how to operate the MX1 beamline. I would also like to mention Joseph Tadros and thank you for your continued mateship and support throughout this degree and my entire academic journey, thanks for being my competition all this time.

A special mention to my fellow team member Sandy Craze, no amount of thanks is enough to recognise your efforts and contributions towards my masters. Thank you for the countless times you collected crystal data for me, the very difficult structures you had to solve, not to mention all the magnetic studies you conducted here and in Japan. Your mateship and dedication towards your friends is something to be envied.

I would like to personally thank Dr Ric Wuhrer of the Advanced Materials Characterisation Facility (AMCF), Dr Laurel George (AMCF), Ms Shamila Salek (AMCF), Dr Meena Mikhael (Mass Spectrometry Laboratory), Dr Chris Gordon (WSU) and Dr Allan Torres (WSU) for their time and training on the various instruments I used throughout this degree. I would also like to thank Assoc Prof Jack Clegg (UQ) and the Australian Synchrotron for allowing me to train and use the MX1 beamline.

Additionally, I would like to thank the following institutes for the provision of training and access to various facilities and instrumentation, Western Sydney University, University of Queensland and the Australian Synchrotron. This research was supported by the Western Sydney University Master of Research stipend.

Finally, I dedicate this text to my partner Laura Cann, thank you for being my source of inspiration.

Statement of Authentication

The work presented in this thesis is, to the best of my knowledge and belief, original except as acknowledged in the text. I hereby declare that I have not submitted this material, either in full or in part, for a degree at this or any other institution.

X [redacted]

(Signature, Date)

Publications and Conference Presentations

Listed below are the publications that the candidate has published as a result of the work conducted throughout the Master's degree.

Published Journal Articles

1. **Howard-Smith, K. J.**, Craze, A. R., Badbhade, M. M., Marjo, C. E., Murphy, T. D., Castignolles, P., Wuhrer, R., Li, F., Synthesis and Structure Investigations of 3d Transition Metal Complexes with a Flexible N_2O_4-Donor Hexadentate Schiff-Base Ligand *Aust. J. Chem.* **2017**, *70*, 581.

Conference Presentations

1. **Howard-Smith, K. J.**, Li, F., (**2016**). Synthesis and Characterisation of Metal Complexes with a Salicylaldehyde Schiff Base. The 8th International Symposium on Nano & Supramolecular Chemistry (ISNSC), July, Brisbane, Australia.
2. **Howard-Smith, K. J.**, Shepherd, N. D., Li, F., (**2016**). Self-Assembly of Homometallic Ni(II)/Ni(II) and Heterometallic Ni(II)/Cu(II) Coordination Cages. Royal Australian Chemical Institute (RACI) NSW Inorganic Symposium, November, Sydney, Australia.

Manuscripts in Preparation

1. **Howard-Smith, K. J.**, Craze, A. R., Badbhade, M. M., Marjo, C. E., Li, F., Investigation of a New N_4O_2 Schiff-base System: Synthesis & Structural Characterisation. Manuscript in preparation.
2. **Howard-Smith, K. J.**, Craze, A. R., Wuhrer, R., Badbhade, M. M., Kepert C. J., Marjo, C. E., Li, F., Synthesis and Spin Crossover Investigations of a New Mononuclear Thioimidazole Schiff-Base Fe^{II} Complex with a High Temperature Spin Transition. Manuscript in preparation.
3. **Howard-Smith, K. J.**, Craze, A. R., Badbhade, M. M., Marjo, C. E., Li, F., Five New Thiazolyimine-based Mononuclear Fe^{II} Complexes in the Presence of Different Anions. Manuscript in preparation.

List of Figures and Schemes

Chapter 1 Figures and Schemes

Chapter 2 Figures and Schemes

Chapter 3 Figures and Schemes

Chapter 4 Figures and Schemes

Chapter 5 Figures and Schemes

List of Tables

Chapter 2 Tables

Chapter 3 Tables

Chapter 4 Tables

Chapter 5 Tables

Abbreviations

AMCF – Advanced Materials Characterisation Facility

FT-IR – Fourier-Transform Infrared Spectroscopy

H_2O – Water

HR ESI-MS – High-Resolution Electrospray Ionisation-Mass Spectrometry

HS – High spin

L – Ligand

LMCT - Ligand-to-Metal Charge Transfer

LS – Low spin

M – Metal

MRI - Magnetic Resonance Imaging

m/z – Mass to charge ratio

PXRD – Powder X-ray Diffraction

QTOF – Quadrupole Time of Flight

SCO – Spin-crossover

SEM-EDS – Scanning Electron Microscopy–Electron Dispersive Spectroscopy

SXRD – Single Crystal X-ray Diffraction

trz – 1,2,4-triazol

UNSW – University of New South Wales

USYD – University of Sydney

UV-Vis – Ultraviolet-Visible Spectroscopy

WSU – Western Sydney University

XDS – X-Ray Spectrometer Detector System

Chapter 1 - Introduction

1.1 Supramolecular Chemistry

Supramolecular chemistry is a diverse and interdisciplinary field that has consistently remained on the forefront of current research, gaining an ever increasing research interest since its establishment some decades ago.[1-5] This relatively new field, in comparison to other fields of chemistry, has become better known as the chemistry "beyond the molecule".[1,2] Supramolecular is primarily concerned with the design and synthesis of supramolecular assemblies, of which, possess the ability to encompass a 'host' or 'guest' (molecule/s or ion/s), these assemblies are typically held together by weak or reversible non-covalent interactions, and hence, form a supermolecule.[1,2,4,5] These weak bond formations can involve and include, hydrogen bonding, hydrophobic forces, metal coordination, π-π interactions and Van der Waals forces.[2,5,6] A predominant research focus within the field is devoted to studying these interactions and their respective functions within these discretely assembled architectures.[1,2,4,5,7-9] Over the last few decades, the extensive field of supramolecular chemistry has provided many developments and contributions in chemistry. Supramolecular assemblies have been shown to exhibit many intriguing properties, including but not limited to magnetic, catalytic, electrochemical, biological and optical properties.[1,2,5]

1.1.1 Origins

The field of supramolecular chemistry has humble, yet subtle origins, the emergence and recognition of the field was a slow process. Deviating from the classical view of molecular chemistry, that only considered strong covalent interactions as a possibility. Supramolecular chemistry is concerned with the non-covalent interactions between a host and guest.[1-5,10] The suggestion of other chemical interaction possibilities was first made by Emil Fisher in 1894, who hypothesised that enzymes interacted non-covalently with their respective substrate, reporting this observation as a "lock-and-key" mechanism, that would later become known

as host-guest chemistry.[10,11] This observation would later revolutionise chemistry and lay the foundations of the field that would become supramolecular chemistry.[10,11]

A breakthrough moment appeared with the discovery of crown ethers by Charles Pederson in the 1960's, depicted in Figure 1. Crown ethers are macrocyclic compounds that feature an ability to 'capture' a positively charged guest, something that had not been demonstrated before that time. [1,3,5,12] The electron donating oxygen atoms within the crown ether point inward 'capturing' the positively charged ion, a key example of the "lock and key" concept and the foundation of supramolecular chemistry. [1,3,5] Charles Pederson would continue to work with coordinative ligands, together with Donald Cram and Jean-Marie Lehn. Later, in 1987, their contributions towards supramolecular chemistry were recognised when they received the Nobel Prize for their development of these highly selective "host-guest" complexes.[1,3,5]

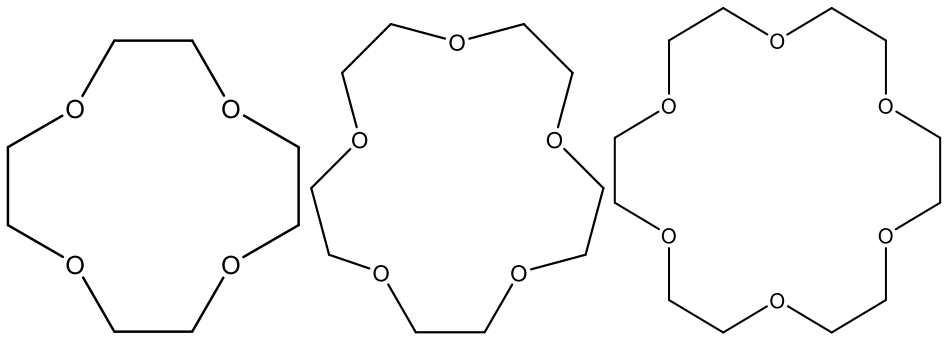

L_1 **L_2** **L_3**

Figure 1. Pederson crown ethers. **L_1** – 12-Crown-4, **L_2** – 15-Crown-5, **L_3**– 18-Crown-6.

1.1.2 Self-Assembly

Although the field of supramolecular chemistry is an extensive and diverse field, it can however, be summarised by two categories, self-assembly and host-guest chemistry.[2,5] it is important to note there exists only a small difference between the two categories and that is, size and shape of the molecules. If both molecules are of similar size and shape they will likely fall into the category of self-assembly, also, if there is a large difference in size they will likely fall under host-guest chemistry.[2,5] With respect to self-assembly, when it is known that

no molecule acts as a host for the other and no significant difference in the size of the molecules is observed, the non-covalent (usually reversible) assembly of the molecules is dubbed *Self-assembly.*[2,5,11] For an assembly to be deemed as such it must react spontaneously, generally only influenced by solvation or crystallisation (in solids).[2,5]

1.1.3 Host-Guest Chemistry

Concerning Host-Guest chemistry, any system labelled as such must feature a 'host' molecule that is able to encapsulate a 'guest' molecule or ion via intermolecular forces.[2,5] With this in mind most host-guest systems are carefully designed using an appropriate synthesised or preformed organic ligand, this chosen molecule acts as the 'host' and will exhibit favourable properties including, size, geometry, chemical nature and appropriate binding sites.[2,5,11] This chosen 'host' is able to encapsulate a 'guest', a smaller positively charged molecule or ion generally a transition or lanthanide metal, and is held together by intermolecular interactions. These weak, generally reversible interactions include π-π interactions, hydrogen bonding, dispersion forces and hydrophobic forces.[1,2,5]

1.1.4 Metallo-Supramolecular Chemistry

Within the field of supramolecular chemistry, there is a vast interest into metallo-supramolecular architectures; these systems consist of pre-formed organic ligands coordinated via non-covalent interactions with metal ion/s.[1,2,5] These systems can exhibit both mono- and multi-dentate ligands, coordinating with one or more metal ions, respectively. Many supramolecular architectures are the products of meticulous planning and design, of a suitable ligand and metal ion, forming structures of various geometries with a high degree of symmetry throughout.[2,5,13,14] This is a crucial element, the ability to plan and manipulate chemical properties, that has made the design and synthesis of these metallo-supramolecular systems a keen research interest for many decades.[2,5,13,14]

1.2 Ligand Selection - The Schiff-Base

The Schiff-base reaction is a well-known and documented organic reaction, with its discovery attributed to Hugo Schiff, an expansive repertoire of literature pertaining to Schiff-bases complexes exists.[15] Much of the respective general properties and mechanism of the Schiff-base is recognised and acknowledged throughout texts and literature.[2,5,15,16] Schiff-base complexes have become a keen focus for chemists, especially amongst supramolecular chemists in recent years due to a number of reasons including, ease of synthesis, strong coordinative abilities and the many intriguing properties such complexes have been shown to exhibit.[2,5,15]

Schiff-bases are formed via the condensation reaction of an activated carbonyl moiety (an aldehyde or ketone), resulting in the formation of a nitrogen analogue (C=N), the resultant imine is the Schiff-base and displayed in Scheme 1.[15,16]

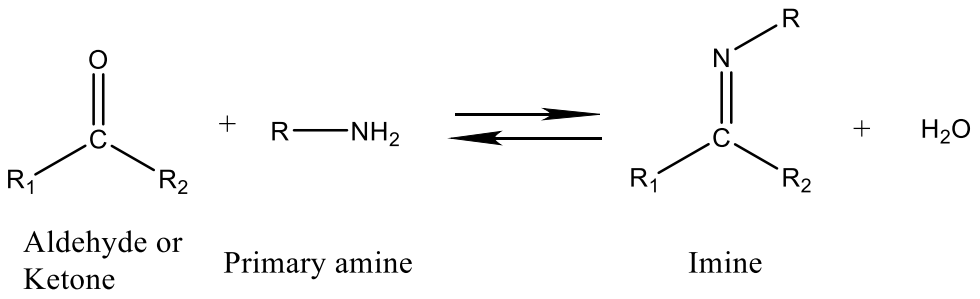

Scheme 1. Schiff-base condensation reaction. R_1 = any substituent (carbon chain), R_2 = carbon chain or H.

The Schiff-base nitrogen moiety (C=N) is a Lewis base (nucleophile) as such it has the ability to donate electrons, it is this feature that enables Schiff-bases to form coordinate complexes with positively charged metal ions, both transition and lanthanide metals.[2,5,17] The nitrogen of the imine, in this case, is a σ-donor, π-acceptor resulting in greater electron density among the non-covalent bond with the metal ion.[2,5] Furthermore, the higher the degree of conjugation within the Schiff-base system, the greater the stability of the complex.[2,5]

Literature suggests that Schiff-base reactions are generally unstable and reversible via hydrolysis.[2,5,16] It is frequently reported, that the stability of Schiff-bases can be improved via the complexation with metal salts largely resulting in the formation of a coordination complex.[2,5,18] The resulting complex exhibits 'host-guest' phenomena observed amid the non-covalent interactions of the metal ion (guest), and the Schiff-base ligand (host). [2,5,18]

In an attempt to counter this drawback, as mentioned above, metal ions can be coordinated with the Schiff-base to improve stability.[18] Additionally, Schiff-bases that contain aliphatic (straight or branched chain) substituents have been reported to be especially susceptible to hydrolysis. However, the use of imine ligands contacting aryl (aromatic) substituents, due to the conjugated π system, are significantly more stable and are less susceptible to hydrolysis.[2,5,18] Therefore, through the careful planning and design of suitable ligands coupled with the use of appropriate metal ions with favourable properties, geometry and binding sites, stable Schiff-base complexes are able to be achieved.

In the field of supramolecular chemistry, Schiff-base ligands in recent times have gained a lot of research interest due mainly to their strong coordinative abilities coupled with their straightforward synthesis.[18] Schiff-bases have become a focal point for many research teams as they form coordinate complexes with a vast array of transition and lanthanide metal ions.[20,21] Similarly, Schiff-base complexes have been found to display an intriguing range of properties including, but not limited to, magnetic, electrochemical, catalytic and optical properties, to name a few.[2,3,5,13,19-23]

There is currently a diverse range of literature available relating to Schiff-base metal complexes, with an extensive amount of research findings relating to the properties and use of such complexes in biological activities. These include but are not limited to, anti-bacterial, anti-fungal, anti-viral, anti-tumour and anti-inflammatory activities.[23-26] Noteworthy Schiff-base complexes include Isatin Schiff-base ligands which have shown to exhibit anti-viral markers potentially useful in the treatment of HIV.[26]

1.2.1 Flexible vs Rigid Ligand Systems

Many supramolecular chemists employ a 'bottom-up' approach when attempting to design a ligand in order to achieve a target compound, through the use of suitable molecular building blocks this is able to be accomplished. Rigid ligand systems (those with high degrees of conjugation and aromacy) tend to result in the formation of more stable and often predictable assemblies, enabling the chemist to have greater control over the system.[7,27-30] The use of rigid ligand systems can limit the possibilities regarding the structures/assemblies that are achievable[27,28] and has been used successfully and reported numerous times to achieve a particular assembly, however, predicting the final assembly still presents a challenge as the use of rigid ligand does not guarantee a predictable geometry.

Feng and co-workers[29] recently communicated the synthesis, characterisation, luminescent, antibacterial and catalytic studies of two new Schiff-base complexes with a rigid bromosalicylaldehyde derivative ligand. The bidentate donor Schiff base ligands L_4 and L_5 (Figure 2) were coordinated in a two-to-one stoichiometric ligand-to-metal ratio with Pd^{II} and Zn^{II}, respectively. The choice of a bidentate donor Schiff-base ligand and metal ions with a favourable square planar and tetrahedral geometry, respectively, has resulted in the formation of the desired complexes in a 2:1 ligand-to-metal ratio.

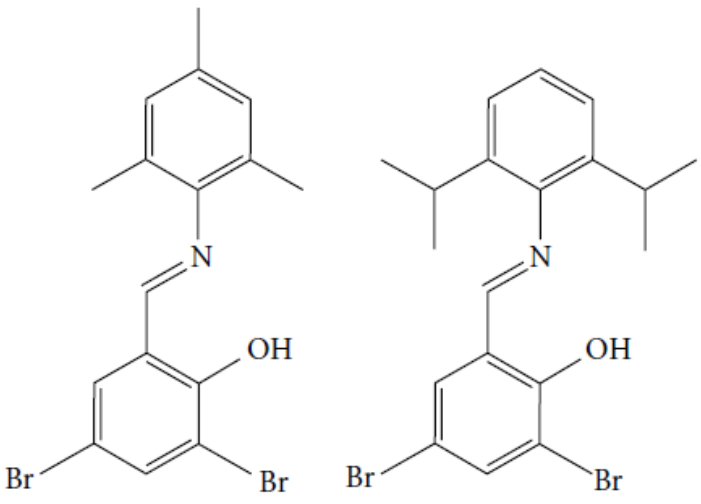

L_4 **L_5**

Figure 2. **L_4** and **L_5** adapted from Feng et. al.[29]

Furthermore, our group recently employed a rigid julolidine-quinoline Schiff base ligand (Figure 3) in an attempt to optimise and predict the geometry of the target coordinate complexes, studied for their respective optical properties.[30] A two-to-one (2:1) stoichiometric ligand-to-metal ratio was favoured for formation Co^{III}, Mn^{II}, Cu^{II} and Zn^{II} complexes, due to the rigid nature of the Schiff-base ligand and the available donor sites. However, it was shown crystallographically that only two of the four respective complexes (Co^{III} & Mn^{II}) crystallised in this stoichiometric ratio, while the other two crystallised in a 1:1 (ligand-to-metal) ratio and was bridged by solvent molecules.[30] This highlights the challenges faced by supramolecular chemists in achieving a favoured target product.

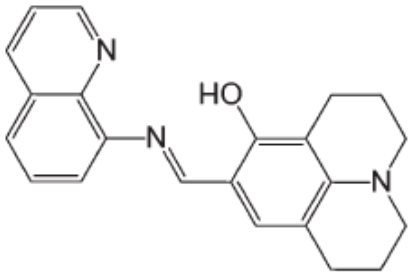

L_6

Figure 3. Julolidine-quinoline Schiff-base ligand **L_6** employed by Fanna et. al.[30]

However, employing a flexible ligand system is one approach in which supramolecular chemists have been able to expand access to a much greater range of metallo-supramolecular architectures. Different conformations are able to be achieved via the use of flexible components. Utilising straight or branched alkyl chains can enable rotation to occur about single bonds thus, introducing flexibility. Other factors including counterions and solvents can also affect the conformation of many metallo-supramolecular architectures.[29] However, it is also noted that the use of flexible ligand systems can result in somewhat unpredictable assemblies and thus, presents a challenge. In order to combat this and maintain some degree of control over the system, metal ions with known or favourable coordination geometries, as well as, ligand systems with a predetermined amount of available donor sites are employed in order to promote control.

As mentioned above counterions, as well as, a flexible ligand system can influence the final nuclearity of a coordinate complex. Abhevré et. al. recently demonstrated the drastic effect counterions play on the nuclearity of Fe^{III} Schiff-base complexes, utilising two flexible N_4-donor tetradentate Schiff-base ligands, one containing an imidazole moiety while the latter contained a pyridine functional moiety (Figure 4).[31] Abhevré and co-workers demonstrated that the choice of counterion is key to tuning the nuclearity of polynuclear metal complexes, describing two new polynuclear ring clusters containing four, six and eight Fe^{III} centres (Figure 5), all complexes were shown to remain in the HS state, Abhevré also suggested that the replacement of NCS^- to CN^- counterion may result in a stronger ligand field and potentially induce spin-crossover.[31]

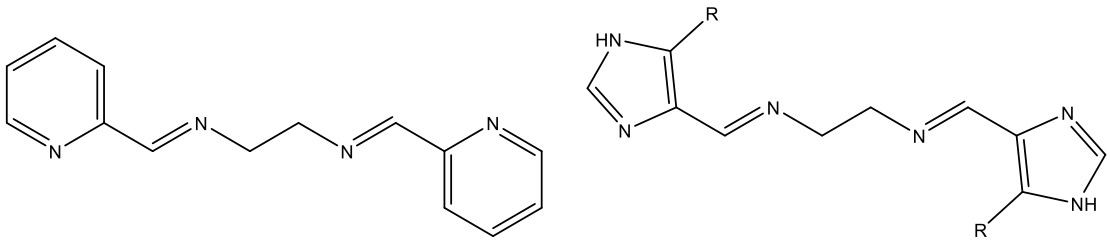

L_7 **L_8** – (R=CH_3) & **L_9** – (R = H)

Figure 4. Pyridine based flexible Schiff-base ligand **L_7** and imidazole based flexible Schiff-base ligands **L_8** and **L_9**, R = H or CH_3 - adapted from Abhevré.[31]

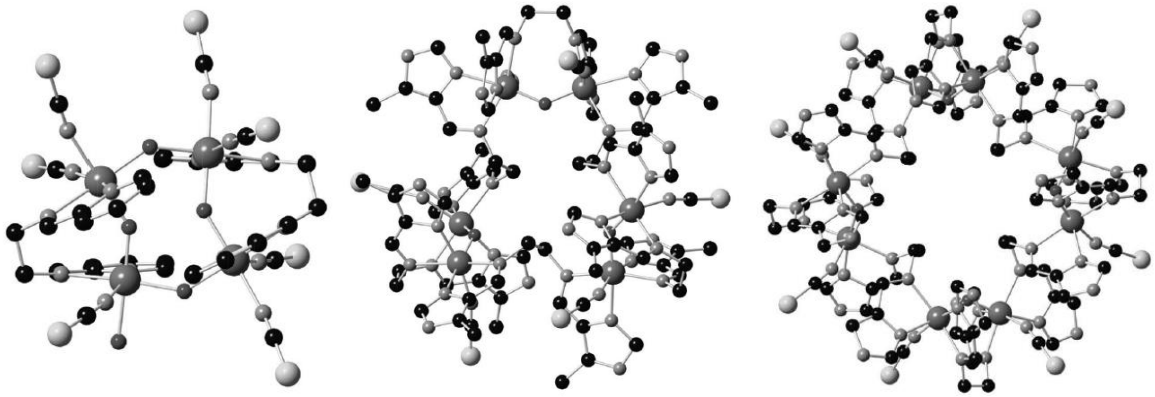

a) b) c)

Figure 5. Molecular representations of complexes a) $[Fe_4(\mathbf{L_7})_2(NCS)_7(OH_2)]$ tetranuclear complex b) $[Fe_6(\mathbf{L_8})_6(NCS)_6]$ hexanuclear complex c) $[Fe_8(\mathbf{L_9})_8(NCS)_8]$ octanuclear complex. Adapted from Abhevré et. al.[31] with permission from the Centre National de la Recherche Scientifique (CNRS) and The Royal Society of Chemistry.

Sanmartín and co-workers demonstrated that the flexibility of a ligand can enable much more fascinating assembly possibilities. They have reported on two separate occasions that the use of a flexible Schiff-base ligand featuring a di-aminobutane alkyl 'spacer' (Figure 6) is capable of resulting in the formation of single and double helicates, demonstrating the effect a flexible ligand can have on nuclearity.[32,33] Sanmartin report the formation of a single helicate when the ligand is coordinated with Co^{II} and Cu^{II},[32] while the formation of a double helicate is favoured when the coordinating metal ion is Ni^{II} and Zn^{II}.[32,33]

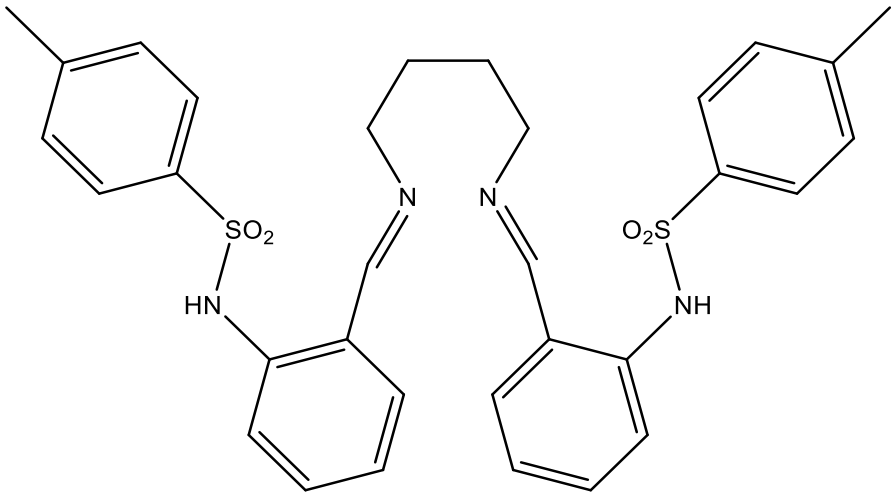

L_{10}

Figure 6. Diaminobutane alkyl flexible 'spacer' ligand **L_{10}** employed by Sanmartin et. al.[32,33]

1.3 Spin-Crossover Phenomenon

With respect to applications, several Schiff-base metal complexes containing d- and f-block metal ions have been shown to exhibit magnetic properties, these can range from single molecular magnetism to spin-crossover (SCO).[34-37] With respect to SCO materials only, several potential applications in many emerging technologies are a possibility, including, molecular data storage devices, switches, displays, and sensors.[38-46]

Spin Crossover (SCO) is a phenomenon in which certain 3d transition metal complexes are able to undergo a transition in spin state, i.e. from low spin to high spin, or vice versa.[36,37,47] Spin Crossover, also commonly referred to as spin transition[36,37] is generally

induced by means of external stimuli, such as temperature, pressure, irradiation or an external magnetic field.[36,37,48-50] Metal complexes coordinated with first row d-block transition metal ions with valence electrons ranging from $3d^4$ – $3d^7$ have the potential to undergo SCO, due to their ability to have configurations in both the low-spin and high-spin states.[36,37] A vast majority of the published literature on SCO complexes pertains to octahedral d^6 Fe^{II} complexes, several d^5 Fe^{III} complexes have also been reported.[36,37,51-55]

When it comes to the design and synthesis of new SCO materials, all of the above factors must be taken into account, as well as, the strength of the ligand fields required to induce SCO.[36,37] Moreover, Sunatsuki and co-workers report the synthesis and magnetic investigations of several new Fe^{II} complexes utilising a semi-flexible ligand with an imidazole-4-carbaldehyde moiety (Scheme 2). The nuclearity of each complex was the result of solvent choice, with methanol yielding mononuclear complexes and nitromethane resulting in the formation of dinuclear triple helicates.[41,44] Sunatsuki and co-workers reported that the nuclearity of the complexes, as well as, solvent and counterions were responsible for the spin states exhibited with all complexes both mononuclear and dinuclear, with the exception of two, remaining in the low-spin state, while, the complexes $[Fe_2(\mathbf{L_{11}})_3]ClO_4$ and $[Fe_2(\mathbf{L_{11}})_3]BF_4$ exhibited an abrupt spin transition from LS → HS at 240 K and 254 K, respectively.[41,44]

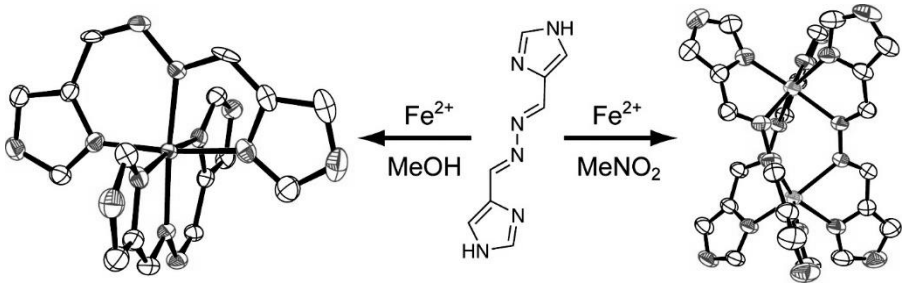

$[Fe(\mathbf{L_{11}})_2]$ $\mathbf{L_{11}}$ $[Fe_2(\mathbf{L_{11}})_3]$

Scheme 2. Adapted with permission from Sunatsuki et. al.[44] Copyright 2017 American Chemical Society.

1.4 Aim and Scope

This project aims to extend upon the work previously conducted by our research team, with an objective to design and synthesise new metallo-supramolecular assemblies that have the potential to undergo a SCO transition or exhibit other physical properties. This will be

achieved by judicious choice of building blocks for the ligand, selection of appropriate metal ions, counterions and solvents in order to achieve the desired target molecule/s. A simplified flow chart has been provided to give an idea as to the process involved in the design and synthesis of all new compounds reported in this thesis.

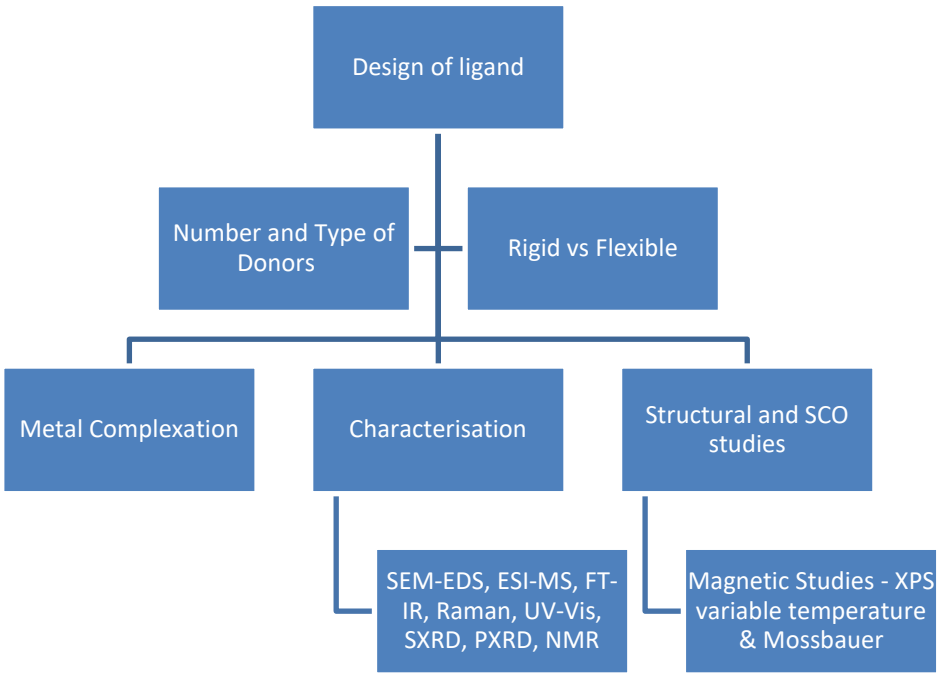

In this present chapter, an introduction to the field of supramolecular chemistry is given. The direction of this thesis is themed throughout the introduction, namely the design, synthesis and characterisation of new Schiff-base metallo-supramolecular architectures designed with the potential to exhibit SCO or other intriguing physical properties.

In chapter 2 five new flexible N_4O_2-donor Schiff-base metal complexes are investigated, their syntheses, characterisation and structural investigations are presented. The aim is to study the effects a flexible ligand can have on the nuclearity and structure of a metal complex.

In chapter 3, extending on the work presented in chapter 2, three new complexes with an N_4O_2-donor Schiff base ligand incorporating an electron withdrawing functional moiety is described. The aim of this chapter is to the determine the effect on structure and nuclearity by the addition of an electron withdrawing functional group, as well as, observe the effect it has on the ligand field and potential physical properties including SCO behaviour.

In chapter 4, a new Fe^{II} thiazolyimine N_6-donor Schiff base complex is presented, the aim was to extend on previously reported SCO materials that contain an imidazole functional moiety, in this case, the functional moiety was replaced with a thioimidazole moiety and studied for magnetic properties including SCO.

In chapter 5, we extend our work presented in chapter 4, this time the length of the ligand backbone has been intentionally shortened and a semi-flexible hydrazine has been employed. This chapter aims to study the effects on the SCO behaviour exhibited on the complex by shortening the backbone as well as counterion effect.

In the conclusion, the author offers a summary and final remarks, the author also makes statements about the future directions of the work as a result of this thesis.

1.5 References

1. J. -M. Lehn, *Supramolecular Chemistry*, VCH, New York, **1995**.
2. J. W. Steed, D. R. Turner and K. J. Wallace, *Core concepts in supramolecular chemistry and nanochemistry*, John Wiley & Sons, Chippenham, United Kingdom, **2007**.
3. B. Daly, J. Ling and P. A. de Silva, *Supramol. Chem.,* **2016**, 28, 201.
4. J. -M. Lehn, *Angew. Chem. Int. Ed. Engl.,* **1988**, 27, 89.
5. J. W. Steed and J. L. Atwood, *Supramolecular Chemistry*, John Wiley & Sons, Chippenham, United Kingdom, **2009**.
6. R. Chakrabarty, P. S and P. Stang, *Chem. Rev.,* **2011**, 111, 6810.
7. P. J. Steel, *Acc. Chem. Res.,* **2005**, 38, 243.
8. P. J. Steel and C. M. Fitchett, *Coord. Chem. Rev.* **2008**. 252, 990.
9. E. C. Constable, *Chem. Soc. Rev.,* **2008**, 252, 842.
10. G. R. Desiraju, *Nature*., **2001**, 412, 397.
11. F. M. Menger, *Proc. Natl. Acad. Sci. USA.,* **2002**, 99, 4818.
12. C. J. Pederson, *Science*., **1988**, 241, 536.
13. F. Reichel, J. K. Clegg, K. Gloe, K. Gloe, J. J. Weigand, J. K. Reynolds, C. -G. Li, J. R. Aldrich-Wright, C. J. Kepert, L. F. Lindoy, H. -C. Yao and F. Li, *Inorg. Chem.*, **2014**, 53, 688.
14. H. -B. Wu and Q. -M. Wang, *Angew. Chem. Int. Ed. Engl.,* **2009**, 48, 7343.
15. W. Qin, S. Long, M. Panunzio and S. Biondi, *Molecules*., **2013**, 18, 12264.
16. D. R. Klein, *Organic Chemistry*, John Wiley & Sons, Hoboken, NJ, 2015.
17. A. A. El-Sherif and M. S. Aljahdali, *J. Coord. Chem.*, **2013**, 66, 3423.
18. A. C. W. Leung and M. J. MacLachlan, *J. Inorg. Organomet. Polym. Mater.*, **2007**, 17, 57.
19. M. Nihei, T. Shiga, Y. Maeda and H. Oshio, *Coord. Chem. Rev.,* **2007**, 251, 2606.
20. P. N. Martinho, B. Gildea, M. M. Harris, T. Lemma, A. D. Naik, H. Müller-Bunz, T. E. Keyes, Y. Garcia and G. G. Morgan, *Angew. Chem. Int. Ed. Engl.,* **2012**, 50, 12765.
21. M. Nihei, T. Shiga, Y. Maeda and H. Oshio, *Coord. Chem. Rev.,* **2007**, 251, 2606.
22. D. E. Goldberg, V. Sharma, A. Oksman, I. Y. Gluzman, T. E. Wellems and D. Piwinca-Worms, *J. Biol. Chem.,* **1997**, 272, 6567.
23. V. K. Gupta, A. K. Jain and G. Maheshwari, *Talanta.,* **2007**, 72, 49.
24. S. Naik, G. Bhattacharjya, V. R. Kavala and B. K. Patel, *Arch. Org. Chem.,* **2004**, 1, 55.
25. A. Xavier and N. Srividhya, *J. App. Chem.*, **2014**, 7, 6.
26. S. B. Ade, M. N. Deshpande and J. H. Deshmukh, *Rasayan. J. Chem.,* **2012**, 5, 10.
27. S. R. Seidel and P. J. Stang. *Acc. Chem. Res.*, **2002**, 35, 972.
28. V. Martins, J. A. L. C. Resende and C. M. Ronconi, *CrystEngComm.*, **2017**, 19, 3103.
29. Z. -Q. Feng, X. -L. Yang and Y. -F, Ye, *Sci. World J.*, **2013**, 2013, 1.
30. D. J. Fanna, Y. Zhang, L. Li, I. Karatchevtseva, N. D. Shepherd, A. Azim, J. R. Price, J. Aldrich-Wright, J. K. Reynolds and F. Li, *Inorg. Chem. Front.*, **2016**, 3, 286.
31. A. Abhervé, J. M. Clemente-Juan, M. Clemente-León, E. Coronado, J. Boonmak and S. Youngme, *New J. Chem.,* **2014**, 38, 2105.
32. M. Vázquez, M. R. Bermejo, M. Fondo, A. Garciá-Deibe, A. M. González and R. Pedrido, *Eur. J. Inorg. Chem.*, **2002**, 465.
33. M. Vázquez, M. R. Bermejo, M. Fondo, A. Garciá-Deibe, J. Mahia, L. Sorace and D. Gattschi, *Eur. J. Inorg. Chem.*, **2001**, 1863.
34. A. B. Gaspar, M. C. Muñoz, J. A. Real and K. Tanaka, *J. Mater. Chem.,* **2006**, 16, 2522.
35. K. S. Murray, *Aust. J. Chem.*, **2009**, 62, 1081.

36. *Spin Crossover in Transition Metal Compounds I, II and III;* P. Gütlich, H. A. Goodwin., Eds.; Springer, **2004**.
37. *Spin-Crossover Materials: Properties and Applications,* M. A. Halcrow., Ed.; Wiley, **2003**.
38. O. Khan, J. Krober and C. Jay, *Adv. Mater.,* **1992**, 4, 718.
39. O. Khan and C. Jay-Martinez, *Science*., **1998**, 279, 44.
40. L. Li, S. M. Neville, A. R. Craze, J. K. Clegg, N. F. Sciortino, K. S. Athukorola Arachchige, O. Mustonen, C. E. Marjo, C. R. McRae, C. J. Kepert, L. F. Lindoy, J. R. Aldrich-Wright and F. Li, *ACS Omega***., 2017**, 2, 3349.
41. Y. Sunatsuki, R. Kawamoto, K. Fujita, H. Maruyama, T. Suzuki, H. Ishida, M. Kojima, S. Iijima and N. Matsumoto, *Coord. Chem. Rev.,* **2010**. 254, 1871.
42. N. Struch, C. Bannwarth, T. K. Ronson, Y. Lorenz, B. Mienert, N. Wagner, M. Engeser, E. Bill, R. Puttreddy, K. Rissanen, J. Beck, S. Grimme, J. R. Nitschke and A. Lützen, *Angew. Chem. Int. Ed.*, **2017**, 56, 4930.
43. J. Kitchen and S. Brooker, *Coord. Chem. Rev.* **2008**, 252, 2072.
44. Y. Sunatsuki, R. Kawamoto, K. Fujita, H. Maruyama, T. Suzuki, H. Ishida, M. Kojima, S. Iijima and N. Matsumoto, *Inorg. Chem.,* **2009**, 48, 8784.
45. J. -F. Létard, P. Guionneau and L. Goux-Capes, *Top. Curr. Chem.*, **2004**, 235, 4590.
46. A. Bousseksou, G. Molnár, L. Salmon and W. Nicolazzi, *Chem. Soc. Rev.*, **2011**, 40, 3313.
47. P. Gütlich, Y. Garcia and H. A. Goodwin, *Chem. Soc. Rev.*, **2000**, 29, 419.
48. J. -F. Létard, *J. Mater. Chem.,* **2006**, 16, 2550.
49. M. A. Halcrow, *Chem. Soc. Rev.*, **2011**, 40, 4119.
50. Y. Ikuta, M. Ooidemizu, Y. Yamahata, M. Yamada, S. Osa, N. Matsumoto, S. Ijima, Y. Sunatsuki, M. Kojima, F. Dahan and J. -P. Tuchages, *Inorg. Chem.*, **2003**, 42, 7001.
51. N. Bréfuel, I. Vang, S. Shova, F. Dahan, J. -P. Costes and J. -P. Tuchagues, *Polyhedron*., **2007**, 26, 1745.
52. N. Struch, C. Bannwarth, T. K. Ronson, Y. Lorenz, B. Mienert, N. Wagner, M. Engeser, E. Bill, R. Puttreddy, K. Rissanen, J. Beck, S. Grimme, J. R. Nitschke and A. Lützen, *Angew. Chem. Int. Ed.*, **2017**, 56, 4930.
53. A. Arroyave, A. Lennarston, A. Dragulescu-Andrasi, K. S. Pedersen, S. Piligkos, S. A. Stoian, S. M. Greer, C. Pak, O. Hietsoi, H. Phan, S. Hill, C. J. McKenzie and M. Shatruk. *Inorg. Chem.,* **2016**, 55, 5904.
54. W. Phonsri, L. C. Darveniza, S. R. Batten and K. S. Murray, *Inorganics*., **2017**, 5, 51.
55. N. Ortega-Villar, A. Y. Guerrero-Estrada, L. Piñero-López, M. C. Muñoz, M. Flores-Ălamo, R. Moreno-Esparza, J. A. Real and V. M. Ulgade-Saldivar, *Inorg. Chem.,* **2015**, 54, 3413.

Chapter 2 – Synthesis and Structure Investigations of 3d Transition Metal Complexes with a Flexible N_2O_4-Donor Hexadentate Schiff-Base Ligand.

*This chapter was published in

Howard-Smith, K. J., Craze, A. R., Badbhade, M. M., Marjo, C. E., Murphy, T. D., Castignolles, P., Wuhrer, R., Li, F. *Aust. J. Chem.* **2017**, *70*, 581.

2.1 Abstract

The syntheses and structure investigations of four new 3d transition metal complexes (**1**–**4**) with a flexible N_4O_2-donor hexadentate Schiff-base ligand are described; three complexes (**1**, **2**, and **4**) of Fe^{III}, Co^{III}, and Cu^{II} metal ions have been investigated by UV-Vis, FT-IR, high-resolution mass spectrometry (HR-MS), and scanning electron microscopy–electron dispersive spectroscopy, as well as single crystal X-ray diffraction. The X-ray structure of Ni^{II} complex **3** is also reported. The molecular structures of the complexes (**1**–**3**) demonstrate distorted octahedral coordination geometry, each exhibiting 1:1 (L:M) ratios and the Cu^{II} complex **4** shows a trinuclear structure with a Cu^{II}:L ratio of 3:2 in the solid state, which has been proven by X-ray diffraction. On the other hand, a mononuclear species of the Cu^{II} complex is formed in solution, which has been identified by electrospray ionisation HR-MS.

2.2 Introduction

Over recent years, there has been increased interest in Schiff-base ligands, which play an important role in metallo-supramolecular chemistry,[1,2] as such metal assemblies may exhibit unique redox, magnetic, and photochemical properties in the potential applications of chemosensors,[3,4] magnetic resonance imaging (MRI) contrast agents,[5] spin crossover (SCO) materials,[6,7] and single molecule magnets.[8] Although several Schiff-base ligands have been well developed, the prediction of their diversified architectures of flexible systems with

different metal ions still represents a significant challenge. By judicious choice of metal and multidentate ligand components, metal-directed self-assembly can successfully act as a simple step in the construction of new polynuclear systems.[9-11]

In earlier studies, the ligand H_2L (Scheme 1) and its Ga^{III} complex were described, and no other metal complexes have been reported.[12] Due to its good chelating properties and its ability to generate polynuclear systems, we now investigate the syntheses, characterisation, and structural properties of four new 3d transition metal complexes (Fe^{III}, Co^{III}, Cu^{II}, and Ni^{II}) with a deprotonated N_4O_2 Schiff-base ligand **L** (Scheme 1). A key feature of our design is to employ flexible components that may give rise to unpredicted architectures, which has been studied in our previous work.[13,14]

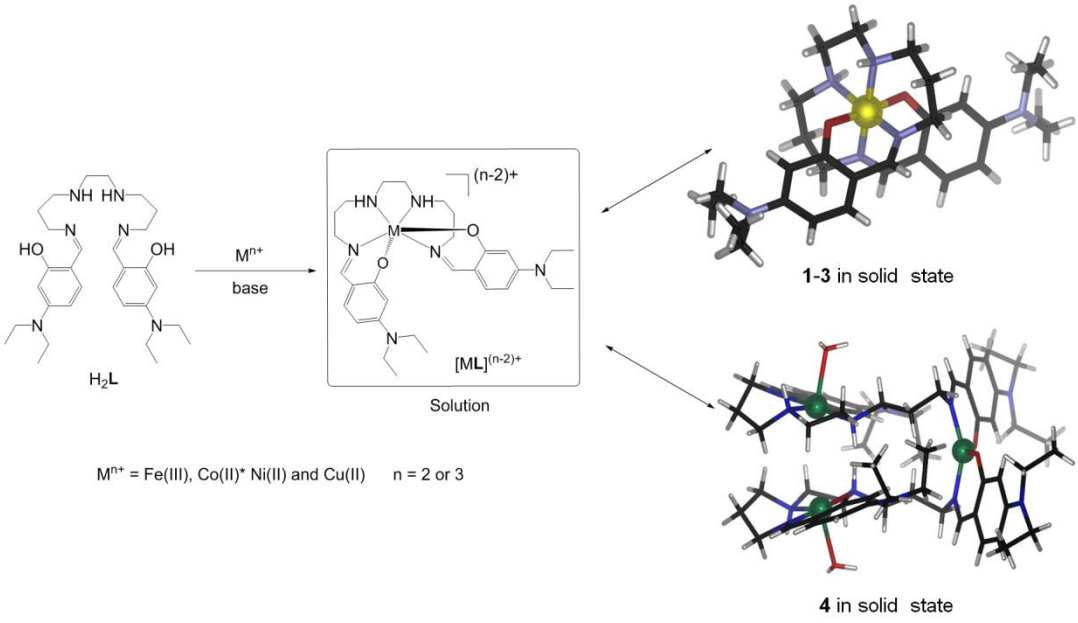

Scheme 1. Schematic representation of the synthesis of complexes **1**-**4**. $^{A}Co^{II}$ oxidised to Co^{III} in air under basic conditions.

2.3 Experimental

2.3.1 Materials and Instrumentation

All chemicals and reagents were purchased from commercial sources and used without further purification. High-resolution electrospray ionisation–mass spectrometry (HR ESI-MS) data were acquired using a Waters Xevo QToF mass spectrometer, operating in positive ion mode. Fourier Transform-Infrared (FT-IR) measurements were undertaken on a Bruker Vertex 70 with a diamond ATR crystal. The solid-state UV-Vis (Ultraviolet-visible) spectra were measured in Nujol at ambient temperature using an Agilent Cary 100 UV-Vis with *WinUV* software. Spectra were collected from 900 to 200 nm with a scan rate of 600 nm per minute. Scanning electron microscopy–electron dispersive spectroscopy (SEM-EDS) analysis was conducted on a Phenom XL instrument. Samples were run at 15 kV in high vacuum without surface coating.

Caution! While we have not experienced any issues with the compounds listed in this work, perchlorate salts are highly explosive and should be handled with care and used in small amounts.

The synthesis of the ligand (H_2**L**) involved a Schiff base condensation reaction adapted and optimised from previously reported methods.[12,15,16]

2.3.2 Synthesis of Ligand H_2**L**

4-(Diethylamino)salicylaldehyde (50 mg, 0.26 mmol) was dissolved in 10 mL of ethanol. To the solution, 1,2-bis(3-aminopropylamino)ethane (22 mg, 0.13 mmol) in 10 mL of ethanol was added dropwise. A few milligrams of *p*-toluenesulfonic acid were added. The reaction mixture was refluxed for 10 hours under nitrogen. After cooling to room temperature, the solvent was evaporated to furnish the crude product as a yellow oil, which was used for the metal complexation without further purification.

2.3.3 Synthesis of Metal Complexes **1**-**4**

*[Fe**L**]ClO_4 (**1**)*

To a solution of [H_2**L**] (0.13 mmol) in 5 mL of ethanol, a 10 mL ethanolic solution of sodium hydroxide (11 mg, 0.27 mmol) was added dropwise and allowed to stir for half an hour, resulting in a green solution. Iron(III) perchlorate nonahydrate (68 mg, 0.13 mmol) in 5 mL of ethanol was added. The resulting dark green solution was heated under reflux for 2 hours. After hot filtration, dark green crystals formed upon slow evaporation, which were allowed to dry in air (56 % yield). λ_{max} (Nujol)/nm 440, 620. ν_{max} (ATR)/cm^{-1} 2971w, 1588s, 1072s, 1010m, 622s. *m/z* (HRMS ESI^+, CH_3CN) 578.2860 [Fe**L**]$^+$. X-Ray quality crystals were used for the X-ray study.

*[Co**L**]NO_3 (**2**)*

To a solution of [H_2L] (0.13 mmol) in 5 mL of ethanol, a 10 mL ethanolic solution of sodium hydroxide (11 mg, 0.27 mmol) was added dropwise and allowed to stir for half an hour, resulting in a green solution. Cobalt(II) nitrate hexahydrate (42 mg, 0.13 mmol) was added. The resulting dark green solution was heated under reflux for 2 hours. After hot filtration, a brown precipitate formed upon slow evaporation, which was allowed to dry in air (63 % yield). λ_{max} (Nujol)/nm 365, 500(sh), 660. ν_{max} (ATR)/cm^{-1} 2980m, 1595s, 1512m, 1351m, 1250m, 1141m. *m/z* (HRMS ESI^+, CH_3OH) 581.2975 [Co**L**]$^+$. The brown precipitate was re-dissolved in ethanol and X-ray quality crystals were obtained by vapour diffusion of diethyl ether into the complex mixture.

*[Ni**L**] (**3**)*

To a solution of [H_2**L**] (0.13 mmol in 5 mL of ethanol), a 10 mL ethanolic solution of sodium hydroxide (11 mg, 0.27 mmol) was added dropwise and allowed to stir for half an hour, resulting in a green solution. Nickel(II) nitrate hexahydrate (40 mg, 0.14 mmol) was added. The resulting dark green solution was heated under reflux for 2 hours. After hot filtration, a few dark green crystals formed upon slow evaporation, which were allowed to dry in air (<3 % yield). Such a small amount of crystals could only be used for the X-ray study and ESI-HRMS. *m/z* (HRMS ESI^+, CH_3OH) 581.3128 [Ni**L** + H]$^+$.

*[Cu_3**L**$_2$] (**4**)*

To a solution of [H_2**L**] (0.13 mmol in 5 mL of ethanol), a 10 mL ethanolic solution of sodium hydroxide (11 mg, 0.27 mmol) was added dropwise and allowed to stir for half an hour, resulting in a green solution. Copper(II) chloride dihydrate (22 mg, 0.13 mmol) was added. The resulting dark green solution was heated under reflux for 2 hours. After hot filtration, dark brown crystals were obtained, which was allowed to dry in air (51 % yield). λ_{max} /nm 350, 650. ν_{max} (ATR)/cm^{-1} 2972(br), 1591s, 1508m, 1348m, 1247s, 1136m, 820m. *m/z* (HRMS ESI$^+$, CH_3OH) 586.3081 [Cu**L** + H]$^+$. X-Ray quality crystals were used for the X-ray study.

2.3.4 Single Crystal X-Ray Diffraction

The single crystal X-ray data for complexes **1**–**4** were collected at the MX1 beamline of the Australian Synchrotron with Silicon Double Crystal monochromated radiation at 100(2) K.[17,18] Data integration and reduction were undertaken with *XDS*.[19] An empirical absorption correction was then applied using *SADABS* at the Australian Synchrotron.[20] The structures were solved by direct methods and the full-matrix least-squares refinements were carried out using a suite of *SHELX* programs[21,22] via the *Olex2* interface.[23] All non-hydrogen atoms were located from the electron density maps and refined anisotropically. Hydrogen atoms bound to carbon atoms were added in the ideal positions and refined using a riding model. Complex **2** crystallised in a chiral space group $P2_12_12_1$, the Flack parameter was refined to a value of 0.41, and refinement suggested use of TWIN/BASF in the subsequent refinement cycles. Therefore, BASF was refined starting from 0.5 which refined to a value of 0.41. This suggests the structure contains racemic twinning. Complex **3** exhibited short intermolecular contacts between O1 and O2A, which are within hydrogen-bonding distance and arise as a result of partially occupied water molecules, one of which makes short hydrogen-bonding contacts with the neighbouring ligand oxygen atom. The difference Fourier of complex **4** showed Q peaks around values of 1.6–2, which are probably due to highly disordered ethanol solvent or partially occupied waters. Therefore, the solvent mask refinement procedure available in *Olex2* was used in the subsequent refinement cycles. The crystallographic data in CIF format has been deposited at the Cambridge Crystallographic Data Centre with CCDC numbers

1519783–1519786. It is available free of charge from the Cambridge Crystallographic Data Centre, 12 Union Road, Cambridge CB2 1 EZ, UK; fax: (+44) 1223-336-033; or email: deposit@ccdc.cam.ac.uk. Specific refinement details and crystallographic data for each structure are presented below.

2.4 Results and Discussion

The flexible N_4O_2-donor hexadentate Schiff-base ligand H_2**L**, as a known compound, was prepared from the reaction of 1,2-bis(3-aminopropylamino)ethane with 4-(diethylamino)salicylaldehyde employing slight modifications of reported procedures.[12,15,16] Metal complexes were synthesised via a self-assembly procedure employing the ligand H_2**L** as a crude product and different metal salts in ethanol under basic conditions. The X-ray quality crystals were obtained by either diffusion of diethyl ether vapour into the ethanol solution or slow evaporation. Three complexes (**1**, **2**, and **4**) of Fe^{III}, Co^{III}, and Cu^{II} metal ions were investigated by UV-Vis, FT-IR, HR-MS, and SEM-EDS, as well as single crystal X-ray diffraction. The X-ray structure of the Ni^{II} complex **3** is also reported.

2.4.1 Structure Description of Complexes **1**-**4**

The crystal data and refinement details for the four complexes **1**–**4** are summarised in Table 1. Complex **1** crystallises in the triclinic space group *P1* (ba). Each complex is chiral and two enantiomers are present in the crystal lattice. These isomers are differentiated by the face orientation of the two benzene moieties in each complex. The Fe^{III} centre adopts a slightly distorted octahedral coordination environment with the basal plane defined by four consecutive nitrogen donors from two imine nitrogens and two secondary amine nitrogens. In addition, the apical positions are occupied by two phenoxo oxygens. This is illustrated from two separate angles in (Figure 1a, b) by rotation around the axial plane. The angle formed by the two axial ligand nitrogen donors and the Fe^{III} site is 173.2(1)°, demonstrating a slight distortion from octahedral geometry. The two Fe^{III}–$O_{phenolic}$ bond distances are 1.879(2) and

1.884(2) Å, the two Fe^{III}–$N_{sec.amine}$ are 2.026(3) and 2.027(3) Å, and the two Fe^{III}–N_{imine} bond distances are 1.952(3) and 1.955(3) Å, similar to previously observed values of equivalent Fe^{III} complexes.[16] These relatively small bond lengths suggest the d^5 Fe^{III} site is in a low spin electronic configuration at the measurement temperature of 100 K, with no electrons occupying the e_g orbitals of the Fe^{III} centre.

Table 1. Crystallographic data and refinement details for complexes **1**–**4**.

Parameter	1	2	3	4
Empirical formula	$C_{30}H_{46}ClFeN_6O_6$	$C_{32}H_{52}CoN_7O_6$	$C_{31}H_{50}N_6NiO_{3.5}$	$C_{30}H_{48}ClCu_{1.5}N_6O_3$
Formula weight	678.03	689.73	621.48	671.50
Temperature [K]	100	100	100.0	100
Crystal system	triclinic	orthorhombic	orthorhombic	monoclinic
Space group	$P\bar{1}$	$P2_12_12_1$	*Pbca*	*P2/n*
a [Å]	7.6630(15)	7.5700(15)	25.035(5)	11.919(2)
b [Å]	14.725(3)	19.646(4)	16.957(3)	12.485(3)
c [Å]	15.088(3)	23.006(5)	30.314(6)	22.433(5)
α [deg.]	109.12(3)	90	90	90
β [deg.]	98.54(3)	90	90	91.50(3)
γ [deg.]	91.01(3)	90	90	90
Volume [Å^3]	1586.7(6)	3421.5(12)	12869(4)	3337.1(12)
Z	2	4	16	4
ρ_{calc} [g cm^{-3}]	1.419	1.339	1.283	1.337
μ [mm^{-1}]	0.612	0.554	0.645	1.083
F(000)	718.0	1472.0	5344.0	1418.0
Radiation	MoKα (λ 0.71073)	MoKα (λ 0.71073)	MoKα (λ 0.71073)	MoKα (λ 0.71073)
2θ range for data collection [deg.]	5.686 to 49.998	2.726 to 54.998	2.686 to 51.996	3.262 to 49.996
Index ranges	$-8 \le h \le 8$, $-17 \le k \le 17$, $-17 \le l \le 17$	$-9 \le h \le 9$, $-25 \le k \le 25$, $-29 \le l \le 29$	$-30 \le h \le 30$, $-20 \le k \le 20$, $-37 \le l \le 37$	$-14 \le h \le 14$, $-14 \le k \le 14$, $-26 \le l \le 26$
Reflections collected	19511	53442	172723	40604
Independent reflections	5066 [R_{int} 0.0372, R_{sigma} 0.0292]	7401 [R_{int} 0.1000, R_{sigma} 0.0481]	12636 [R_{int} 0.1485, R_{sigma} 0.0479]	5869 [R_{int} 0.0945, R_{sigma} 0.0439]
Data/restraints/parameters	5066/0/401	7401/0/422	12636/25/800	5869/1/385
Goodness-of-fit on *F*2	1.023	1.069	1.043	1.043
Final *R* indexes [$I \ge 2\sigma(I)$]	R_1 0.0488, wR_2 0.1219	R_1 0.0513, wR_2 0.1183	R_1 0.0589, wR_2 0.1239	R_1 0.0854, wR_2 0.2159
Final *R* indexes [all data]	R_1 0.0602, wR_2 0.1303	R_1 0.0671, wR_2 0.1273	R_1 0.0972, wR_2 0.1459	R_1 0.1051, wR_2 0.2335
Largest diff. peak/hole [e Å^{-3}]	0.86/−0.88	0.63/−0.92	0.79/−0.71	3.04/−1.44
Flack parameter		0.41(2)		

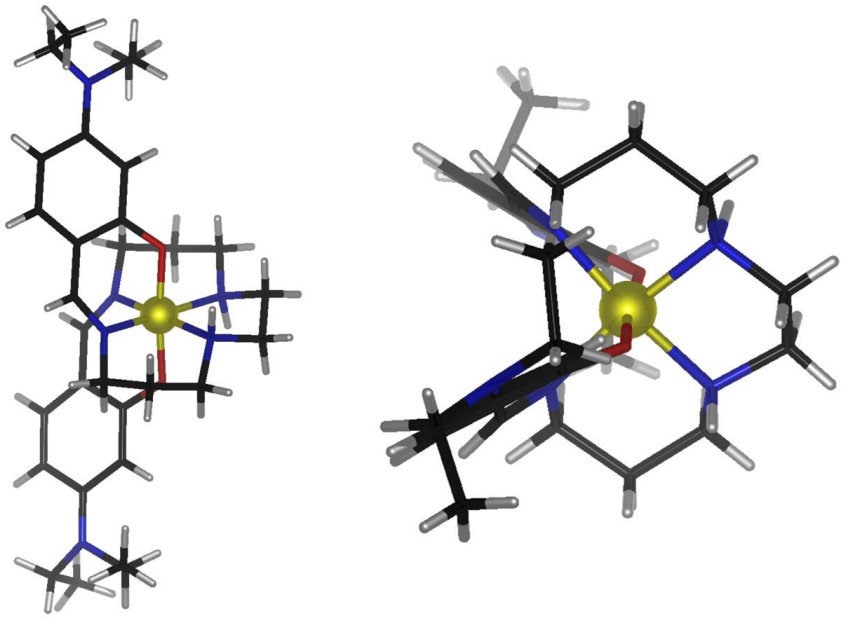

Figure 1. Schematic representations of the X-ray crystal structure of [Fe**L**]ClO_4 (**1**). Figures (a) and (b) show the structure rotated around the axial plane for clarity. The anion is not shown.

The ClO_4^- counter ions participate in hydrogen bonding with the axial $N_{sec.amine,}$ with an average N–H···O–ClO_3 distance being 2.24 Å. The complexes pack in repeating one-dimensional chains along the crystallographic *a*-axis (Figure 2), in which inverted isomeric complexes are orientated in a slightly offset undulating manner, so as to permit closer packing of the complexes, separating the complex cations of [Fe**L**]$^+$ to reduce electrostatic repulsion. The terminal diethyl groups participate in weak van der Waals interactions as a result of their proximity.

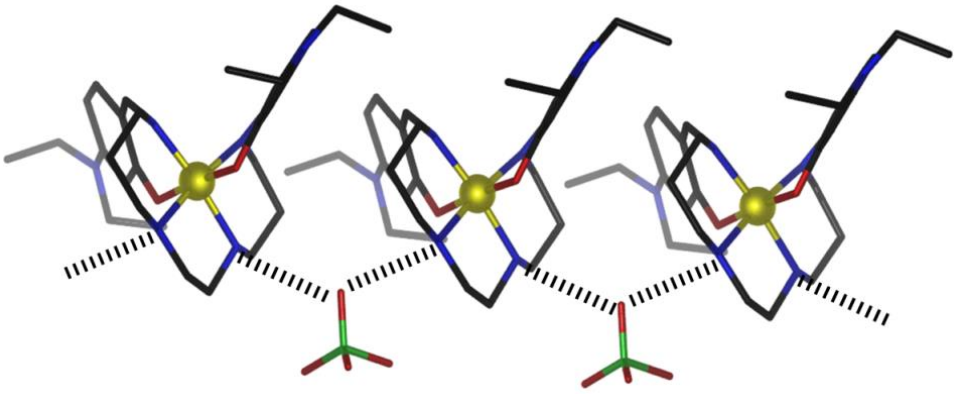

Figure 2. Schematic representation of part of the packing in the crystal X-ray structure of [Fe**L**]ClO_4 (**1**), illustrating the one-dimensional chain formed via the hydrogen bond involving the ClO_4^- anion and the complex cation [Fe**L**]$^+$. H atoms omitted for clarity.

Complex **2** crystallises in the orthorhombic space group $P2_12_12_1$, with one complex molecule in the asymmetric unit. The coordination geometry is almost identical to that of complex **1** with the Co^{III} centre exhibiting a slightly distorted octahedral geometry (Figure 3a, b). Although this distortion is not as severe as the previous complex, with an angle of 176.1(2)° formed between the two axial N donors and the Co^{III} centre.

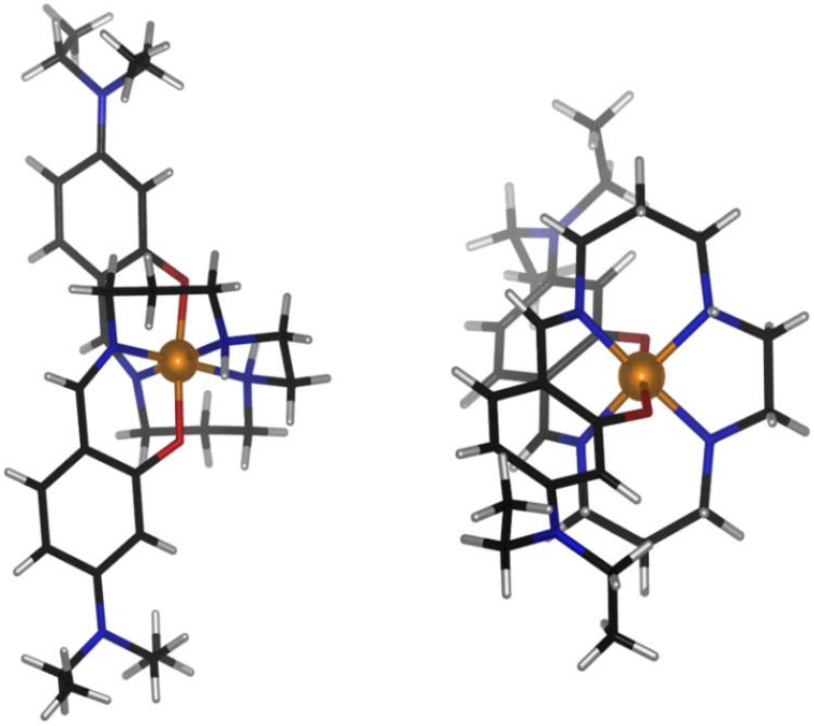

a) **b)**

Figure 3. Schematic representation of the X-ray crystal structure of [Co**L**]NO_3 (**2**). Figures (a) and (b) show the structure rotated around the axial plane for clarity. The NO_3^- anion and ethanol solvent are not shown.

The NO_3^- counter ions participate in hydrogen bonding with the two $N_{sec.amine}$ hydrogens and one –OH hydrogen from ethanol. The infinite one-dimensional chains are also formed via hydrogen-bonding interactions. The $N_{sec.amine}$–H···O–NO_2 distances are 2.09 and 2.04 Å. Each NO_3^- counter ion interacts via hydrogen bonding with two adjacent metal complexes, with the NO_3^- ions situated in the cavities between the cationic lattice (Figure 4).

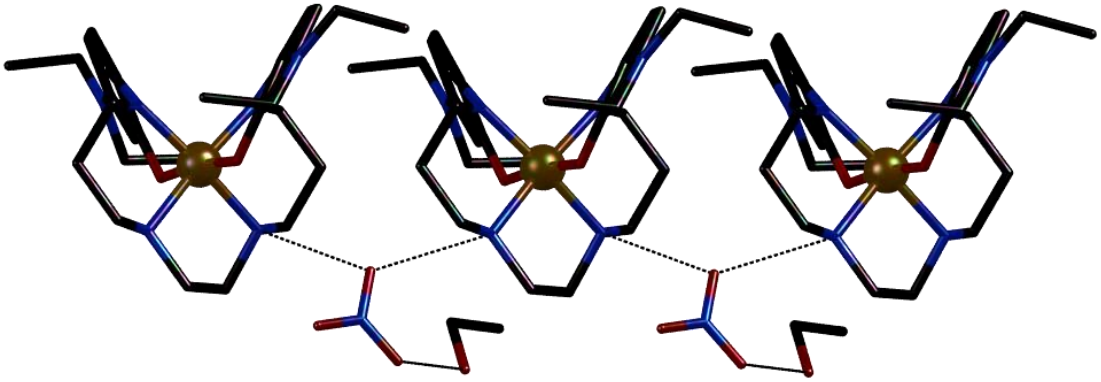

Figure 4. Schematic representation of the single crystal structure of [Co**L**]NO_3 (**2**), showing the hydrogen-bonding interaction of each complex with two NO_3^- counter ions, and the effective hydrogen-bonding bridging of the NO_3^- counter ions. H atoms omitted for clarity.

Complex **3** forms a neutral species, [Ni**L**], and the coordination geometry of the Ni^{II} centre is again very similar to the previous two crystal systems, crystallising in the orthorhombic *Pbca* space group (Figure 5a, b), with two complex molecules in the asymmetric unit. The Ni^{II} centre again adopts a distorted octahedral geometry, with the axial $N_{sec.amine}$, and N_{imine} donors making an angle of 169.1(1)° with the Ni^{II} ion. Ethanol solvent molecules participate in hydrogen-bonding interactions with an equatorial $O_{phenolic}$ and $N_{sec.amine}$ of the same complex, while further hydrogen bonding is observed between water molecules and two equatorial $O_{phenolic}$ of two separate complexes.

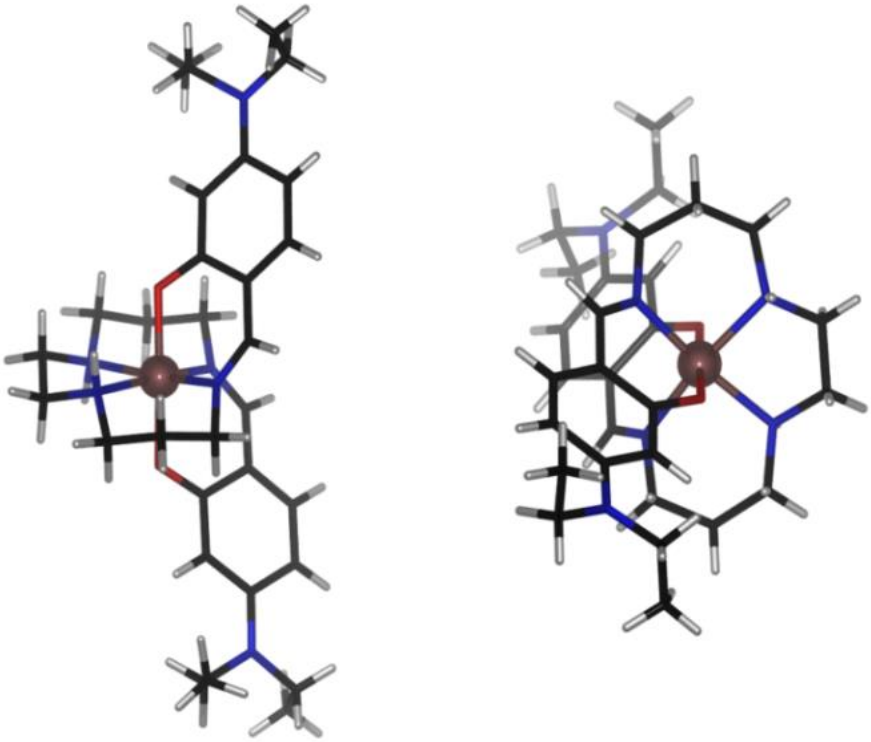

a) **b)**

Figure 5. Schematic representation of the X-ray crystal structure of [Ni**L**] (**3**). Figures (a) and (b) show the structure inverted and rotated around the axial plane for clarity. The solvent molecules are not shown.

The molecular coordination of the longer flexible ligand **L** with the five coordinate Cu^{II} metal ion is very different to that of the six coordinate Fe^{III}, Co^{III}, and Ni^{II} reported above (Figure 6a, b). This interesting structure results from the flexibility of **L**, which has less preorganization. Complex **4** is a discrete trinuclear architecture, which crystallises in the monoclinic space group *P*2/*n* with a two-fold rotation along the *b*-axis at 1/4, *y*, 1/4, and C_2 symmetry passing through the centre of Cu01. In contrast to the above structures, complex **4** exhibits two of the Cu^{II} centres coordinated in a distorted square pyramidal geometry and one four-coordination Cu^{II} centre in a distorted tetrahedral/square planar ('triangular-based pyramidal') geometry (Figure 6a, b). For the two five-coordinate Cu^{II} centres, a water molecule sits on the axial position, while the equatorial donors are the two $N_{sec.amine}$ as well as one N_{imine} (1.956–2.052 Å) and one $O_{phenolic}$ (1.906–1.922 Å) atoms at only one end of one ligand, with distances typical for these types of bonds. Each of the two ligands present in the complex coordinate one Cu^{II} ion in this manner. In addition, the two approximately square pyramidal d^9 Cu^{II} centres exhibit elongation of the axial bond as a result of Jahn–Teller

distortions, with a O_{water}–Cu^{II} coordinate bond distance of 2.370(5) Å. The third Cu^{II} site is coordinated by one N_{imine} and one $O_{phenolic}$ of each of the other ends of the two ligands, resulting in a coordination geometry somewhere between square planar and tetrahedral. The angle formed by the immines and the metal centre, N_{imine}–Cu^{II}–$N_{imine,}$ is 152.8(3)°, and that formed by $O_{phenolic}$–Cu^{II}–$O_{phenolic}$ is 147.5(3)° (as opposed to 180° in a square planar complex). The angle formed by adjacent atoms and the metal centre, $O_{phenolic}$–Cu^{II}–N_{imine}, is 95.2(2)°, as opposed to 90 in a square planar complex.

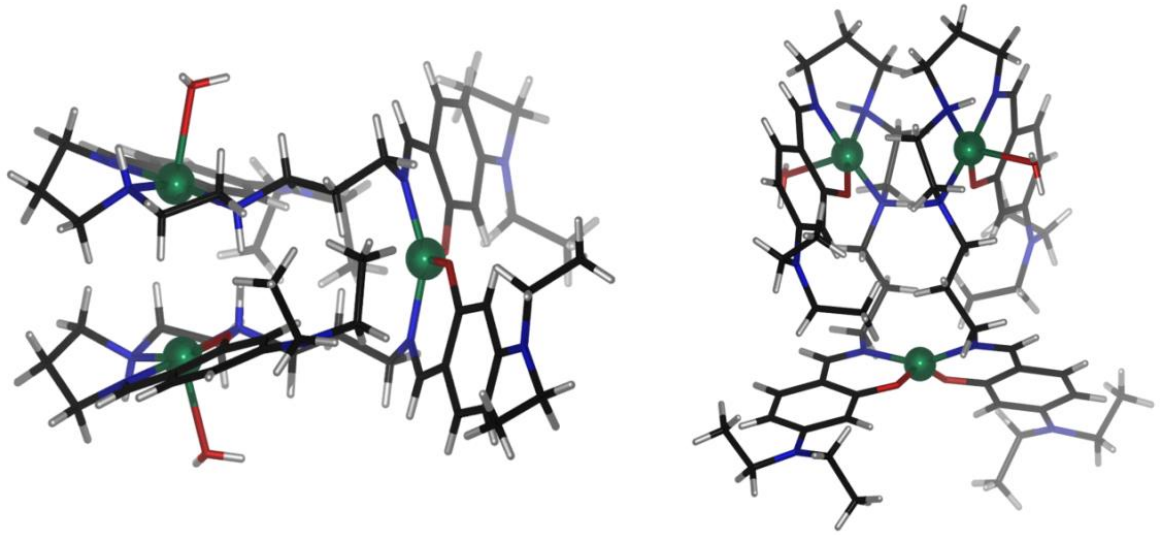

a) **b)**

Figure 6. Schematic representations of the X-ray crystal structure of [Cu_3**L**$_2$] (**4**). Figures (a) and (b) show the structure rotated around the crystallographic *c*-axis for clarity. The anion and solvent are not shown.

The structure is stabilised by intramolecular hydrogen-bonding interactions between the $O_{phenolic}$ and $HN_{sec.amine}$ of opposing equatorial five coordinate Cu^{II} metal centres, with $O_{phenolic}\cdots HN_{sec.amine}$ bond distances of 2.04 Å. Hydrogen-bonding interactions occur between the Cl^- counter ions and H–OH, with a bond distance of 2.32 Å.

The complexes pack in layers, with complexes in each layer orientated in the same direction along the *b* and *c*-axis, separated by an ethanol solvent molecule and Cl^- counter ions. From one adjacent layer to the next, extending along the *a*-axis, the complexes are inverted, with an inversion centre at [0,0,0] (Figure 7).

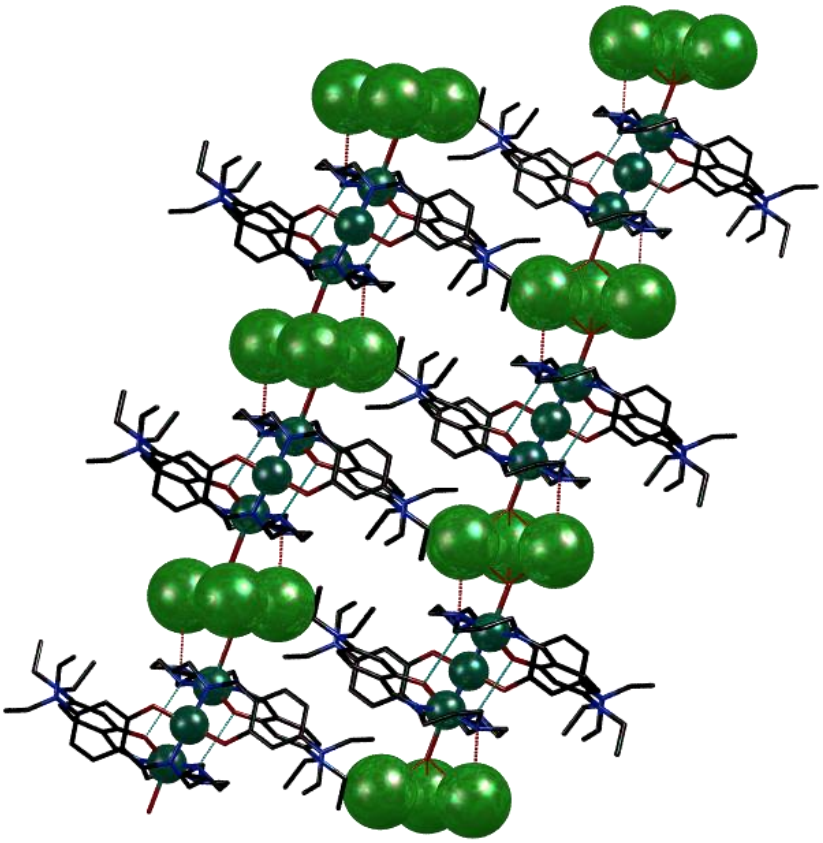

Figure 7. Schematic representation of the packing in the X-ray crystal structure of [$Cu_3\mathbf{L}_2$] (**4**), illustrating the layered packing structure of the complexes. The Cl^- anions and ethanol solvents are shown in spacefilling representation (larger light green balls: Cl^- anions, small dark green balls: Cu^{2+}). H atoms omitted for clarity.

Furthermore, Figure 8 demonstrates how these layers are stabilised by hydrogen bonding between the coordinated waters of each five coordinate Cu^{II} and Cl^- ions between each layer.

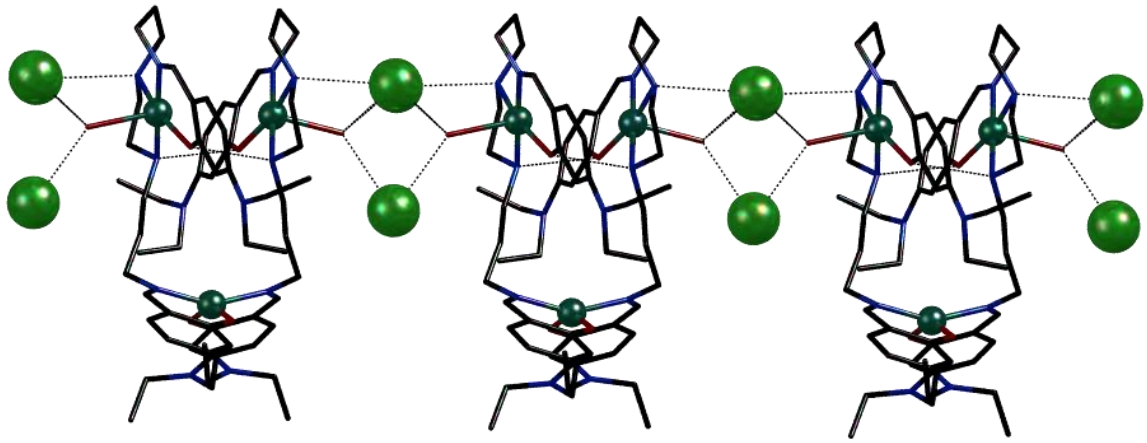

Figure 8. Schematic representation of hydrogen-bonding interactions, stabilising adjacent layers in the crystal X-ray structure of [$Cu_3\mathbf{L}_2$] **4**. (green balls: Cl^- anions, small dark green balls: Cu^{2+}). H atoms omitted for clarity.

2.4.2 SEM-EDS

SEM images (Figures S1–S3, S = Supplementary Materials) indicated that complex **1** is formed in large single crystals whereas **2** and **4** are microcrystalline powders. The needle crystals of complex **1** undergo rapid decay due to loss of solvent. In addition, SEM-EDS analysis confirmed the presence of C, Cl, Fe, N, and O in [Fe**L**]ClO_4 (**1**) (Figure S1), C, Co, N, and O in [Co**L**]NO_3 (**2**) (Figure S2), and C, Cu, Cl, N, and O in [Cu_3**L**$_2$] (**4**) (Figure S3).

2.4.3 HR-ESI Mass Spectrometry

HR ESI-MS provided evidence that singly charged species of type [Fe**L**]$^+$, [Co**L**]$^+$, [Ni**L** + H]$^+$, and [Cu**L** + H]$^+$ persist in solution (Figures S4–S7). The expected isotope patterns for such charged species for the four complexes **1**–**4** were all found to be in excellent agreement with their simulated patterns (inserts in Figures S4 and S5, Figs S6 and S7, Supplementary Material). In regard to complex **2**, a Co^{III} complex with a 1:1 stoichiometry was observed as a major peak at *m/z* 581.2975 (calc. 581.3015), as the Co^{II} complex is oxidised to the Co^{III} complex under the experimental conditions.[3] For complex **4**, a trinuclear species of the Cu^{II} complex was found in the solid state (see above), but its mononuclear species is formed when it is dissolved in solution.

2.4.4 UV-Vis Spectroscopy

The solid-state UV-Vis spectra of **1**, **2**, and **4** are shown in Figure S8. The electronic spectrum of complex **1** exhibits a low energy charge-transfer band centred at 620 nm and a higher energy band at 440 nm. The lower energy band may be assigned to the low spin Fe^{III} form and the higher energy band to the high spin form,[24,25] which will be of interest for future studies of magnetic properties in our laboratory. For complex **2**, the UV-Vis spectrum exhibits a weak absorption band at 660 nm in addition to a strong broad absorption band at 365 nm with a shoulder at approx. 500nm, which are similar to those of the previously reported Co^{III}

complexes of N_4O_2 Schiff-base analogues.[25] The UV-Vis spectrum of complex **4** shows an intense broad absorption band at 350 nm in the UV region and a weak band at 650 nm in the visible region. The former absorption peak is assigned to a ligand-to-metal charge transfer (LMCT) transition and the latter band as a d–d transition of the Cu^{II} ion in a square-pyramidal geometry.[26]

2.4.5 IR Spectroscopy

FT-IR spectra of complexes **1**, **2**, and **4** were recorded at room temperature (Figures S9–S11, Supplementary Material). The FT-IR spectra show absorptions in the region of 1595–1585 cm^{-1} that are typical of imine (C=N) stretching modes. In the region 3400–2800 cm^{-1}, the spectra exhibit an alkyl C–H stretch and N–H stretch of a secondary amine, which is assigned to alkyl secondary amines in all three complexes. In addition, the absorptions at 1072 and 622 cm^{-1} indicate the presence of the perchlorate counter ion in complex **1**.

2.5 Conclusion

We describe the synthesis and structure investigations of four new 3d transition metal complexes **1**–**4** with a long flexible N_4O_2-donor hexadentate Schiff-base ligand. Three complexes (**1**, **2**, and **4**) of Fe^{III}, Co^{III}, and Cu^{II} metal ions have been investigated by UV-Vis, FT-IR, HR-MS, and SEM-EDS, as well as single crystal X-ray diffraction. The X-ray structure of the Ni^{II} complex **3** is also reported. Further studies are underway to optimise the synthetic method to produce a larger amount of the Ni^{II} complex and other metal complexes and to explore their magnetic and optical properties.

2.6 Acknowledgements

The research described herein was supported by Western Sydney University. The authors acknowledge Western Sydney University for the use of the Advanced Materials Characterisation Facility and mass spectrometry facilities. The crystallographic data for **1**–**4** were collected on the MX1 beamline at the Australian Synchrotron, Victoria, Australia. A.R.C. also acknowledges the AINSE honours scholarship program. In addition, K.J.H.-S. acknowledges the Western Sydney University Scholarship for the Master's program.

2.7 References

1. E. L. Gavey and M. Pilkington, *Coord. Chem. Rev.*, **2015**, *296*, 125.
2. M. Rezaeivala and H. Keypour, *Coord. Chem. Rev.*, **2014**, *280*, 203.
3. D. J. Fanna, Y. Zhang, L. Li, I. Karatchevtseva, N. D. Shepherd, A. Azim, J. R. Price, J. Aldrich-Wright, J. K. Reynolds and F. Li, *Inorg. Chem. Front.,* **2016**, *3*, 286.
4. D. J. Fanna, Y. Zhang, A. Salih, J. K. Reynolds and F. Li, *J. Coord. Chem.,* **2016**, *69*, 1883.
5. H. Eguchi, M. Umemura, R. Kurotani, H. Fukumura, I. Sato, J.-H. Kim, Y. Hoshino, J. Lee, N. Amemiya, M. Sato, K. Hirata, D. J. Singh, T. Masuda, M. Yamamoto, T. Urano, K. Yoshida, K. Tanigaki, M. Yamamoto, M. Sato, S. Inoue, I. Aoki and Y. Ishikawa, *Scientific Reports.*, **2015**, *5*, 9194.
6. S. Wang, W.-T. Xu, W.-R. He, S. Takaishi, Y.-H. Li, M. Yamashita and W. Huang, *Dalton. Trans.,* **2016**, *45*, 5676.
7. S. Hayami, Z. Gu, H. Yoshiki, A. Fujishima and O. Sato, *J. Am. Chem. Soc.*, **2001**, *123*, 11644.
8. V. Mougel, L. Chatelain, J. Pécaut, R. Caciuffo, E. Colineau, J.-C. Griveau and M. Mazzanti, *Nat. Chem.*, **2012**, *4*, 1011.
9. L. Li, Y. Zhang, M. Avdeev, L.F. Lindoy, D.G. Harman, R. Zheng, Z. Cheng, J.R. Aldrich-Wright and F. Li, *Dalton Trans.*, **2016**, *45,* 9407.
10. F. Reichel, J. K. Clegg, K. Gloe, K. Gloe, J. J. Weigand, J. K. Reynolds, C.-G. Li, J. R. Aldrich-Wright, C. J. Kepert, L. F. Lindoy, H.-C. Yao and F. Li, *Inorg. Chem.*, **2014**, *53*, 688.
11. W. J. Ramsay and J. R. Nitschke, *J. Am. Chem. Soc.*, **2014**, *136*, 7038.
12. B. W. Tsang, C. J. Mathias, P. E. Fanwick and M. A. Green, *J. Med. Chem.,* **1994**, *37*, 4400.
13. F. Li, J. K. Clegg, L.F. Lindoy, R. B. Macquart and G. V. Meehan, *Nature Commun.*, **2011**, *2*: 205.
14. F. Li, J. K. Clegg, D. Price and C. J. Kepert, *Inorg. Chem.*, **2011**, 50, 726.
15. L Li, A. R. Craze, D. J. Fanna, A. J. Brock, J. K. Clegg, L. F. Lindoy, J. R. Aldrich-Wright, J. K. Reynolds and F. Li, *Polyhedron.*, **2017**, 125, 44.
16. R. Kannappan, S. Tanase, I. Mutikainen, U. Turpeinen and J. Reedijk, *Polyhedron.,* **2006**, *25*, 1646.
17. T.M. McPhillips, S.E. McPhillips, H.J. Chiu, A.E. Cohen, A.M. Deacon, P.J. Ellis, E. Garman, A. Gonzalez, N.K. Sauter, R.P. Phizackerley, S.M. Soltis and P. Kuhn, BlueIce, *J. Synchrotron Rad.,* **2002**, *9*, 401.
18. N. P. Cowieson, D. Aragao, M. Clift, D. J. Ericsson, C. Gee, S.J. Harrop, N. Mudie, S. Panjikar, J.R. Price, A. Riboldi-Tunnicliffe, R. Williamson and T. Caradoc-Davies, *J. Synchrotron Rad.,* **2015**, *22*, 187.
19. W. Kabsch, *J. Appl. Cryst.*, **1993**, *26*, 795.
20. G. M. Sheldrick, SADABS: Empirical Absorption and Correction Software, University of Göttingen, Germany, **1996**.
21. G. M. Sheldrick, *Acta Cryst.,* **2008**, *A64*, 112.
22. G. M. Sheldrick, *Acta Cryst.,* **2015**, *A71*, 3.
23. O. V. Dolomanov, L. J. Bourhis, R. J. Gildea, J. A. K. Howard, H. Puschmann, *J. Appl. Cryst.,* **2009**, *42*, 339.
24. M. F. Tweedle and L.J. Wilson, *J. Am. Chem. Soc.,* **1976**, 98, 4824.
25. A. S. Rothin, H. J. Banbery, F. J. Berry, T. A. Hamor, C. J. Jones and J. A. McCleverty, *Polyhedron*, **1989**, *8*, 491.
26. S. Biswas, A. Dutta, M. Dolai, K. K. Das and M. Ali, *Dalton Trans.,* **2013**, *42*, 13210.

2.8 Supplementary Materials

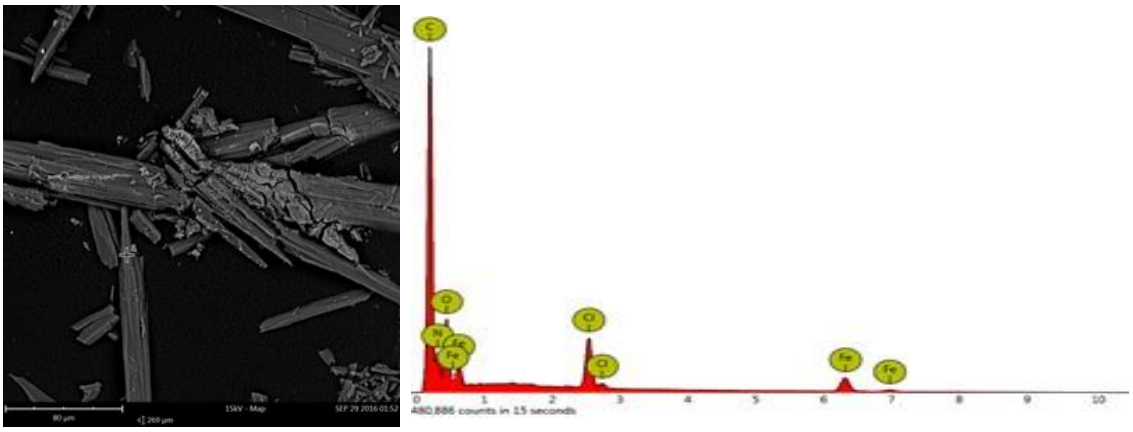

Figure S1. A backscattered SEM micrograph (left) and an EDS spectrum (right) of complex **1**.

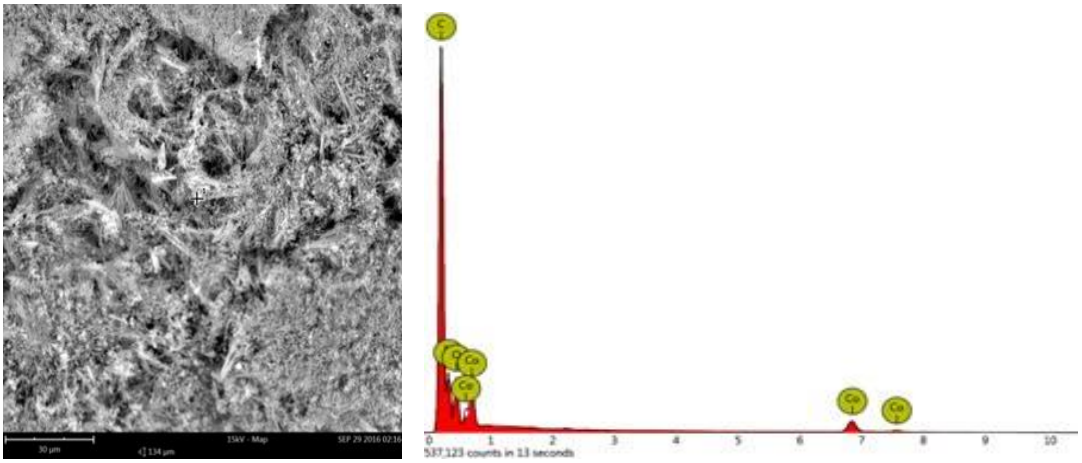

Figure S2. A backscattered SEM micrograph (left) and an EDS spectrum (right) of complex **2**.

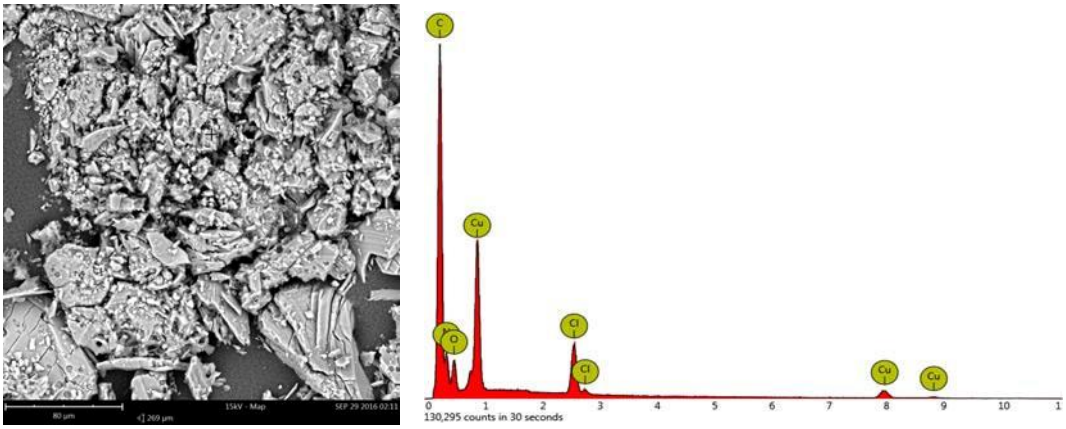

Figure S3. A backscattered SEM micrograph (left) and an EDS spectrum (right) of complex **3**.

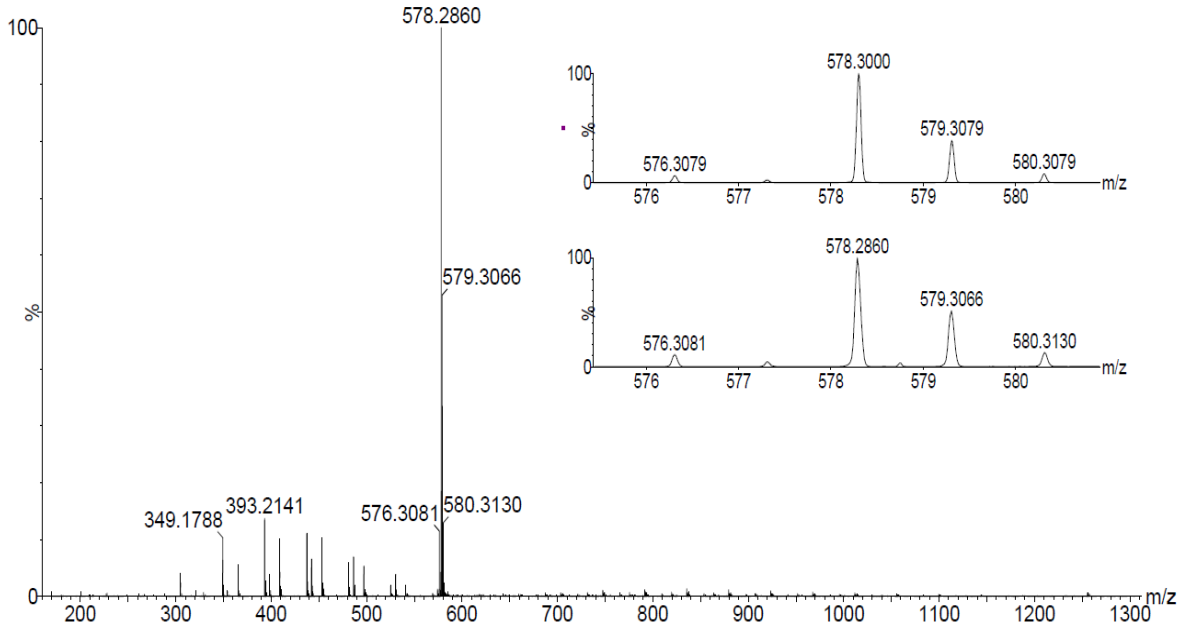

Figure S4. HR ESI-MS spectrum of **1**. The inset shows the isotope pattern for [Fe**L**]$^{+}$ (top calculated; bottom experimental).

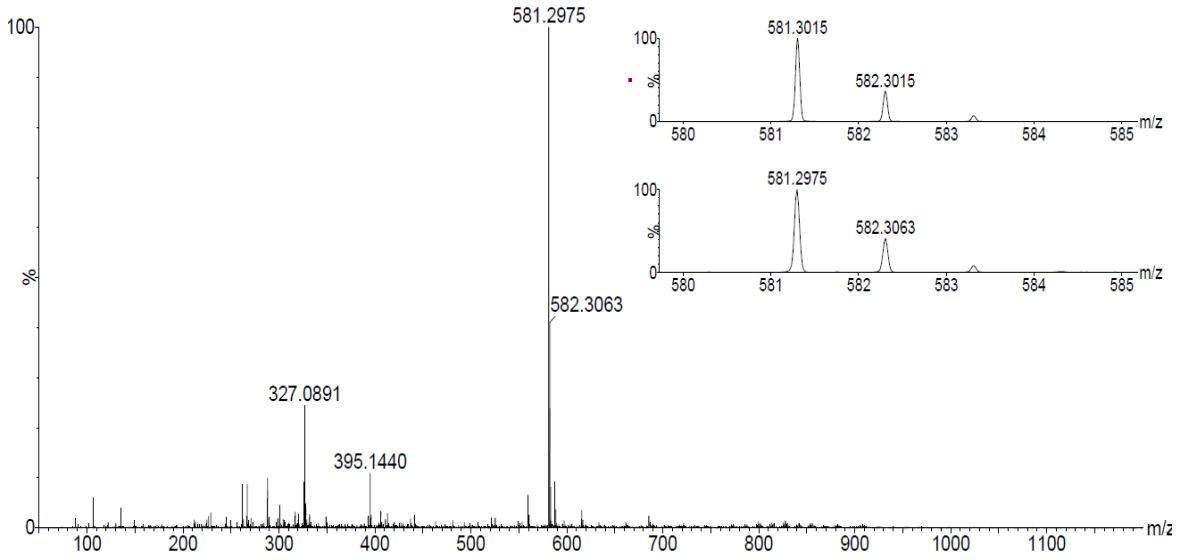

Figure S5. HR ESI-MS spectrum of complex **2**. The inset shows the isotope pattern for [Co**L**]$^{+}$ (top calculated; bottom experimental).

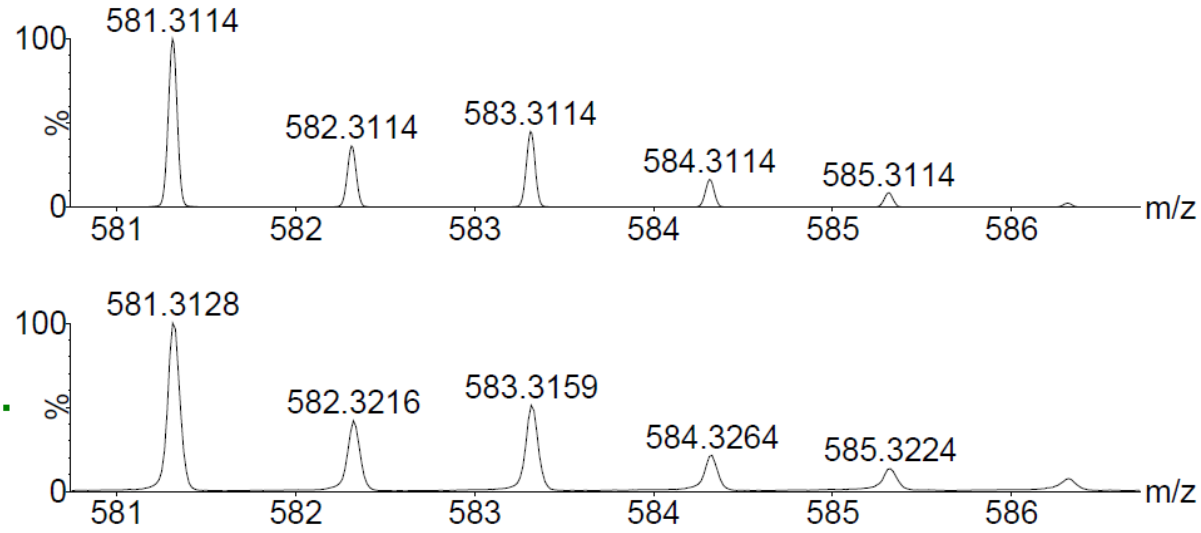

Figure S6. HR ESI-MS spectrum of the isotope pattern for $[NiL + H]^+$ (top calculated; bottom experimental).

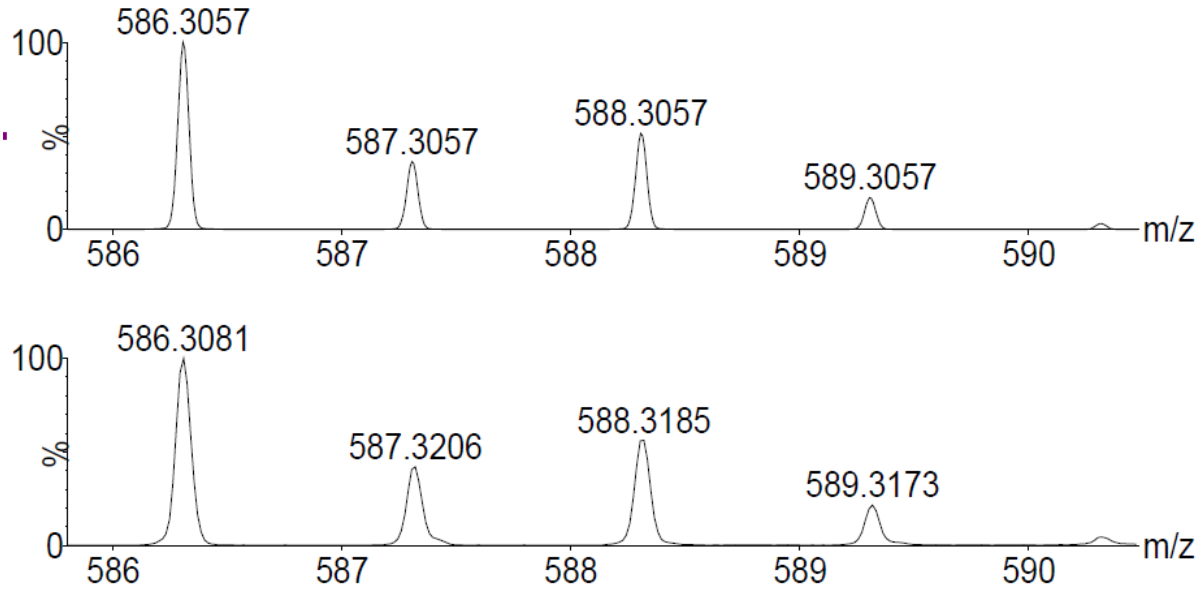

Figure S7. HR ESI-MS spectrum of the isotope pattern for $[CuL]^+$ (top calculated; bottom experimental).

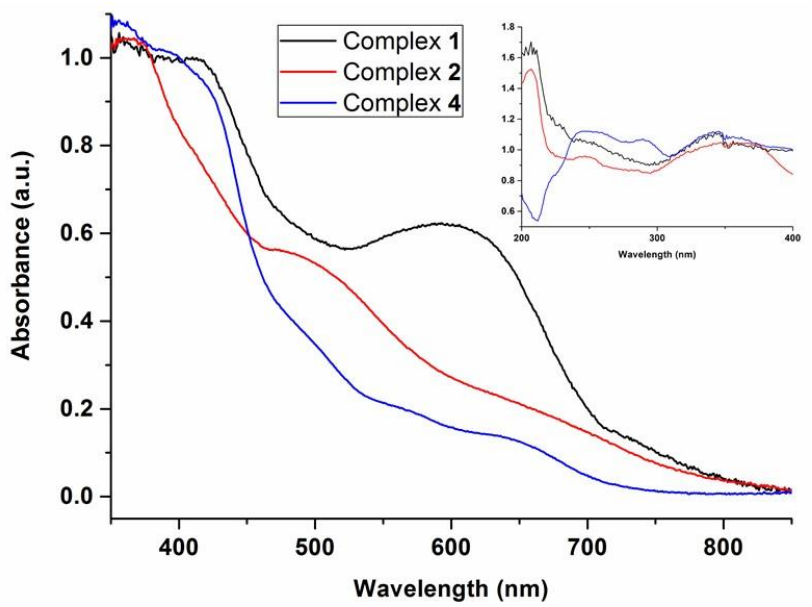

Figure S8. Solid state UV-Vis absorption spectra of **1**-**2** and **4** in nujol. The inset shows the relatively high intensity transition in region 200-400 nm.

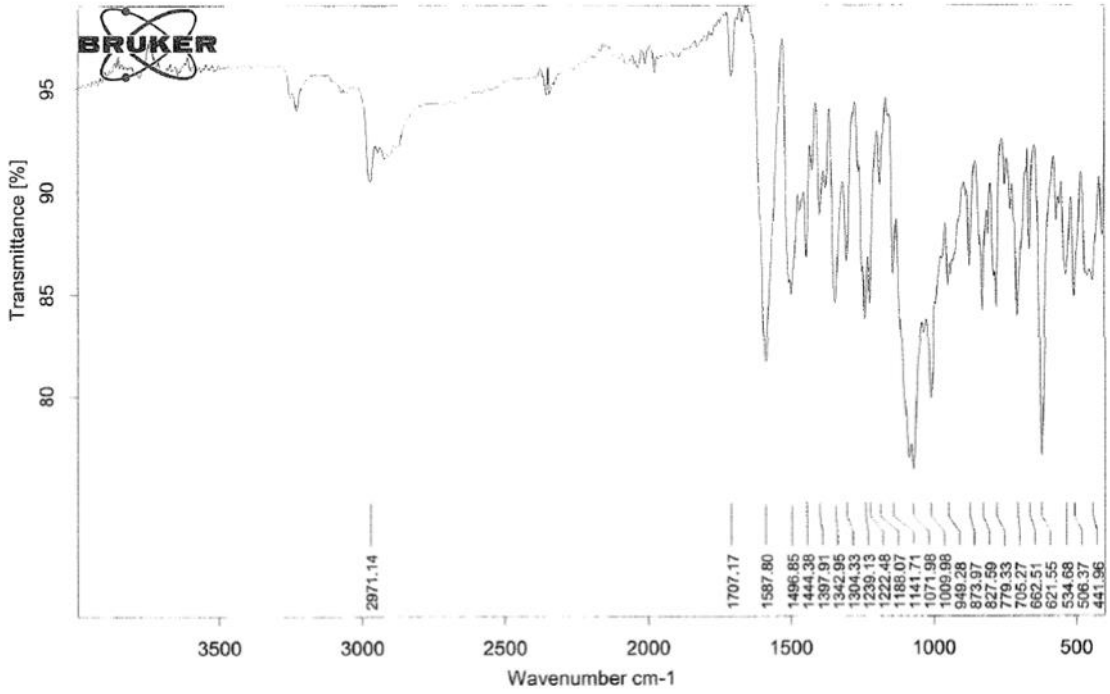

Figure S9: FT-IR spectrum of complex **1** [Fe**L**]ClO_4.

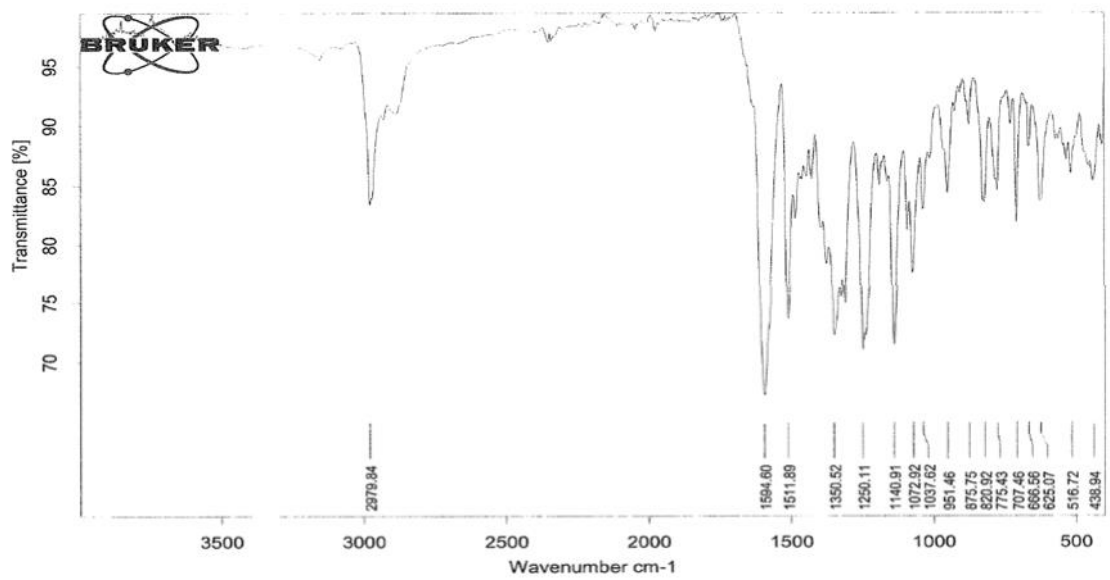

Figure S10: FT-IR spectrum of complex **2** [Co**L**]NO_3.

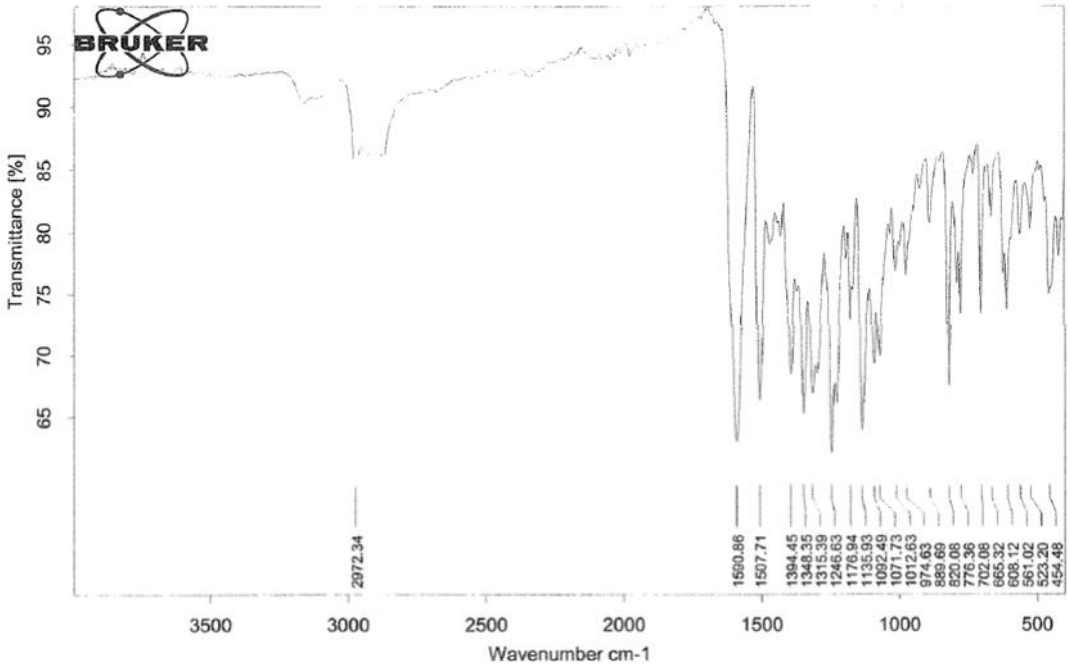

Figure S11: FT-IR spectrum of complex **4** [Ni**L**].

Chapter 3 – Investigation of a New N_4O_2 Schiff-base System: Synthesis & Structural Characterisation.

Authors: Kyle J. Howard-Smith[A], Alexander R. Craze[A], Mohan M. Badbhade[B] Chris Marjo[B] and Feng Li[A*]

[A]School of Science and Health, Western Sydney University, Locked Bag 1797, Penrith, NSW 2751, Australia.

[B] Mark Wainwright Analytical Centre, University of New South Wales, NSW, 2052, Australia.

3.1 Abstract

The design and synthesis of three new metal complexes, [Fe**L**]BF_4 (**1**), [Co**L**]PF_6 (**2**) and [Mn**L**]PF_6 (**3**) with a N_4O_2-donor hexadentate Schiff-base ligand is described herein. The three complexes **1**-**3** have been characterised by scanning electron microscopy-electron dispersive spectroscopy (SEM-EDS), FT-IR, Raman spectroscopy, solid-state UV-Vis, high-resolution electrospray ionisation-mass spectrometry (HR ESI-MS) and single crystal X-ray diffraction. Single crystal XRD reveals the molecular structure of the complexes **1**-**3** consists of mononuclear species in a distorted octahedral geometry with the phenolate oxygen groups being *trans* to each other around the central metal ion.

3.2 Introduction

In recent years, an ever-increasing research effort has been concerned with Schiff-base metallo-supramolecular assemblies, due in part by their straightforward ligand synthesis and intriguing properties, including, biological, photochemical, catalytic and magnetic.[1-4] Concerning the latter, many Schiff-base metal complexes have been demonstrated to exhibit interesting magnetic properties including, single molecular magnetism and spin-crossover (SCO) transitions. These assemblies have been well documented with potential applications in a variety of emerging technologies such as molecular switches, displays, sensors, and molecular storage devices.[5-8] Among these complexes, a vast amount of research has been focused towards Fe^{II} complexes[9-11] due in part by their magnetic and frequently optically distinct bi-stability states.[10-11] These bi-stability states refer to the low-spin (LS – $^1A_{1g}$)

diamagnetic and the high-spin (HS – $^5T_{2g}$) paramagnetic states, which is often reported as being easily incited by external stimuli including, pressure, light irradiation, temperature and external magnetic fields.[5,9-11] While several ligand coordination spheres have been shown to exhibit SCO behaviour such as N_6,[8,9,12] N_4O_2[13,14] and N_3O_3[15] among others, there exists an inherent challenge in designing SCO materials as no defined conditions exist.[10,11] Instead, many supramolecular research groups have employed a bottom-up approach, designing a ligand with a favourable coordination sphere, while studying the effect that small changes to the ligand field may have on the promotion of SCO behaviour.[5,10,11] Kannappan et. al. synthesised an Fe^{III} hexacoordinate N_4O_2-donor Schiff-base ligand. The ligand synthesis was achieved by reacting 1,2-bis(3-aminopropylamino)ethane with 2 equivalents of Salicylaldehyde, the complexation was achieved in a 1:1 metalation. The resulting complex was studied for magnetic properties and found to exist in the low spin state in the temperature region of 70K to 296K. This illustrates the challenges faced by supramolecular chemists in regards to designing SCO materials.

The addition of certain functional moieties such as electron withdrawing or electron donating groups can affect the SCO behaviour by introducing electron induction effects on the system resulting in strengthening or weakening of the ligand field and is a method that has been utilised previously.[5,16] In a recent study conducted by our team we continued the efforts of Kannappan et. al. by employing an electron donating functional moiety to the N_4O_2-donor Schiff-base ligand. This was achieved by reacting 1,2-bis(3-aminopropylamino)ethane and 2 equivalents of 4-(diethylamino)salicylaldehyde.

In the present contribution, we report an adapted synthetic route resulting in the synthesis of three new N_4O_2-donor Schiff-base metal complexes, the synthetic methods were adapted from our previously reported work.[1] We first synthesised a new ligand [H_2**L**], similar to our previously reported ligand[1] except, in this case, we have employed an electron withdrawing functional moiety (R-Br). Utilising a N_4O_2 deprotonated Schiff-base ligand, we report the synthesis, characterisation, structural properties of three new complexes [Fe**L**]BF_4 (**1**), [Co**L**]PF_6 (**2**) and [Mn**L**]PF_6 (**3**) (Scheme 1).

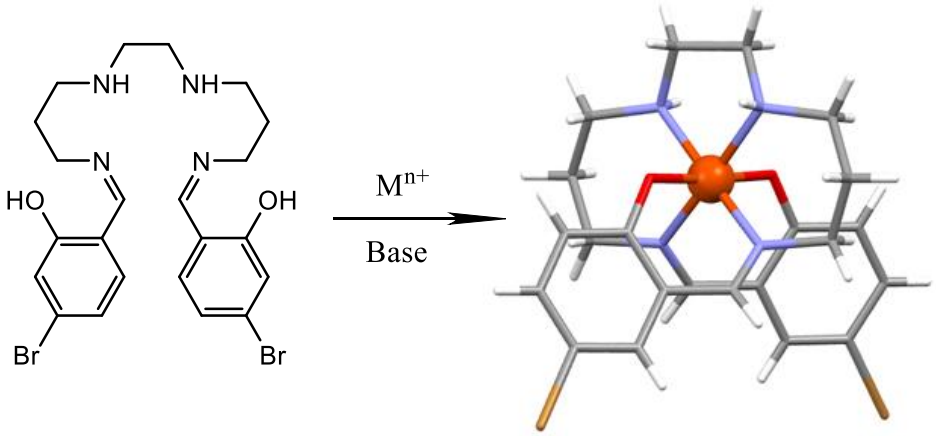

Scheme 1. Schematic representation of the synthesis of complexes **1**-**3**.

3.3 Experimental

3.3.1 Materials and Instrumentation

All chemicals and reagents were purchased from commercial sources and used without further purification. High-resolution electrospray ionisation–mass spectrometry (HR ESI-MS) data were acquired using a Waters Xevo QToF mass spectrometer, operating in positive ion mode. FT-IR measurements were undertaken on a Bruker Vertex 70 with a diamond ATR crystal. Raman Spectra were recorded using a Bruker Senterra spectrometer, all samples were subjected to an Ar excitation laser of 532 nm wavelength. Spectra were recorded over a 400-4000 cm^{-1} range. The solid-state UV-Vis spectra were measured in Nujol at ambient temperature using an Agilent Cary 100 UV-Vis with *WinUV* software. Spectra were collected from 900 to 200 nm with a scan rate of 600 nm per minute. Scanning electron microscopy–electron dispersive spectroscopy (SEM-EDS) analysis was conducted on a Phenom XL instrument. Samples were run at 15 kV in high vacuum without surface coating.

The synthesis of ligand [H_2**L**] was adapted from our previously reported methods on a similar N_4O_2 ligand.[1] The synthesis involved a Schiff-base condensation reaction performed using a di-primary amine and a brominated salicylaldehyde.

3.3.2 Synthesis of Metal Complexes **1**-**4**

*[Fe**L**]BF_4 (**1**)*

The formation of the complex was achieved via subcomponent self-assembly,[17,18] forming the ligand [H_2**L**] first via the use of simple building blocks and completing the complexation via the direct addition of the metal salt to the stirring solution. 5-Bromosalicylaldehyde (500 mg, 2.48 mmol) was dissolved in 10 mL of ethanol. To the solution, 1,2-bis(3-aminopropylamino)ethane (216 mg, 1.24 mmol) in 10 mL of ethanol was added dropwise. A few milligrams of *p*-toluenesulfonic acid were added. The reaction mixture was refluxed for 10 h under nitrogen. To a stirring solution of [H_2**L**] (672 mg, 1.24 mmol), iron(III) tetrafluoroborate hexahydrate (420 mg, 1.24mmol) in 10 mL of ethanol was added dropwise. Sodium hydroxide (100 mg, 2.48 mmol) in 5 mL of ethanol and a few drops of H_2O was added dropwise. The resulting dark green solution was heated for 4 hours. Upon hot filtration, a small amount of precipitate was obtained, the solvent from the remaining filtrate was slowly evaporated, yielding dark green X-Ray quality crystals. The crystals were allowed to dry in air (yield 53%). λ_{max} (Nujol)/nm 396, 610. ν_{max} (ATR)/cm^{-1} 3249, 2869, 1614, 1033. *m/z* (HRMS ESI^+, CH_3CN) 593.9741 [Fe$\mathbf{L}^{2-}$]$^+$. X-Ray quality crystals were used for single crystal X-Ray studies.

*[Co**L**]PF_6 (**2**)*

The formation of the complex was achieved via subcomponent self-assembly,[17,18] forming the ligand [H_2**L**] first via the use of simple building blocks and completing the complexation via the direct addition of the metal salt to the stirring solution. 5-Bromosalicylaldehyde (500 mg, 2.48 mmol) was dissolved in 10 mL of ethanol. To the solution, 1,2-bis(3-aminopropylamino)ethane (216 mg, 1.24 mmol) in 10 mL of ethanol was added dropwise. A few milligrams of *p*-toluenesulfonic acid were added. The reaction mixture was refluxed for 10 h under nitrogen. To a stirring solution of [H_2**L**] (672 mg, 1.24 mmol), cobalt(II) acetate tetrahydrate (311 mg, 1.24 mmol) in 10 mL ethanol was added dropwise, the resultant mixture turned a bright red/orange. A few drops of hydrogen peroxide (200 mg, 6.24 mmol) was also added dropwise to the complex mixture. The resulting dark brown solution was heated for 2 hours. The reaction mixture was hot filtered and an excess of ammonium hexafluorophosphate (649 mg, 3.97 mmol) in 10 mL of ethanol was added to the

filtrate. The resulting dark coloured solution was heated for 4 hours. Upon hot filtration, a small amount of precipitate was obtained, the solvent from the remaining filtrate was slowly evaporated, dark green crystals were obtained. The resultant crystals were allowed to dry in air (yield 54%). λ_{max} (Nujol)/nm 405, 640. ν_{max} (ATR)/cm^{-1} 3244, 2920, 1625, 819. *m/z* (HRMS ESI^+, CH_3CN) 596.9664 $[Co\mathbf{L}^{2-}]^+$. X-Ray quality crystals were utilised from X-Ray studies.

*[Mn**L**]PF_6 (**3**)*

The formation of the complex was achieved via subcomponent self-assembly,[17,18] forming the ligand [H_2**L**] first via the use of simple building blocks and completing the complexation via the direct addition of the metal salt to the stirring solution. 5-Bromosalicylaldehyde (500 mg, 2.48 mmol) was dissolved in 10 mL of ethanol. To the solution, 1,2-bis(3-aminopropylamino)ethane (216 mg, 1.24 mmol) in 10 mL of ethanol was added dropwise. A few milligrams of *p*-toluenesulfonic acid were added. The reaction mixture was refluxed for 10 h under nitrogen. To a stirring solution of [H_2**L**] (672 mg, 1.24 mmol), manganese (III) acetate dehydrate (333 mg, 1.24 mmol) in 10 mL of ethanol was added dropwise, the resultant mixture was dark red. The reaction mixture was heated for 2 hours, it was then hot filtered and an excess of ammonium hexafluorophosphate (649 mg, 3.97 mmol) in 10 mL of ethanol was added to the filtrate. The resulting dark coloured solution was heated for 4 hours. Upon hot filtration, a small amount of precipitate was obtained, the solvent from the remaining filtrate was slowly evaporated, yielding dark coloured brown/green crystals. The resultant crystals were allowed to dry in air (yield 58%). λ_{max} (Nujol)/nm 375, 550. ν_{max} (ATR)/cm^{-1} 3290, 2867, 1614, 819. *m/z* (HRMS ESI^+, CH_3CN) 592.9810 $[Mn\mathbf{L}^{2-}]^+$. X-Ray quality crystals were utilised from X-Ray studies.

3.3.3 Single Crystal X-Ray Diffraction

The single crystal X-ray data obtained for complexes [Fe**L**]BF_4 (**1**), [Co**L**]PF_6 (**2**) and [Mn**L**]PF_6 (**3**) were collected using the MX1 beamline at the Australian Synchrotron with Silicon Double Crystal monochromated radiation at 100(2) K.[19,20] Data integration and reduction were undertaken with XDS.[21] An empirical absorption correction was then applied using SADABS at the Australian Synchrotron.[22] The structures were solved by direct methods

and the full-matrix least-squares refinements were carried out using a suite of SHELX program[23,24] via the Olex2 interface.[25] All non-hydrogen atoms were located from the electron density maps and refined anisotropically. Hydrogen atoms bound to carbon atoms were added in the ideal positions and refined using a riding model.

3.4 Results and Discussion

3.4.1 Structure Description of Complexes **1**-**3**

The crystal data & refinement details are shown in Table 1, selected bond angles and bond lengths are shown in Table S1. The molecular structure of complex **1** [Fe**L**]BF_4 is shown in Figure 1. All atomic numbering for non-carbon and non-hydrogen atoms is shown in Figure S1. Complex **1** crystallises in a triclinic space group P-1, the lattice of complex **1** is made up of cations of $[Fe\mathbf{L}]^+$ and uncoordinated tetrafluoroborate anions and ethanol solvent molecules. The hexadentate Fe^{III} metal centre of complex **1** is encompassed by the N_4O_2 donor atoms of the deprotonated Schiff-base ligand $\mathbf{L}^{2-}$. This coordination sphere is defined by two imine nitrogens, two secondary amine nitrogens and two phenolate oxygens. Figure 1 demonstrates how the deprotonated hexadentate $\mathbf{L}^{2-}$ ligand envelops the Fe^{III}, the phenolate oxygens are *trans* to each other, demonstrated by the angle formed from $O_{Phenolic}$-Fe^{III}-$O_{Phenolic}$ = 176.63(13)°. Similarly, the angle formed by the axial nitrogens N_{amine}-Fe^{III}-N_{imine} = 174.30(2)° demonstrating a slightly distorted octahedral geometry. The two Fe^{III}-$O_{phenolic}$ bond distances are 1.892(4) and 1.888(4) Å, the two Fe^{III}-N_{amine} bond distances are 2.018(5) and 2.004(5) Å and the two Fe^{III}-N_{imine} bond distance is 1.967(5) and 1.965(5) Å. The bond distances of Fe^{III}-N_{imine} are shorter than that of Fe^{III}-N_{amine} and are consistent with similar reported Fe^{III} complexes that exhibit a low-spin state, this is suggestive that complex **1** is in a low-spin electron configuration at 100 K.[1,4]

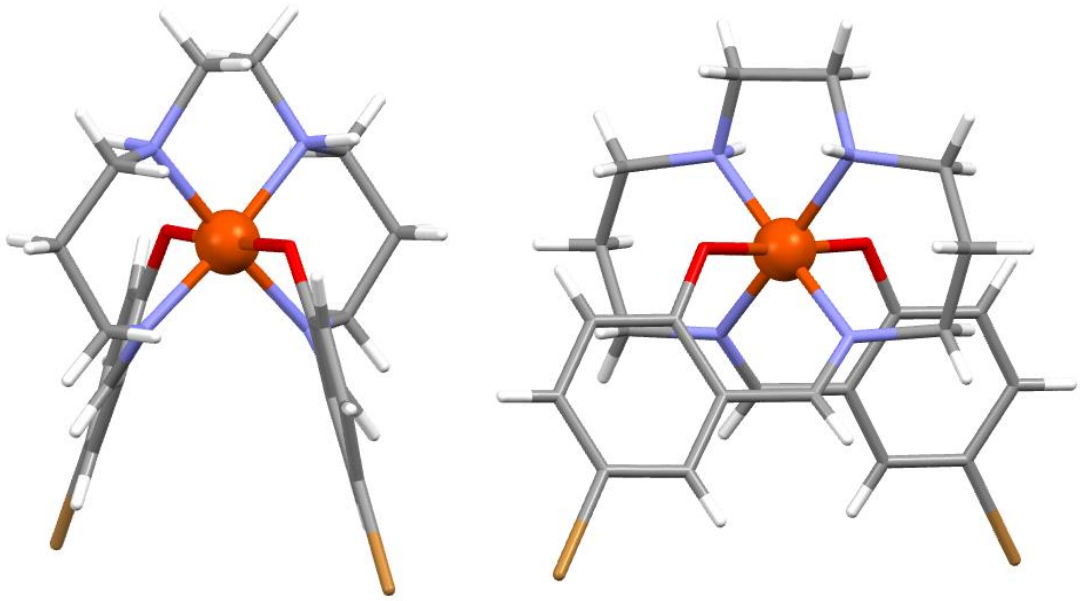

a) b)

Figure 1. Molecular representation of X-ray crystal structure of [Fe**L**]BF_4 (**1**) the anion BF_4^- and ethanol solvent molecule have been excluded for clarity. a) and b) illustrate the structure rotated about the y-axis for clarity. White indicates hydrogen, grey – carbon, red – oxygen, light blue – nitrogen, brown/yellow – bromine and orange – iron.

The molecular structure of complex [Co**L**]PF_6 (**2**) is shown in Figure 2. All atomic numbering for non-carbon and non-hydrogen atoms are illustrated in Figure S2. Complex **2** crystallises in an orthorhombic Pbcn space group, the asymmetric unit consists of one-half of the complex [Co**L**]PF_6. The lattice of complex **2** is made up of $[Co\mathbf{L}]^+$ cations and uncoordinated hexafluorophosphate anions and disordered ethanol molecules. The hexadentate Co^{III} metal centre is encompassed by the N_4O_2 donor atoms of the deprotonated Schiff-base ligand $\mathbf{L}^{2-}$. This coordination sphere is defined by two imine nitrogens, two secondary amine nitrogens and two phenolate oxygens. The *trans* configuration relative to the two phenolate oxygens $O_{phenolic}$-Co^{III}-$O_{phenolic}{}^1$ = 172.00(3)°, demonstrates how the flexible deprotonated Schiff-base ligand $\mathbf{L}^{2-}$ wraps around the Co^{III} metal centre encompassing it. The angle formed between the two axial nitrogens N_{imine}-Co^{III}-$N_{amine}{}^1$ = 175.94(2)° demonstrates a slightly distorted octahedral geometry. The Co^{III}-$O_{phenolic}$ bond distance is 1.889(4) Å, the Co^{III}-N_{amine} bond distance is 1.932(5) Å and the Co^{III}-N_{imine} bond distance is 1.932(5) Å. The bond distances and angles are consistent with those of previously published results on a similar Co^{III} N_4O_2 Schiff-base complex.[1,26]

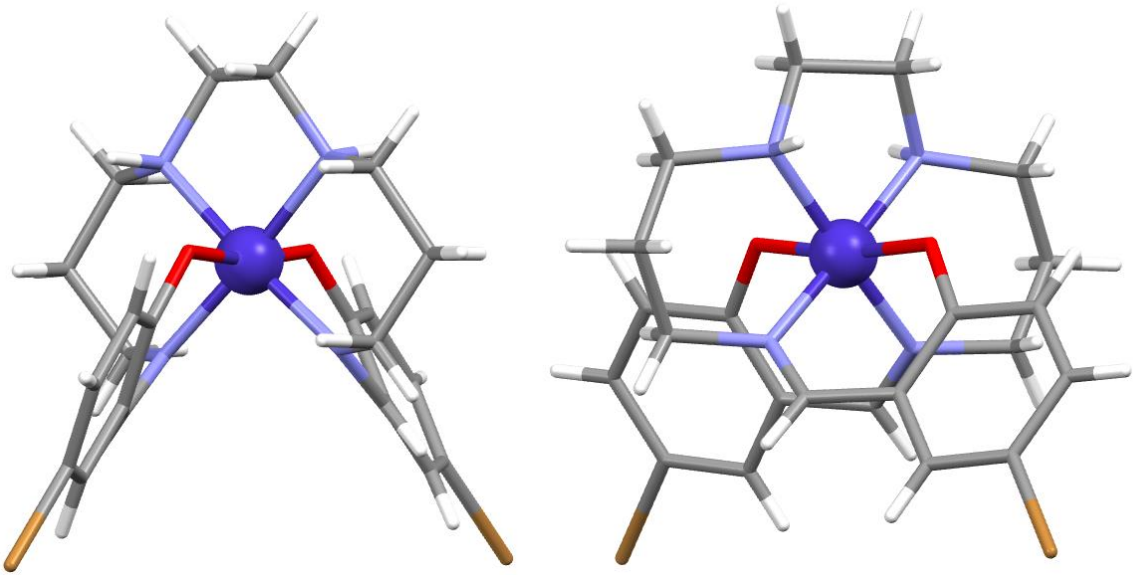

a) b)

Figure 2. Molecular representation of X-ray crystal structure of [Co**L**]PF_6 (**2**) the anion PF_6^- and solvent molecules have been excluded for clarity. a) and b) illustrate the structure rotated about the y-axis for clarity. White indicates hydrogen, grey – carbon, red – oxygen, light blue – nitrogen, brown/yellow – bromine and dark blue – cobalt.

The molecular structure of complex [Mn**L**]PF_6 (**3**) is shown in Figure 3. All atomic numbering for non-carbon and non-hydrogen atoms are illustrated in Figure S3. Complex **3** crystallises in an orthorhombic Pbcn space group, the asymmetric unit consists of one-half of the complex [Co**L**]PF_6. The lattice of the complex is made up of cations of $[Mn\mathbf{L}]^+$ and uncoordinated distorted hexafluorophosphate $(PF_6)^-$ anions. The N_4O_2 donor atoms of the deprotonated Schiff-base ligand $\mathbf{L}^{2-}$ encompasses the hexadentate Mn^{III} metal centre. This coordination environment is characterised by two imine nitrogens, two secondary amine nitrogens and two phenolate oxygens. Figure 3 demonstrates how the deprotonated hexadentate $\mathbf{L}^{2-}$ ligand encompasses the Mn^{III} metal centre, the phenolate oxygens are *trans* to each other, demonstrated by the angle formed from $O_{phenolic}$-Mn^{III}-$O_{phenolic}{}^1$ = 178.40(3)°. The angle formed between the two axial nitrogens N_{imine}-Mn^{III}-$N_{amine}{}^1$ = 170.70(3)° demonstrates a distorted octahedral geometry. The Mn^{III}-$O_{phenolic}$ bond distances are 1.878(5) Å, the Mn^{III}-N_{amine} bond distances are 2.081(6) Å and the Mn^{III}-N_{imine} bond distance is 2.016(7) Å.

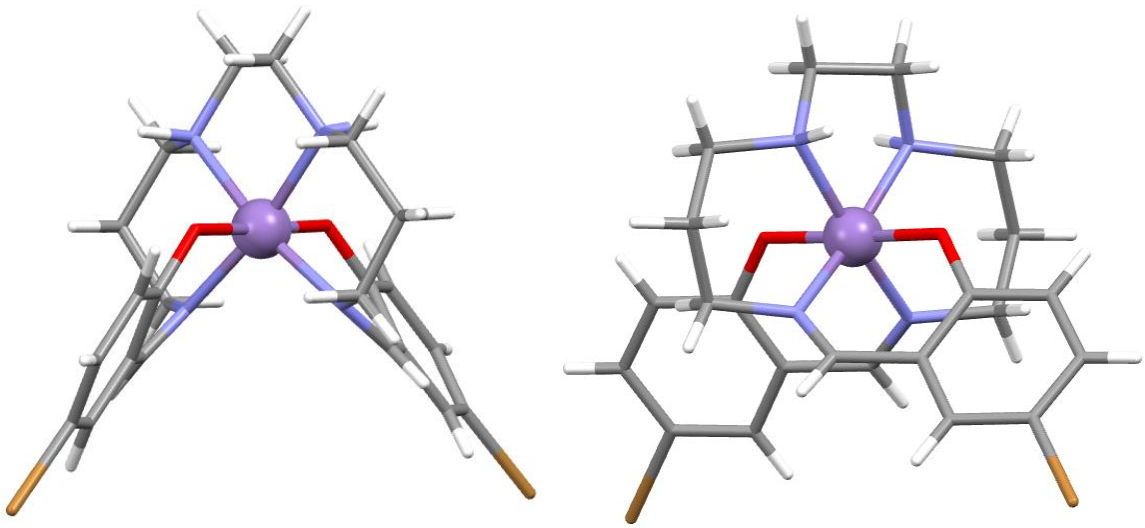

a) **b)**

Figure 3. Molecular representation of X-ray crystal structure of [Mn**L**]PF_6 (**3**) the anion PF_6^- has been excluded for clarity. a) and b) illustrate the structure rotated about the y-axis for clarity. White indicates hydrogen, grey – carbon, red – oxygen, light blue – nitrogen, brown/yellow – bromine and purple – manganese.

Table 1. Crystallographic data and refinement details for complexes **1**-**3**.

	1	**2**	**3**
Empirical formula	$[(C_{22}H_{26}FeN_4O_2Br_2)BF_4]\cdot C_2H_4OH$	$[(C_{24}H_{26}CoN_4O_2Br2)PF6]\cdot C_2H_4OH$	$[(C_{22}H_{26}MnN_4O_2Br_2)]PF6$
Formula weight	727.01	788.25	738.20
Temperature/K	100	100	100
Crystal system	triclinic	orthorhombic	orthorhombic
Space group	P-1	Pbcn	Pbcn
a/Å	8.4000(17)	8.3720(17)	13.205(3)
b/Å	9.6900(19)	27.664(6)	26.477(5)
c/Å	17.570(4)	13.458(3)	8.7550(18)
α/°	84.86(3)	90	90
β/°	81.27(3)	90	90
γ/°	81.42(3)	90	90
Volume/$Å^3$	1394.5(5)	3116.9(11)	3061.0(11)
Z	2	4	4
$\rho_{calc}g/cm^3$	1.731	1.680	1.602
μ/mm^{-1}	3.467	3.234	3.156
F(000)	730.0	1576.0	1464.0
Radiation	MoKα (λ = 0.71073)	MoKα (λ = 0.71073)	MoKα (λ = 0.71073)
2Θ range for data collection/°	2.35 to 52.744	4.222 to 60.99	3.076 to 52.744
Index ranges	-10 ≤ h ≤ 10, -12 ≤ k ≤ 12, -21 ≤ l ≤ 21	-11 ≤ h ≤ 11, -39 ≤ k ≤ 39, -18 ≤ l ≤ 18	-15 ≤ h ≤ 15, -32 ≤ k ≤ 32, -9 ≤ l ≤ 9
Reflections collected	33760	53278	34657
Independent reflections	5377 [R_{int} = 0.0655, R_{sigma} = 0.0431]	4585 [R_{int} = 0.0749, R_{sigma} = 0.0292]	2920 [R_{int} = 0.0581, R_{sigma} = 0.0246]
Data/restraints/parameters	5377/0/354	4585/178/203	2920/36/200
Goodness-of-fit on F^2	1.162	1.237	1.073

Final R indexes [I>=2σ (I)]	R_1 = 0.0531, wR_2 = 0.1434	R_1 = 0.0913, wR_2 = 0.2213	R_1 = 0.0938, wR_2 = 0.2805
Final R indexes [all data]	R_1 = 0.0629, wR_2 = 0.1471	R_1 = 0.0946, wR_2 = 0.2225	R_1 = 0.1188, wR_2 = 0.3079
Largest diff. peak/hole / e $Å^{-3}$	1.34/-1.21	2.90/-1.94	1.41/-1.99

3.4.2 SEM-EDS

Scanning electron microscopy (SEM) micrographs (Figures S4-6) indicated that complexes **1**-**3** all exist as large single crystals, complexes **1** and **3** are thin needle crystals. The needle crystals of complex **1** undergo rapid decay due to loss of solvent, there is evident cracking along the edges. Additionally, energy dispersive spectroscopy (EDS) confirmed the presence of C, N, O, F, B, Br and Fe in complex **1** [Fe**L**]BF_4 (Figure S4), C, N, O, F, P, Br and Co in complex **2** [Co**L**]PF_6 (Figure S5) and C, N, O, F, P, Br and Mn in complex **3** [Mn**L**]PF_6 (Figure S6).

3.4.3 IR Spectroscopy

FT-IR spectra for complexes [Fe**L**]BF_4 (**1**), [Co**L**]PF_6 (**2**) and [Mn**L**]PF_6 (**3**) were all recorded at room temperature and are shown in Figures S7-9, respectively. The FT-IR spectra exhibit absorptions in the region 1625-1600 cm^{-1}, these are attributable to imine (C=N) stretching modes. Evidenced in the region 3300-2900 cm^{-1} are absorptions typical of C-H alkyl and N-H secondary alkyl stretches, this is attributed to the secondary amine in all complexes.

3.4.4 Raman Spectroscopy

Raman spectra for complexes **1**-**3** are presented Figures S10-12, respectively. With respect to all complexes **1**-**3** shown in Figures S10-12, the Raman spectra shows absorptions in the region 1620-1600 cm^{-1} typical of an imine (C=N) stretching mode. Absorptions in the region 1460-1440 cm^{-1} are typical for an aromatic ring stretch and are attributable to the aromatic rings present in complexes **1**-**3**. Lastly, Raman spectra for complexes **1**-**3** also exhibit

alky C-H and secondary N-H stretching modes in the region 3200-2700 cm^{-1}, this is attributed to the secondary amine in all complexes.

3.4.5 UV-Vis Spectroscopy

The solid-state UV-Vis spectra of complexes [Fe**L**]BF_4 (**1**), [Co**L**]PF_6 (**2**) and [Mn**L**]PF_6 (**3**) are shown in Figure S13. The electronic spectrum of complex [Fe**L**]BF_4 (**1**) exhibits a low-energy charge transfer band at 610 nm and also exhibits a higher band at 396 nm. Similar to our previous studies this low and high energy bands can be attributed to the low spin and high spin energy state of the Fe^{III}, respectively.[1] Complex [Co**L**]PF_6 (**2**) exhibits a broad band centred at 640nm and another band centred at 405 nm similar to our previously reported N_4O_2 Schiff-base Co^{III} complex.[1] Complex [Mn**L**]PF_6 (**3**) exhibits a broad band centred at 550 nm and a strong band centred at 375 nm. The bands observed in the region 550-640 nm in complexes **1**-**3** can be attributed to the d-d transitions associated with the octahedral coordination environment around the respective metal centres, while the absorptions in the region 375-405 nm can be attributed to ligand-to-metal charge transfer (LMCT).[1,27,28]

3.4.6 HR ESI Mass Spectrometry

High-resolution electrospray ionisation-mass spectrometry (HR ESI-MS) provided indication that singly charged complex species of [Fe$\mathbf{L}^{2-}$]$^+$, [Co$\mathbf{L}^{2-}$]$^+$ and [Mn$\mathbf{L}^{2-}$]$^+$ (**1**-**3**) all persist in solution (Figures S14-16). The experimentally calculated isotopic distribution patterns for all three complexes (**1**-**3**) are in excellent agreement with the theoretically generated patterns (inserts Figures S14-16). With respect to all complexes (**1**-**3**) [Fe**L**]BF_4, [Co**L**]PF_6 and [Mn**L**]PF_6 were observed to be in a 2:1 stoichiometric ratio of L:M (Ligand-to-Metal) with major peaks observed at m/z [Fe$\mathbf{L}^{2-}$]$^+$ = 593.9684 (calc. 593.9741), [Co$\mathbf{L}^{2-}$]$^+$ = 596.9664 (calc. 596.9755) and [Mn$\mathbf{L}^{2-}$]$^+$ = 592.9810 (calc. 593.9803), respectively.

3.5 Conclusion

We describe the synthesis, characterisation and structural investigations on three new N_4O_2-donor Schiff-base metal complexes. All complexes have been investigated by scanning electron microscopy-electron dispersive spectroscopy (SEM-EDS), FT-IR, Raman spectroscopy, solid state UV-Vis, high-resolution electrospray ionisation-mass spectrometry (HR ESI-MS) and single crystal X-ray diffraction. Further studies are underway to investigate the magnetic properties of these new complexes.

3.6 Acknowledgements

The research described herein was supported by Western Sydney University (WSU). The author acknowledges the AMCF and Mass Spectrometry facilities at Western Sydney University. The crystallographic data presented was collected on the MX1 beamline at the Australian Synchrotron, Victoria, Australia. K. J. H.-S. and A. R. C. acknowledge the Western Sydney University Masters of Research scholarship program. A. R. C. also acknowledges the AINSE honours scholarship program.

3.7 References

1. K. J. Howard-Smith, A. R. Craze, M. Badbhade, C. E. Marjo, T. D. Murphy, P. Castignolles, R. Wuhrer and F. Li, *Aust. J. Chem.,* **2017**, 70, 581.
2. D. J. Fanna, Y. Zhang, L. Li, I. Karatchevtseva, N. D. Shepherd, A. Azim, J. R. Price, J. Aldrich-Wright, J. K. Reynolds and F. Li, *Inorg. Chem. Front.,* **2016**, *3*, 286.
3. D. J. Fanna, Y. Zhang, A. Salih, J. K. Reynolds and F. Li, *J. Coord. Chem.,* **2016**, *69*, 1883.
4. R. Kannappan, S. Tanase, I. Mutikainen, U. Turpeinen and J. Reedijk, *Polyhedron.,* **2006**, 7, 1646.
5. *Spin-Crossover Materials: Properties and Applications,* M. A. Halcrow., Ed.; Wiley, **2013**.
6. O. Khan, J. Krober and C. Jay, *Adv. Mater.,* **1992**, 4, 718.
7. O. Khan and C. Jay-Martinez, *Science*., **1998**, 279, 44.
8. L. Li, S. M. Neville, A. R. Craze, J. K. Clegg, N. F. Sciortino, K. S. Athukorola Arachchige, O. Mustonen, C. E. Marjo, C. R. McRae, C. J. Kepert, L. F. Lindoy, J. R. Aldrich-Wright and F. Li, *ACS Omega*., **2017**, 2, 3349.
9. *Spin Crossover in Transition Metal Compounds I, II and III;* P. Gütlich, H. A. Goodwin., Eds.; Springer, **2004**.
10. N. Bréfuel, I. Vang, S. Shova, F. Dahan, J. -P. Costes and J. -P. Tuchagues, *Polyhedron*., **2007**, 26, 1745.
11. N. Struch, C. Bannwarth, T. K. Ronson, Y. Lorenz, B. Mienert, N. Wagner, M. Engeser, E. Bill, R. Puttreddy, K. Rissanen, J. Beck, S. Grimme, J. R. Nitschke and A. Lützen, *Angew. Chem. Int. Ed.*, **2017**, 56, 4930.
12. P. Gütlich, Y. Garcia and H. A. Goodwin, *Chem. Soc. Rev.*, **2000**, 29, 419.
13. B. Weber, E. Kaps, J. Weigand, C. Cabonera, J. -F. Létard, K. Achterhold and F. G. Parak, *Inorg. Chem*., **2008**, 47, 487.
14. J. Klingele, D. Kaase, J. Hilgert, G. Steinfeld, M. H. Klingele and J. Lach, *Dalton Trans.*, **2010**, 39, 4495.
15. K. Dankhoff, C. Lochenie, F. Puchtler and B. Weber, *Eur. J. Inorg. Chem.*, **2016**, 2016, 2136.
16. J. G. Park, I. -R. Jeon and T. D. Harris, *Inorg. Chem.*, **2015**, 54, 359.
17. J. R. Nitschke, *Acc. Chem. Res.,* **2007**, 40, 103.
18. A. M. Castilla, W. J. Ramsay and J. R Nitschke, *Acc. Chem. Res.,* **2014**, 47, 2063.
19. T. M. McPhillips, S. E. McPhillips, H. J. Chiu, A. E. Cohen, A. M. Deacon, P. J. Ellis, E. Garman, A. Gonzalez, N. K. Sauter, R. P. Phizackerley, S. M. Soltis and P. Kuhn, BlueIce, *J. Synchrotron Rad.,* **2002**, *9*, 401.
20. N. P. Cowieson, D. Aragao, M. Clift, D. J. Ericsson, C. Gee, S. J. Harrop, N. Mudie, S. Panjikar, J. R. Price, A. Riboldi-Tunnicliffe, R. Williamson and T. Caradoc-Davies, *J. Synchrotron Rad.,* **2015**, *22*, 187.
21. W. Kabsch, *J. Appl. Cryst.*, **1993**, *26*, 795.
22. G. M. Sheldrick, SADABS: Empirical Absorption and Correction Software, University of Göttingen, Germany, **1996**.
23. G. M. Sheldrick, *Acta Cryst.,* **2008**, *A64*, 112.
24. G. M. Sheldrick, *Acta Cryst.,* **2015**, *A71*, 3.
25. O. V. Dolomanov, L. J. Bourhis, R. J. Gildea, J. A. K. Howard and H. Puschmann, *J. Appl. Cryst.,* **2009**, *42*, 339.
26. M. Dolai and M. Ali, *J. Chem. Sci. (Berlin, Ger.).,* **2014**, 126, 1647.
27. A. Vijayaraj, R. Prabu, N. Sivakumar, R. S. Kumari, V. Kaviyarsan and V. Narayanan, *Int. J. ChemTech. Res.,* **2017**, 10, 2455.
28. S. P. Kumar, R. Suresh, K. Giribabu, R. Manigandan, S. Munusamy, S. Muthamizh and V. Narayanan. *Spectrochim. Acta, Part A.,* **2015**, 139, 431.

3.8 Supplementary Materials

Table S1. Summary of bond angles and bond lengths of complexes **1**-**3**.

Bond lengths (Å)		**Bond angles (°)**	
1			
Fe03-O1	1.892(4)	O2- Fe03-O1	176.63(18)
Fe03-O2	1.888(4)	O2- Fe03-N1	92.4(2)
Fe03-N1	1.967(5)	O2- Fe03-N2	86.9(2)
Fe03-N2	2.018(5)	O2- Fe03-N3	90.4(2)
Fe03-N3	2.004(5)	O2- Fe03-N4	89.6(2)
Fe03-N4	1.965(5)	N1- Fe03-N2	91.2(2)
Bond angles (°)		N1- Fe03-N3	175.5(2)
O1- Fe03-N1	89.5(2)	N3- Fe03-N2	85.4(2)
O1- Fe03-N2	90.2(2)	N4- Fe03-N1	93.5(2)
O1- Fe03-N3	87.6(2)	N4- Fe03-N2	174.3(2)
O1- Fe03-N4	93.1(2)	N4- Fe03-N3	90.1(2)
2			
Co02-O004	1.889(4)	O004-Co02-N006^{1}	93.8(2)
Co02-O004^{1}	1.889(4)	O004-Co02-N007^{1}	85.97(19)
Co02-N006	1.932(5)	O004-Co02-N007	88.20(19)
Co02-N006^{1}	1.932(5)	O004^{1}-Co02-N007	85.97(19)
Co02-N007	1.987(5)	O004^{1}-Co02-N007^{1}	88.20(19)
Co02-N007^{1}	1.987(5)	N006^{1}-Co02-N006	93.7(3)
Bond angles (°)		N006^{1}-Co02-N007	176.0(2)
O004^{1}-Co02-O004	172.0(3)	N006^{1}-Co02-N007^{1}	89.8(2)
O004^{1}-Co02-N006	93.8(2)	N006-Co02-N007	89.8(2)
O004^{1}-Co02-N006^{1}	91.7(2)	N006-Co02-N007^{1}	176.0(2)
O004-Co02-N006	91.7(2)	N007^{1}-Co02-N007	86.9(3)
3			
Mn1-O004^{1}	1.878(5)	O004-Mn1-N1^{1}	87.0(2)
Mn1-O004	1.878(5)	O004-Mn1-N2	89.1(3)
Mn1-N1^{1}	2.081(6)	O004^{1}-Mn1-N2^{1}	89.1(3)
Mn1-N1	2.081(6)	O004-Mn1-N2^{1}	91.9(3)
Mn1-N2	2.016(7)	O004^{1}-Mn1-N2	91.9(3)
Mn1-N2^{1}	2.016(7)	N1^{1}-Mn1-N1	83.8(4)
Bond angles (°)		N2^{1}-Mn1-N1^{1}	87.9(3)
O004-Mn1-O004^{1}	178.4(3)	N2-Mn1-N1^{1}	170.7(3)
O004^{1}-Mn1-N1	87.0(2)	N2^{1}-Mn1-N1	170.7(3)
O004^{1}-Mn1-N1^{1}	91.8(2)	N2-Mn1-N1	87.9(3)
O004-Mn1-N1	91.8(2)	N2-Mn1-N2^{1}	100.6(4)

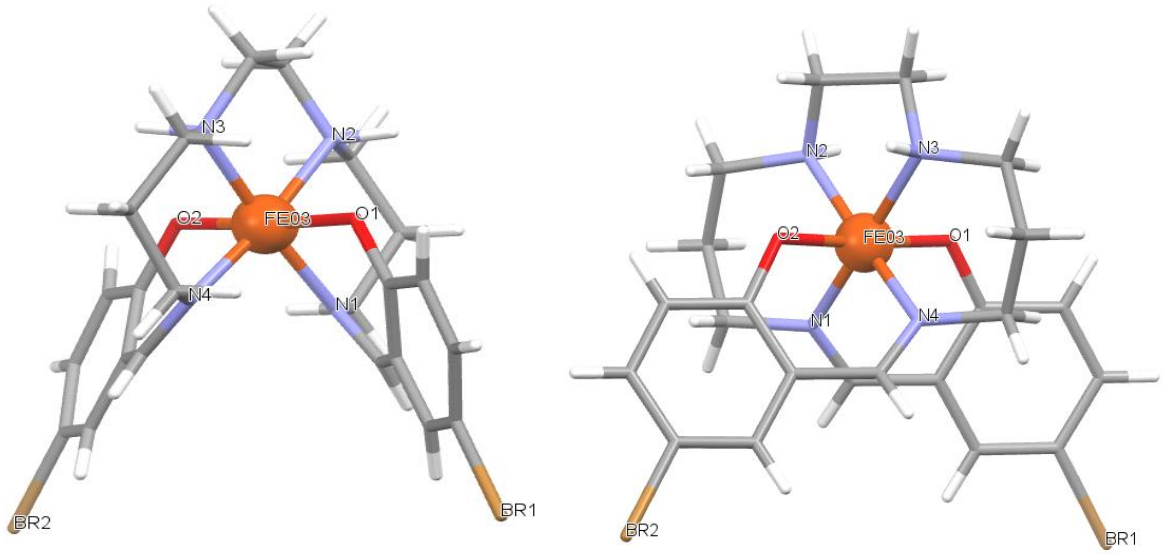

a) **b)**

Figure S1. Molecular representation of X-ray crystal structure of [Fe**L**]BF_4 (**1**) the anion BF_4^- and ethanol solvent molecule have been excluded for clarity. a) and b) illustrate the structure rotated about the y-axis for clarity.

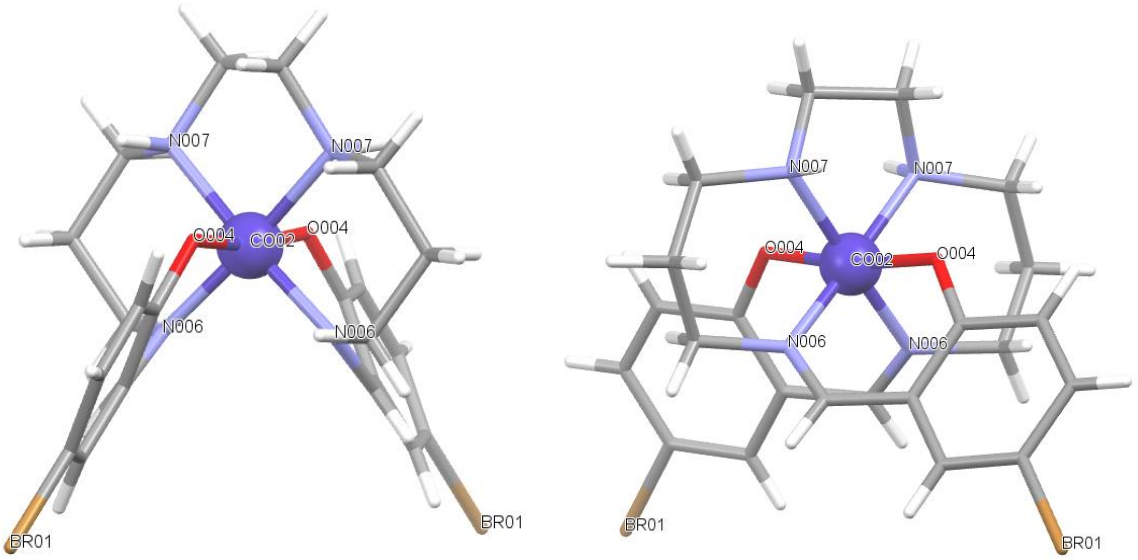

a) **b)**

Figure S2. Molecular representation of X-ray crystal structure of [Co**L**]PF_6 (**2**) the anion PF_6^- and solvent molecules have been excluded for clarity. a) and b) illustrate the structure rotated about the y-axis for clarity.

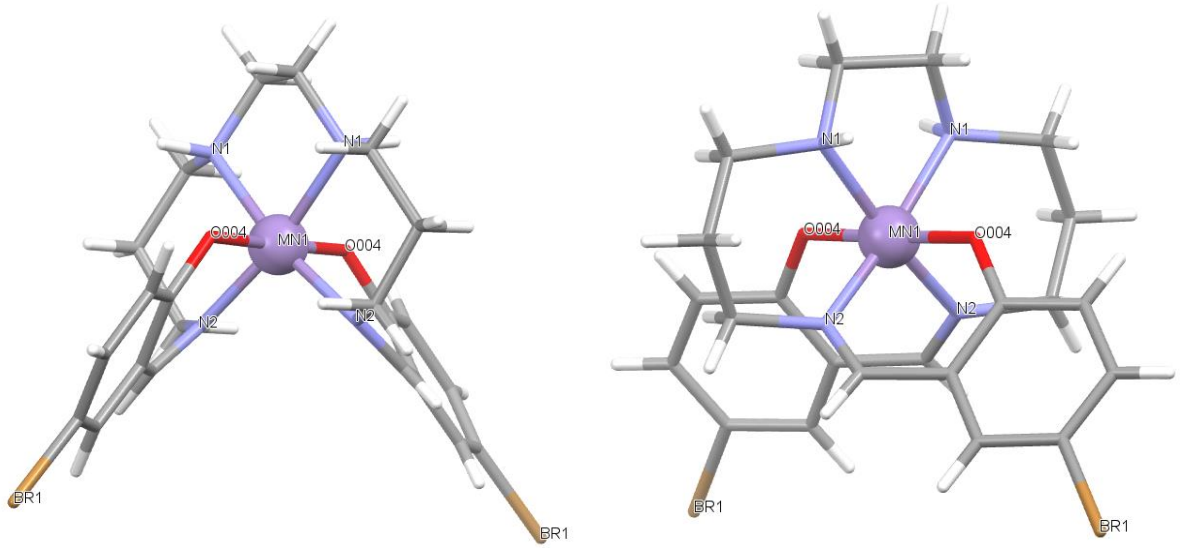

a) **b)**

Figure S3. Molecular representation of X-ray crystal structure of [Mn**L**]PF_6 (**3**) the anion PF_6^- has been excluded for clarity. a) and b) illustrate the structure rotated about the y-axis for clarity.

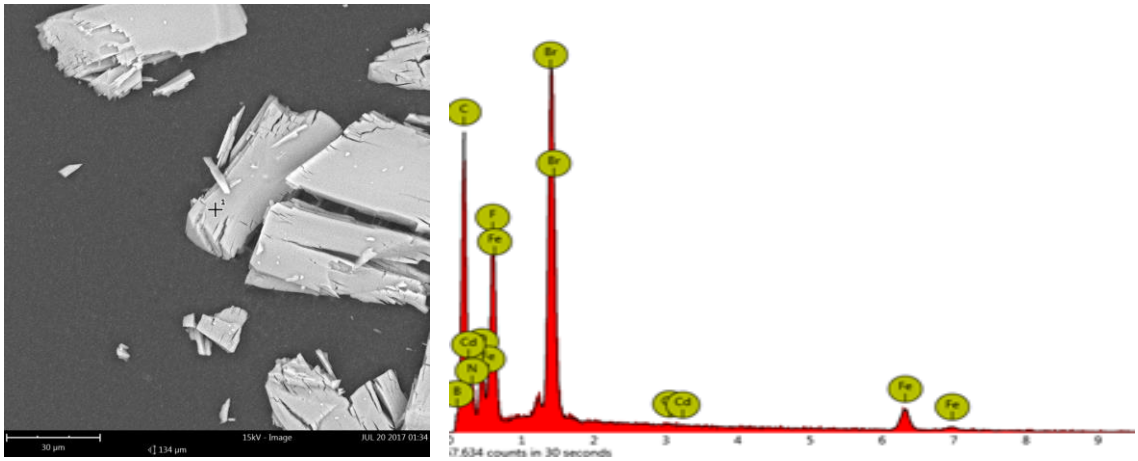

Figure S4. [Fe**L**]BF_4 x1000 magnification SEM micrograph of complex **1** (right) with an EDS spectrum (left).

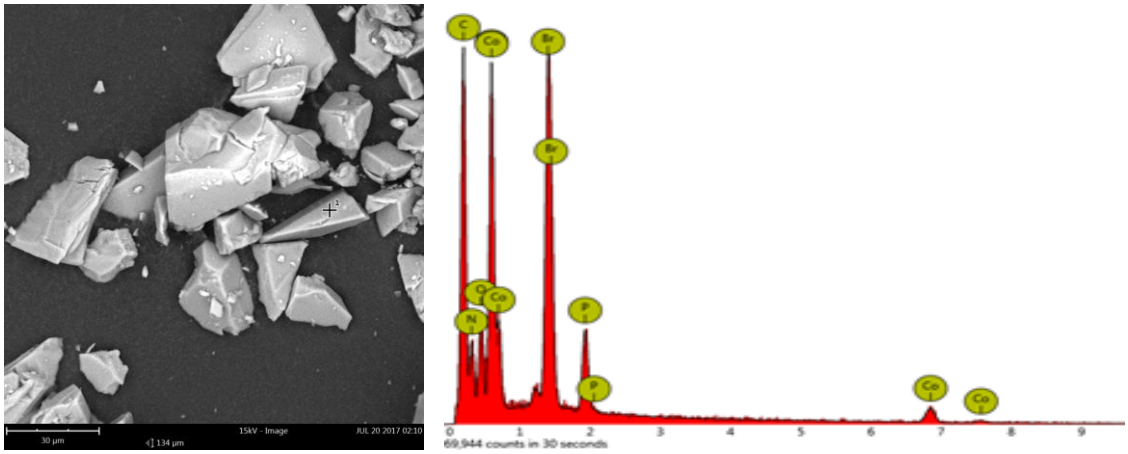

Figure S5. [Co**L**]PF_6 x2000 magnification SEM micrograph of complex **2** (right) with an EDS spectrum (left).

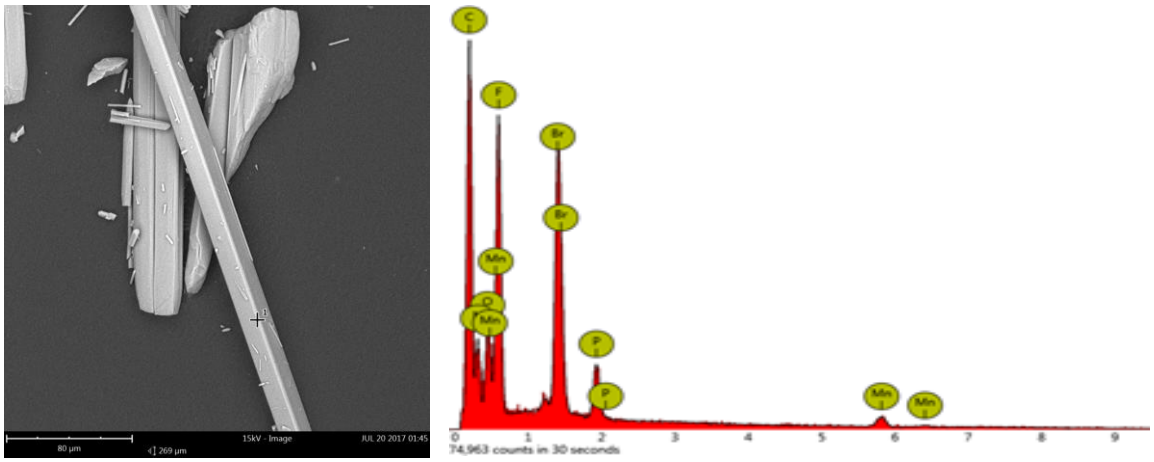

Figure S6. [Mn**L**]PF_6 - x1000 magnification SEM micrograph of complex **3** (right) with an EDS spectrum (left).

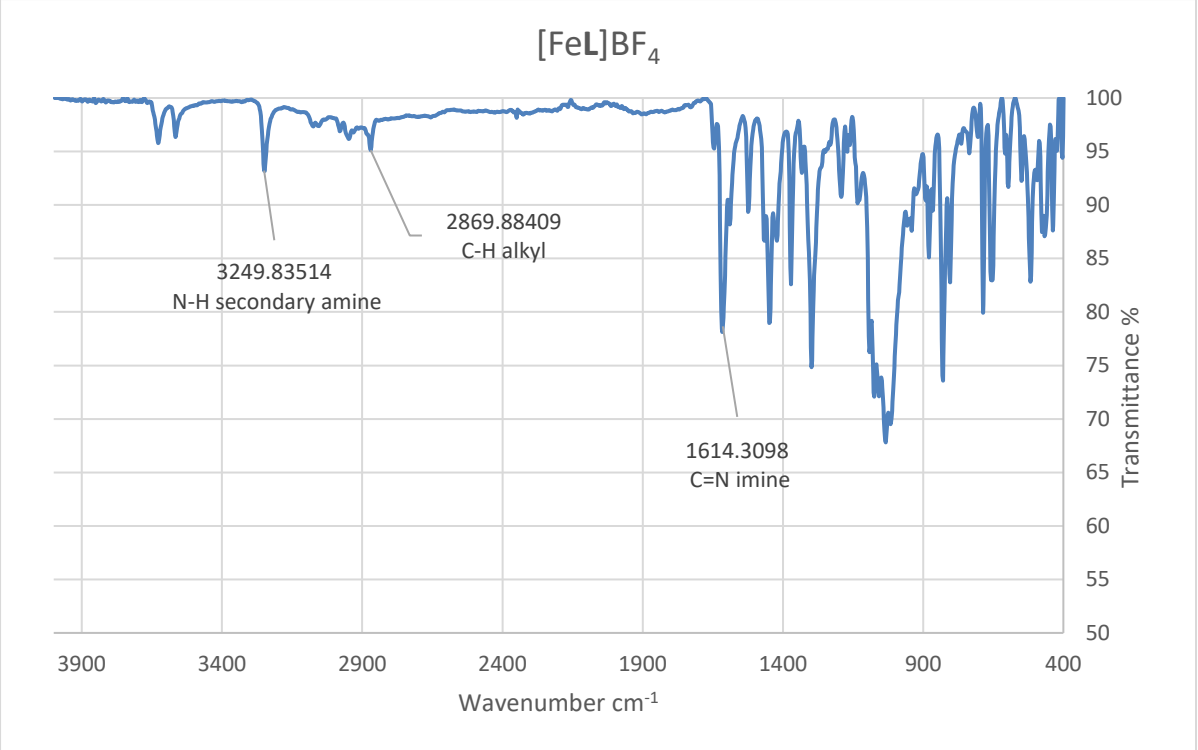

Figure S7. FT-IR spectrum of complex **1** [Fe**L**]BF_4.

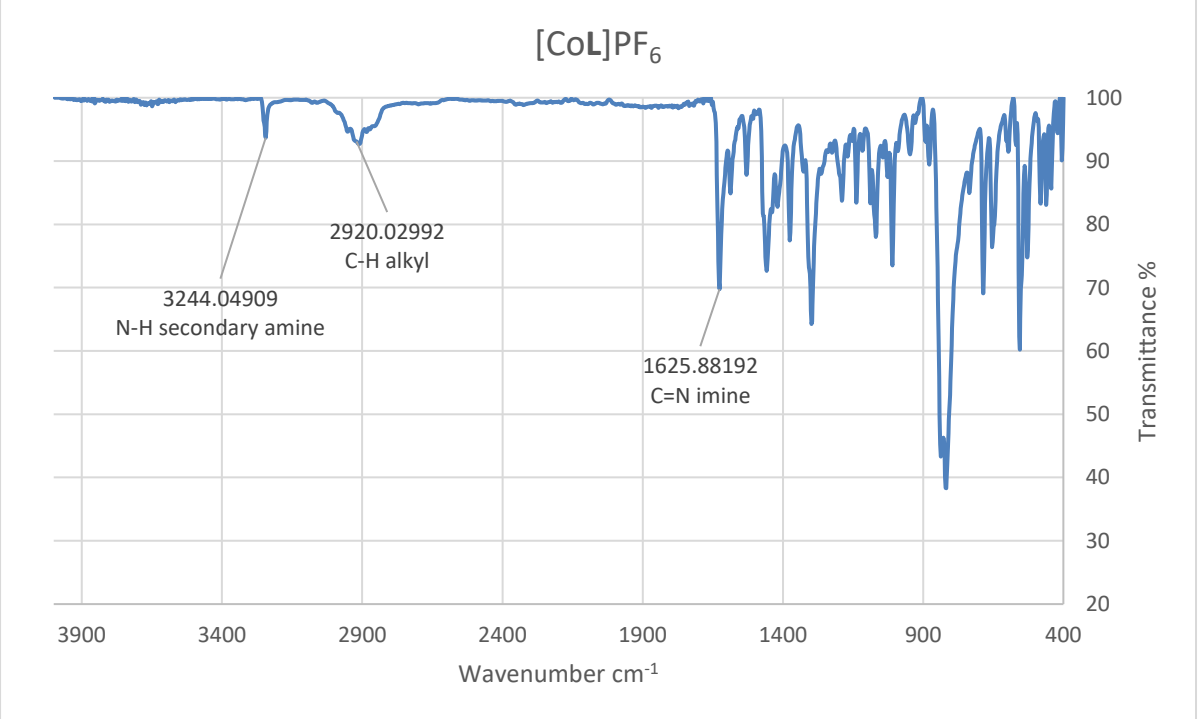

Figure S8. FT-IR spectrum of complex **2** [Co**L**]PF_6.

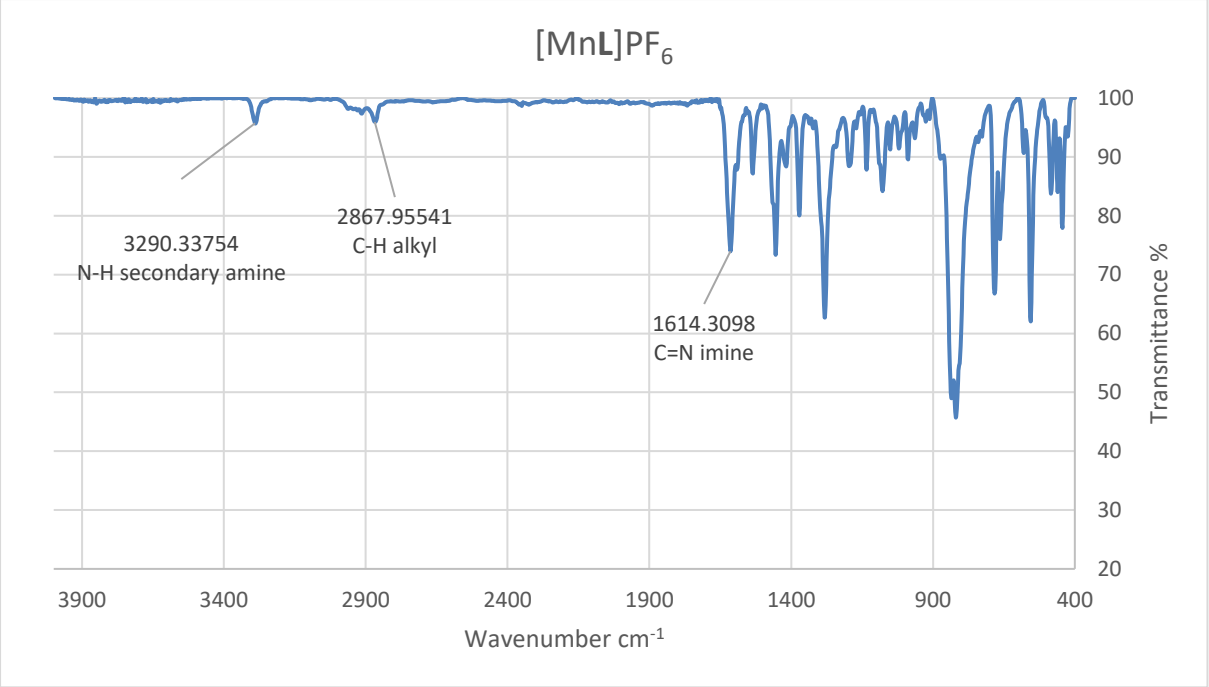

Figure S9.FT-IR spectrum of complex **3** [Mn**L**]PF_6.

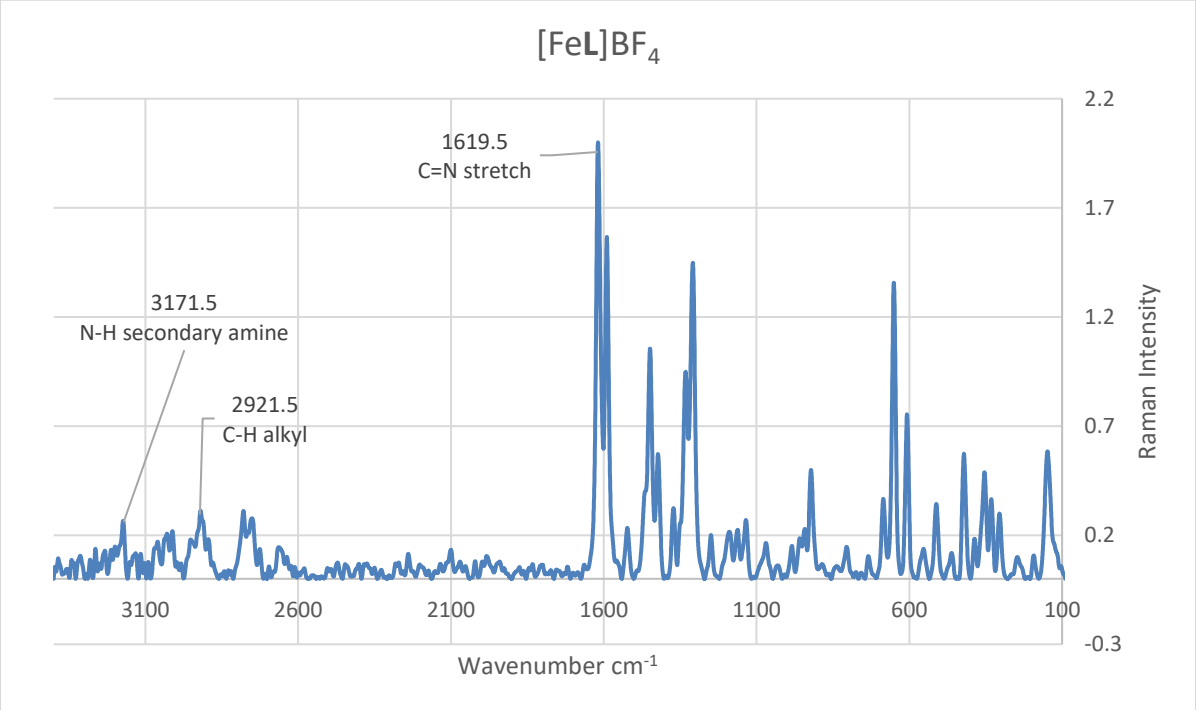

Figure S10. Raman spectrum of complex **1** [Fe**L**]BF_4.

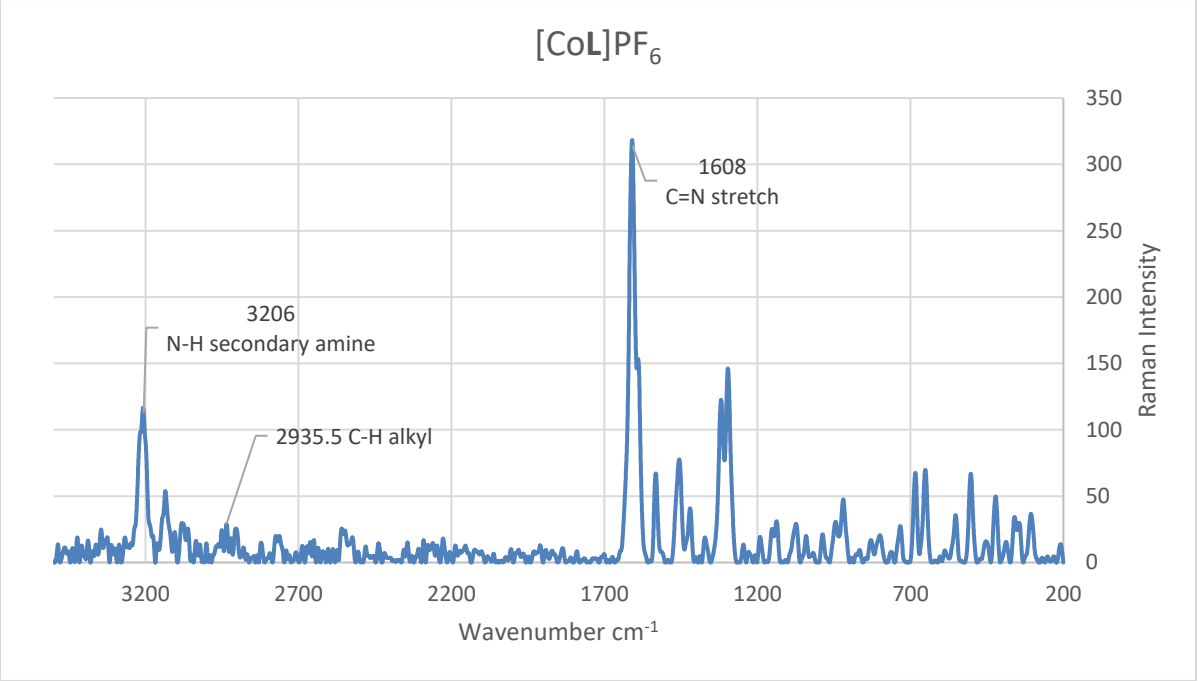

Figure S11. Raman spectrum of complex **2** [Co**L**]PF_6.

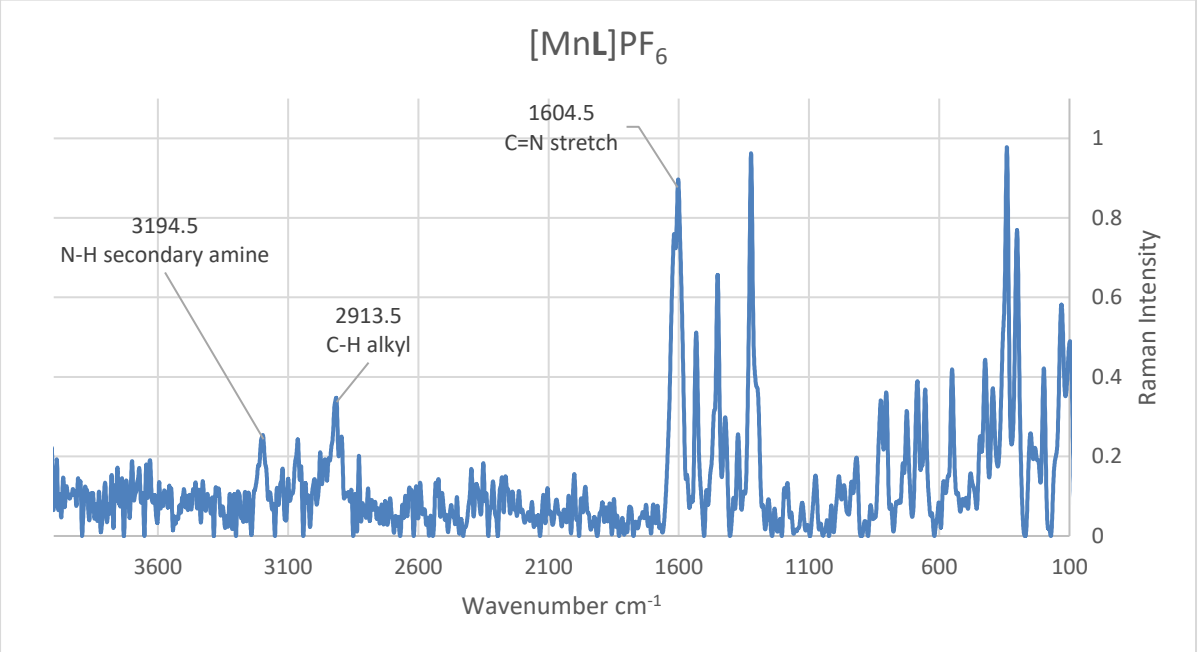

Figure S12. Raman spectrum of complex **3** [Mn**L**]PF_6.

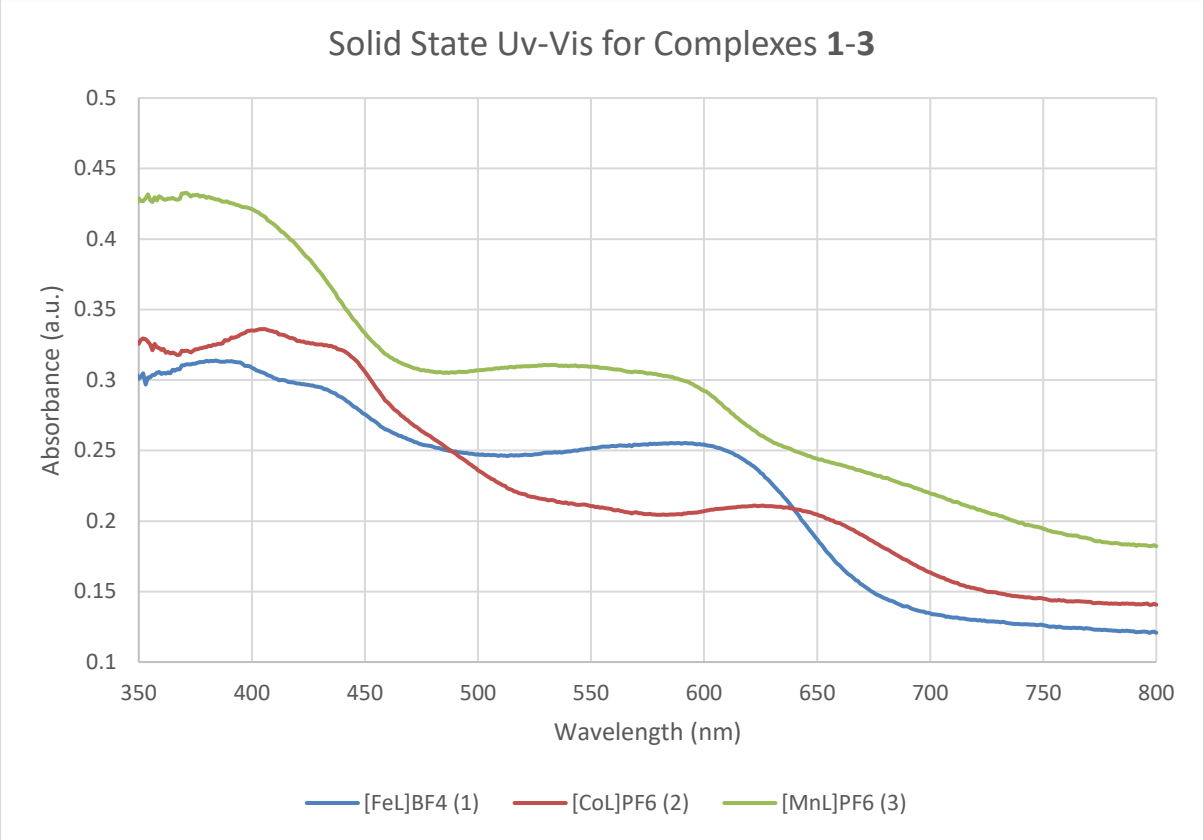

Figure S13. UV-Vis solid-state spectra of complexes **1**-**3**.

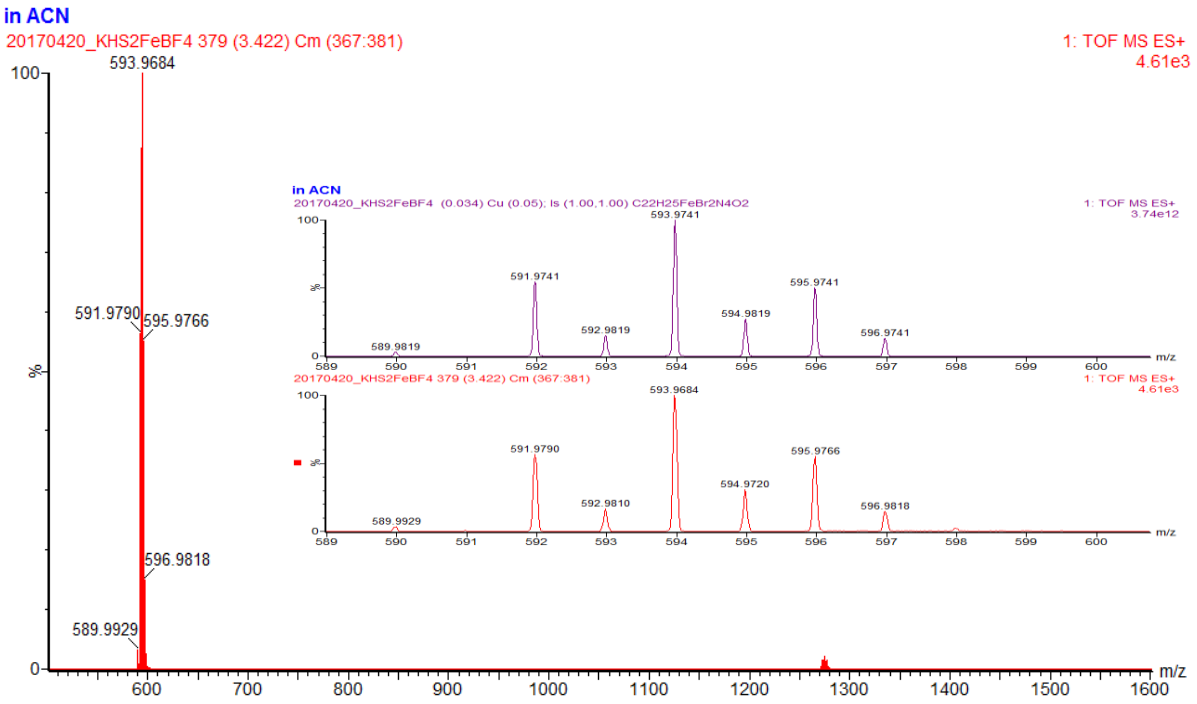

Figure S14. $[FeL]^+$ HR-ESI MS calculated m/z 593.9741 upper insert, experimental m/z 593.9684 lower insert.

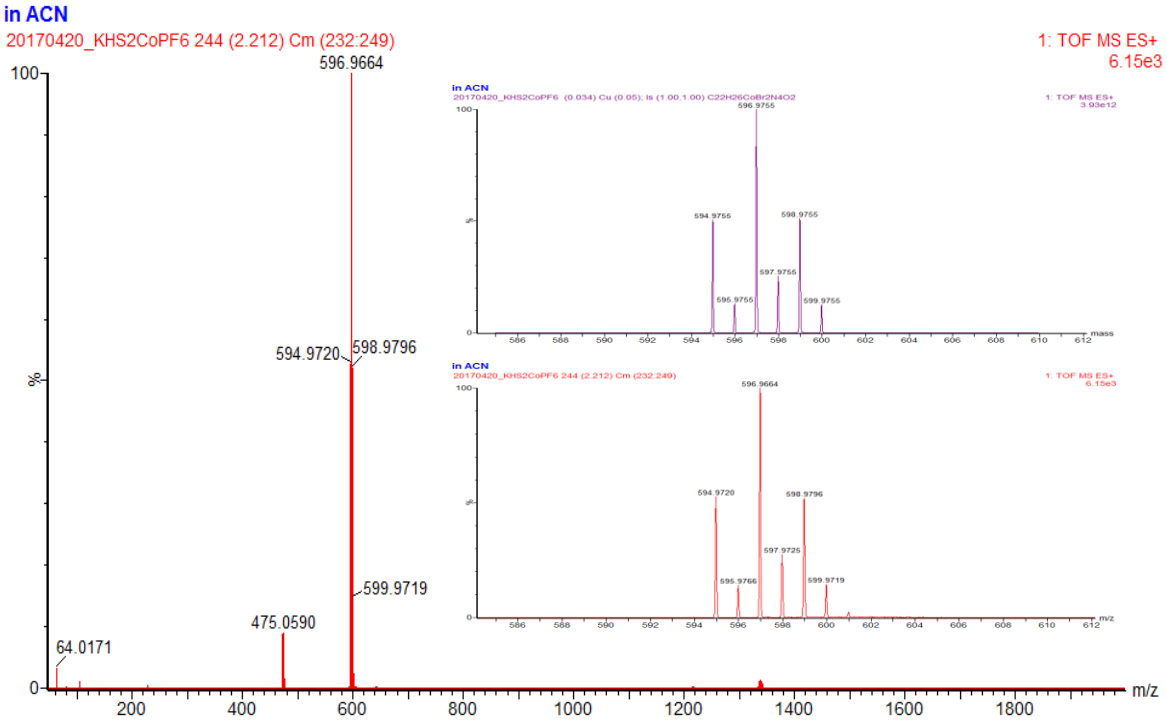

Figure S15. [Co**L**]$^{+}$ HR-ESI MS calculated m/z = 596.9755 upper insert, experimental m/z = 596.9664 lower insert.

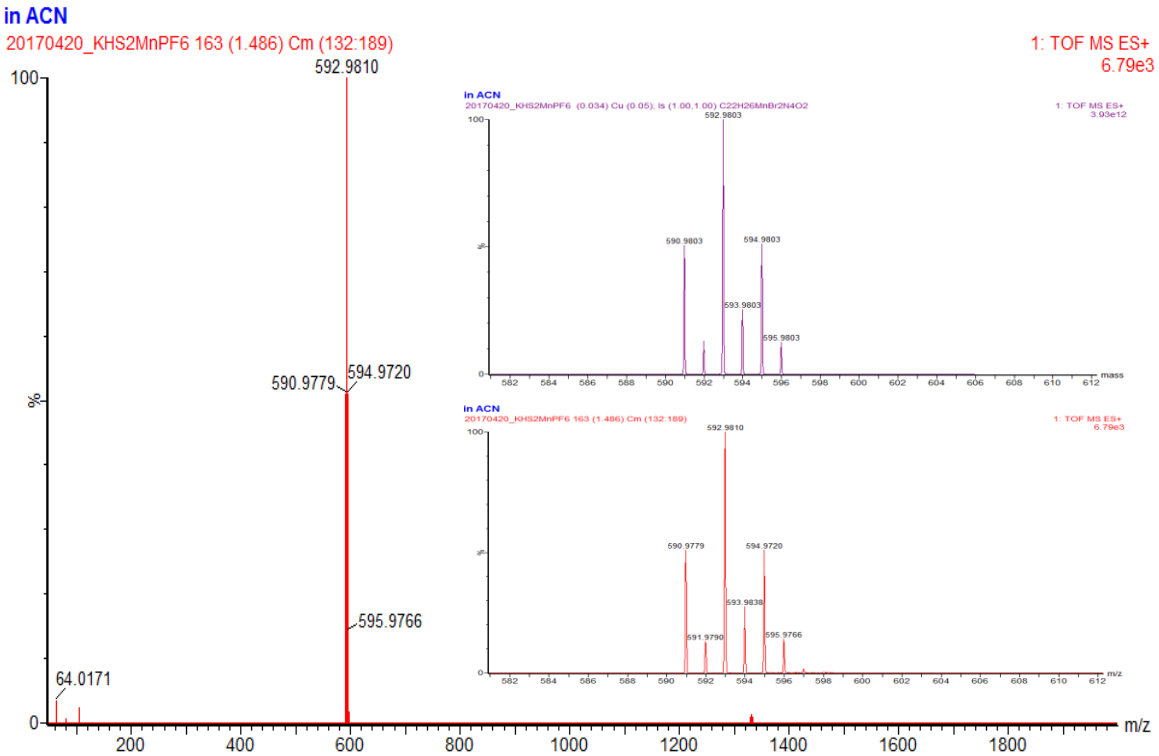

Figure S16. [Mn**L**]$^{+}$ HR-ESI MS calculated m/z = 592.9803 upper insert, experimental m/z = 592.9810 lower insert.

Chapter 4 – Synthesis and Spin Crossover Investigations of a New Mononuclear Thioimidazole Schiff-Base Fe^{II} Complex with a High Temperature Spin Transition.

AUTHORS: Kyle J. Howard-Smith[A#], Alexander R. Craze[A#], Ric Wuhrer[B], Mohan Badbhade[C], Cameron J. Kepert[D], Christopher E. Marjo[C] and Feng Li[A*]

[A]School of Science and Health, Western Sydney University, Locked Bag 1797, Penrith, NSW 2751, Australia.

[B]Advanced Materials Characterisation Facility, Western Sydney University, Locked Bag 1797, Penrith, NSW, 2751, Australia.

[C]Mark Wainwright Analytical Centre, University of New South Wales, NSW, 2052, Australia.

[D]School of Chemistry, University of Sydney, NSW, 2006, Australia.

# denotes equal contribution by both co-first authors

*This chapter is currently being prepared for manuscript submission and was written with the co-first author and has been presented as is with slight alterations.

4.1 Abstract

The exploration of new room-temperature and above spin-crossover (SCO) compounds plays a vital part in understanding the mechanism of spin-transitions and important factors in their informed design. This study presents the new mononuclear complex (**1**), of the form [Fe**L**]$(BF_4)_2$, incorporating the 4-thioimidazole donor moiety, which was found to exhibit a high temperature spin-transition ($T_{1/2}$ of 375 ↓ and 370 ↑at 4 $Kmin^{-1}$) and thermal hysteresis (5 K). The effect of scan rate was investigated, with magnetic susceptibility being measured at 4, 2 and 1 $Kmin^{-1}$ and the thermal hysteresis decreased with slower scan rates. The magnetometry results were confirmed by single crystal X-ray diffraction (150 and 400 K) experiments, which showed excellent correlation. Examination of the single crystal structure revealed the existence of two isomers in the crystal lattice, of opposite handedness (Λ and Δ). Hydrogen bonding along a single crystallographic axis formed chains of Λ---Λ and Δ---Δ.

4.2 Introduction

The discipline of spin-crossover (SCO) materials continues to receive attention from many fronts. Be it theoretical, experimental or from an application standpoint, understanding and controlling the magnetic properties of molecular materials is of high priority in chemical research.[1–4] The most thoroughly studied compounds to this point are those based on Fe^{II} (d^6 electronic configuration) for which the transition from the paramagnetic high-spin (HS) state (S = 2, $^5T_{2g}$) to the diamagnetic low-spin (LS) state (S = 0, $^1A_{1g}$) has been observed to occur with temperature under an appropriate ligand field.[2,5–10]

An important aspect of SCO research lies in the ability to control the temperature of transitions, and expand the range of transition temperatures achievable, which still represents a significant challenge to the SCO research community.[11] Recently we, along with Halcrow and co-workers, have investigated the scarcely reported 2,4-thioimidazole chemical moiety in a mononuclear thioimidazoleimine donor SCO complex.[12,13] A great deal of previous work has focused on various derivatives of the imidazoleimine donor group, which tend to demonstrate SCO behaviour at lower temperatures.[14–17] Nitrogen substitutions at various positions in the imidazole ring have the advantage of hydrogen-bond donor and acceptor addition.[15] On the other hand, our group has recently demonstrated the 2,4-thioimidazole group has the ability to stabilise the LS electronic state at higher temperatures, resulting in higher temperature SCO (manuscript in preparation). Such SCO materials may potentially be useful for above room temperature applications, such as molecular sensing devices.

To date, much of the research into high temperature discrete Fe^{II} compounds has focused on the 1,2,4-triazol (trz) ligand system.[11] Tris(pyrazole-1-yl)methane Fe^{II} complexes have also been shown to exhibit SCO at high temperature.[18–20] The current work presents a mononuclear, high temperature Fe^{II} SCO complex **1** ([Fe**L**]$(BF_4)_2$) utilising a ditopic N_6 hexadentate ligand **L** (Figure 1). The temperature dependant spin-transition of complex **1** was explored using SQUID magnetometry and further evidence was provided by variable temperature single-crystal X-ray diffraction. These experiments all demonstrated excellent correlation of the SCO behaviour. The compound was further characterised by PXRD, HRESI-MS, SEM-EDS, FT-IR and UV-vis spectroscopy.

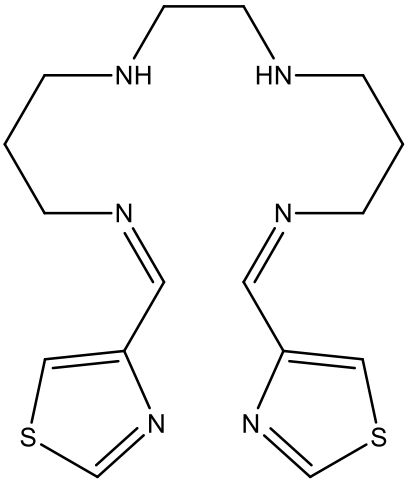

Figure 1. Schematic representation of **L**.

4.3 Experimental

4.3.1 Materials and Instrumentation

All chemicals and reagents were sourced and purchased from commercial sources and used without further purification. A Waters Xevo QToF mass spectrometer was used to collect all high-resolution ESI-MS data, this was conducted in positive ion mode. A Waters lock spray system was used to calibrate the high-resolution masses. A Bruker Vertex 70 with a diamond ATR crystal was used to obtain all FT-IR measurements. Using an Agilent Cary 100 UV-Vis with WinUV software, all solid-state UV-Vis spectra were measured in Nujol at ambient room temperature, the spectra were collected at a scan rate of 600nm per minute from 900-200nm. Scanning electron microscopy–electron dispersive spectroscopy (SEM-EDS) analysis was conducted on a Phenom XL tabletop instrument. Samples were run at 15 kV in high vacuum without surface coating.

4.3.2 Powder X-Ray Diffraction

Powder X-Ray diffraction measurements were conducted on a Bruker D8 ADVANCE diffractometer with a LynxEye position sensitive detector (PSD). The X-ray source was a

Copper K-α1 at 1.54 Å at 40 kV and a current of 40mA. The sample scan range was 5-55 degrees 2θ with a step size of 0.019°. Data processing was conducted using Bruker's EVA software.

4.3.3 Single Crystal X-Ray Diffraction

Crystallographic data was collected using a Bruker kappa-II CCD diffractometer at 150 K, employing an IμS Incoatec Microfocus Source with Mo-Kα radiation (λ = 0.710723 Å). For 400 K measurements, the crystal was mounted on a glass fibre and secured with superglue. Data integration and reduction were undertaken with CrysAlisPro.[21] The structures were solved by direct methods and the full-matrix least-squares refinements were carried out using a suite of *SHELX* programs[22,23] via the *Olex2* interface.[24] Non-hydrogen atoms were refined anisotropically. Carbon-bound hydrogen atoms were included in idealised positions and refined using a riding model.

4.3.4 Magnetic Susceptibility Measurements

Data for magnetic susceptibility measurements were collected on a Quantum Design Versalab Measurement System with a Vibrating Sample Magnetometer (VSM) attachment. Measurements were taken continuously under an applied field of 0.5 T. A polycrystalline sample of complex **1** was cycled over the temperature range 250-400 K at heating rates of 4, 2 and 1 $Kmin^{-1}$.

4.3.5 Synthesis of Complex $[Fe\mathbf{L}](BF_4)_2$ (**1**)

The formation of complex **1** was achieved via subcomponent self-assembly[25,26] utilising simple building blocks to form the coordinate complex $[Fe\mathbf{L}](BF4)_2$. Thiazole-4-carboxaldehyde (300 mg, 2.66 mmol) was dissolved in 10 mL of ethanol, to this stirring solution, 1,2-Bis(3-aminopropylamino)ethane (230 mg, 1.33 mmol) dissolved in 10mL ethanol

was added dropwise. The reaction mixture was then refluxed for 6 hours under a nitrogen atmosphere. To a stirring solution of the ligand (**L**) (1.33 mmol) in 20mL ethanol, a 10 mL (ethanol) solution of iron(II) tetrafluoroborate hexahydrate (447 mg, 1.33 mmol) was added dropwise. The resulting deep blood red solution was stirred for 4 hours. Upon filtration and washing of the crude product with small aliquots of ethanol, 560 mg (71% yield) of dark red precipitate was obtained. The dark red precipitate was redissolved in acetonitrile, vapour diffusion of diethyl ether into the complex mixture yielded X-ray quality crystals. *m/z* (HRMS ESI$^+$, CH_3CN) 592.9810 [Fe + **L**]$^+$ 210.0468. λ_{max} (Nujol)/nm 410, 560. ν_{max} (ATR)cm^{-1} 3296, 2937, 1589.

4.4 Results and Discussion

4.4.1 Magnetic Susceptibility Measurements

A polycrystalline sample of complex **1** was cycled between 250 and 400 K at scan rates of 4, 2 and 1 Kmin^{-1}, with a field of 0.5 T (Figure 2). The molar magnetic susceptibility ($\chi_M T$) at 250 K was 0.06358 cm^3·K·mol^{-1}, corresponding to an almost complete diamagnetic LS ($^1A_1$, S = 0) state. The $\chi_M T$ increased gradually in a single step manner to a value of 1.76 cm^3·K·mol^{-1} at 400 K, at which point c.a 50 % of the Fe^{II} metal centres have undergone a thermally induced spin transition to the HS ($^5T_2$, S = 2) electronic configuration. At a rate of 4 Kmin^{-1}, the heating and cooling modes proceed with a thermal hysteresis of 5 K (Figure 3), with a $T_{1/2}$ of 375 ↓ and 370 ↑ in the cooling and heating modes respectively. At scan rates of 2 and 1 Kmin^{-1}, the spin-transition profile retained its shape, although the thermal hysteresis was found to decrease with slower scan rates.

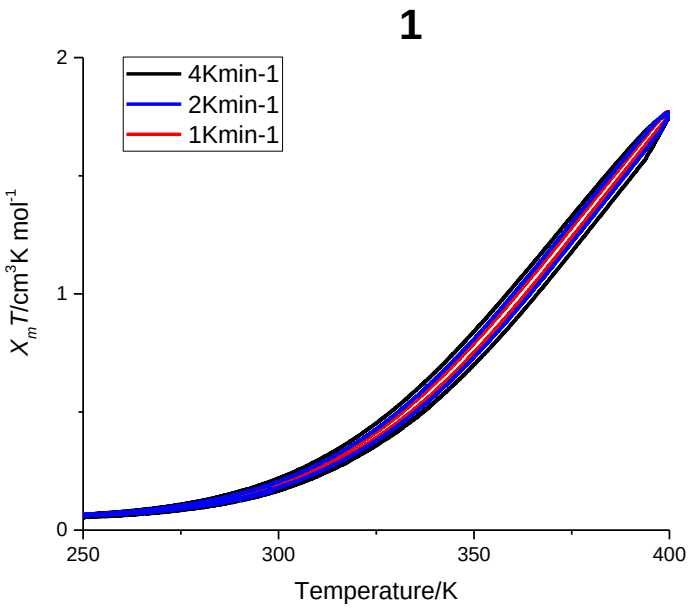

Figure 2. Magnetic susceptibility measurements for compound **1** at 4, 2 and 1 Kmin^{-1}.

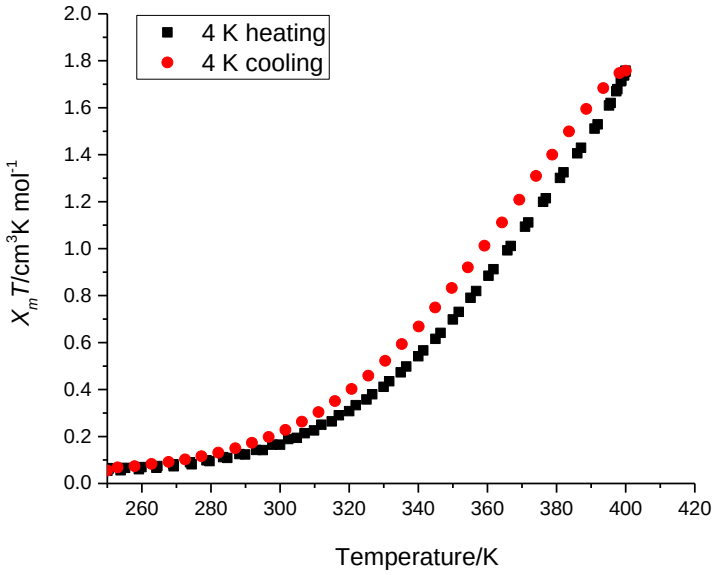

Figure 3. Heating (black squares) and cooling (red circles) modes of complex **1** at 400 Kmin^{-1}, displaying a thermal hysteresis of 5 K.

4.4.2 Magneto-structural Correlation

At 100 K, complex **1** crystallised in the monoclinic space group $P2_1/n$. The coordination sphere is composed of six nitrogen donors; two adjacent thioimidazole nitrogens, two *cis*

imine nitrogens and two adjacent amine nitrogens (Figure 4). As the hexadentate ligand wraps around the Fe^{II} metal centre in a distorted octahedral geometry (Σ 56.1°), this along with average N···Fe bond lengths of 2.00 Å (Table 1), are indicative of a LS Fe^{II} centre, which is in accordance with the magnetic susceptibility results.[10,27-29]

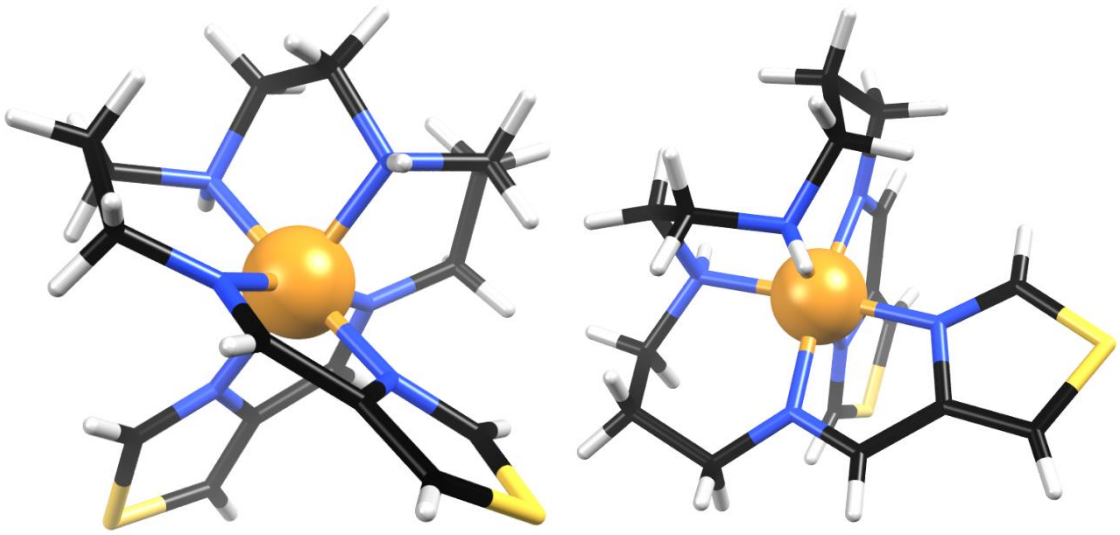

a b

Figure 4. Schematic representation of the crystal structure of complex **1** at 100 K, as shown from two separate angles, a and b. Cations have been excluded for clarity. White represents hydrogen atoms, black - carbon, blue - nitrogen, yellow - sulphur and orange - iron.

As per Figure 5 a, complex **1** packs in an undulating manner along the *b* and *c*-crystallographic axes, and in straight rows along the *a*-axis (Figure 5 b). Along the *b*-axis, hydrogen bonding between amine N-H and tetrafluoroborate counter ions (N···F 2.95 and 2.92 Å) links adjacent complexes in a chain-like manner (Figure 6). Intermolecular interactions, particularly hydrogen bonding, have been demonstrated to be an important factor in the cooperativity of spin-transitions.[10,27,30,31] The gradual nature of the spin-transition profile could be influenced by the hydrogen bonding along only one axis, which provides a relatively small degree of cooperativity between Fe^{II} centres of the crystal lattice.

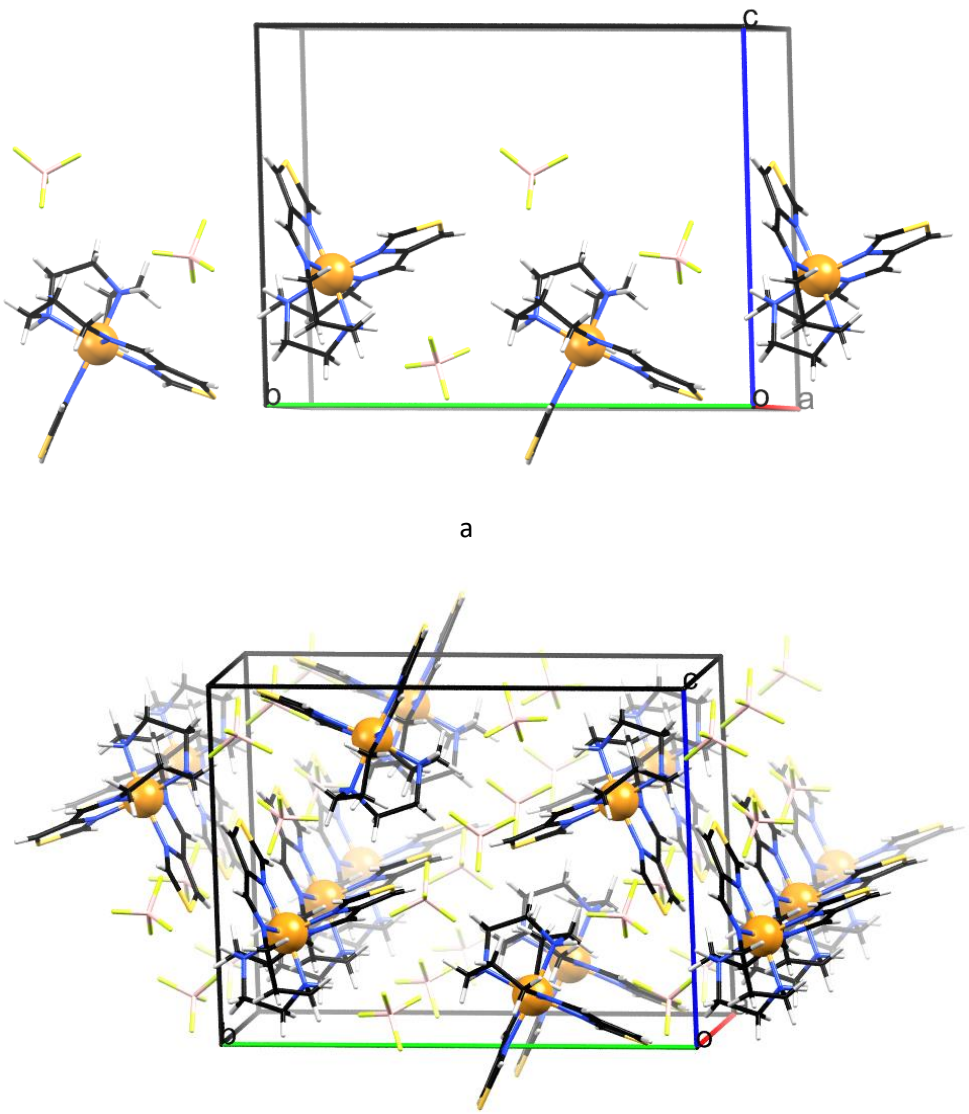

Figure 5. Schematic representation of the crystal packing in complex **1**. The Green line indicates the *b*-axis, red the *a*-axis and blue the *c*-axis.

Furthermore, two distinct isomers are observed within the crystal lattice, characterised by the direction with which the thioimidazole ring is facing around the metal centre after being locked in position by coordination bonding – in a right (Δ - green) or left (Λ - red) handed direction (Figure 7). The unit cell consists of two Λ and two Δ molecules (Figures 8 and 9). As can be seen in figure 10 a, these isomers are distributed in straight rows of similar handedness along the *c*-axis, with adjacent rows possessing opposite handedness. The adjacent rows pack together in an undulating manner. Along the *b*-axis on the other hand, these rows of similar

handedness consist of undulating complexes inverted relative to one another (figure 10 b). The compounds connected by hydrogen bonding interactions along the *b*-axis are of the same handedness, forming chains of Λ---Λ and Δ---Δ.

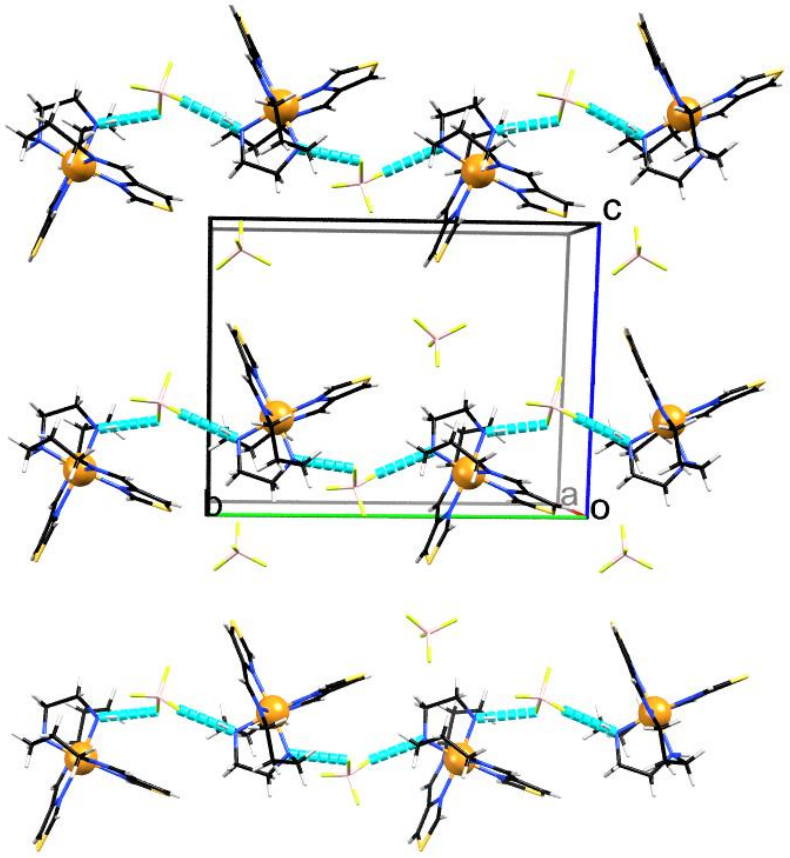

Figure 6. Schematic representation of the hydrogen bonding interactions (represented by light blue dotted lines) present within the crystal lattice of complex **1**. Hydrogen bonding links complexes in rows along the *b*-axis.

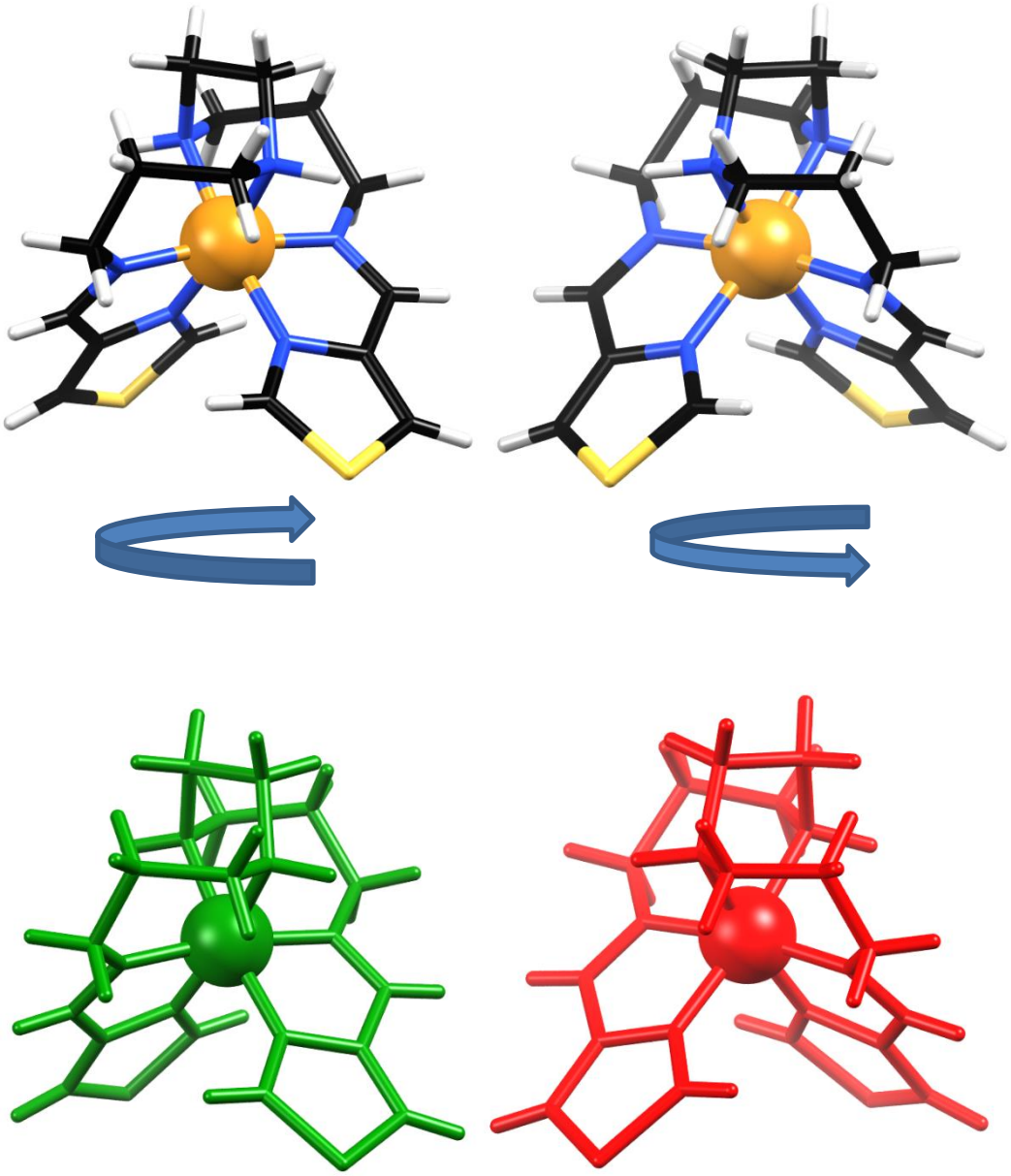

Figure 7. Single crystal structure of complex **1**, the top images showing the manner of the left and right-handedness in the two isomers present in the crystal lattice and the bottom images demonstrating the colour assignment of the two isomers.

Both Isomers share the same bond lengths and octahedral distortion (Σ), and therefore may also possess very similar ligand fields, which may help explain why only one step is observed in the spin transition profile. Although as only half of the material has undergone a LS to HS transition at 400 K, we cannot comment on the nature of the curve beyond 400 K and this will be subject to further investigation.

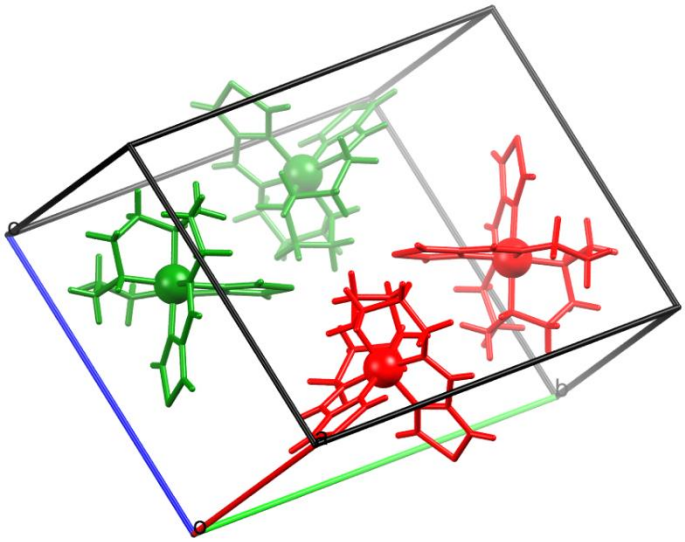

Figure 8. Schematic representation of the unit cell of complex **1**, in which two Λ (red) and two Δ (green) compounds are present.

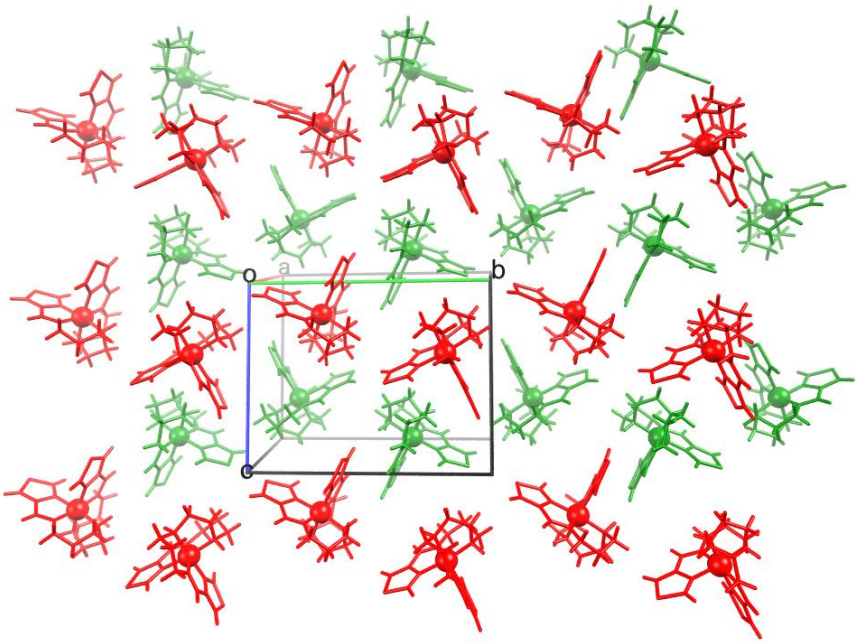

Figure 9. Schematic representation of the packing of the Λ (red) and Δ (green) isomers in the crystal lattice of complex **1**. Counter ions have been removed for clarity.

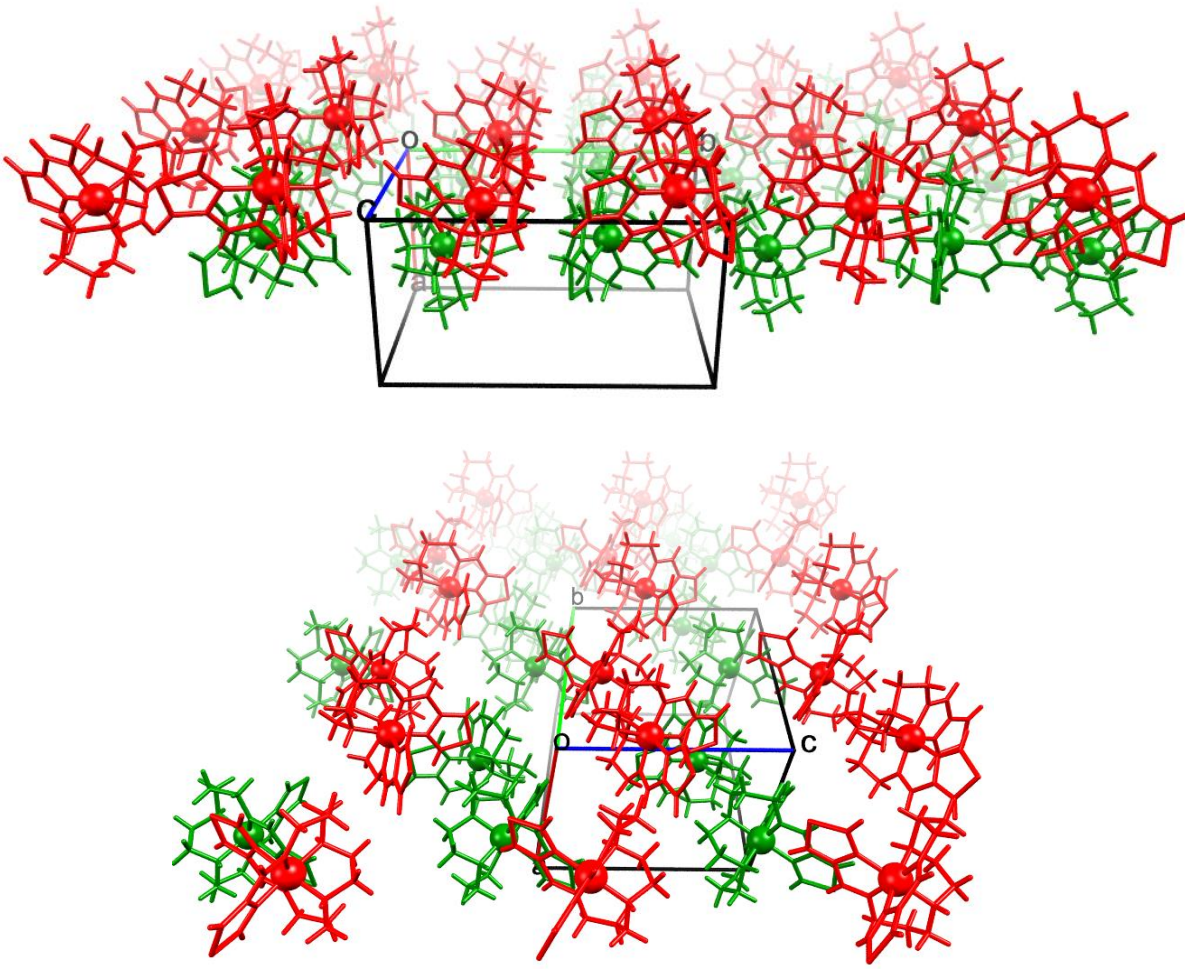

Figure 10. Schematic representation of the crystal packing of complex **1**, showing the packing of isomers a) in straight rows along the *c*-axis, and b) in undulating rows along the *b*-axis.

At 400 K, the crystal structure of complex **1** retains monoclinic space group $P2_1/n$. The blood red crystals showed excellent stability at higher temperatures, the 400 K data finishing with an R_{int} of 8.32 % and an R1 of 7.06 %. The 400 K structure shows identical packing arrangements and similarly, the two isomers are also present with two of each in the unit cell. The average Fe···N bond lengths and octahedral distortion parameter (Σ) were found to increase slightly to values of 2.08 Å and 58.6° respectively. These bond lengths are indicative of a mixed HS and LS spin-state population within the crystal lattice, which confirms magnetic susceptibility data that suggests a population of around 50 % of the Fe^{II} centres are in HS state at 400 K.[27-29,32] Although, the change in the octahedral distortion parameter is only slight, a larger change in Σ is commonly observed in Fe^{II} SCO compounds with an N_6 arrangement of donor atoms. The small change in the distortion of the octahedron may contribute to the high stability at such temperatures, producing a smaller change in the packing orientation and

volume of the cell, resulting in a reduced strain on the crystal lattice. The unit cell volume increases by 164.6 Å from 2298.1 Å at 150 K to 2462.70 Å at 400 K. The other cell parameters (other than the two 90.0° monoclinic angles) also increase in the 400 K structure (Table 2). Previously, it has been shown that greater differences in the distortion between the HS and LS states corresponds to lower transition temperatures.[29] The very low change in distortion accompanying the spin transition in complex **1** may therefore, be a factor in the very high transition temperature ($T_{1/2}$ 375 ↓ and 370 ↑). The measured distortion parameters, average Fe···N bond lengths and cell parameters can be found in Table 1.

Table 1. Important crystallographic values indicating the structural differences between complex **1** at 150 and 400 K.

	1 at 150 K	**1** at 400 K
Average Fe···N bond lengths (Å)	2.00	2.08
Σ (degrees)	56.1	58.6
Unit cell volume (Å)	2298.10	2462.70
a	9.77	10.06
b	17.50	17.42
c	13.66	14.22
α	90.0	90.0
β	100.3	98.7
γ	90.0	90.0

4.4.3 SEM-EDS

Scanning electron microscopy (SEM) micrographs (Figure S1) indicated that complex [Fe**L**]BF_4 (**1**) exists as large single needle crystals. The needle crystals of complex **1** undergo rapid decay due to loss of solvent, there is evident cracking throughout the entirety. Additionally, energy dispersive spectroscopy (EDS) confirmed the presence of C, N, F, B, S and Fe in complex [Fe**L**]BF_4 (**1**) (Figure S1 inset).

4.4.4 IR Spectroscopy

The FT-IR spectrum for complex [Fe**L**]BF_4 (**1**) was recorded at room temperature (Figure S2). The FT-IR spectrum show absorptions in the region of 1595-1585 cm^{-1} that are typical of

imine (C=N) stretching modes. In the region 3300-2985 cm^{-1} and 2945-2930 cm^{-1}, the spectrum exhibits an N-H stretch of a secondary amine and alkyl C-H stretch, respectively.

4.4.5 HR ESI Mass Spectrometry

Electrospray ionisation high resolution mass spectrometry (ESI-HRMS) provided indication that the doubly charged complex species $[Fe\mathbf{L}]^{2+}$ persists in solution. The isotopic distribution patterns for complex **1** that were determined experimentally (Figure S3) are in excellent agreement with the theoretically calculated patterns (insert in Figure S3). With respect to $[Fe\mathbf{L}]BF_4$ (**1**) a 1:1 stoichiometric ratio was observed with major peaks occurring at m/z 210.0468 (calc. 210.0450)

4.4.6 UV-Vis Spectroscopy

The solid-state UV-Vis spectrum of complex **1** is shown in Figure S4. The electronic spectrum of the complex $[Fe\mathbf{L}](BF_4)_2$ (**1**) exhibits a low-energy charge transfer band centred at 560 nm and also exhibits a higher band at 410 nm. These low and high energy bands can be attributed to the low spin and high spin energy state of the Fe^{II}, respectively.

4.4.7 Powder X-Ray Diffraction

The Powder X-ray spectrum of the bulk polycrystalline material matches very well with the spectrum simulated from the single crystal structure at 100 K, confirming that the monoclinic $P2_1/n$ compound is representative of the bulk sample (Figure S5).

4.5 Conclusion

In conclusion, the new complex **1** synthesised by complexation of **L** and $Fe(BF_4)_2$, demonstrated a high temperature thermally induced spin-transition ($T_{1/2}$ of 375 ↓ and 370 ↑at 4 $Kmin^{-1}$), with a 5 K hysteresis between warming and cooling modes. At slower scan rates (2 $Kmin^{-1}$), the profile shape was retained, and the size of the hysteresis decreased. The spin state at variable temperature was further investigated with 150 and 400 K single crystal X-ray diffraction, all of which show good agreement. Examination of the crystal structure at both 150 and 400 K revealed the presence of two isomers (Λ and Δ), which hydrogen bonding connected to other like isomers in chains along the *b*-axis.

4.6 Acknowledgements

The research described herein was supported by Western Sydney University (WSU). The author acknowledges the AMCF and Mass Spectrometry facilities at Western Sydney University. XPS and single crystal experiments were conducted at the Mark Wainwright facility at the University of New South Wales. Magnetometry measurements were performed at Sydney University. K. J. H.-S. and A. R. C acknowledge the Western Sydney University Masters of Research scholarship program. A. R. C. also acknowledges the AINSE honours scholarship program.

4.7 References

1. *Spin-Crossover Materials: Properties and Applications,* M. A. Halcrow., Ed.; Wiley, **2013**.
2. *Spin Crossover in Transition Metal Compounds I, II and III;* P. Gütlich, H. A. Goodwin., Eds.; Springer, **2004**.
3. A. Bousseksou, G. Molnár, L. Salmon and W. Nicolazzi, W. *Chem. Soc. Rev.,* **2011**, *40*, 3313.
4. K. Senthil, and M. Ruben, *Coord. Chem. Rev.,* **2017**, *346* (Supplement C), 176.
5. G. Dupouy, M. Marchivie, S. Triki, J. Sala-Pala, C. J. Gómez-García, S. Pillet, C. Lecomte and J. -F. Létard, *Chem. Commun.,* **2009**, 3404.
6. Y. Garcia, V. Niel, M. C Muñoz and J. A. Real, In: *Spin Crossover in Transition Metal Compounds I*; Topics in Current Chemistry; Springer, Berlin, Heidelberg, **2004**; pp 229–257.
7. P. Gütlich, Y. Garcia and H. A Goodwin, *Chem. Soc. Rev.,* **2000**, *29*, 419.
8. X. -H. Zhao, S. -L. Zhang, D. Shao and X. -Y. Wang, *Inorg. Chem.,* **2015**, *54*, 7857.
9. B. Weber, *Coord. Chem. Rev.,* **2009**, *253*, 2432.
10. E. Milin, B. Benaicha, F. E. Hajj, V. Patinec, S. Triki, M. Marchivie, C. J Gómez-García and S. Pillet, *Eur. J. Inorg. Chem.,* **2016**, 5282.
11. I. Šalitroš, N. T. Madhu, R. Boča, J. Pavlik and M. Ruben, *Monatshefte Für Chem. - Chem. Mon.,* **2009**, *140*, 695.
12. L. Li, S. M. Neville, A. R. Craze, J. K. Clegg, N. F. Sciortino, K. S. A. Arachchige, O. Mustonen, C.E. Marjo, C. R. McRae, C. J. Kepert, L. F. Lindoy, J. R. Aldrich-Wright and F. Li, *ACS Omega.,* **2017**, *2*, 3349.
13. R. Kulmaczewski, O. Cespedes and M. A. Halcrow, *Inorg. Chem.,* **2017**, 56, 3144.
14. L. Li, N. Saigo, Y. Zhang, D. J. Fanna, N. D. Shepherd, J. K. Clegg, R. Zheng, S. Hayami, L. F. Lindoy, J. R. Aldrich-Wright, C. -G. Li, J. K. Reynolds, D. G. Harman and F. Li, *Mater. Chem.,* **2015**, *3*, 7878.
15. F. Tuna, M. R. Lees, G. J. Clarkson and M. J. Hannon, M. J. *Chem. Weinh. Bergstr. Ger.,* **2004**, *10*, 5737.
16. H. Phan, J. J. Hrudka, D. Igimbayeva, L. M. Daku, M. Shatruk, *J. Am. Chem. Soc.,* **2017**, *139*, 6437.
17. T. Fujinami, K. Nishi, N. Matsumoto, S. Iijima, M. A. Halcrow, Y. Sunatsuki and M. Kojima, *Dalton Trans.,* **2011**, *40*, 12301.
18. O. G. Shakirova, L. G. Lavrenova, V. A. Daletsky, E. A. Shusharina, T. P. Griaznova, S. A. Katsyuba, V. V. Syakaev, V. V. Skripacheva, A. R. Mustafina and S. E. Solovieva, *Inorganica Chim. Acta.,* **2010**, *363*, 4059.
19. O. G. Shakirova, L. G. Lavrenova, D. Y. Naumov, V. A. Daletsky and L. A. Sheludyakova, *Polyhedron.,* **2012**, *31*, 64.
20. C. J. Schneider, B. Moubaraki, J. D. Cashion, D. R. Turner, B. A. Leita, S. R. Batten and K. S. Murray, *Dalton Trans.,* **2011**, *40*, 6939.
21. J. R. Nitschke, *Acc. Chem. Res.,* **2007**, 40, 103.
22. A. M. Castilla, W. J. Ramsay and J. R. Nitschke, *Acc. Chem. Res.,* **2014**, 47, 2063.
23. A. Technologies, *CrystalAtlasPro*; Agilent Technologies Ltd: UK, **2009**.
24. G. M. Sheldrick, *SHELX-2014: Programs for Crystal Structure Analysis*; University of Göttingen: Göttingen, **2014**.
25. G. M. Sheldrick, *Acta Crystallogr. Sect. C Struct. Chem.,* **2015**, *71*, 3.
26. O. V. Dolomanov, L. J. Bourhis, R. J. Gildea, J. A. K. Howard and H. Puschmann, *J. Appl. Cryst.,* **2009**, *42*, 339.
27. G. Dupouy, M. Marchivie, S. Triki, J. Sala-Pala, J. Salaün C. J. Gómez-García and P. Guionneau, *Inorg. Chem.* **2008**, *47*, 8921.
28. M. Marchivie, P. Guionneau, J. -F. Létard and D. Chasseau, D. *Acta Crystallogr. Sect. B.,* **2005**, *61*, 25.

29. P. Guionneau, M. Marchivie, G. Bravic, J. -F. Letard and D. Chasseau, *ChemInform.,* **2005**, *36*, no-no.
30. M. Marchivie, P. Guionneau, J. -F. Létard and D. Chasseau, *Acta Crystallogr. Sect. B.,* **2003**, *59*, 479.
31. D. J. Harding, W. Phonsri, P. Harding, I. A. Gass, K. S. Murray, B. Moubaraki, J. D. Cashion, L. Liu and S. G. Telfer, *Chem. Commun.,* **2013**, *49*, 6340.
32. D. Pelleteret, R. Clérac, C. Mathonière, E. Harté, W. Schmitt and P. E. Kruger, *Chem. Commun.,* **2009**, 2, 221.
33. A. P. Grosvenor, B. A. Kobe, M. C. Biesinger and N. S. McIntyre, *Surf. Interface Anal.,* **2004**, *36*, 1564.

4.8 Supplementary Materials

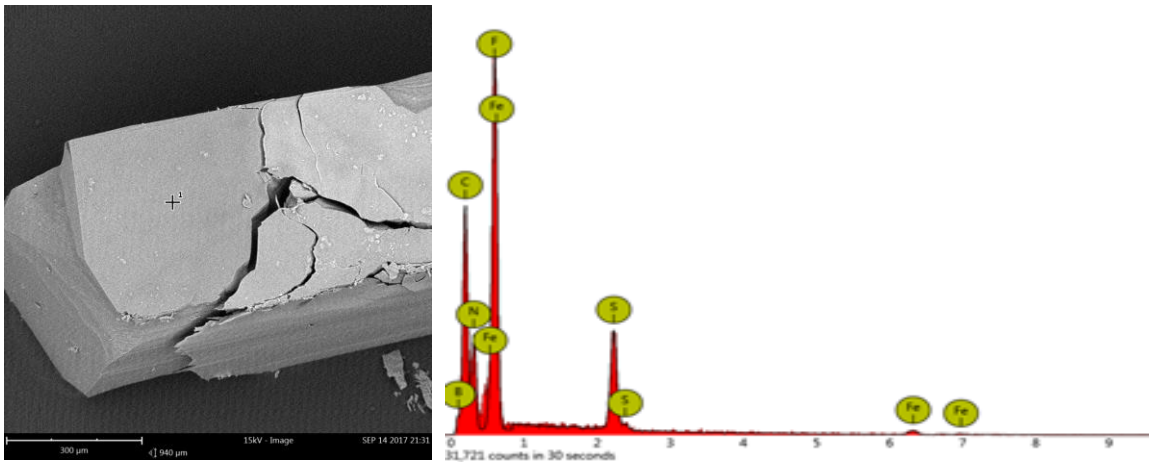

Figure S1. [Fe**L**]BF_4 – SEM micrograph of complex **1** at x285 magnification (left) and EDS spectrum (left).

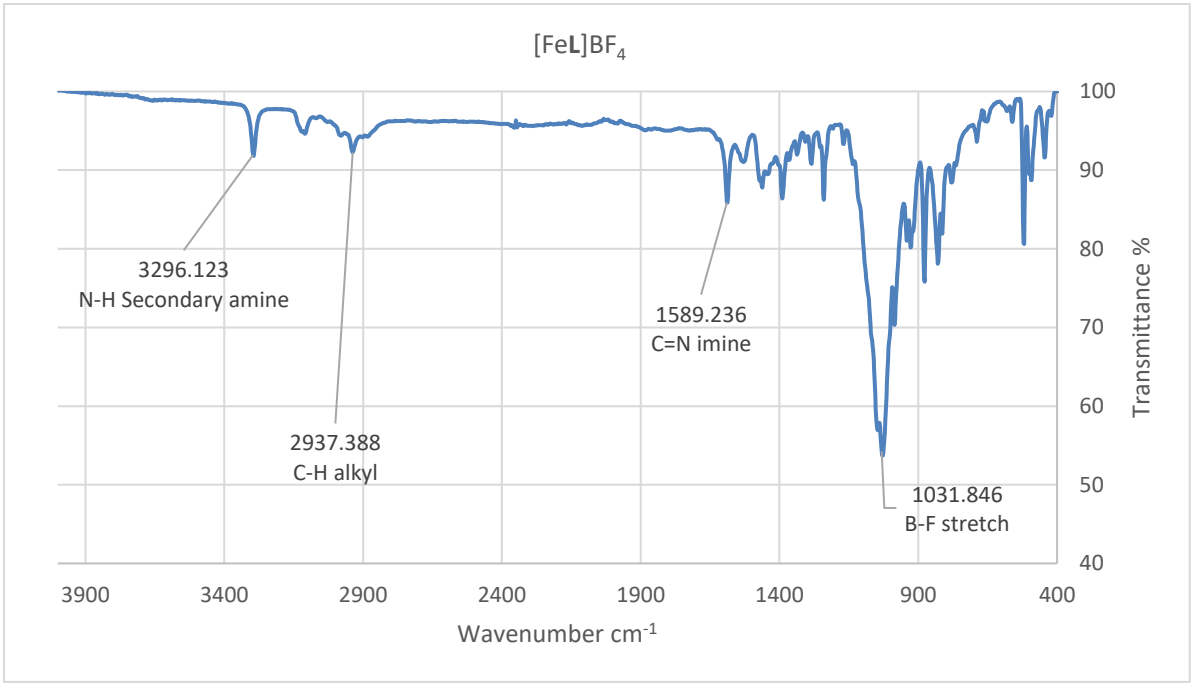

Figure S2. FT-IR spectrum of complex **1** [Fe**L**]$(BF_4)_2$.

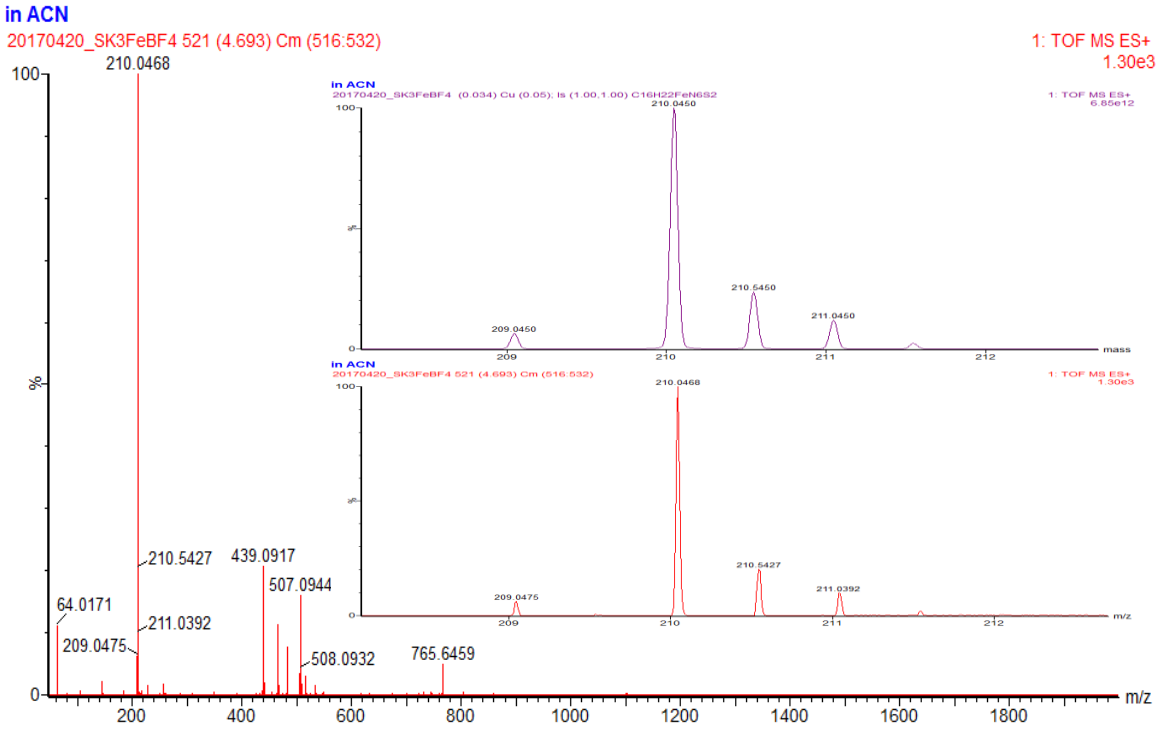

Figure S3. [Fe**L**]$^{2+}$ HR-ESI MS calculated m/z 210.0450 upper insert, experimental m/z 210.0468 lower insert.

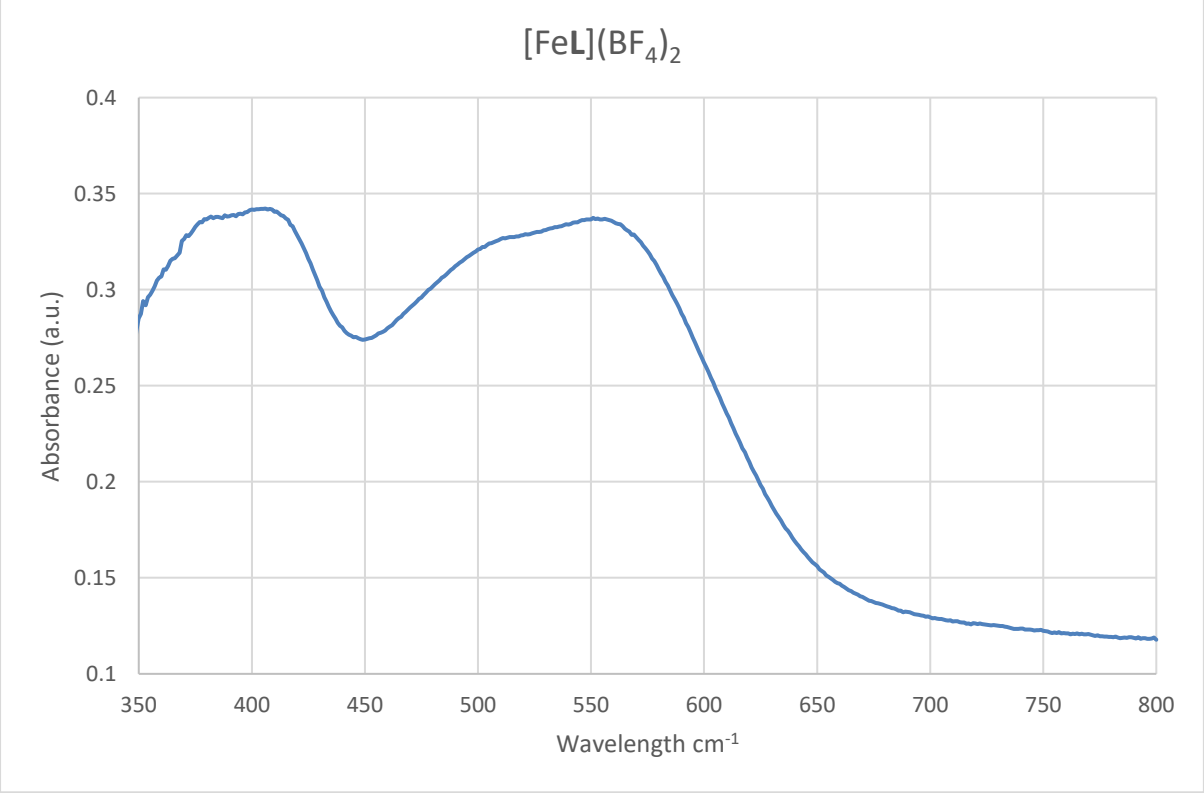

Figure S4. UV-Vis solid-state spectrum of complex **1** [Fe**L**](BF$_4$)$_2$.

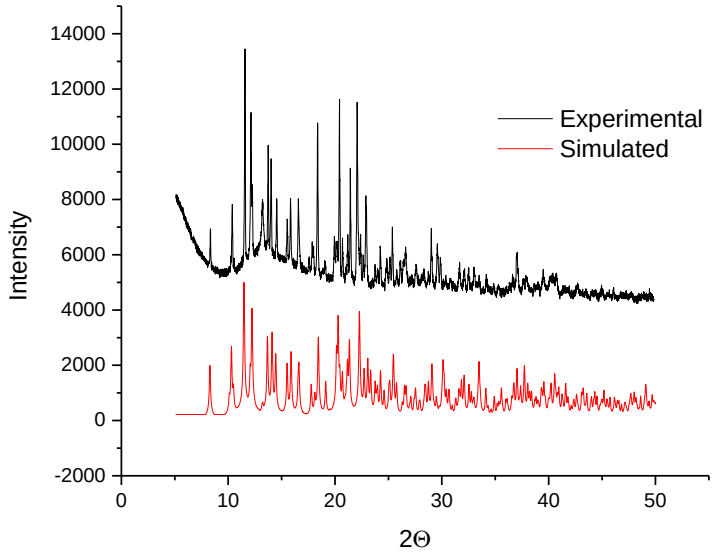

Figure S5. Experimental Powder X-ray diffraction vs simulated powder X-ray diffraction patterns of complex **1.**

Chapter 5 – Five New Thiazolyimine-based Mononuclear Fe^{II} Complexes in the Presence of Different Anions.

Authors: Kyle J. Howard-Smith[A], Alexander R. Craze[A], Mohan M. Badbhade[B], Christopher E. Marjo[B], and Feng Li[A*]

[A]School of Science and Health, Western Sydney University, Locked Bag 1797, Penrith, NSW 2751, Australia.

[B] Mark Wainwright Analytical Centre, University of New South Wales, NSW, 2052, Australia.

5.1 Abstract

Five mononuclear Fe^{II} complexes incorporating different anions (BF_4^-, BPh_4^-, Cl^-, Br^-, I^-) of a new N_3-donor thiazolyimine ligand (**L**) have been designed and synthesised. All complexes were unambiguously characterised by SEM-EDS (scanning electron microscopy-electron dispersive spectroscopy), FT-IR, Raman spectroscopy, solid state UV-Vis, HR ESI-MS (high-resolution electrospray ionisation-mass spectrometry). Single crystal X-ray structures of four complexes have been investigated in LS (low spin) state at 100K. Measurements confirmed the molecular structures of the complexes to be mononuclear assemblies in a distorted octahedral geometry with a stoichiometric ligand-to-metal ratio of 2:1.

5.2 Introduction

Metal-directed self-assembly including supramolecular architectures of nanoscale dimensions is currently an area of intense research activity. By judicious choice of metal and multidentate ligand components, the resulting polymetallic assemblies may exhibit unique redox, magnetic and photochemical properties, and have the potential to bind guest substrates.[1-8] In recent work, both group[9] along with another group[10] have reported thiazolyimine as a functional group for Fe^{II} spin-crossover (SCO) studies at higher temperature. The phenomenon of SCO is a molecular bi-stability exhibited by a select number of octahedral metal complexes containing $3d^4$-$3d^7$ transition metal ions. This bi-stability is characterised by the ability of the metal complex to undergo a transition between low-spin (LS) and high-spin (HS) states, it is well documented that this bi-stability can be induced by external stimuli including, light irradiation, temperature, magnetic field and even counterions and solvent molecule exchange.[11-14]

As an extension of our previous studies of SCO materials incorporating the thiazolyimine moiety, we now describe the design and preparation of the five new mononuclear Fe^{II} complexes with a new N_3-donor thiazolyimine ligand (**L**) using a semi-flexible group, which can be converted between two configurations (see below) for the different metallo-supramolecular assemblies to meet a suitable coordination geometry of an Fe^{II} ion.

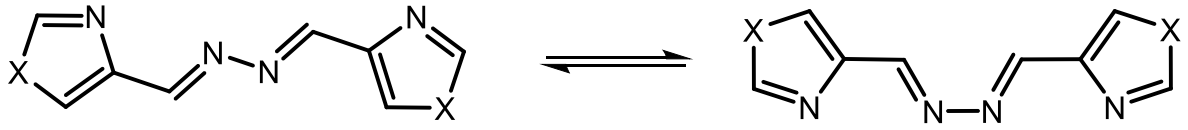

L, X = S
L^{1}, X=NH

Figure 1. Representation of ligand **L** that we have presented in this work compared to ligand **L**^{1} presented by Sunatsuki and co-workers.[15,16]

Previous studies by Sunatsuki and co-workers[15,16] have unambiguously demonstrated the potential of similar ligands utilising the same semi-flexible group with an imidazolyimine ligand (**L**^{1}) for Fe^{II} complexes in the investigation of SCO materials. In addition, the nuclearity of each complex was the result of solvent choice, with methanol yielding mononuclear complexes and nitromethane resulting in the formation of dinuclear triple helicates.[15,16] Sunatsuki and co-workers reported that all complexes both mononuclear and dinuclear, with the exception of one, remained in the low-spin state, while, the complex $[Fe_2(\mathbf{L^1})_3]$ resulted in the formation of a triple helicate which was shown to exhibit an abrupt spin transition from LS → HS dependent on temperature.[15,16]

In this report, we also present the structural characterisation of four complexes, $[Fe\mathbf{L_2}](BF_4)_2$ (**1**), $[Fe\mathbf{L_2}](BPh_4)_2$ (**2**), $[Fe\mathbf{L_2}]Br_2$ (**4**) and $[Fe\mathbf{L_2}]I_2$ (**5**).

5.3 Experimental

5.3.1 Materials and Instrumentation

All chemicals and reagents were purchased from commercial sources and used without further purification. High-resolution electrospray ionisation–mass spectrometry (HR ESI-MS) data were acquired using a Waters Xevo QToF mass spectrometer, operating in positive ion mode. FT-IR measurements were undertaken on a Bruker Vertex 70 with a diamond ATR crystal. Raman spectra were recorded using a Bruker Senterra spectrometer, all samples were subjected to Ar excitation laser of 785 nm wavelength. Spectra were recorded over a 400-4000 cm^{-1} range. A Varian Mercury 300MHz NMR Spectrometer was used to obtain all NMR spectra, 1H was recorded at 300Hz and 13C was recorded at 75Hz. The solid-state UV-Vis spectra were measured in Nujol at ambient temperature using an Agilent Cary 100 UV-Vis with *WinUV* software. Spectra were collected from 900 to 200 nm with a scan rate of 600 nm per minute. Scanning electron microscopy–electron dispersive spectroscopy (SEM-EDS) analysis was conducted on a Phenom XL instrument. Samples were run at 15 kV in high vacuum without surface coating.

The synthesis of ligand [**L**] was adapted and modified from previously reported methods on a similar N_3-donor Schiff-base ligand.[6,11] The synthesis involved a Schiff base condensation reaction performed using a dipodal amine (hydrazine) and 4-thiazole carboxaldehyde.

5.3.2 Synthesis of Ligand [**L**]

4-thiazole carboxaldehyde (1000 mg, 7.80 mmol) was dissolved in 10mL of methanol. To the stirring solution, hydrazine hydrochloride (196 mg, 3.90 mmol) was added dropwise. The reaction mixture was refluxed under atmospheric conditions for 24 hours. After cooling to room temperature, the reaction mixture was filtered and an opaque white precipitate was obtained (yield 80%). *m/z* (HRMS ESI^+, CH_3CN) 244.9779 = [**L** + Na^+], ν_{max} (ATR)/cm^{-1} 1631. ^1H NMR (DMSO): 9.25 (s, 2H), 8.76 (s, 2H), 8.39 (s, 2H). ^{13}C NMR (DMSO): 156.08 (s), 151.49 (s), 124.47 (s).

5.3.3 Synthesis of Metal Complexes **1**-**5**

Complexes **1** and **2** were synthesised in a 3:2 ligand-to-metal (L:M) ratio, in order to favour the formation of a helicate, single crystal X-ray diffraction (SXRD) later showed all attempts resulted in a 2:1 (L:M) complex. Yields have been adjusted to reflect the correct stoichiometric ratios. The results presented in this recent work are those pertaining to complexes formed in methanol, as solvent choice proved to have no impact on the final complex geometry and were hence excluded.

*$[Fe\mathbf{L}_2](BF_4)_2$ (**1**)*

To a stirring solution of [**L**] (200 mg, 0.74 mmol) in 10 mL of methanol, a solution of iron(II) tetrafluoroborate (167 mg, 0.49 mmol) in 10 mL of methanol was added dropwise. The resulting deep purple solution was heated for 8 hours. The resulting reaction mixture was chilled and filtered, a deep purple crystalline precipitate was obtained (yield 65%). The deep purple crystalline precipitate was re-dissolved in acetonitrile and X-ray quality crystals were obtained by vapour diffusion of diethyl ether into the complex mixture. *m/z* (HRMS ESI^+, CH_3CN) 249.9589 = $[Fe\mathbf{L}_2]^{2+}$. ν_{max} (ATR)/cm^{-1} 1614. λ_{max} (Nujol)/nm 580.

*$[Fe\mathbf{L}_2](BPh_4)_2$ (**2**)*

To a stirring solution of [**L**] (200 mg, 0.74 mmol) in 10 mL of methanol, a solution of anhydrous iron(II) chloride (63 mg, 0.49 mmol) in 10 mL of methanol was added dropwise. The reaction mixture was heated for 30 minutes. A 10 mL methanolic solution of excess sodium tetraphenylborate (338 mg, 0.99 mmol) was added dropwise. The reaction mixture was heated for 8 hours. The resulting reaction mixture was chilled and filtered, a deep purple crystalline precipitate was obtained (yield 85%). The deep crystalline precipitate was re-dissolved in acetonitrile and X-ray quality crystals were obtained by vapour diffusion of diethyl ether into the complex mixture. *m/z* (HRMS ESI^+, CH_3CN) 500.0155 = $[Fe\mathbf{L}_2]^+$. ν_{max} (ATR)/cm^{-1} 1618. λ_{max} (Nujol)/nm 580.

*[Fe**L**$_2$]Cl$_2$ (**3**)*

To a stirring solution of [**L**] (200 mg, 0.74 mmol) in 10 mL of methanol, a 10 mL methanolic solution of anhydrous iron(II) chloride (47mg, 0.37 mmol) was added dropwise. The resulting deep purple solution was heated for 8 hours. The reaction mixture was then chilled and the solvent was slowly evaporated, a deep purple crystalline precipitate was obtained (yield 56%). The deep crystalline precipitate was re-dissolved in hot methanol and X-ray quality crystals were obtained by vapour diffusion of diethyl ether into the complex mixture. *m/z* (HRMS ESI$^+$, CH_3CN) 249.9489 = [Fe**L**$_2$]$^{2+}$. ν_{max} (ATR)/cm^{-1} 1612. λ_{max} (Nujol)/nm 580.

*[Fe**L**$_2$]Br$_2$ (**4**)*

To a stirring solution of [**L**] (200 mg, 0.74 mmol), in 10 mL of methanol, a 10 mL methanolic solution of anhydrous iron(II) bromide (80mg, 0.37 mmol) was added dropwise. The resulting deep purple solution was heated for 8 hours. The reaction mixture was then chilled and the solvent was slowly evaporated, a deep purple crystalline precipitate was obtained (yield 58%). The deep crystalline precipitate was re-dissolved in hot methanol and X-ray quality crystals were obtained by vapour diffusion of diisopropyl ether into the complex mixture. *m/z* (HRMS ESI$^+$, CH_3CN) 249.9789 = [Fe**L**$_2$]$^{2+}$. ν_{max} (ATR)/cm^{-1} 1614. λ_{max} (Nujol)/nm 600.

*[Fe**L**$_2$]I$_2$ (**5**)*

To a stirring solution of [**L**] (200 mg, 0.74 mmol), in 10 mL of methanol, a 10 mL methanolic solution of anhydrous iron(II) iodide (115 mg, 0.37 mmol) was added dropwise. The resulting deep purple solution was heated for 8 hours. The reaction mixture was then chilled and the solvent was slowly evaporated, a deep purple crystalline precipitate was obtained (yield 58%). The deep crystalline precipitate was re-dissolved in acetonitrile and X-ray quality crystals were obtained by vapour diffusion of diethyl ether into the complex mixture. *m/z* (HRMS ESI$^+$, CH_3CN) 249.9689 = [Fe**L**$_2$]$^{2+}$. ν_{max} (ATR)/cm^{-1} 1614. λ_{max} (Nujol)/nm 600.

5.3.4 Single Crystal X-Ray Diffraction

The single crystal X-ray data obtained for complexes $[FeL_2](BF_4)_2$ (**1**), $[FeL_2](BPh_4)_2$ (**2**), $[FeL_2]Br_2$ (**4**) and $[FeL_2]I_2$ (**5**) were collected using the MX1 beamline at the Australian Synchrotron with Silicon Double Crystal monochromated radiation at 100(2) K.[17,18] Data integration and reduction were undertaken with XDS.[19] An empirical absorption correction was then applied using SADABS at the Australian Synchrotron.[20] The structures were solved by direct methods and the full-matrix least-squares refinements were carried out using a suite of SHELX program[21,22] via the Olex2 interface.[23] Where possible, all non-hydrogen atoms were located from the electron density maps and refined anisotropically. Hydrogen atoms bound to carbon atoms were added in the ideal positions and refined using a riding model. Some complexes had poor data due to the relatively high disorder of the hydrazine moiety and as such, some atoms had to be left isotropic.

5.4 Results and Discussion

5.4.1 Structure Descriptions of Complexes **1**, **2**, **4** & **5**

The crystal data and refinement details are shown in Table 1. Selected bond angles and bond lengths are shown in shown in Table S1, crystal refinement data can be found in the appendices. Molecular structures of complexes **1, 2, 4** & **5**, were determined by single crystal X-ray diffraction and is shown in Figure **2**. Figure 2 is representative of the molecular structure (excluding anions and solvent molecules) of all complexes **1, 2, 4** & **5** and hence, only one figure is presented. The molecular structures of ligand **L** and complex **3** were unable to be determined due to poor quality data, future work will involve attempts to obtain X-ray quality crystals. Complex **1** crystallises in a triclinic space group P1. The lattice of complex **1** is made up of $[Fe\mathbf{L_2}]^{2+}$ cations and uncoordinated tetrafluoroborate anions. The hexadentate Fe^{II} metal centre is coordinated to three of the four nitrogens present in the N_3-donor Schiff-base ligand in a 2:1 ligand-to-metal (L:M) stoichiometric ratio. The coordination sphere consists of six imine nitrogens (four from the thiazole and two from hydrazine moieties). The asymmetric unit shows disorder with respect to the coordination between the central metal ion Fe^{II} and

the hydrazine moiety taking two separate positions. Hence, the asymmetric unit (which is an average of all repeating units) shows a disordered coordinate bond occurring between the Fe^{II} centre and each hydrazine donor nitrogen, while in fact, only 1 bond exists at any given time in each repeating unit. The angle formed between the two axial imine (thiazole) nitrogens N_{imine}-Fe^{II}-N_{imine} = 174.00(5)° and demonstrates a distorted octahedral geometry. The two Fe^{II}-$N_{hydrazine.imine}$ bond distances are 1.945(16) and 1.910(14) Å and the four Fe^{II}-N_{imine} bond distances are 1.962(13), 1.963(13), 1.929(13) and 1.967(15) Å, these short bond distances are suggestive of a of a low spin Fe^{II} centre and similar to our previous reported Fe^{II} complex in chapter 4.

a) **b)**

Figure 2. Molecular representation of X-ray crystal structures of complexes **1**, **2**, **4** and **5** all counter ions and solvent molecules are not shown. Figures a) and b) illustrate the structure rotated about the y-axis for clarity. White represents hydrogen, yellow – sulfur, grey – carbon, light blue – nitrogen, orange – Fe^{II}

The molecular structure of complex **2** is represented in Figure **2**. Complex **2** crystallises in a monoclinic $P2_{1/C}$ space group. The lattice of complex **2** is made up of $[Fe\mathbf{L_2}]^{2+}$ cations and uncoordinated tetraphenylborate anions. The hexadentate Fe^{II} metal centre is coordinated to three of the four nitrogens present in the N_3-donor Schiff-base ligand in a 2:1 (L:M) stoichiometric ratio. The coordination sphere consists six imine nitrogens. Interestingly, with respect to the hydrazine nitrogen donors, complex **2** was disordered in a similar manner to that described above and correspondingly was modelled accordingly. The angle formed between the two axial secondary nitrogens N_{imine}-Fe^{II}-N_{imine} = 172.50(5)° and demonstrates a distorted octahedral geometry. The two Fe^{II}-$N_{hydrazine.imine}$ bond distances are 1.963(14) and

1.978(2) Å and the four Fe^{II}-N_{imine} bond distances are 1.966(14), 1.961(14), 1.971(13) and 1.967(13) Å, again these short bond distances are suggestive that the Fe^{II} metal centre is in a LS electronic configuration.

The molecular structure of complex (**4**) is shown in Figure **2**. Complex **4** crystallises in a monoclinic $P2_{1/n}$ space group. The lattice of complex **4** is made up of $[Fe\mathbf{L_2}]^{2+}$ cations and uncoordinated bromine (Br^-) anions. The hexadentate Fe^{II} metal centre is coordinated to three of the four nitrogens present in the N_3-donor Schiff-base ligand in a 2:1 (L:M) stoichiometric ratio. The coordination sphere was again made up of six imine nitrogens. Once again, the hydrazine nitrogen donors displayed the same disorder as described above. The angle formed between the two axial secondary nitrogens N_{imine}-Fe^{II}-N_{imine} = 172.10(5)° and demonstrates a distorted octahedral geometry. The data collected for this particular complex was not great and indicated by the relatively high R_{int} value, multiple atoms had to be left isotropic, although the data indicates that the complex in agreement with the structure presented. The two Fe^{II}-$N_{hydrazine.imine}$ bond distances are 1.934(18) and 1.965(12) Å and the four Fe^{II}-N_{imine} bond distances are 1.960(11), 1.972(11), 1.956(14) and 1.936(13) Å, again these short bond distances are indicative of a LS state.

The molecular structure of complex **5** is shown in Figure **2**. Complex **5** crystallises in a monoclinic space group $P2_{1/n}$. The lattice of complex **5** is made up of $[Fe\mathbf{L_2}]^{2+}$ cations and uncoordinated iodine anions. The hexadentate Fe^{II} metal centre is coordinated to three of the four nitrogens present in the N_3-donor Schiff-base ligand in a 2:1 (L:M) stoichiometric ratio. The coordination sphere is yet again made up of the same six imine nitrogens. The disorder with regards to the hydrazine nitrogen donors was the same once again as reported above. The angle formed between the two axial secondary nitrogens N_{imine}-Fe^{II}-N_{imne} = 176.00(17)° and demonstrates a distorted octahedral geometry. The two Fe^{II}-$N_{hydrazine.imine}$ bond distances are 1.951(4) and 1.955(8) Å and the four Fe^{II}-N_{imine} bond distances are 1.969(4), 1.954(4), 1.962(4) and 1.951(4) Å, once more indicating a LS Fe^{II} centre.

Table 1. Crystallographic data and refinement details for complexes **1, 2, 4 & 5**.

	1	**2**	**4**	**5**
Empirical formula	$[C_{16}H_{12}FeN_8S_4]\cdot B_2F_8$	$[C_{16}H_{12}FeN_8S_4]\cdot B_2C_{48}H_{40}$	$[C_{18}H_{20}Fe\ N_8\ S_4](Br_2)\cdot C_2H_8O_2$	$[C_{16}H_{12}FeN_8S_4](I)_4C_2H_2N$
Formula weight	674.05	1138.84	724.33	1048.07
Temperature/K	100	100	100	293(2)
Crystal system	triclinic	monoclinic	monoclinic	monoclinic
Space group	P1	$P2_1/c$	$P2_1/n$	$P2_1/n$
a/Å	8.6440(17)	11.654(2)	8.6690(17)	8.7710(18)
b/Å	8.8000(18)	22.362(5)	17.524(4)	30.380(6)
c/Å	16.261(3)	21.505(4)	19.320(4)	11.331(2)
α/°	89.91(3)	90	90	90
β/°	75.82(3)	98.16(3)	101.98(3)	101.47(3)
γ/°	89.92(3)	90	90	90
Volume/Å^3	1199.2(4)	5548(2)	2871.0(10)	2959.0(11)
Z	2	4	4	4
ρ_{calc}g/cm^3	1.867	1.364	1.676	2.353
μ/mm^{-1}	1.066	0.473	3.631	4.992
F(000)	672.0	2368.0	1440.0	1948.0
Radiation	MoKα (λ = 0.71073)	MoKα (λ = 0.71073)	MoKα (λ = 0.71073)	MoKα (λ = 0.71073)
2Θ range for data collection/°	2.584 to 52.734	2.642 to 56.566	3.17 to 56.56	2.682 to 56.564
Index ranges	-10 ≤ h ≤ 10, -10 ≤ k ≤ 10, -20 ≤ l ≤ 20	-15 ≤ h ≤ 15, -28 ≤ k ≤ 29, -28 ≤ l ≤ 28	-10 ≤ h ≤ 10, -23 ≤ k ≤ 23, -25 ≤ l ≤ 25	-11 ≤ h ≤ 11, -40 ≤ k ≤ 40, -14 ≤ l ≤ 14
Reflections collected	16965	88126	47743	49217
Independent reflections	8547 [R_{int} = 0.0613, R_{sigma} = 0.0927]	13663 [R_{int} = 0.0270, R_{sigma} = 0.0154]	6568 [R_{int} = 0.1722, R_{sigma} = 0.0771]	7259 [R_{int} = 0.0270, R_{sigma} = 0.0143]
Data/restraints/parameters	8547/3/623	13663/42/748	6568/3/333	7259/21/344
Goodness-of-fit on F^2	1.059	1.035	1.081	1.073
Final R indexes [I>=2σ (I)]	R_1 = 0.0889, wR_2 = 0.2307	R_1 = 0.0386, wR_2 = 0.1029	R_1 = 0.1322, wR_2 = 0.3732	R_1 = 0.0432, wR_2 = 0.0975
Final R indexes [all data]	R_1 = 0.0947, wR_2 = 0.2365	R_1 = 0.0393, wR_2 = 0.1036	R_1 = 0.1656, wR_2 = 0.3993	R_1 = 0.0461, wR_2 = 0.0990
Largest diff. peak/hole / e Å^{-3}	2.37/-1.28	1.63/-0.47	2.92/-2.18	1.99/-2.04
Flack parameter	0.036(13)			

5.4.2 SEM-EDS

Scanning electron microscopy (SEM) micrographs (Figures S2-6) indicated that complexes **1**-**5** exist as large single crystals, complexes **1**, **2**, **4** and **5** are needle crystals, while complex **3** is large block crystals. SEM micrograph of the ligand [**L**] (Figure S1) indicates the ligand exist as small block crystals. It is evident that complexes **3** and **4** undergo decay due to loss of solvent. Additionally, scanning electron microscopy-energy dispersive spectroscopy (SEM-EDS) analysis provided evidence confirming the presence of C, N and S in [**L**] (Figure S1), C, N, S, B, F and Fe in [Fe**L**$_2$](BF$_4$)$_2$ (**1**) (Figure S2), C, N, S, B and Fe in [Fe**L**$_2$](BPh$_4$)$_2$ (**2**) (Figure S3), C,

N, S, Cl and Fe in [Fe**L$_2$**]Cl_2 (**3**) (Figure S4), C, N, S, Br and Fe in [Fe**L$_2$**]Br_2 (**4**) (Figure S5) and C, N, S, I and Fe in [Fe**L$_2$**]I_2 (**5**) (Figure S6).

5.4.3 IR Spectroscopy

FT-IR spectra for ligand [**L**] and complexes [Fe**L$_2$**]$(BF_4)_2$ (**1**), [Fe**L$_2$**]$(BPh_4)_2$ (**2**), [Fe**L$_2$**]Cl_2 (**3**), [Fe**L$_2$**]Br_2 (**4**) and [Fe**L$_2$**]I_2 (**5**) were all recorded at room temperature and are shown in Figures S7-12, respectively. With respect to ligand [**L**] shown in Figure S7, FT-IR spectra absorptions in the region 1631 cm^{-1} that is attributable to imine (C=N) stretching modes. Similarly, the absorptions in the region 1620-1610 cm^{-1} for complexes **1**-**5** shown in Figures S8-12, respectively, are all in agreement with each other, exhibiting characteristic imine (C=N) stretching modes.

5.4.4 Raman Spectroscopy

Raman spectra for ligand [**L**] and complexes **1**-**5** are shown in Figures S13-18, respectively. With respect to ligand [**L**] shown in Figure S13, absorptions in the region 1600-1550 cm^{-1} are typical of an imine (C=N) stretching mode. Complexes **1**-**5,** shown in Figure S14-18 respectively, are all in agreement with one another, the spectra show very similar absorptions in characteristic regions. Complexes **1**-**5** show absorptions in the regions of 1600-1500 cm^{-1}, typical of an imine (C=N) functional moiety.

5.4.5 UV-Vis Spectroscopy

The solid-state UV-Vis spectra of complexes [Fe**L$_2$**]$(BF_4)_2$ (**1**), [Fe**L$_2$**]$(BPh_4)_2$ (**2**), [Fe**L$_2$**]Cl_2 (**3**), [Fe**L$_2$**]Br_2 (**4**) and [Fe**L$_2$**]I_2 (**5**) are shown in Figure S19. Complexes **1**-**3** exhibit broad bands centred at 580 nm, while complexes **4** & **5** exhibit broad bands centred at 600 nm. The bands observed in the region 580-600 nm in complexes **1**-**5** can be attributed to the d-d transitions associated with the octahedral coordination environment around the respective metal centres.

5.4.5 HR ESI Mass Spectrometry

High-resolution electrospray ionisation mass-spectrometry (HR ESI-MS) provided indication that the neutral charged ligand [**L**] persists in solution (Figure S20). The experimentally calculated m/z obtained for the ligand [**L**] [**L** + Na^+] = 244.9779, is in excellent agreement with the theoretical calculated m/z (insert Figure S20). Figures S21, S23-25, shows the doubly charged complexes **1, 3, 4** & **5**, [Fe**L**]$^{2+}$, while Figure S22, shows the singly charged complex **2** [Fe**L**]$^+$. The experimentally calculated isotopic distribution patterns for all complexes (**1**-**5**) are in excellent agreement with the theoretically generated patterns (inserts Figures S21-25). With respect to complexes **1-5**, all were observed to be in a 2:1 stoichiometric ratio of L:M (Ligand-to-Metal) with major peaks observed at m/z [Fe**L**]$^{2+}$ (**1**) = 249.9589 (calc. 249.9732), [Fe$\mathbf{L_2}$]$^+$ = 500.0155 (calc. 499.9356), [Fe$\mathbf{L_2}$]$^{2+}$ (**3**) = 249.9489 (calc. 249.9732), [Fe$\mathbf{L_2}$]$^{2+}$ (**4**) = 249.9789 (calc. 249.9732) and [Fe$\mathbf{L_2}$]$^{2+}$ (**5**) = 249.9689 (calc. 249.9732).

5.5 Conclusion

We describe the synthesis and characterisation of a series of five new mononuclear Fe^{II} N_3-donor thiazolyimine Schiff-base complexes. All complexes have been investigated and unambiguously characterised by scanning electron microscopy-electron dispersive spectroscopy (SEM-EDS), FT-IR, Raman spectroscopy, solid state UV-Vis, high-resolution electrospray ionisation-mass spectrometry (HR ESI-MS). We also present the structural characterisation of four complexes, $[FeL_2](BF_4)_2$ (**1**), $[FeL_2](BPh_4)_2$ (**2**), $[FeL_2]Br_2$ (**4**) and $[FeL_2]I_2$ (**5**), characterised by means of single crystal X-ray diffraction. Further studies are underway to investigate whether the nuclearity is a thermally favoured product rather than kinetic. Magnetic studies will also be carried out on all complexes in order to determine if a SCO transition exists.

5.6 Acknowledgements

The research described herein was supported by Western Sydney University (WSU). The author acknowledges the AMCF and Mass Spectrometry facilities at Western Sydney University. The crystallographic data presented was collected on the MX1 beamline at the Australian Synchrotron, Victoria, Australia. K. J. H.-S. & A. R. C acknowledge the Western Sydney University Masters of Research scholarship program. A. R. C. also acknowledges the AINSE honours scholarship program.

5.6 References

1. E. L. Gavey and M. Pilkington, *Coord. Chem. Rev.*, **2015**, *296*, 125.
2. M. Rezaeivala and H. Keypour, *Coord. Chem. Rev.*, **2014**, *280*, 203.
3. D. J. Fanna, Y. Zhang, L. Li, I. Karatchevtseva, N. D. Shepherd, A. Azim, J. R. Price, J. Aldrich-Wright, J. K. Reynolds and F. Li, *Inorg. Chem. Front.,* **2016**, *3*, 286.
4. D. J. Fanna, Y. Zhang, A. Salih, J. K. Reynolds and F. Li, *J. Coord. Chem.,* **2016**, *69*, 1883.
5. H. Eguchi, M. Umemura, R. Kurotani, H. Fukumura, I. Sato, J.-H. Kim, Y. Hoshino, J. Lee, N. Amemiya, M. Sato, K. Hirata, D. J. Singh, T. Masuda, M. Yamamoto, T. Urano, K. Yoshida, K. Tanigaki, M. Yamamoto, M. Sato, S. Inoue, I. Aoki and Y. Ishikawa, *Scientific Reports.*, **2015**, *5*, 9194.
6. S. Wang, W.-T. Xu, W.-R. He, S. Takaishi, Y.-H. Li, M. Yamashita and W. Huang, *Dalton. Trans.,* **2016**, *45*, 5676.
7. S. Hayami, Z. Gu, H. Yoshiki, A. Fujishima and O. Sato, *J. Am. Chem. Soc.*, **2001**, *123*, 11644.
8. V. Mougel, L. Chatelain, J. Pécaut, R. Caciuffo, E. Colineau, J.-C. Griveau and M. Mazzanti, *Nat. Chem.*, **2012**, *4*, 1011.
9. L. Li, S. M. Neville, A. R. Craze, J. K. Clegg, N. F. Sciortino, K. S. Athukorala Arachchige, O. Mustonen, C. E. Marjo, C. R. McRae, C. J. Kepert, L. F. Lindoy, J. R. Aldrich-Wright and F. Li, *ACS Omega*., **2017**, 2, 3349.
10. R. Kulmaczewski, O. Cespedes and M. A. Halcrow, *Inorg. Chem.,* **2017**, 56, 3144.
11. *Spin-Crossover Materials: Properties and Applications,* M. A. Halcrow., Ed.; Wiley, **2013**.
12. O. Khan, J. Krober, C. Jay, *Adv. Mater.,* **1992**, 4, 718.
13. O. Khan, C. Jay-Martinez, *Science*., **1998**, 279, 44.
14. *Spin Crossover in Transition Metal Compounds I, II and III;* P. Gütlich and H. A. Goodwin., Eds.; Springer, **2004**.
15. Y. Sunatsuki, R. Kawamoto, K. Fujita, H. Maruyama, T. Suzuki, H. Ishida, M. Kojima, S. Iijima and N. Matsumoto, *Coord. Chem. Rev.,* **2010**. 254, 1871.
16. Y. Sunatsuki, R. Kawamoto, K. Fujita, H. Maruyama, T. Suzuki, H. Ishida, M. Kojima, S. Iijima and N. Matsumoto, *Inorg. Chem.,* **2009**, 48, 8784.
17. T. M. McPhillips, S. E. McPhillips, H. J. Chiu, A. E. Cohen, A. M. Deacon, P. J. Ellis, E. Garman, A. Gonzalez, N. K. Sauter, R. P. Phizackerley, S. M. Soltis and P. Kuhn, BlueIce, *J. Synchrotron Rad.,* **2002**, *9*, 401.
18. N. P. Cowieson, D. Aragao, M. Clift, D. J. Ericsson, C. Gee, S. J. Harrop, N. Mudie, S. Panjikar, J. R. Price, A. Riboldi-Tunnicliffe, R. Williamson and T. Caradoc-Davies, *J. Synchrotron Rad.,* **2015**, *22*, 187.
19. W. Kabsch, *J. Appl. Cryst.*, **1993**, *26*, 795.
20. G. M. Sheldrick, SADABS: Empirical Absorption and Correction Software, University of Göttingen, Germany, **1996**.
21. G. M. Sheldrick, *Acta Cryst.,* **2008**, *A64*, 112.
22. G. M. Sheldrick, *Acta Cryst.,* **2015**, *A71*, 3.
23. O. V. Dolomanov, L. J. Bourhis, R. J. Gildea, J. A. K. Howard and H. Puschmann, *J. Appl. Cryst.,* **2009**, *42*, 339.

5.7 Supplementary Materials

Table S1. Summary of bond angles and bond lengths of complexes **1, 2, 4 & 5**.

Bond lengths (Å)		Bond angles (°)			
1					
Fe01-N00K	1.962(12)	N00K-Fe01-N00N	89.5(5)	N013-Fe01-N00N	91.8(6)
Fe01-N00N	1.963(13)	N00K-Fe01-N00S	173.6(5)	N013-Fe01-N00S	92.5(7)
Fe01-N00O	1.929(13)	N00N-Fe01-N00S	90.4(5)	N01X-Fe01-N00K	93.7(6)
Fe01-N00S	1.967(15)	N00O-Fe01-N00K	89.4(5)	N01X-Fe01-N00N	82.7(8)
Fe01-N0013	1.945(16)	N00O-Fe01-N00N	174.0(5)	N01X-Fe01-N00O	91.6(8)
Fe01-N01X	1.910(14)	N00O-Fe01-N00S	91.3(5)	N01X-Fe01-N00S	92.7(6)
Fe02-N00J	1.961(12)	N00O-Fe01-N013	93.9(6)	N01X-Fe01-N013	172.4(7)
		N013-Fe01-N00K	81.1(6)		
2					
Fe01-N006	1.9675(14)	N006-Fe01-N008	91.75(5)	N009-Fe01-N01A	94.77(9)
Fe01-N007	1.9607(14)	N006-Fe01-N01A	91.98(8)	N00A-Fe01-N006	80.76(6)
Fe01-N008	1.9714(13)	N007-Fe01-N006	172.50(5)	N00A-Fe01-N008	93.48(5)
Fe01-N009	1.9672(13)	N007-Fe01-N008	90.63(5)	N00A-Fe01-N009	93.35(5)
Fe01-N00A	1.9634(14)	N007-Fe01-N009	88.40(5)	N00A-Fe01-N01A	169.11(9)
Fe01-N01A	1.978(2)	N007-Fe01-N00A	92.00(6)	N2-Fe01-N006	90.51(11)
Fe01-N2	1.956(4)	N007-Fe01-N01A	95.47(8)	N2-Fe01-N007	96.25(11)
		N008-Fe01-N01A	78.55(9)	N2-Fe01-N008	97.08(14)
		N009-Fe01-N006	90.07(5)	N2-Fe01-N009	76.27(14)
		N009-Fe01-N008	173.13(6)	N2-Fe01-N00A	166.50(13)
4					
Fe03-N008	1.936(13)	N008-Fe03-N009	172.1(5)	N00B-Fe03-N00A	173.3(5)
Fe03-N009	1.956(14)	N008-Fe03-N00A	91.2(5)	N00B-Fe03-N00C	82.0(6)
Fe03-N00A	1.972(11)	N008-Fe03-N00B	88.4(5)	N00B-Fe03-N00F	93.7(10)
Fe03-N00B	1.960(11)	N008-Fe03-N00C	95.1(5)	N00C-Fe03-N00A	91.3(6)
Fe03-N00C	1.965(12)	N008-Fe03-N00F	75.6(10)	N00C-Fe03-N00F	169.9(10)
Fe03-N00E	1.934(18)	N009-Fe03-N00A	90.6(5)	N00E-Fe03-N008	96.2(8)
Fe03-N00f	2.01(3)	N009-Fe03-N00B	90.7(5)	N00E-Fe03-N009	76.0(8)
		N009-Fe03-N00C	92.6(6)	N00E-Fe03-N00A	91.9(7)
		N009-Fe03-N00F	96.7(10)	N00E-Fe03-N00B	94.8(6)
		N00A-Fe03-N00F	92.7(10)	N00E-Fe03-N00C	168.2(8)
5					
Fe05-N00A	1.969(4)	N00B-Fe05-N00A	90.24(16)	N00E-Fe05-N00A	81.52(18)
Fe05-N00B	1.964(4)	N00B-Fe05-N0AA	77.7(4)	N00E-Fe05-N00B	92.51(18)
Fe05-N00C	1.954(4)	N00C-Fe05-N00A	174.20(17)	N00E-Fe05-N00C	92.70(19)
Fe05-N00D	1.962(4)	N00C-Fe05-N00B	90.51(17)	N00E-Fe05-N00D	92.92(18)
Fe05-N00E	1.951(4)	N00C-Fe05-N00D	91.09(16)	N00E-Fe05-N00R	168.4(3)
Fe05-N00R	1.955(8)	N00C-Fe05-N00R	93.5(3)	N00E-Fe05-N0AA	168.7(3)
Fe05-N0aa	1.964(9)	N00C-Fe05-N0AA	93.1(3)	N00R-Fe05-N00A	92.1(3)
		N00D-Fe05-N00A	88.73(16)	N00R-Fe05-N00B	97.2(3)
		N00D-Fe05-N00B	174.26(18)	N00R-Fe05-N00D	77.2(3)
		N00D-Fe05-N0AA	96.7(4)	N0AA-Fe05-N00A	92.7(3)

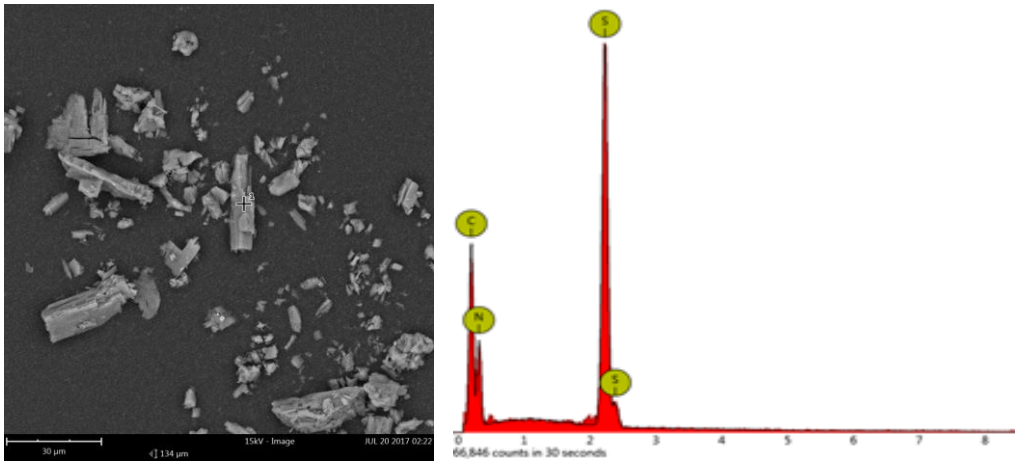

Figure S1. [**L**] – x2000 magnification SEM micrograph of ligand **L** (right) with an EDS spectrum (left).

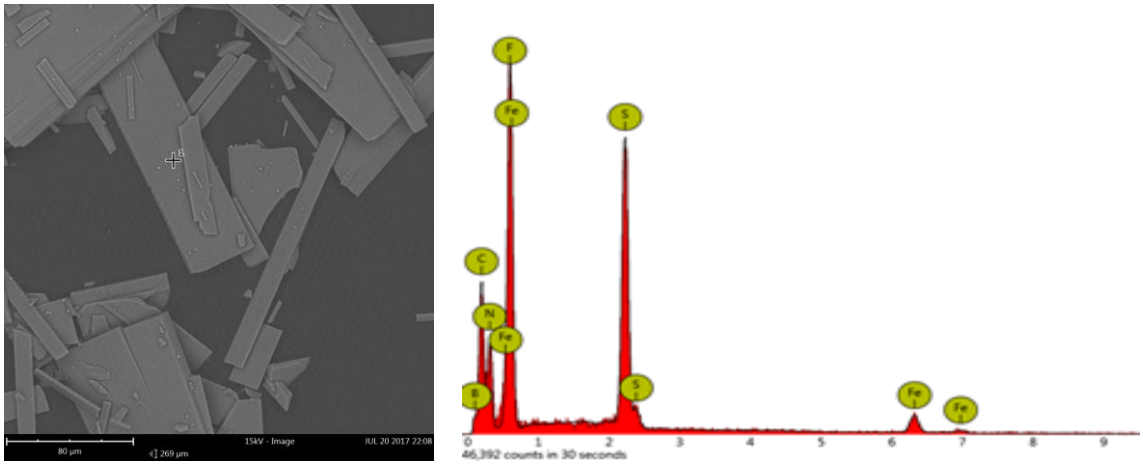

Figure S2. [Fe**L**$_2$](BF$_4$)$_2$ - x1000 magnification SEM micrograph of complex **1** (right) with an EDS spectrum (left).

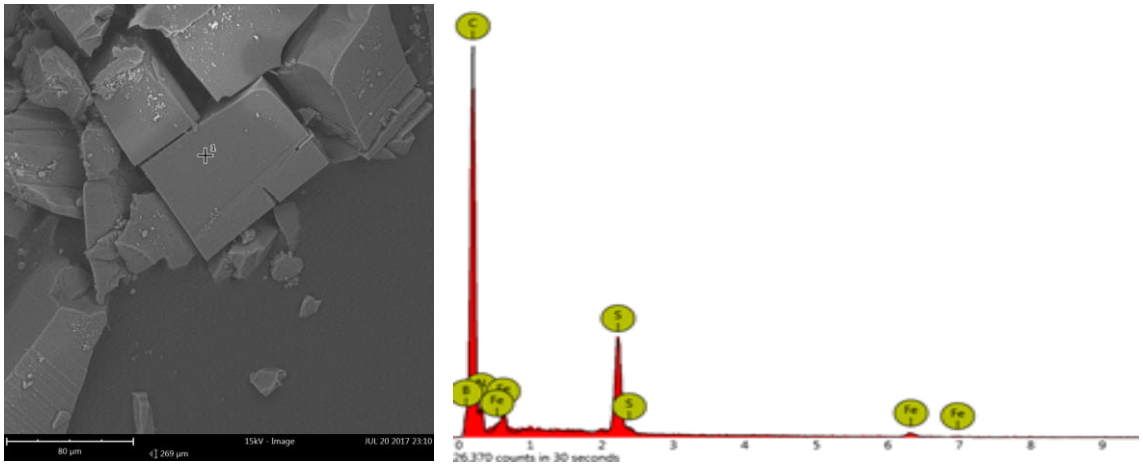

Figure S3. [Fe**L**$_2$](BPh$_4$)$_2$ - x1000 magnification SEM micrograph of complex **2** (right) with an EDS spectrum (left).

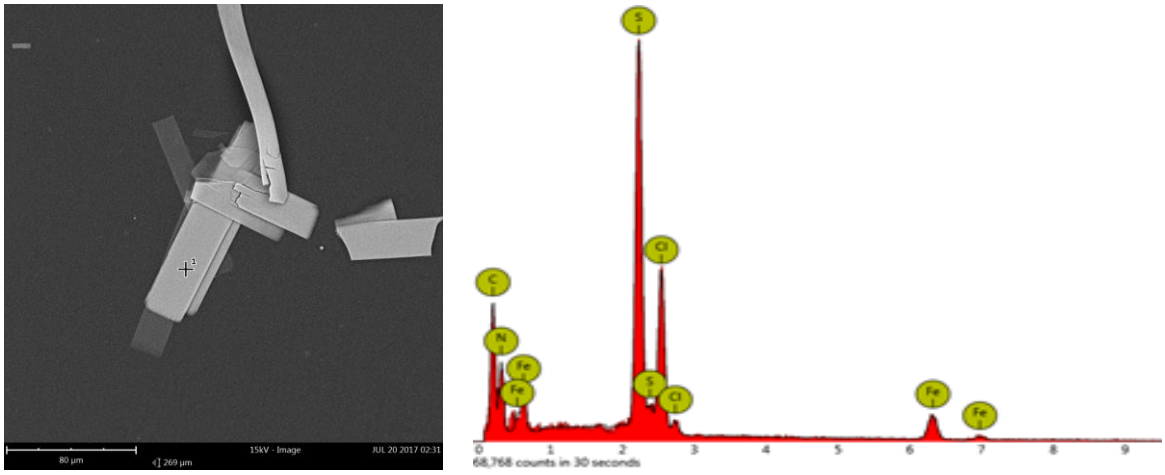

Figure S4. [Fe**L**$_2$]Cl_2 - x1000 magnification SEM micrograph of complex **3** (right) with an EDS spectrum (left). The crystals were observed to bend and flex under vacuum.

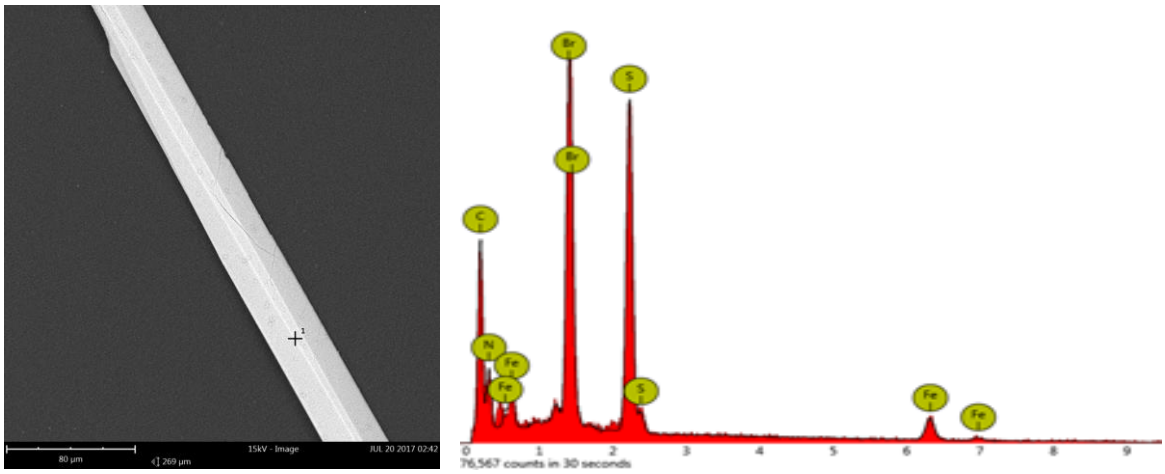

Figure S5. [Fe**L**$_2$]Br_2 - x1000 magnification SEM micrograph of complex **4** (right) with an EDS spectrum (left).

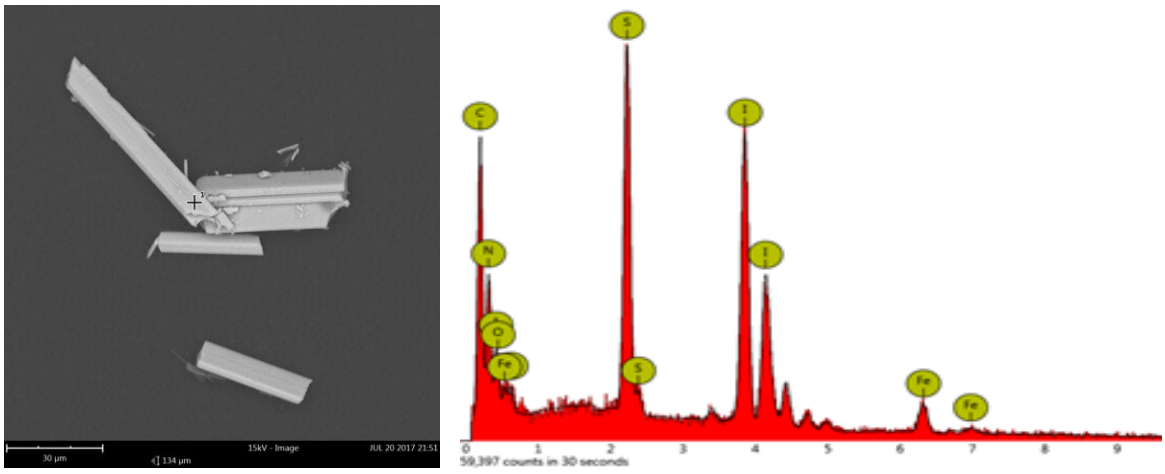

Figure S6. [Fe**L**$_2$]I_2 – x2000 magnification SEM micrograph of complex **5** (right) with an EDS spectrum (left).

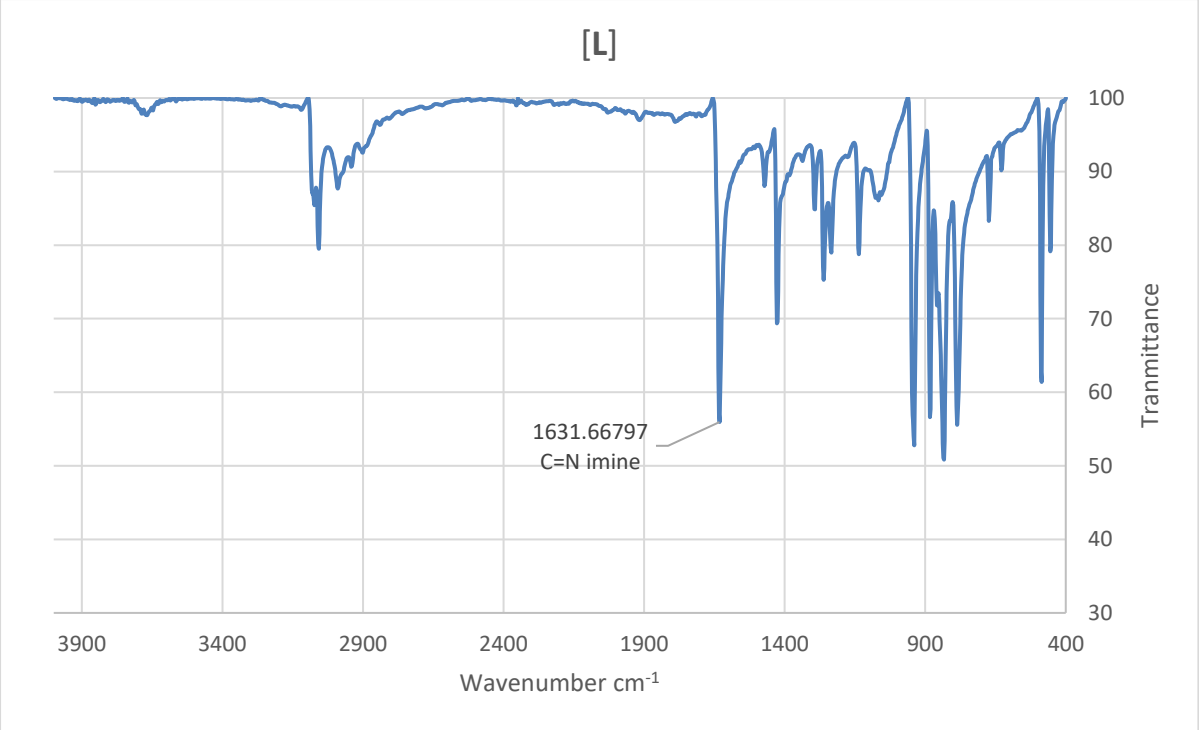

Figure S7. FT-IR spectrum of ligand [**L**].

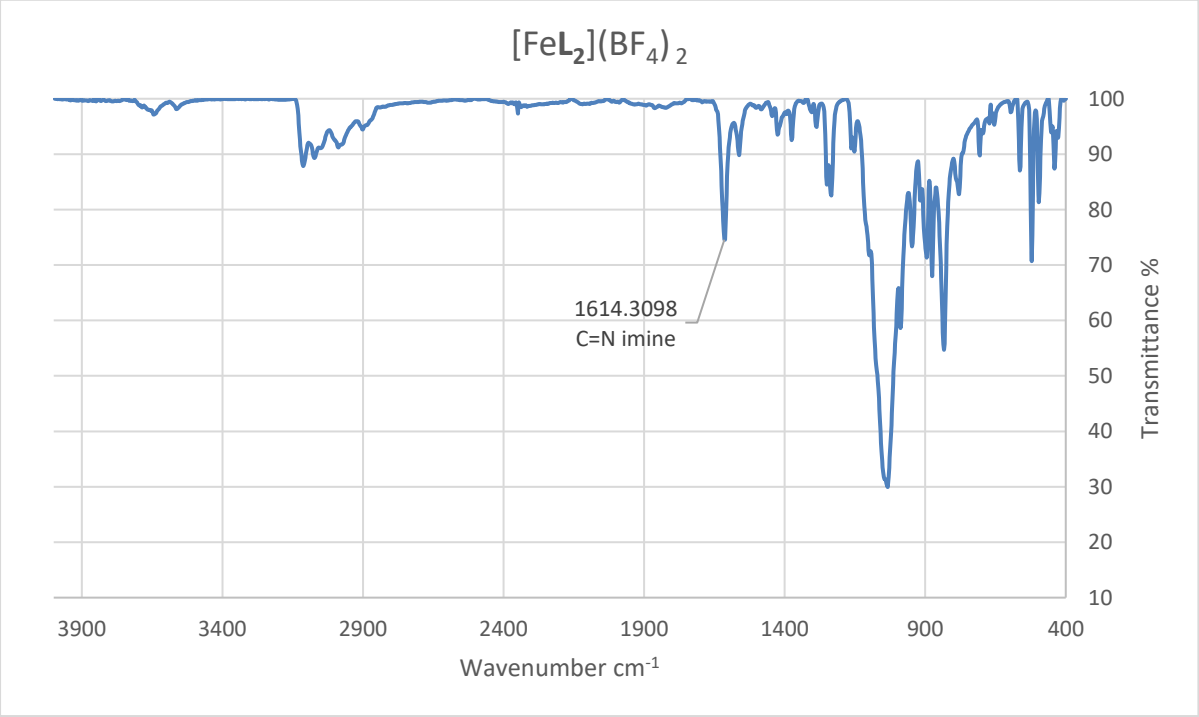

Figure S8. FT-IR spectrum of complex **1** [Fe**L**$_2$](BF$_4$)$_2$.

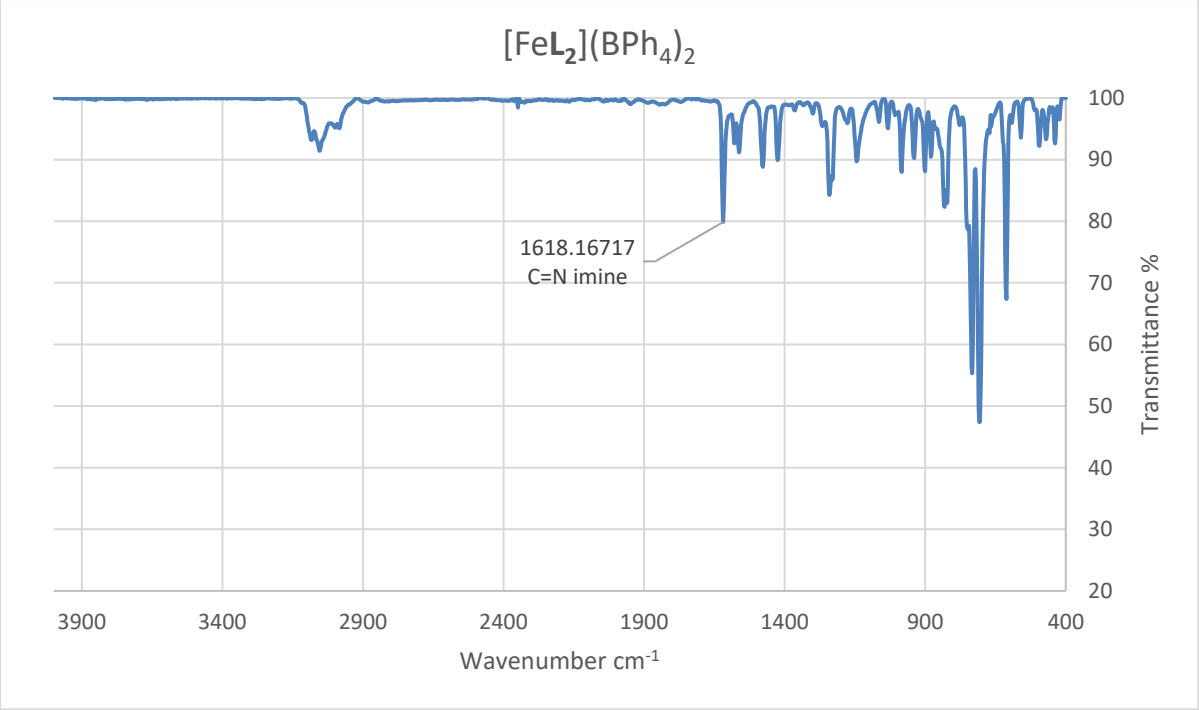

Figure S9. FT-IR spectrum of complex **2** [Fe**L**$_2$](BP$_4$)$_2$.

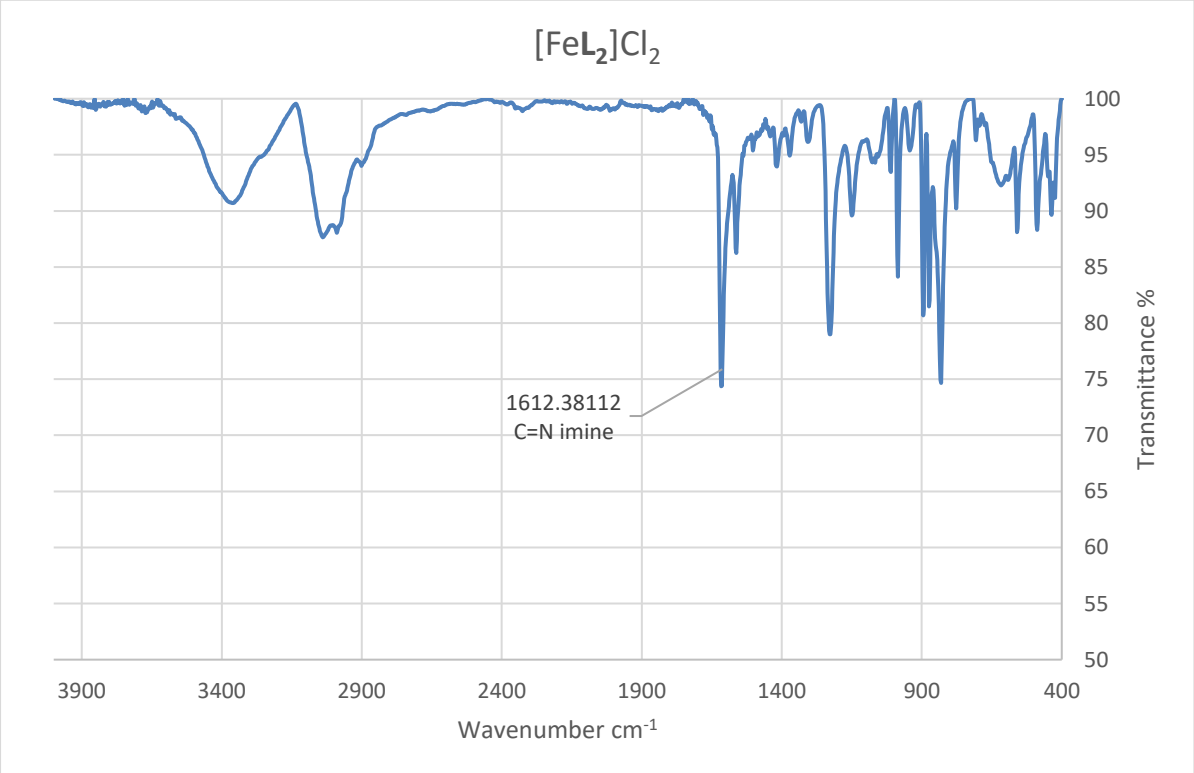

Figure S10. FT-IR spectrum of complex **3** [Fe**L**$_2$]Cl$_2$.

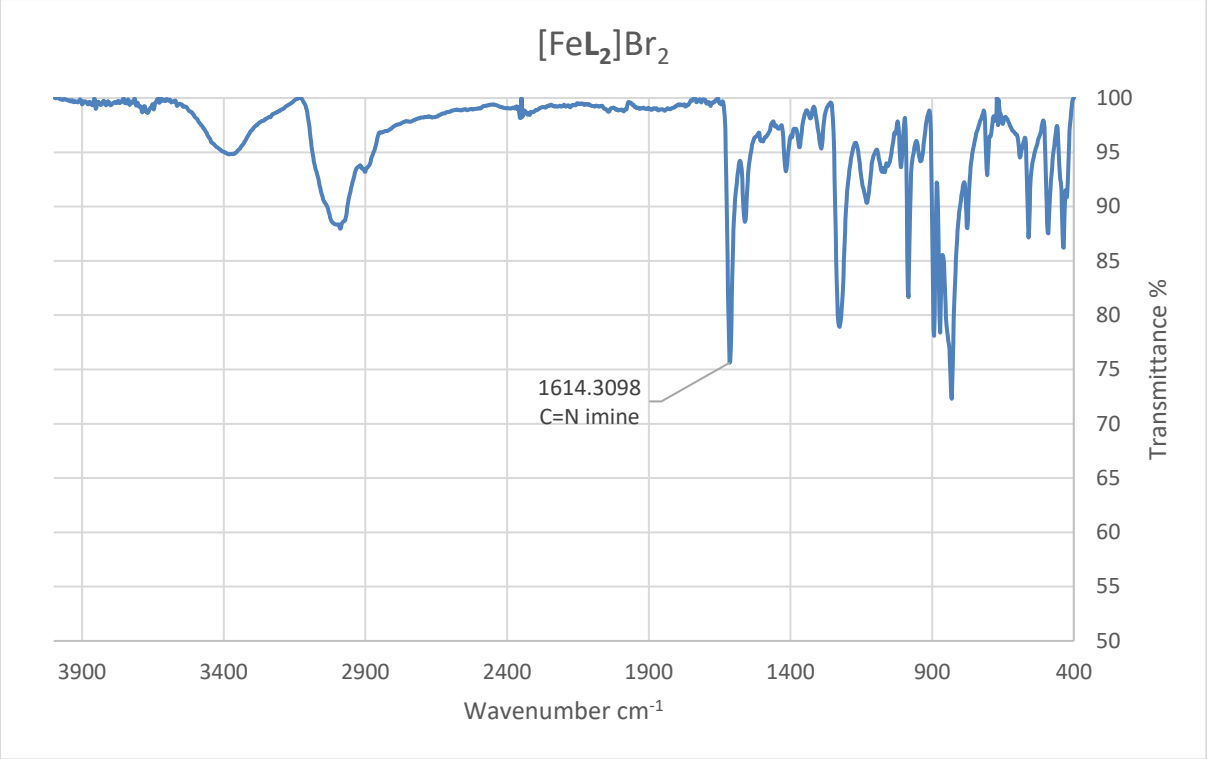

Figure S11. FT-IR spectrum of complex **4** [Fe**L**$_2$]Br$_2$.

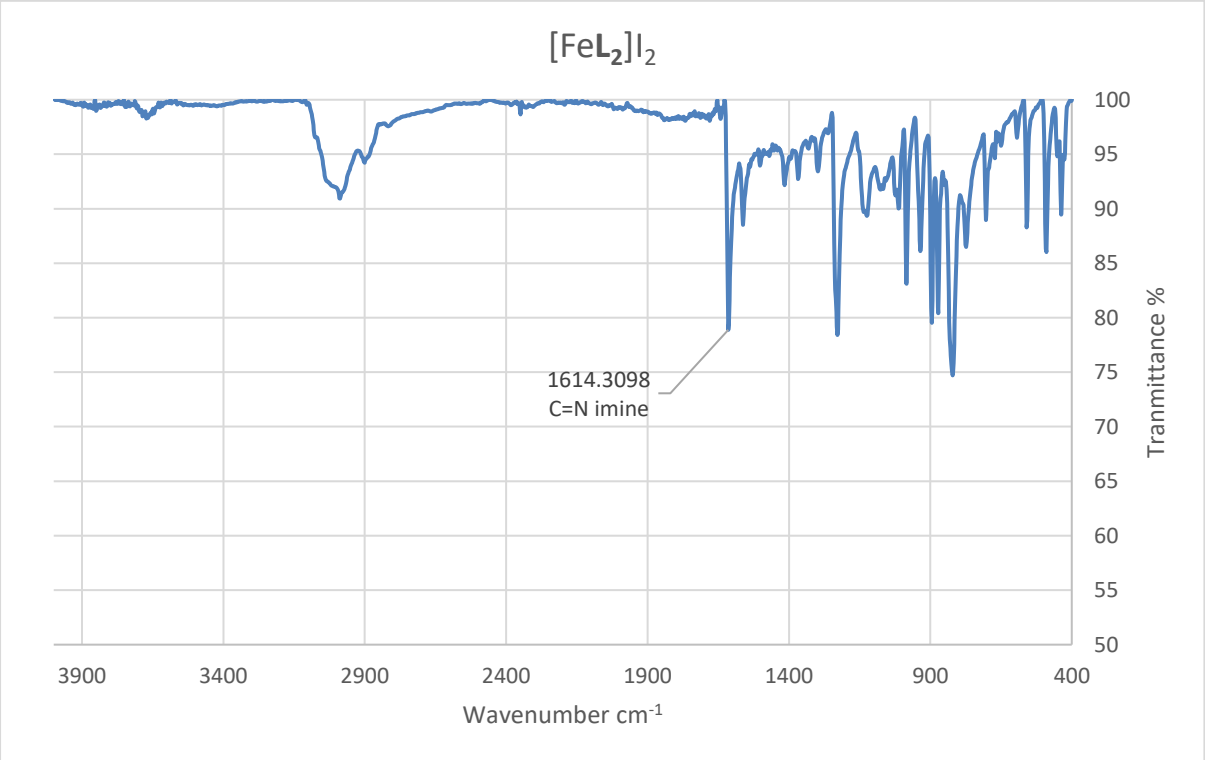

Figure S12. FT-IR spectrum of complex **5** [Fe**L**$_2$]I$_2$.

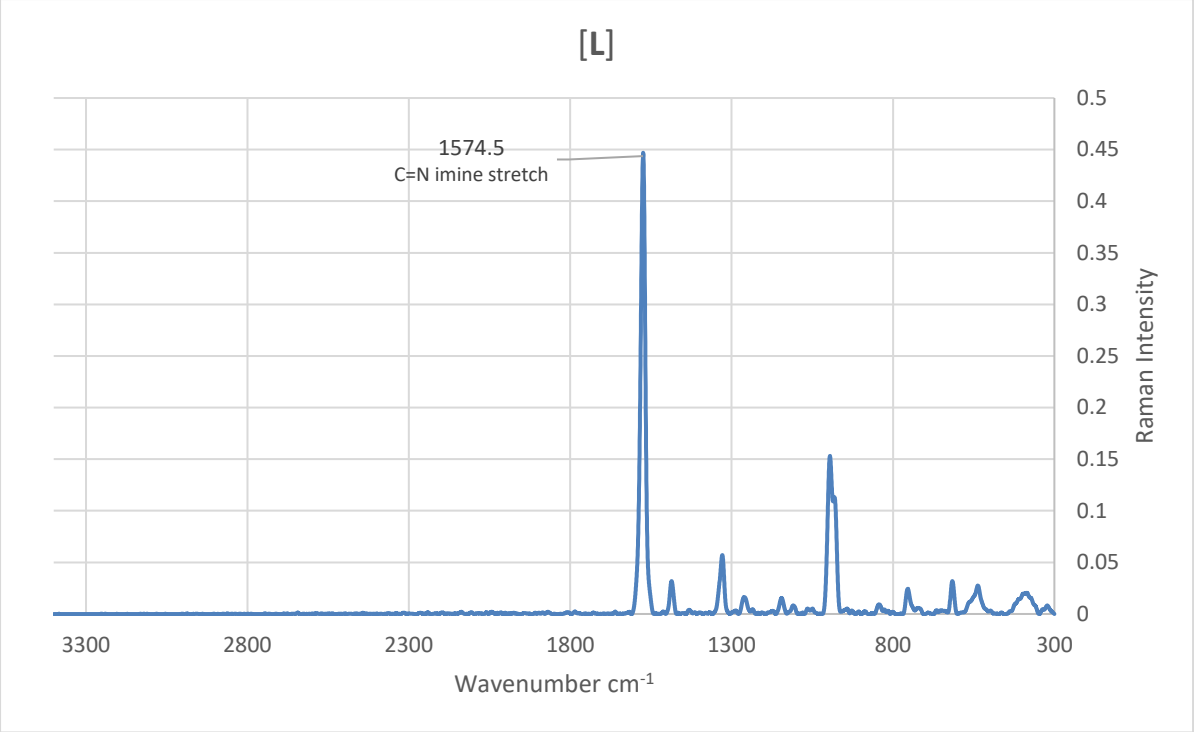

Figure S13. Raman Spectrum of Ligand [**L**].

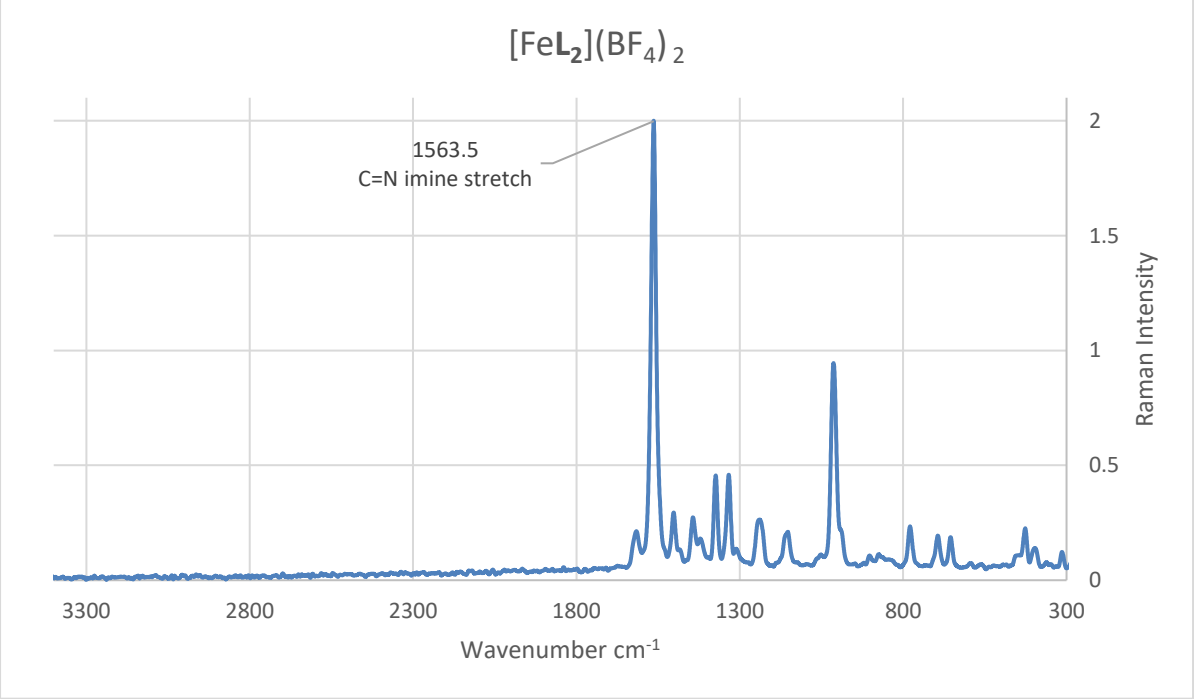

Figure S14. Raman Spectrum of Complex **1** $[FeL_2](BF_4)_2$.

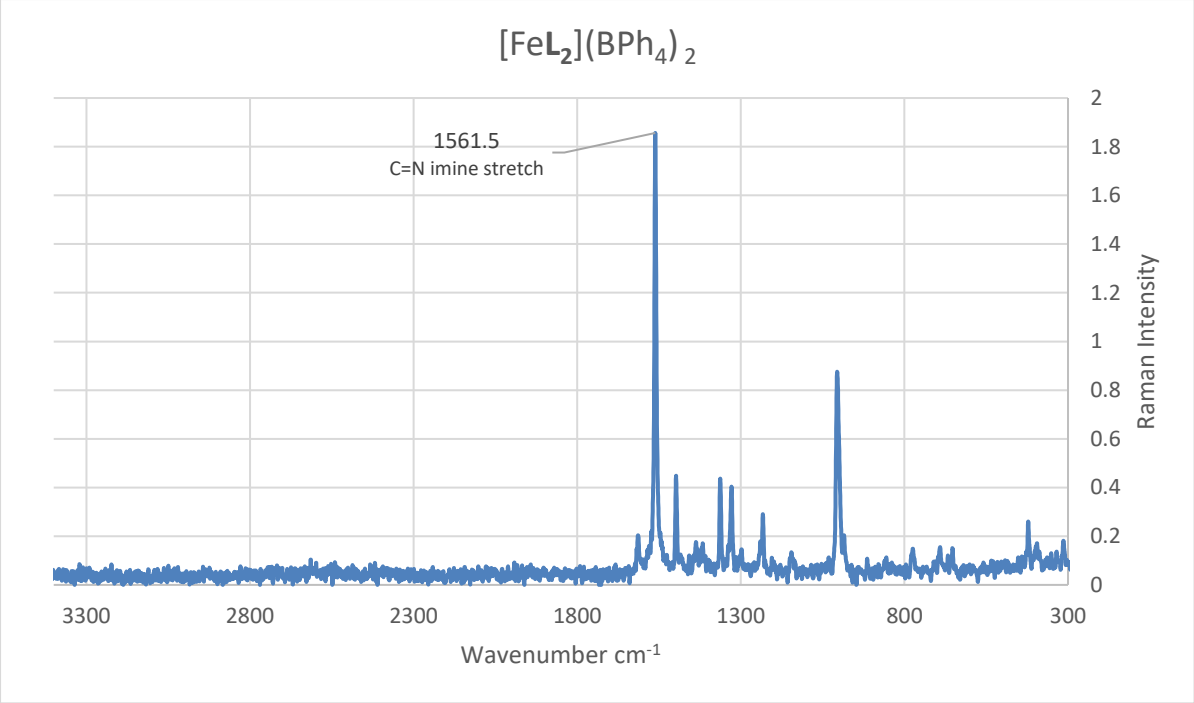

Figure S15. Raman Spectrum of Complex **2** [Fe**L**$_2$](BPh$_4$) $_2$.

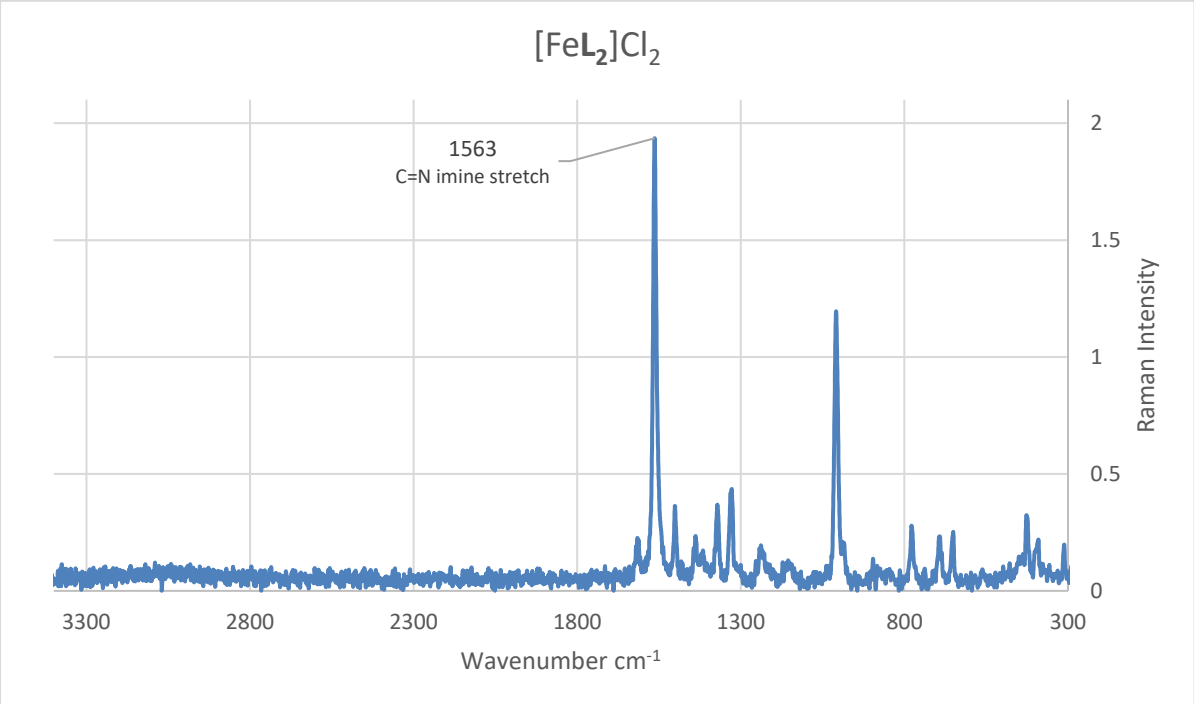

Figure S16. Raman Spectrum of Complex **3** [Fe**L**$_2$]Cl$_2$.

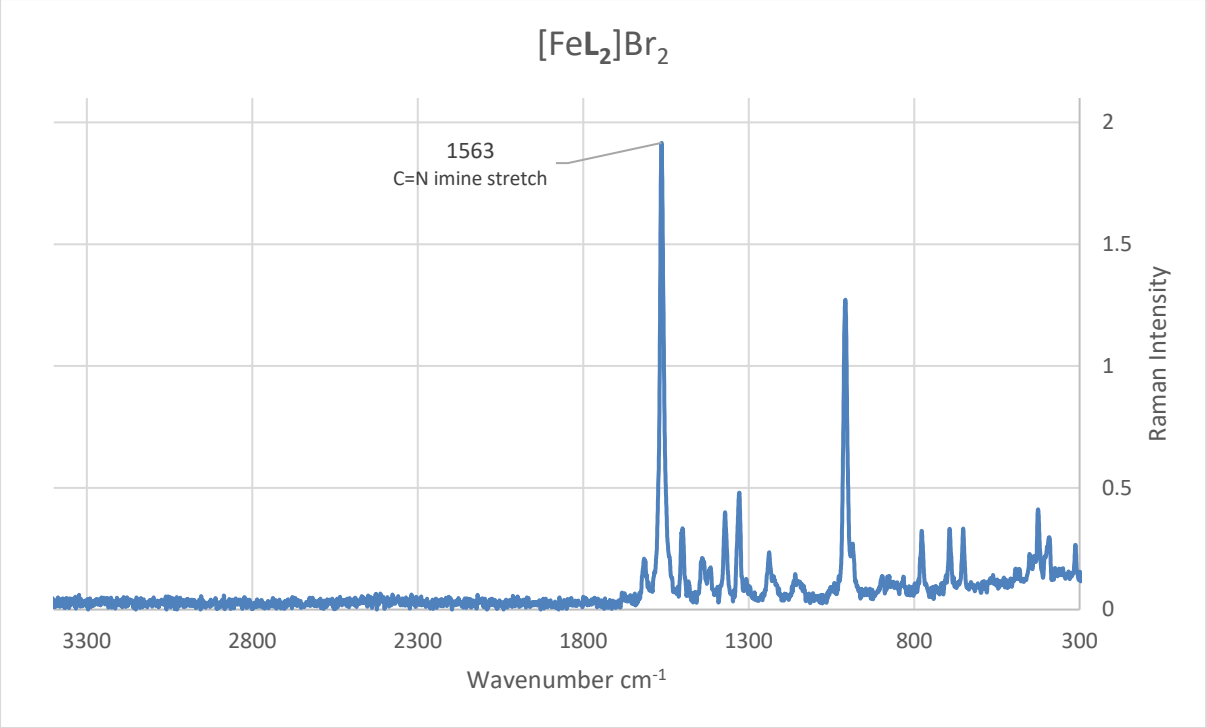

Figure S17. Raman Spectrum of Complex **4** [Fe**L**$_2$]Br$_2$.

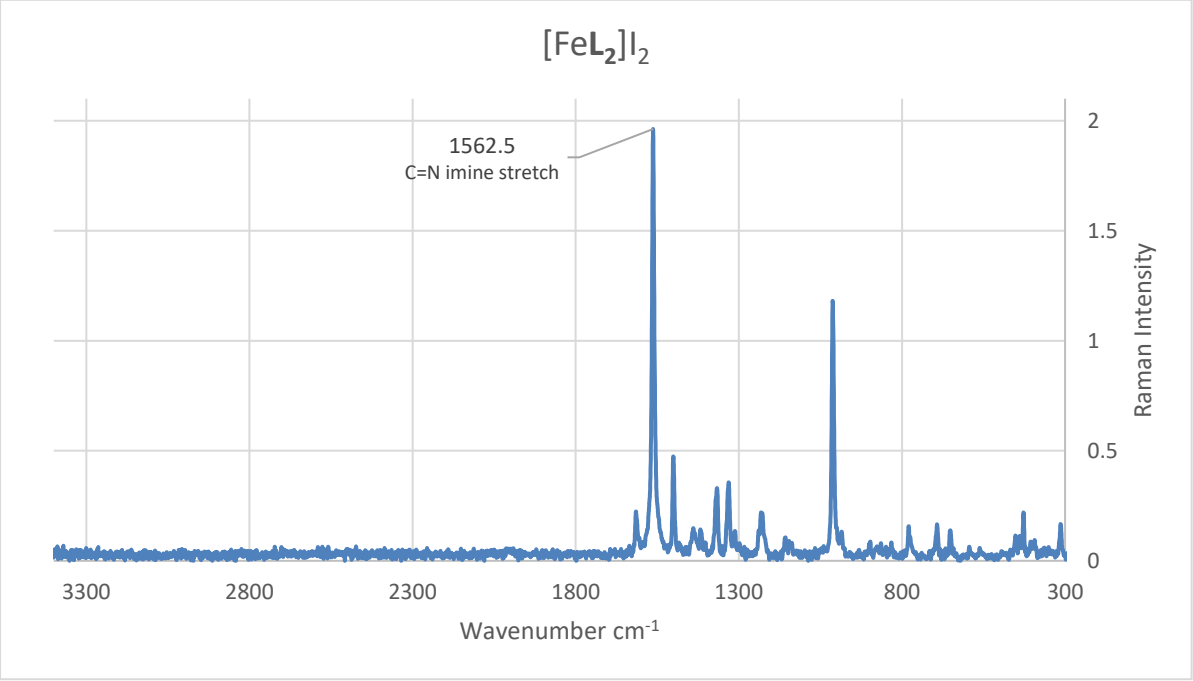

Figure S18. Raman Spectrum of Complex **5** [Fe**L**$_2$]I$_2$.

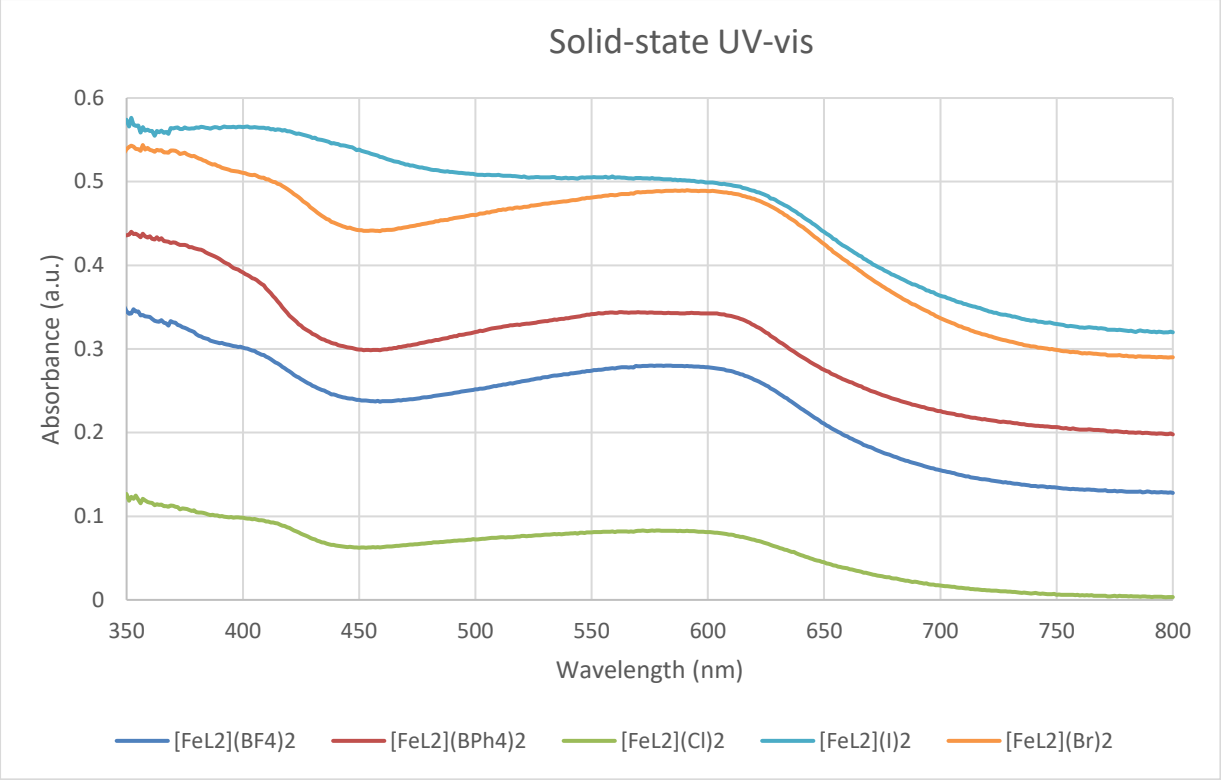

Figure 19. Solid-state UV-Vis spectrum complexes **1**-**5**.

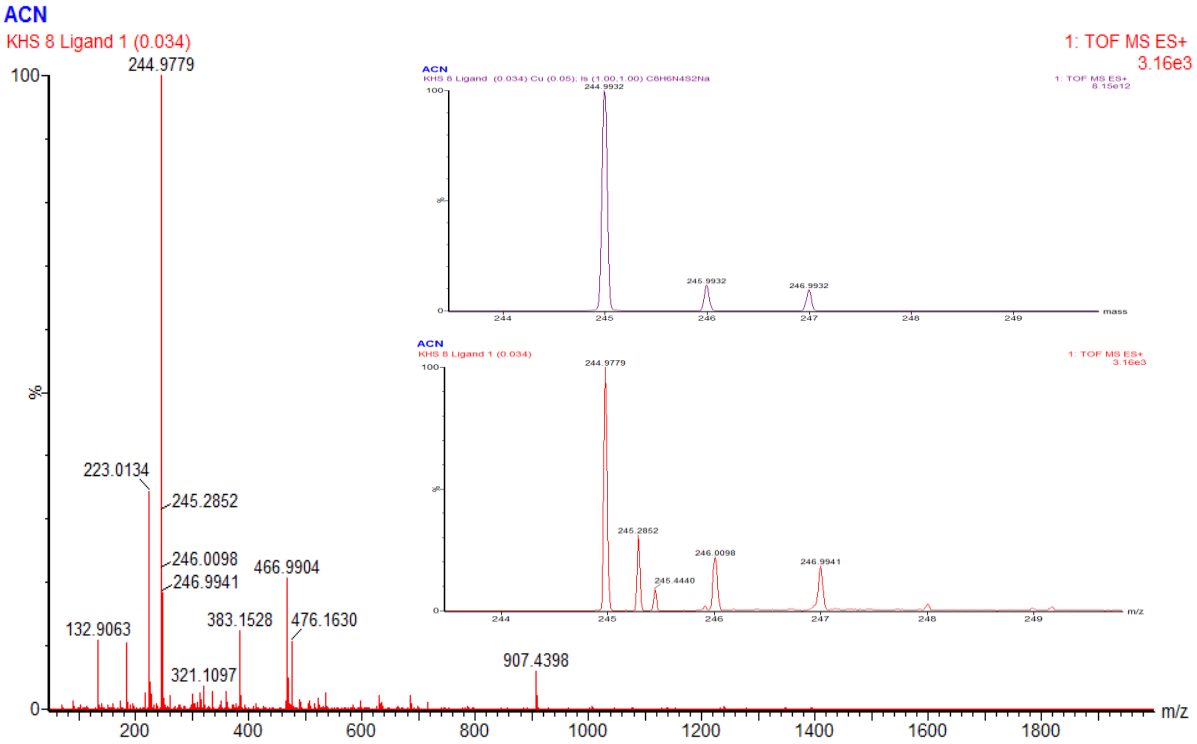

Figure S20. [**L** + Na^+] HR ESI-MS calculated m/z 244.9932 upper insert, experimental m/z 244.9779 lower insert.

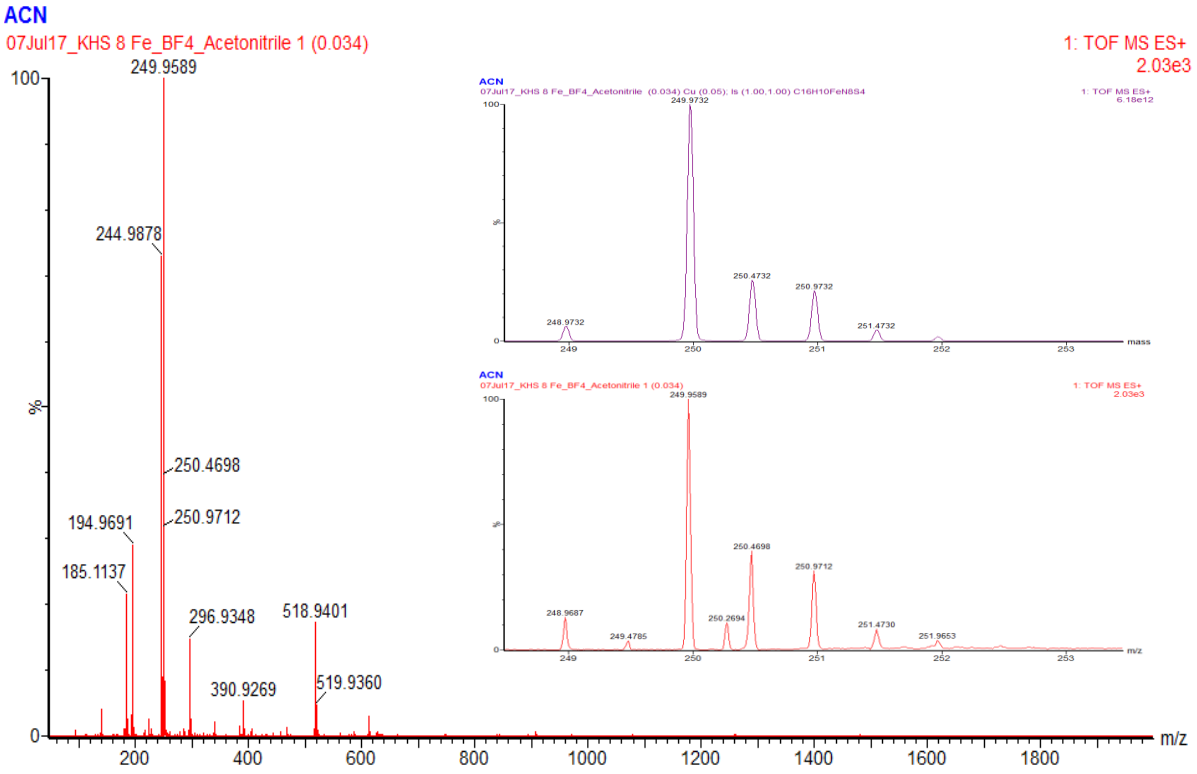

Figure S21. $[FeL_2]^{2+}$ HR ESI-MS calculated m/z 249.9732 upper insert, experimental m/z 249.9589 lower insert.

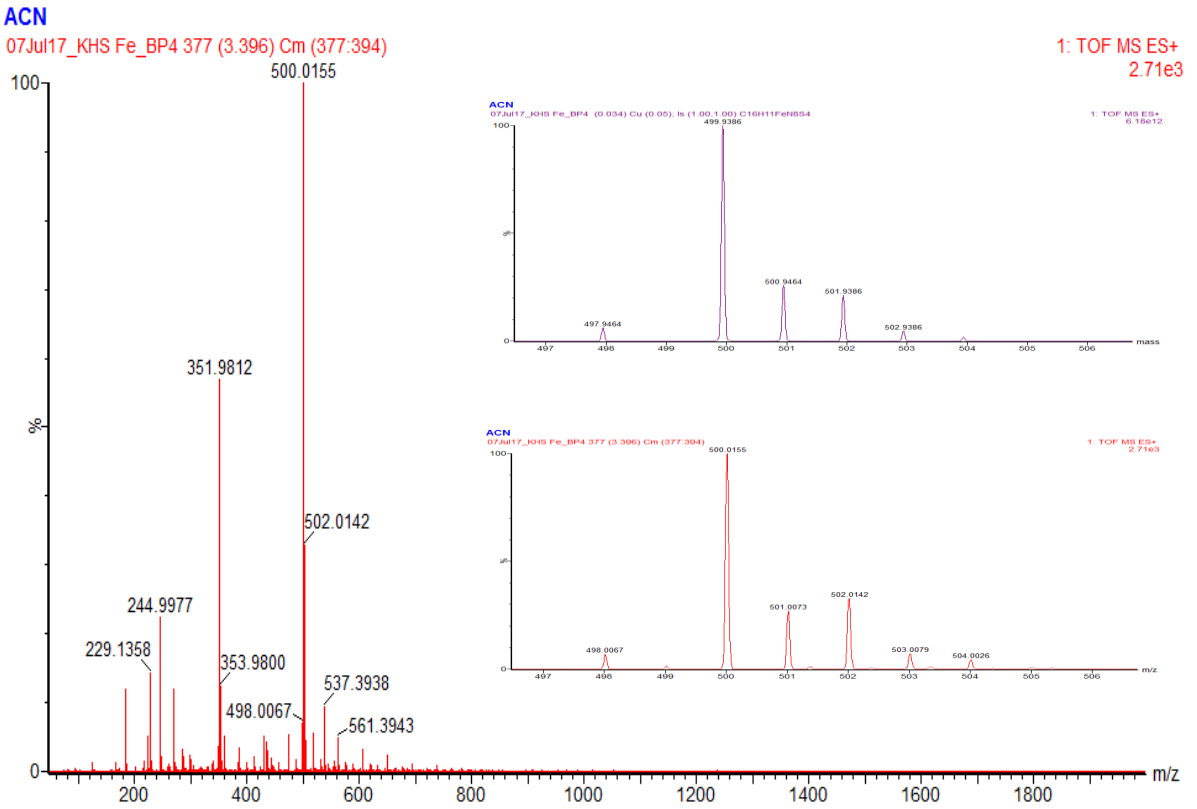

Figure S22. $[FeL_2]^{+}$ HR ESI-MS calculated m/z 500.0155 upper insert, experimental m/z 499.9386 lower insert.

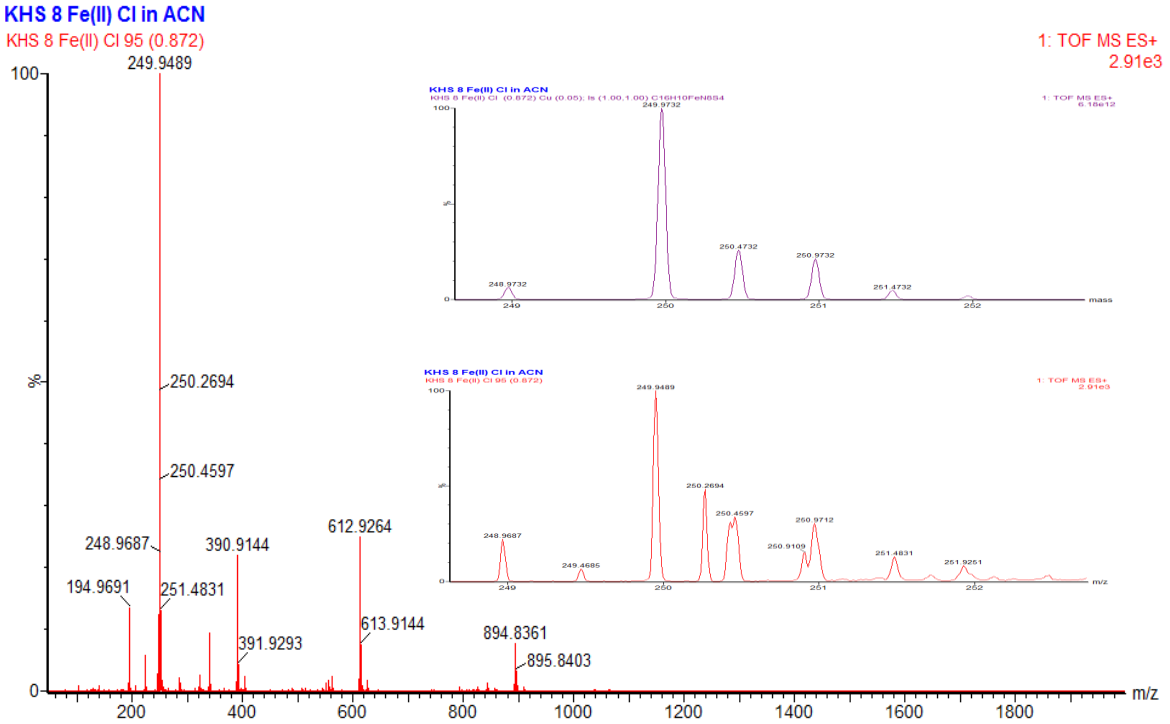

Figure S23. $[FeL_2]^{2+}$ HR ESI-MS calculated m/z 249.9489 upper insert, experimental m/z 249.9732 lower insert.

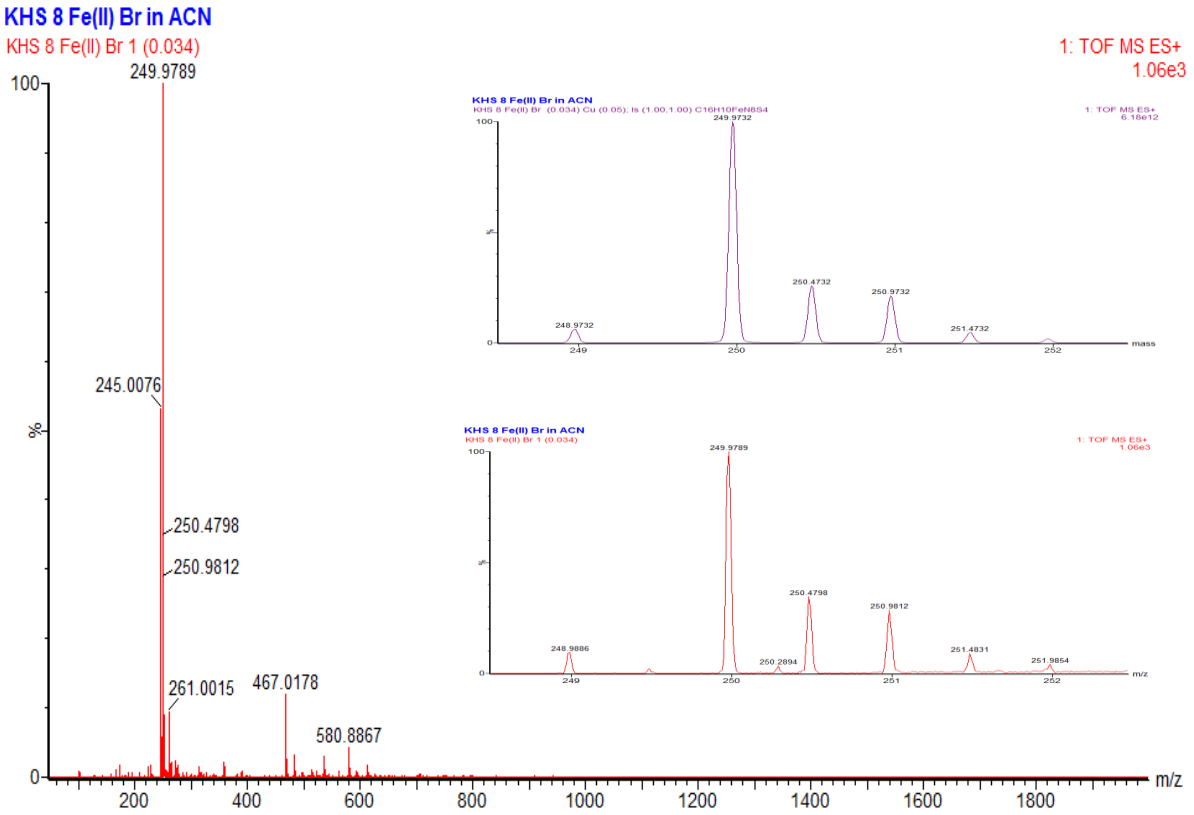

Figure S24. $[FeL_2]^{2+}$ HR ESI-MS calculated m/z 249.9789 upper insert, experimental m/z 249.9732 lower insert.

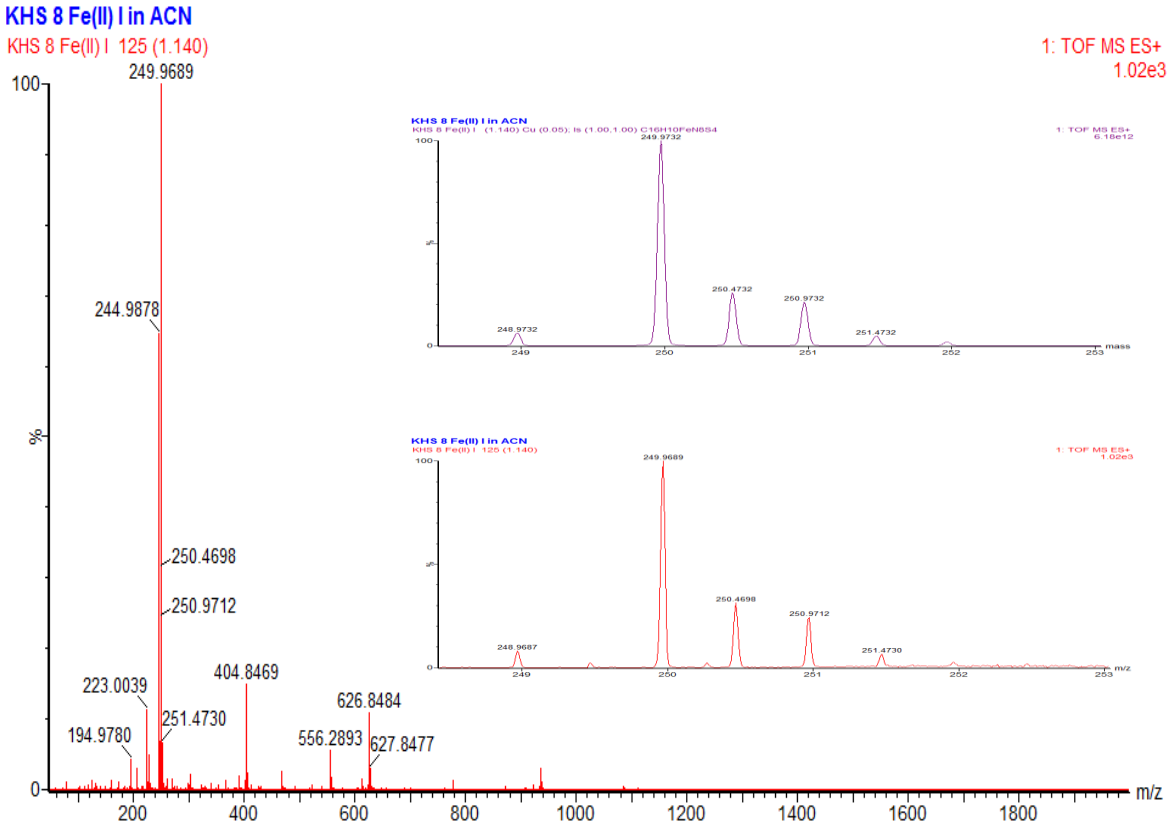

Figure S25. $[FeL_2]^{2+}$ HR ESI-MS calculated m/z 249.9689 upper insert, experimental m/z 249.9732 lower insert.

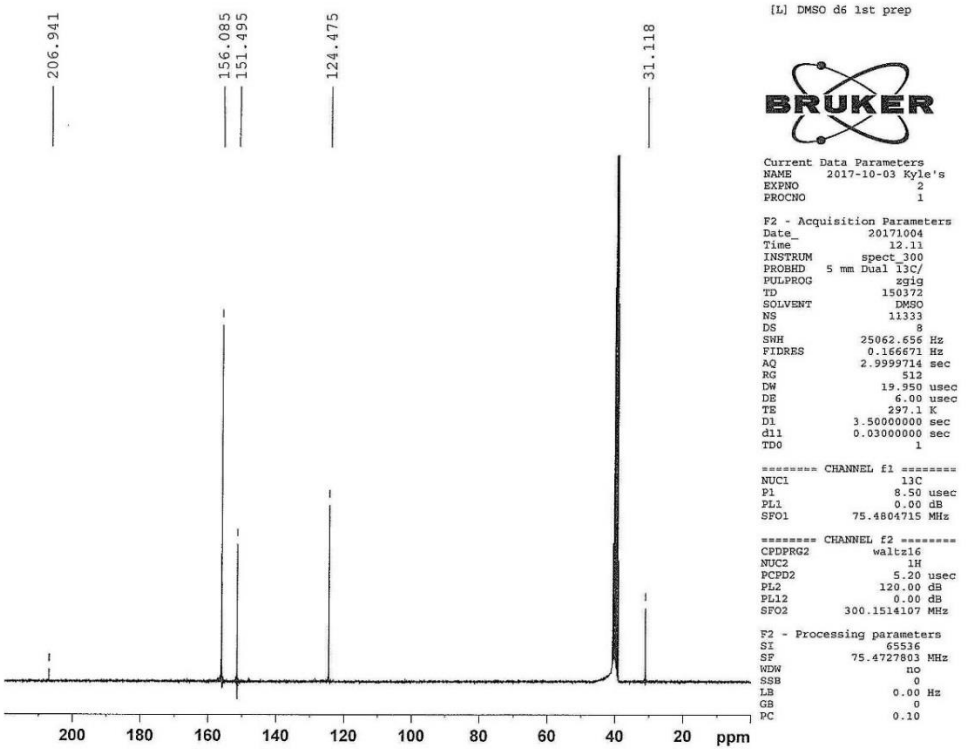

Figure S26. ^{1}H – NMR spectrum of ligand **L** in DMSO.

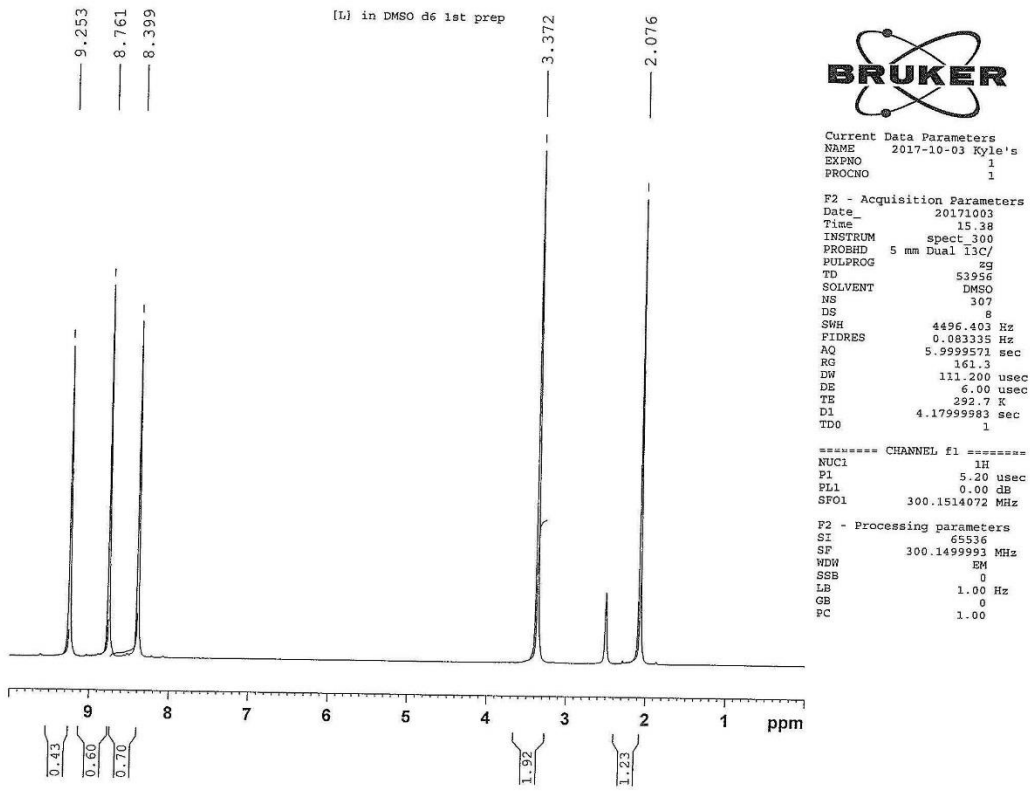

Figure S27. ^{13}C – NMR spectrum of ligand **L** in DMSO.

Chapter 6 – Conclusions and Future Work

Several new metallo-supramolecular assemblies incorporating Schiff-base ligands were designed and successfully synthesised as a result of the research conducted as part of this thesis. Several characterisation techniques were employed throughout to characterise each ligand and metal complex, such as, FT-IR, NMR, SEM-EDS, solid-state UV-Vis, Raman, HR ESI-MS. Structural characterisations were conducted by performing single crystal X-ray diffraction experiments using the MX1 beamline at the Australian Synchrotron and a Bruker kappa-II CCD diffractometer at the Mark Wainwright Analytical Centre at University of New South Wales (UNSW). Magnetic studies were conducted on a Quantum Design Versalab Measurement System with a Vibrating Sample Magnetometer (VSM) attachment at University of Sydney (USYD).

With regards to chapter two, a flexible N_4O_2-donor Schiff-base ligand containing a bis-(aminopropylamino)ethane backbone incorporating a 4-(diethylamino)salicylaldehyde functional moiety was employed. As a result, four new mononuclear complexes were designed, synthesised and characterised unambiguously. The four new metal complexes containing Fe^{III}, Co^{III}, Ni^{II} and Cu^{II} metal centres were characterised unambiguously. Structural characterisations revealed that complexes [Fe**L**]ClO_4, [Co**L**]NO_3 and [Ni**L**] exist in a 1:1 (L:M) stoichiometric ratio, while the Cu^{II} complex ([Cu_3**L**$_2$]) was shown to exhibit an unexpected 3:2 (L:M) stoichiometric ratio. Further work will be conducted to improve the synthetic methods in order to obtain a larger amount of the Ni^{II} complex. Focus will also be made to synthesise a Mn^{III} complex. Magnetic studies will be performed on complexes containing Fe^{III}, Co^{III} and Mn^{III} to determine whether the implementation of an electron donating group can induce SCO, this will extend the research efforts communicated by Kannappan et. al.[1] who reported the design and synthesis of a similar Fe^{III} complex incorporating salicylaldehyde that remained in low spin. The results of which will be published in a relevant journal.

In chapter three, the design, synthesis and characterisation of three new mononuclear N_4O_2-donor Schiff-base complexes (similar to those presented in chapter two) were reported. Each complex incorporated a ligand flexible design achieved by utilising a bis-(aminopropylamino)ethane backbone reacted with a bromo-salicylaldehyde functional moiety. The structural characterisation of new Fe^{III}, Mn^{III} and Co^{III} complexes revealed that all

complexes persist in a predictable 1:1 (L:M) stoichiometric ratio. Following the trend of chapter two, magnetic studies will be employed on the three new complexes in order to determine the effect that an electron withdrawing bromine moiety has on the SCO behaviours, more in depth structural characterisations will also be conducted. The results of which will be published in a relevant journal.

Concerning chapter four, a mononuclear Fe^{II} complex was synthesised, the ligand incorporated the scarcely studied thiazolyimine functional moiety. Magnetic studies of the complex revealed that a high-temperature spin-transition ($T_{1/2}$ of 375 ↓ and 370 ↑at 4 $Kmin^{-1}$), with a 5 K hysteresis between warming and cooling modes. Structural characterisations revealed two isomers (Λ and Δ) of opposite handedness (left and right) and that the isomers are linked by hydrogen bonding along the *b*-axis. Variable temperature X-ray photoelectron spectroscopy (XPS) will be conducted in future studies. The results obtained in this chapter are currently being prepared for manuscript submission, any XPS results will also be added.

Lastly, chapter 5 reported the design and synthesis of a semi-flexible N_3-donor thiazolyimine Schiff-base ligand with a hydrazine (N-N) backbone. The synthesis and characterisations of five new Fe^{II} complexes $[Fe\mathbf{L_2}](A)_2$ (A = BF_4^-, BPh_4^-, Cl^-, Br^- & I^-) were reported. Structural characterisation proved difficult in all complexes in this chapter, this was due mainly to the disorder in the asymmetric unit with respect to the two hydrazine nitrogens. As a result, some atoms had to be left isotropic. More single crystal experiments will be conducted to obtain better structural data of all complexes, especially the ligand **L** and complex **3** $[Fe\mathbf{L_2}](Cl)_2$ in which no usable data could be acquired. Magnetic studies will be employed on all complexes in order to observe any SCO behaviour that may be exhibited.

6.1 References

1. R. Kannappan, S. Tanase, I. Mutikainen, U. Turpeinen and J. Reedijk, *Polyhedron.,* **2006**, *25*, 1646.

Appendices

Chapter 2 Appendices

Crystal CIF Files

The crystallographic data in CIF format for chapter 2 has been deposited at the Cambridge Crystallographic Data Centre with CCDC numbers 1519783–1519786. It is available free of charge from the Cambridge Crystallographic Data Centre, 12 Union Road, Cambridge CB2 1 EZ, UK; fax: (+44) 1223-336-033; or email: deposit@ccdc.cam.ac.uk. Specific refinement details and crystallographic data for each structure are presented below.

Chapter 3 Appendices

Crystals Refinement Data for Complex **1** [Fe**L**]BF_4

Table 1 Crystal data and structure refinement for FL258_a.

Identification code	FL258_a
Empirical formula	$C_{24}H_{32}BBr_2F_4FeN_4O_3$
Formula weight	727.01
Temperature/K	293(2)
Crystal system	triclinic
Space group	P-1
a/Å	8.4000(17)
b/Å	9.6900(19)
c/Å	17.570(4)
α/°	84.86(3)
β/°	81.27(3)
γ/°	81.42(3)
Volume/$Å^3$	1394.5(5)
Z	2
$\rho_{calc}g/cm^3$	1.731
μ/mm^{-1}	3.467
F(000)	730.0
Radiation	MoKα (λ = 0.71073)
2Θ range for data collection/°	2.35 to 52.744
Index ranges	-10 ≤ h ≤ 10, -12 ≤ k ≤ 12, -21 ≤ l ≤ 21
Reflections collected	33760
Independent reflections	5377 [R_{int} = 0.0655, R_{sigma} = 0.0431]
Data/restraints/parameters	5377/0/354
Goodness-of-fit on F^2	1.162
Final R indexes [I>=2σ (I)]	R_1 = 0.0531, wR_2 = 0.1434
Final R indexes [all data]	R_1 = 0.0629, wR_2 = 0.1471
Largest diff. peak/hole / e $Å^{-3}$	1.34/-1.21

Table 2 Fractional Atomic Coordinates ($\times10^4$) and Equivalent Isotropic Displacement Parameters ($Å^2\times10^3$) for FL258_a. U_{eq} is defined as 1/3 of of the trace of the orthogonalised U_{IJ} tensor.

Atom	*x*	*y*	*z*	U(eq)
Br1	-2362.8(8)	2772.7(6)	4312.0(4)	15.52(17)
Br2	7260.1(8)	7463.1(7)	5596.1(4)	14.31(17)
Fe03	2917(1)	7592.9(8)	2346.5(5)	7.0(2)
O1	1158(5)	6801(4)	2089(2)	10.1(9)
O2	4667(5)	8454(4)	2550(2)	10.0(9)
N1	1631(6)	8044(5)	3347(3)	8.6(10)
N2	2053(7)	9462(5)	1854(3)	13.1(11)

N3	4073(7)	7203(6)	1288(3)	11.6(11)
N4	3962(6)	5788(5)	2758(3)	8.9(10)
C1	-1264(7)	4045(6)	3605(4)	10.2(12)
C2	-636(7)	5094(6)	3902(4)	10.1(12)
C3	198(7)	6050(6)	3398(3)	8.3(12)
C4	343(7)	5958(6)	2589(3)	7.3(11)
C5	-419(8)	4934(6)	2314(4)	11.0(12)
C6	-1202(7)	3984(6)	2820(4)	12.1(12)
C7	636(7)	7246(7)	3715(4)	10.8(12)
C8	1585(8)	9432(6)	3643(4)	14.5(13)
C9	892(8)	10558(7)	3086(4)	17.2(14)
C10	1941(8)	10707(6)	2308(4)	16.2(14)
C11	3064(9)	9656(7)	1098(4)	17.7(14)
C12	3363(9)	8276(7)	729(4)	17.3(14)
C13	4133(9)	5779(7)	1030(4)	16.7(14)
C14	4937(9)	4651(7)	1552(4)	17.7(14)
C15	4001(8)	4488(6)	2366(4)	12.3(13)
C16	4779(7)	5706(6)	3325(3)	8.9(12)
C17	5225(7)	6899(6)	3644(3)	7.0(11)
C18	5841(7)	6699(6)	4357(3)	7.5(11)
C19	6446(8)	7756(6)	4630(4)	12.4(13)
C20	6534(8)	9035(6)	4199(4)	12.0(13)
C21	5982(7)	9237(6)	3492(4)	11.3(12)
C22	5264(7)	8198(6)	3208(3)	9.2(12)
F1	6673(7)	10976(6)	1024(3)	47.5(15)
F2	8477(5)	9757(5)	1765(3)	31.0(11)
F3	6876(6)	11716(4)	2178(3)	29.2(10)
F4	8920(7)	11912(7)	1206(3)	55.0(16)
B1	7715(10)	11117(9)	1532(5)	21.1(17)
O1S	7487(6)	7447(6)	1164(3)	28.0(12)
C1S	8231(10)	6494(9)	-62(5)	29.2(18)
C2S	8728(9)	7353(8)	511(4)	20.5(15)

Table 3 Anisotropic Displacement Parameters ($Å^2×10^3$) for FL258_a. The Anisotropic displacement factor exponent takes the form: $-2\pi^2[h^2a^{*2}U_{11}+2hka^*b^*U_{12}+\ldots]$.

Atom	**U_{11}**	**U_{22}**	**U_{33}**	**U_{23}**	**U_{13}**	**U_{12}**
Br1	14.8(3)	8.7(3)	20.6(3)	4.8(2)	2.6(2)	-2.4(2)
Br2	18.1(3)	15.7(3)	11.1(3)	-1.9(2)	-7.7(2)	-2.5(2)
Fe03	7.8(4)	5.2(4)	7.6(4)	-1.2(3)	-1.1(3)	0.7(3)
O1	11(2)	12(2)	8(2)	0.3(17)	-1.0(16)	-0.9(17)
O2	11(2)	8(2)	9(2)	2.5(16)	-1.7(17)	0.4(17)
N1	8(2)	5(2)	13(3)	-1(2)	-6(2)	2.5(19)
N2	12(3)	11(3)	17(3)	0(2)	-6(2)	1(2)
N3	13(3)	12(3)	9(2)	-2(2)	-2(2)	-2(2)

N4	10(3)	6(2)	11(2)	-4(2)	-1(2)	0.4(19)
C1	7(3)	5(3)	16(3)	3(2)	-1(2)	3(2)
C2	7(3)	13(3)	10(3)	-1(2)	-2(2)	0(2)
C3	6(3)	7(3)	12(3)	-4(2)	-2(2)	2(2)
C4	5(3)	6(3)	9(3)	0(2)	-1(2)	3(2)
C5	13(3)	10(3)	11(3)	-4(2)	-2(2)	-1(2)
C6	9(3)	8(3)	19(3)	-5(2)	-2(2)	2(2)
C7	9(3)	14(3)	9(3)	-5(2)	-1(2)	1(2)
C8	15(3)	9(3)	22(3)	-8(3)	-6(3)	0(2)
C9	18(3)	11(3)	23(4)	-10(3)	-7(3)	7(3)
C10	21(4)	4(3)	23(4)	-3(3)	-9(3)	5(2)
C11	24(4)	14(3)	14(3)	8(3)	-6(3)	-2(3)
C12	21(4)	22(4)	9(3)	1(3)	-4(3)	-4(3)
C13	23(4)	16(3)	13(3)	-6(3)	-4(3)	-3(3)
C14	24(4)	11(3)	18(3)	-11(3)	-3(3)	2(3)
C15	17(3)	5(3)	16(3)	-6(2)	-4(3)	1(2)
C16	10(3)	4(3)	13(3)	2(2)	-3(2)	0(2)
C17	2(3)	5(3)	13(3)	-4(2)	1(2)	2(2)
C18	6(3)	6(3)	9(3)	0(2)	2(2)	1(2)
C19	14(3)	9(3)	12(3)	-3(2)	3(2)	2(2)
C20	12(3)	6(3)	20(3)	-4(2)	-5(3)	-1(2)
C21	7(3)	9(3)	18(3)	2(2)	-1(2)	-3(2)
C22	5(3)	11(3)	11(3)	2(2)	0(2)	2(2)
F1	57(4)	58(4)	38(3)	15(3)	-35(3)	-23(3)
F2	19(2)	28(2)	48(3)	-16(2)	-13(2)	6.2(18)
F3	40(3)	15(2)	29(2)	0.9(18)	3(2)	-0.1(19)
F4	48(3)	65(4)	53(4)	7(3)	11(3)	-35(3)
B1	20(4)	29(4)	16(4)	1(3)	-1(3)	-9(3)
O1S	21(3)	36(3)	30(3)	-17(2)	3(2)	-10(2)
C1S	30(4)	32(4)	26(4)	-11(3)	5(3)	-8(3)
C2S	17(3)	23(4)	22(4)	2(3)	-3(3)	-7(3)

Table 4 Bond Lengths for FL258_a.

Atom	**Atom**	**Length/Å**	**Atom**	**Atom**	**Length/Å**
Br1	C1	1.906(6)	C3	C7	1.447(8)
Br2	C19	1.907(7)	C4	C5	1.413(8)
Fe03	O1	1.892(4)	C5	C6	1.388(9)
Fe03	O2	1.888(4)	C8	C9	1.510(9)
Fe03	N1	1.967(5)	C9	C10	1.517(10)
Fe03	N2	2.018(5)	C11	C12	1.509(10)
Fe03	N3	2.004(5)	C13	C14	1.510(9)
Fe03	N4	1.965(5)	C14	C15	1.531(9)
O1	C4	1.327(7)	C16	C17	1.449(8)
O2	C22	1.318(7)	C17	C18	1.413(8)

N1	C7	1.286(8)	C17	C22	1.416(8)
N1	C8	1.479(8)	C18	C19	1.361(9)
N2	C10	1.489(8)	C19	C20	1.399(9)
N2	C11	1.478(9)	C20	C21	1.379(9)
N3	C12	1.488(8)	C21	C22	1.410(9)
N3	C13	1.482(8)	F1	B1	1.370(9)
N4	C15	1.483(7)	F2	B1	1.431(10)
N4	C16	1.283(8)	F3	B1	1.369(10)
C1	C2	1.385(9)	F4	B1	1.387(9)
C1	C6	1.378(9)	O1S	C2S	1.428(9)
C2	C3	1.412(9)	C1S	C2S	1.505(10)
C3	C4	1.417(8)			

Table 5 Bond Angles for FL258_a.

Atom	**Atom**	**Atom**	**Angle/˚**	**Atom**	**Atom**	**Atom**	**Angle/˚**
O1	Fe03	N1	89.5(2)	C4	C3	C7	121.0(5)
O1	Fe03	N2	90.2(2)	O1	C4	C3	122.2(5)
O1	Fe03	N3	87.6(2)	O1	C4	C5	119.6(5)
O1	Fe03	N4	93.1(2)	C5	C4	C3	118.2(5)
O2	Fe03	O1	176.63(18)	C6	C5	C4	121.1(6)
O2	Fe03	N1	92.4(2)	C1	C6	C5	119.9(6)
O2	Fe03	N2	86.9(2)	N1	C7	C3	123.8(6)
O2	Fe03	N3	90.4(2)	N1	C8	C9	109.7(5)
O2	Fe03	N4	89.6(2)	C8	C9	C10	114.7(6)
N1	Fe03	N2	91.2(2)	N2	C10	C9	112.2(5)
N1	Fe03	N3	175.5(2)	N2	C11	C12	107.7(5)
N3	Fe03	N2	85.4(2)	N3	C12	C11	107.2(5)
N4	Fe03	N1	93.5(2)	N3	C13	C14	112.9(5)
N4	Fe03	N2	174.3(2)	C13	C14	C15	114.2(6)
N4	Fe03	N3	90.1(2)	N4	C15	C14	108.7(5)
C4	O1	Fe03	121.8(4)	N4	C16	C17	124.5(5)
C22	O2	Fe03	121.9(4)	C18	C17	C16	118.8(5)
C7	N1	Fe03	122.2(4)	C18	C17	C22	119.7(5)
C7	N1	C8	117.0(5)	C22	C17	C16	121.0(5)
C8	N1	Fe03	120.2(4)	C19	C18	C17	120.3(6)
C10	N2	Fe03	117.1(4)	C18	C19	Br2	119.5(5)
C11	N2	Fe03	107.3(4)	C18	C19	C20	120.9(6)
C11	N2	C10	110.5(5)	C20	C19	Br2	119.5(5)
C12	N3	Fe03	108.0(4)	C21	C20	C19	119.6(6)
C13	N3	Fe03	117.6(4)	C20	C21	C22	121.2(6)
C13	N3	C12	110.6(5)	O2	C22	C17	122.2(6)
C15	N4	Fe03	120.9(4)	O2	C22	C21	119.7(5)
C16	N4	Fe03	121.6(4)	C21	C22	C17	118.1(5)
C16	N4	C15	117.1(5)	F1	B1	F2	108.6(7)

C2	C1	Br1	118.2(5)	F1	B1	F4	112.2(7)
C6	C1	Br1	120.7(5)	F3	B1	F1	110.3(7)
C6	C1	C2	121.0(6)	F3	B1	F2	108.0(6)
C1	C2	C3	119.9(6)	F3	B1	F4	109.3(7)
C2	C3	C4	119.7(5)	F4	B1	F2	108.4(7)
C2	C3	C7	118.5(5)	O1S	C2S	C1S	108.4(6)

Table 6 Hydrogen Bonds for FL258_a.

D	H	A	d(D-H)/Å	d(H-A)/Å	d(D-A)/Å	D-H-A/°
N3	H3	O1S	0.98	1.91	2.886(8)	171.7
O1S	H1S	F2	0.82	2.05	2.839(7)	160.4

Table 7 Hydrogen Atom Coordinates (Å×10^4) and Isotropic Displacement Parameters (Å^2×10^3) for FL258_a.

Atom	*x*	*y*	*z*	U(eq)
H2	952	9396	1753	16
H3	5203	7357	1280	14
H2A	-765	5167	4432	12
H5	-395	4895	1786	13
H6	-1684	3307	2630	15
H7	171	7449	4214	13
H8A	2675	9578	3704	17
H8B	917	9478	4144	17
H9A	725	11446	3321	21
H9B	-164	10358	3003	21
H10A	1489	11531	2017	19
H10B	3025	10838	2388	19
H11A	4089	9942	1166	21
H11B	2506	10373	773	21
H12A	2350	8034	613	21
H12B	4109	8334	251	21
H13A	4723	5734	512	20
H13B	3033	5602	1011	20
H14A	6014	4860	1592	21
H14B	5067	3766	1316	21
H15A	2901	4323	2337	15
H15B	4529	3696	2654	15
H16	5107	4821	3546	11
H18	5834	5842	4640	9
H20	6962	9745	4389	14
H21	6086	10073	3197	14
H1S	7630	8055	1433	42
H1SA	9086	6368	-490	44

H1SB	7259	6968	-245	44
H1SC	8030	5598	182	44
H2SA	9753	6916	670	25
H2SB	8868	8282	279	25

Crystal structure determination of [FL258_a]

Crystal Data for $C_{24}H_{32}BBr_2F_4FeN_4O_3$ (*M* =727.01 g/mol): triclinic, space group P-1 (no. 2), a = 8.4000(17) Å, b = 9.6900(19) Å, c = 17.570(4) Å, α = 84.86(3)°, β = 81.27(3)°, γ = 81.42(3)°, V = 1394.5(5) Å^3, Z = 2, T = 293(2) K, μ(MoKα) = 3.467 mm^{-1}, *Dcalc* = 1.731 g/cm^3, 33760 reflections measured (2.35° ≤ 2Θ ≤ 52.744°), 5377 unique (R_{int} = 0.0655, R_{sigma} = 0.0431) which were used in all calculations. The final R_1 was 0.0531 (I > 2σ(I)) and wR_2 was 0.1471 (all data).

Refinement model description

Number of restraints - 0, number of constraints - unknown.

Details:

1. Fixed Uiso
 At 1.2 times of:
  All C(H) groups, All C(H,H) groups, All N(H) groups
 At 1.5 times of:
  All C(H,H,H) groups, All O(H) groups
2.a Ternary CH refined with riding coordinates:
 N2(H2), N3(H3)
2.b Secondary CH2 refined with riding coordinates:
 C8(H8A,H8B), C9(H9A,H9B), C10(H10A,H10B), C11(H11A,H11B), C12(H12A,H12B),
 C13(H13A,H13B), C14(H14A,H14B), C15(H15A,H15B), C2S(H2SA,H2SB)
2.c Aromatic/amide H refined with riding coordinates:
 C2(H2A), C5(H5), C6(H6), C7(H7), C16(H16), C18(H18), C20(H20), C21(H21)
2.d Idealised Me refined as rotating group:
 C1S(H1SA,H1SB,H1SC)
2.e Idealised tetrahedral OH refined as rotating group:
 O1S(H1S)

Crystal Refinement Data for Complex **2** [Co**L**]PF_6

Table 1 Crystal data and structure refinement for p222_a.

Identification code	p222_a
Empirical formula	$C_{24}H_{32}Br_2CoF_6N_4O_3P$
Formula weight	788.25
Temperature/K	293(2)
Crystal system	orthorhombic
Space group	Pbcn
a/Å	8.3720(17)
b/Å	27.664(6)
c/Å	13.458(3)
α/°	90
β/°	90
γ/°	90
Volume/Å^3	3116.9(11)
Z	4
ρ_{calc}g/cm^3	1.680
μ/mm^{-1}	3.234
F(000)	1576.0
Radiation	MoKα (λ = 0.71073)
2Θ range for data collection/°	4.222 to 60.99
Index ranges	-11 ≤ h ≤ 11, -39 ≤ k ≤ 39, -18 ≤ l ≤ 18
Reflections collected	53278
Independent reflections	4585 [R_{int} = 0.0749, R_{sigma} = 0.0292]
Data/restraints/parameters	4585/178/203
Goodness-of-fit on F^2	1.237
Final R indexes [I>=2σ (I)]	R_1 = 0.0913, wR_2 = 0.2213
Final R indexes [all data]	R_1 = 0.0946, wR_2 = 0.2225
Largest diff. peak/hole / e Å^{-3}	2.90/-1.94

Table 2 Fractional Atomic Coordinates (×10^4) and Equivalent Isotropic Displacement Parameters (Å^2×10^3) for p222_a. U_{eq} is defined as 1/3 of of the trace of the orthogonalised U_{IJ} tensor.

Atom	*x*	*y*	*z*	U(eq)
Br01	10714.5(9)	7451.4(3)	5040.9(7)	33.6(2)
Co02	5000	5881.3(4)	2500	10.8(2)
P003	0	4635.7(9)	2500	23.3(5)
O004	6579(5)	5833.5(15)	3498(3)	14.2(8)
F005	-1041(6)	4640(3)	1505(4)	57.6(18)
N006	6229(6)	6359.0(18)	1785(4)	14.4(9)
N007	6130(6)	5359.8(17)	1768(4)	13.6(9)

F008	1597(6)	4643(3)	1862(4)	59.0(18)
F009	0	5208(3)	2500	69(3)
C00A	7457(7)	6198(2)	3803(4)	14.6(10)
C00B	5246(7)	4908(2)	1964(4)	15.7(11)
C00C	9376(8)	6945(3)	4543(5)	23.6(12)
C00D	6305(7)	6339(2)	695(4)	17(1)
C00E	7220(7)	6649.7(19)	2223(4)	14.1(10)
C00F	7712(7)	6624(2)	3242(5)	17.3(10)
C00G	7239(8)	5887(2)	401(5)	20.1(11)
C00H	8698(7)	6995(2)	3620(5)	18.8(11)
C00I	9148(8)	6525(3)	5119(5)	25.5(13)
C00J	6378(8)	5422(2)	674(4)	18.8(11)
C00K	8215(8)	6163(2)	4738(5)	21.2(12)
F00L	0	4070(3)	2500	122(5)
O1	4383(16)	3107(6)	2443(14)	59(5)
C0AA	1620(20)	2965(7)	2637(16)	45(4)
C3A	2889(19)	3311(6)	2437(13)	35(3)

Table 3 Anisotropic Displacement Parameters ($Å^2×10^3$) for p222_a. The Anisotropic displacement factor exponent takes the form: $-2π^2[h^2a^{*2}U_{11}+2hka^*b^*U_{12}+…]$.

Atom	U_{11}	U_{22}	U_{33}	U_{23}	U_{13}	U_{12}
Br01	22.0(3)	33.2(4)	45.5(4)	-23.0(3)	-5.1(3)	-7.0(3)
Co02	10.5(4)	10.3(4)	11.5(4)	0	-0.8(4)	0
P003	14(1)	19.7(10)	36.3(13)	0	-3.8(9)	0
O004	12.8(18)	16.1(18)	13.8(17)	1.1(14)	-2.3(14)	-1.4(15)
F005	24(2)	110(5)	39(3)	-30(3)	-9(2)	7(3)
N006	14(2)	14(2)	14(2)	-0.5(16)	2.2(17)	-1.8(17)
N007	13(2)	14(2)	14(2)	-2.3(16)	0.4(17)	-0.5(17)
F008	16(2)	120(6)	41(3)	-23(3)	0(2)	-3(3)
F009	123(9)	27(3)	58(5)	0	4(6)	0
C00A	11(2)	18(2)	15(2)	-4.4(18)	-1.4(18)	-0.2(19)
C00B	13(2)	14(2)	20(3)	-3.1(19)	-1(2)	0.2(19)
C00C	12(2)	30(3)	29(3)	-17(2)	-2(2)	0(2)
C00D	17(3)	21(3)	13(2)	1(2)	1.2(19)	-2(2)
C00E	16(2)	9(2)	18(2)	-2.5(17)	3.7(19)	-1.9(18)
C00F	15(2)	18(2)	19(2)	-3.7(19)	1(2)	-2(2)
C00G	18(3)	24(3)	17(3)	0(2)	5(2)	0(2)
C00H	15(3)	19(3)	22(3)	-9(2)	4(2)	-3(2)
C00I	15(3)	36(3)	25(3)	-13(2)	-8(2)	3(2)
C00J	20(3)	21(3)	15(2)	-5(2)	1(2)	0(2)
C00K	19(3)	25(3)	20(3)	-1(2)	-5(2)	1(2)
F00L	95(9)	18(3)	252(17)	0	-20(10)	0
O1	42(6)	76(10)	59(12)	38(10)	0(7)	1(6)
C0AA	47(8)	38(8)	50(11)	-6(8)	2(8)	11(7)

C3A	47(7)	28(6)	30(7)	-6(6)	-2(6)	13(6)

Table 4 Bond Lengths for p222_a.

Atom	Atom	Length/Å	Atom	Atom	Length/Å
Br01	C00C	1.915(6)	N006	C00E	1.298(7)
Co02	O004[1]	1.889(4)	N007	C00B	1.476(7)
Co02	O004	1.889(4)	N007	C00J	1.496(8)
Co02	N006[1]	1.932(5)	C00A	C00F	1.415(8)
Co02	N006	1.932(5)	C00A	C00K	1.412(8)
Co02	N007	1.987(5)	C00B	C00B[1]	1.499(12)
Co02	N007[1]	1.987(5)	C00C	C00H	1.373(9)
P003	F005[2]	1.598(5)	C00C	C00I	1.410(11)
P003	F005	1.598(5)	C00D	C00G	1.526(9)
P003	F008	1.589(5)	C00E	C00F	1.434(9)
P003	F008[2]	1.589(5)	C00F	C00H	1.412(8)
P003	F009	1.584(8)	C00G	C00J	1.521(9)
P003	F00L	1.565(9)	C00I	C00K	1.369(9)
O004	C00A	1.313(7)	O1	C3A	1.372(15)
N006	C00D	1.469(7)	C0AA	C3A	1.45(3)

[1]1-X,+Y,1/2-Z; [2]-X,+Y,1/2-Z

Table 5 Bond Angles for p222_a.

Atom	Atom	Atom	Angle/˚	Atom	Atom	Atom	Angle/˚
O004[1]	Co02	O004	172.0(3)	F00L	P003	F008[2]	90.7(3)
O004[1]	Co02	N006	93.8(2)	F00L	P003	F009	180.0
O004[1]	Co02	N006[1]	91.7(2)	C00A	O004	Co02	124.0(4)
O004	Co02	N006	91.7(2)	C00D	N006	Co02	119.6(4)
O004	Co02	N006[1]	93.8(2)	C00E	N006	Co02	122.5(4)
O004	Co02	N007[1]	85.97(19)	C00E	N006	C00D	116.7(5)
O004	Co02	N007	88.20(19)	C00B	N007	Co02	106.7(3)
O004[1]	Co02	N007	85.97(19)	C00B	N007	C00J	110.0(4)
O004[1]	Co02	N007[1]	88.20(19)	C00J	N007	Co02	118.1(4)
N006[1]	Co02	N006	93.7(3)	O004	C00A	C00F	123.9(5)
N006[1]	Co02	N007	176.0(2)	O004	C00A	C00K	118.5(6)
N006[1]	Co02	N007[1]	89.8(2)	C00K	C00A	C00F	117.6(5)
N006	Co02	N007	89.8(2)	N007	C00B	C00B[1]	108.1(4)
N006	Co02	N007[1]	176.0(2)	C00H	C00C	Br01	119.0(6)
N007[1]	Co02	N007	86.9(3)	C00H	C00C	C00I	121.6(6)
F005[2]	P003	F005	179.2(6)	C00I	C00C	Br01	119.4(5)
F008	P003	F005	90.3(3)	N006	C00D	C00G	108.2(5)
F008	P003	F005[2]	89.7(3)	N006	C00E	C00F	126.0(5)

F008[2]	P003	F005	89.7(3)	C00A	C00F	C00E	120.5(5)
F008[2]	P003	F005[2]	90.3(3)	C00H	C00F	C00A	120.1(6)
F008	P003	F008[2]	178.5(6)	C00H	C00F	C00E	118.4(6)
F009	P003	F005	89.6(3)	C00J	C00G	C00D	112.8(5)
F009	P003	F005[2]	89.6(3)	C00C	C00H	C00F	119.6(6)
F009	P003	F008	89.3(3)	C00K	C00I	C00C	118.3(6)
F009	P003	F008[2]	89.3(3)	N007	C00J	C00G	113.6(5)
F00L	P003	F005[2]	90.4(3)	C00I	C00K	C00A	122.7(6)
F00L	P003	F005	90.4(3)	O1	C3A	C0AA	113.2(14)
F00L	P003	F008	90.7(3)				

[1]1-X,+Y,1/2-Z; [2]-X,+Y,1/2-Z

Table 6 Hydrogen Atom Coordinates (Å×10[4]) and Isotropic Displacement Parameters (Å[2]×10[3]) for p222_a.

Atom	***x***	***y***	***z***	**U(eq)**
H007	7187.58	5325.01	2071.19	16
H00A	5920.67	4630.78	1826.9	19
H00B	4311.12	4889.48	1540.57	19
H00C	6831.84	6624.9	438.95	20
H00D	5234.8	6325.15	419.61	20
H00E	7652.2	6897.44	1840.93	17
H00F	7424.3	5892.04	-309.97	24
H00G	8271.08	5892.69	728.85	24
H00H	8885.75	7272.06	3246.38	23
H00I	9620.14	6493.77	5740.93	31
H00J	5347.1	5416.98	345.69	23
H00K	6991.47	5149.66	426.49	23
H00L	8073.59	5882.97	5109.47	25
H1	4533.01	2970.95	2975.88	88
H0AA	1580.62	2732.15	2109.14	67
H0AB	619.67	3132	2678.34	67
H0AC	1833.21	2803.62	3253.97	67
H3AA	2702.49	3458.72	1793.91	42
H3AB	2849.55	3564.93	2933.99	42

Table 7 Atomic Occupancy for p222_a.

Atom	***Occupancy***	**Atom**	***Occupancy***	**Atom**	***Occupancy***
O1	0.5	H1	0.5	C0AA	0.5
H0AA	0.5	H0AB	0.5	H0AC	0.5
C3A	0.5	H3AA	0.5	H3AB	0.5

Crystal structure determination of [p222_a]

Crystal Data for $C_{24}H_{32}Br_2CoF_6N_4O_3P$ (*M* =788.25 g/mol): orthorhombic, space group Pbcn (no. 60), *a* = 8.3720(17) Å, *b* = 27.664(6) Å, *c* = 13.458(3) Å, *V* = 3116.9(11) Å^3, *Z* = 4, *T* = 293(2) K, μ(MoKα) = 3.234 mm^{-1}, *Dcalc* = 1.680 g/cm^3, 53278 reflections measured (4.222° ≤ 2Θ ≤ 60.99°), 4585 unique (R_{int} = 0.0749, R_{sigma} = 0.0292) which were used in all calculations. The final R_1 was 0.0913 (I > 2σ(I)) and wR_2 was 0.2225 (all data).

Refinement model description

Number of restraints - 178, number of constraints - unknown.

Details:

1. Fixed Uiso
 At 1.2 times of:
  All C(H) groups, All C(H,H) groups, All N(H) groups
 At 1.5 times of:
  All C(H,H,H) groups, All O(H) groups
2. Restrained distances
 O1-C3A
 1.4 with sigma of 0.02
3. Uiso/Uaniso restraints and constraints
C0AA: within 1.7A with sigma of 0.04 and sigma for terminal atoms of 0.08
O1 ≈ C3A: within 1.7A with sigma of 0.04 and sigma for terminal atoms of
0.08
4. Rigid body (RIGU) restrains
 All non-hydrogen atoms
 with sigma for 1-2 distances of 0.004 and sigma for 1-3 distances of 0.004
5. Others
 Fixed Sof: O1(0.5) H1(0.5) C0AA(0.5) H0AA(0.5) H0AB(0.5) H0AC(0.5) C3A(0.5)
 H3AA(0.5) H3AB(0.5)
6.a Ternary CH refined with riding coordinates:
 N007(H007)
6.b Secondary CH2 refined with riding coordinates:
 C00B(H00A,H00B), C00D(H00C,H00D), C00G(H00F,H00G), C00J(H00J,H00K), C3A(H3AA,
 H3AB)
6.c Aromatic/amide H refined with riding coordinates:
 C00E(H00E), C00H(H00H), C00I(H00I), C00K(H00L)
6.d Idealised Me refined as rotating group:
 C0AA(H0AA,H0AB,H0AC)
6.e Idealised tetrahedral OH refined as rotating group:
 O1(H1)

Crystal Refinement Data for Complex **3** [Mn**L**]PF_6

Table 1 Crystal data and structure refinement for FL259_a.

Empirical formula	$C_{22}H_{26}Br_2F_6MnN_4O_2P$
Formula weight	738.20
Temperature/K	293(2)
Crystal system	orthorhombic
Space group	Pbcn
a/Å	13.205(3)
b/Å	26.477(5)
c/Å	8.7550(18)
α/°	90
β/°	90
γ/°	90
Volume/Å^3	3061.0(11)
Z	4
ρ_{calc}g/cm^3	1.602
μ/mm^{-1}	3.156
F(000)	1464.0
Radiation	MoKα (λ = 0.71073)
2Θ range for data collection/°	3.076 to 52.744
Index ranges	-15 ≤ h ≤ 15, -32 ≤ k ≤ 32, -9 ≤ l ≤ 9
Reflections collected	34657
Independent reflections	2920 [R_{int} = 0.0581, R_{sigma} = 0.0246]
Data/restraints/parameters	2920/36/200
Goodness-of-fit on F^2	1.073
Final R indexes [I>=2σ (I)]	R_1 = 0.0938, wR_2 = 0.2805
Final R indexes [all data]	R_1 = 0.1188, wR_2 = 0.3079
Largest diff. peak/hole / e Å^{-3}	1.41/-1.99

Table 2 Fractional Atomic Coordinates (×10^4) and Equivalent Isotropic Displacement Parameters (Å^2×10^3) for FL259_a. U_{eq} is defined as 1/3 of of the trace of the orthogonalised U_{IJ} tensor.

Atom	*x*	*y*	*z*	U(eq)
Br1	7424.6(11)	4979.1(4)	7989.9(14)	98.4(6)
Mn1	5000	6682.2(6)	2500	52.0(5)
O004	6018(4)	6692.3(19)	3997(6)	55.7(13)
N1	4220(4)	7267(3)	3565(8)	56.7(15)
N2	4207(5)	6196(3)	3807(8)	61.4(16)
C1	4439(6)	7737(3)	2681(11)	65(2)
C2	3094(6)	7208(3)	3790(11)	66(2)
C3	2821(6)	6735(4)	4665(12)	73(3)

C4	3087(6)	6241(4)	3869(12)	72(2)
C5	4608(6)	5906(3)	4793(11)	67(2)
C6	5680(6)	5899(3)	5218(10)	61.9(19)
C7	6016(7)	5507(4)	6151(11)	72(2)
C8	6985(8)	5515(3)	6696(10)	73(2)
C9	7639(7)	5897(4)	6339(11)	72(2)
C10	7305(6)	6295(4)	5402(10)	67(2)
C11	6324(6)	6302(3)	4853(9)	59.3(19)
P1	5000	7943(2)	7500	84.9(12)
F1	5472(16)	8415(8)	6470(40)	187(11)
F2	4165(12)	8273(11)	7000(20)	118(6)
F3	3945(11)	7945(10)	6534(19)	105(6)
F4	5483(13)	7856(9)	5859(17)	97(5)
F5	5446(15)	7603(8)	6420(20)	111(6)
F6	4221(19)	7438(9)	6970(20)	162(8)

Table 3 Anisotropic Displacement Parameters ($Å^2×10^3$) for FL259_a. The Anisotropic displacement factor exponent takes the form: $-2\pi^2[h^2a^{*2}U_{11}+2hka^*b^*U_{12}+\ldots]$.

Atom	**U_{11}**	**U_{22}**	**U_{33}**	**U_{23}**	**U_{13}**	**U_{12}**
Br1	139.0(12)	82.5(8)	73.7(9)	17.5(5)	5.4(6)	36.1(7)
Mn1	36.2(8)	53.6(9)	66.0(11)	0	4.7(7)	0
O004	42(3)	56(3)	69(3)	8(2)	3(2)	0(2)
N1	31(3)	66(4)	73(4)	-10(3)	0(3)	2(3)
N2	49(3)	58(4)	77(4)	-1(3)	6(3)	-5(3)
C1	53(5)	66(5)	77(6)	1(4)	-8(4)	6(4)
C2	35(4)	74(5)	87(6)	-12(4)	6(4)	0(3)
C3	39(4)	93(6)	88(7)	-14(5)	10(4)	-2(4)
C4	41(4)	88(6)	86(6)	4(5)	5(4)	-11(4)
C5	51(4)	66(5)	83(6)	7(4)	14(4)	-9(4)
C6	60(5)	60(4)	65(5)	8(4)	9(4)	1(4)
C7	64(5)	72(5)	78(6)	11(5)	17(4)	11(4)
C8	96(7)	62(5)	61(5)	7(4)	14(5)	19(5)
C9	63(5)	83(6)	71(6)	7(5)	0(4)	20(4)
C10	58(5)	67(5)	74(6)	12(4)	1(4)	10(4)
C11	56(4)	60(4)	62(5)	0(4)	10(3)	3(3)
P1	46.6(17)	140(4)	68(2)	0	5.8(15)	0
F1	130(13)	137(12)	300(30)	89(15)	110(18)	27(10)
F2	58(8)	198(16)	98(13)	49(12)	-3(7)	30(9)
F3	47(6)	195(19)	73(9)	26(11)	1(5)	26(8)
F4	64(8)	167(16)	60(7)	-9(8)	5(6)	-23(9)
F5	76(10)	140(12)	116(14)	-44(10)	-31(9)	38(10)
F6	166(17)	195(16)	125(15)	-25(13)	41(13)	-96(14)

Table 4 Bond Lengths for FL259_a.

Atom	Atom	Length/Å	Atom	Atom	Length/Å
Br1	C8	1.905(9)	C6	C11	1.402(11)
Mn1	O004[1]	1.878(5)	C7	C8	1.366(14)
Mn1	O004	1.878(5)	C8	C9	1.367(14)
Mn1	N1[1]	2.081(6)	C9	C10	1.406(12)
Mn1	N1	2.081(6)	C10	C11	1.381(12)
Mn1	N2[1]	2.016(7)	P1	F1[2]	1.662(17)
Mn1	N2	2.016(7)	P1	F1	1.662(17)
O004	C11	1.340(10)	P1	F2[2]	1.472(17)
N1	C1	1.494(12)	P1	F2	1.472(17)
N1	C2	1.507(9)	P1	F3[2]	1.630(15)
N2	C4	1.485(10)	P1	F3	1.630(15)
N2	C5	1.271(11)	P1	F4	1.589(15)
C1	C1[1]	1.514(17)	P1	F4[2]	1.589(15)
C2	C3	1.513(13)	P1	F5[2]	1.435(18)
C3	C4	1.522(13)	P1	F5	1.435(18)
C5	C6	1.464(13)	P1	F6[2]	1.750(18)
C6	C7	1.393(12)	P1	F6	1.750(18)

[1]1-X,+Y,1/2-Z; [2]1-X,+Y,3/2-Z

Table 5 Bond Angles for FL259_a.

Atom	Atom	Atom	Angle/˚	Atom	Atom	Atom	Angle/˚
O004	Mn1	O004[1]	178.4(3)	C10	C11	C6	118.7(8)
O004[1]	Mn1	N1	87.0(2)	F1	P1	F6[2]	119.9(11)
O004[1]	Mn1	N1[1]	91.8(2)	F1[2]	P1	F6[2]	130.5(16)
O004	Mn1	N1	91.8(2)	F2	P1	F1[2]	55.5(13)
O004	Mn1	N1[1]	87.0(2)	F2[2]	P1	F1[2]	71.1(12)
O004	Mn1	N2	89.1(3)	F2[2]	P1	F2	107(2)
O004[1]	Mn1	N2[1]	89.1(3)	F2[2]	P1	F3[2]	37.3(10)
O004	Mn1	N2[1]	91.9(3)	F2	P1	F3[2]	142.3(19)
O004[1]	Mn1	N2	91.9(3)	F2[2]	P1	F4	93.0(10)
N1[1]	Mn1	N1	83.8(4)	F2	P1	F4[2]	93.0(10)
N2[1]	Mn1	N1[1]	87.9(3)	F2	P1	F4	96.9(11)
N2	Mn1	N1[1]	170.7(3)	F2[2]	P1	F4[2]	96.9(12)
N2[1]	Mn1	N1	170.7(3)	F2	P1	F6[2]	166.4(17)
N2	Mn1	N1	87.9(3)	F2	P1	F6	86.2(13)
N2	Mn1	N2[1]	100.6(4)	F2[2]	P1	F6	166.4(17)
C11	O004	Mn1	126.6(5)	F2[2]	P1	F6[2]	86.2(13)
C1	N1	Mn1	107.0(5)	F3[2]	P1	F1	87.6(12)
C1	N1	C2	110.2(6)	F3	P1	F1	92.1(14)
C2	N1	Mn1	118.1(5)	F3[2]	P1	F3	180(2)
C4	N2	Mn1	119.1(6)	F3	P1	F6[2]	130.0(17)

C5	N2	Mn1	123.7(6)	F3[2]	P1	F6[2]	50.3(11)
C5	N2	C4	116.0(7)	F4[2]	P1	F1[2]	57.9(12)
N1	C1	C1[1]	107.4(5)	F4	P1	F1[2]	138.6(16)
N1	C2	C3	112.7(7)	F4[2]	P1	F3[2]	82.8(9)
C2	C3	C4	115.1(8)	F4	P1	F3[2]	97.3(9)
N2	C4	C3	108.4(7)	F4	P1	F4[2]	163.2(17)
N2	C5	C6	125.7(8)	F4	P1	F6	83.3(9)
C7	C6	C5	117.9(8)	F4	P1	F6[2]	83.9(10)
C7	C6	C11	120.5(8)	F4[2]	P1	F6	83.9(10)
C11	C6	C5	121.3(7)	F4[2]	P1	F6[2]	83.3(9)
C8	C7	C6	119.5(9)	F5	P1	F1	87.7(13)
C7	C8	Br1	118.8(7)	F5[2]	P1	F1	170.0(16)
C7	C8	C9	121.5(8)	F5[2]	P1	F3	89.7(11)
C9	C8	Br1	119.7(8)	F5	P1	F3	90.5(10)
C8	C9	C10	119.3(9)	F5[2]	P1	F5	102(2)
C11	C10	C9	120.5(9)	F5	P1	F6[2]	57.0(11)
O004	C11	C6	122.1(7)	F5[2]	P1	F6[2]	65.5(12)
O004	C11	C10	119.2(7)	F6[2]	P1	F6	80(2)

[1]1-X,+Y,1/2-Z; [2]1-X,+Y,3/2-Z

Table 6 Hydrogen Atom Coordinates (Å×10[4]) and Isotropic Displacement Parameters (Å[2]×10[3]) for FL259_a.

Atom	***x***	***y***	***z***	**U(eq)**
H1	4520.24	7310.59	4579.75	68
H1A	4264.47	8032.92	3280.37	78
H1B	4046.38	7742.81	1745.19	78
H2A	2765.67	7199.58	2799.58	79
H2B	2838.12	7500.07	4338.47	79
H3A	2098.7	6738.34	4863.99	88
H3B	3164.45	6743.35	5644.57	88
H4A	2802.41	5958.41	4427.91	86
H4B	2809.13	6238.71	2843.46	86
H5	4183.04	5678.69	5287.88	80
H7	5584.27	5241.83	6400.23	86
H9	8298.49	5894.45	6712.27	87
H10	7746.92	6555.29	5149.47	80

Table 7 Atomic Occupancy for FL259_a.

Atom	***Occupancy***	**Atom**	***Occupancy***	**Atom**	***Occupancy***
F1	0.5	F2	0.5	F3	0.5
F4	0.5	F5	0.5	F6	0.5

Crystal structure determination of [FL259_a]

Crystal Data for $C_{22}H_{26}Br_2F_6MnN_4O_2P$ (*M* =738.20 g/mol): orthorhombic, space group Pbcn (no. 60), *a* = 13.205(3) Å, *b* = 26.477(5) Å, *c* = 8.7550(18) Å, *V* = 3061.0(11) Å^3, *Z* = 4, *T* = 293(2) K, μ(MoKα) = 3.156 mm^{-1}, *Dcalc* = 1.602 g/cm^3, 34657 reflections measured (3.076° ≤ 2Θ ≤ 52.744°), 2920 unique (R_{int} = 0.0581, R_{sigma} = 0.0246) which were used in all calculations. The final R_1 was 0.0938 (I > 2σ(I)) and wR_2 was 0.3079 (all data).

Refinement model description

Number of restraints - 36, number of constraints - unknown.

Details:

1. Fixed Uiso
 At 1.2 times of:
  All C(H) groups, All C(H,H) groups, All N(H) groups
2. Rigid body (RIGU) restrains
 P1, F1, F2, F3, F4, F5, F6
 with sigma for 1-2 distances of 0.004 and sigma for 1-3 distances of 0.004
3. Others
 Fixed Sof: F1(0.5) F2(0.5) F3(0.5) F4(0.5) F5(0.5) F6(0.5)
4.a Ternary CH refined with riding coordinates:
 N1(H1)
4.b Secondary CH2 refined with riding coordinates:
 C1(H1A,H1B), C2(H2A,H2B), C3(H3A,H3B), C4(H4A,H4B)
4.c Aromatic/amide H refined with riding coordinates:
 C5(H5), C7(H7), C9(H9), C10(H10)

This report has been created with Olex2, compiled on 2017.08.10 svn.r3458 for OlexSys. Please let us know if there are any errors or if you would like to have additional features.

Chapter 4 Appendices

Crystal Refinement Data for Complex **1** [Fe**L**](BF4) at 150 K

Table 1 Crystal data and structure refinement for SK3FeBF4_150K_0m_a.

Identification code	SK3FeBF4_150K_0m_a
Empirical formula	$C_{16}H_{24}B_2F_8FeN_6S_2$
Formula weight	594.00
Temperature/K	150.01
Crystal system	monoclinic
Space group	$P2_1/n$
a/Å	9.7734(7)
b/Å	17.4949(14)
c/Å	13.6597(11)
α/°	90
β/°	100.286(2)
γ/°	90
Volume/Å^3	2298.1(3)
Z	4
ρ_{calc}g/cm^3	1.717
μ/mm^{-1}	0.922
F(000)	1208.0
Crystal size/mm^3	0.02 × 0.01 × 0.01
Radiation	MoKα (λ = 0.71073)
2Θ range for data collection/°	3.822 to 50
Index ranges	-11 ≤ h ≤ 11, -20 ≤ k ≤ 20, -16 ≤ l ≤ 16
Reflections collected	51435
Independent reflections	4040 [R_{int} = 0.0589, R_{sigma} = 0.0260]
Data/restraints/parameters	4040/0/316
Goodness-of-fit on F^2	1.176
Final R indexes [I>=2σ (I)]	R_1 = 0.1175, wR_2 = 0.3196
Final R indexes [all data]	R_1 = 0.1228, wR_2 = 0.3225
Largest diff. peak/hole / e Å^{-3}	3.71/-1.08

Table 2 Fractional Atomic Coordinates (×10^4) and Equivalent Isotropic Displacement Parameters (Å^2×10^3) for SK3FeBF4_150K_0m_a. U_{eq} is defined as 1/3 of of the trace of the orthogonalised U_{IJ} tensor.

Atom	*x*	*y*	*z*	U(eq)
Fe01	6731.3(17)	8271.2(9)	3418.3(12)	15.4(4)
S1	8584(4)	9324.9(19)	6392(2)	24.4(7)
S2	6043(4)	5973.8(19)	4799(3)	27.7(8)
F5	3036(9)	5777(6)	4800(6)	45(2)

F6	772(9)	5670(5)	4143(7)	44(2)
F7	2412(11)	5207(5)	3296(6)	47(2)
F8	2127(11)	6485(5)	3453(8)	53(3)
N1	7444(11)	8781(6)	4722(8)	22(2)
N2	4936(11)	8623(6)	3737(8)	23(2)
N3	5832(11)	7857(6)	2065(8)	22(2)
N4	7034(11)	9230(6)	2677(8)	21(2)
N5	8583(10)	7845(6)	3308(7)	19(2)
N6	6547(11)	7254(6)	4029(7)	19(2)
C1	8660(13)	8900(7)	5276(9)	22(3)
C2	6805(14)	9343(8)	6087(10)	27(3)
C3	6410(14)	9048(7)	5162(9)	22(3)
C4	5032(14)	8959(7)	4589(10)	24(3)
C5	3522(13)	8451(8)	3235(10)	26(3)
C6	3388(14)	8290(8)	2133(10)	29(3)
C7	4348(13)	7645(8)	1941(10)	26(3)
C8	6129(15)	8371(8)	1284(9)	28(3)
C9	6233(16)	9194(8)	1638(10)	29(3)
C10	8510(14)	9474(7)	2701(10)	26(3)
C11	9392(14)	8892(8)	2300(11)	28(3)
C12	9751(13)	8212(8)	2977(10)	28(3)
C13	8797(13)	7155(7)	3623(9)	21(3)
C14	7710(13)	6805(7)	4047(9)	20(3)
C15	7623(15)	6081(7)	4458(10)	27(3)
C16	5594(14)	6878(7)	4420(10)	26(3)
B2	2096(15)	5780(8)	3924(11)	23(3)
F1	8198(13)	6917(5)	1015(10)	69(4)
F2	6624(9)	6277(5)	1745(6)	40(2)
F3	8628(8)	5699(5)	1458(7)	37(2)
F4	6924(10)	5996(8)	185(7)	71(4)
B1	7594(18)	6233(9)	1108(12)	30(3)

Table 3 Anisotropic Displacement Parameters ($Å^2×10^3$) for SK3FeBF4_150K_0m_a. The Anisotropic displacement factor exponent takes the form: $-2\pi^2[h^2a^{*2}U_{11}+2hka^*b^*U_{12}+\ldots]$.

Atom	U_{11}	U_{22}	U_{33}	U_{23}	U_{13}	U_{12}
Fe01	15.1(9)	13.8(8)	17.5(9)	0.1(7)	3.5(6)	0.9(7)
S1	27.3(17)	23.7(16)	21.3(16)	-5.2(13)	1.9(13)	-2.4(13)
S2	28.9(18)	20.9(16)	32.3(18)	7.8(14)	2.2(14)	-1.4(14)
F5	33(5)	75(7)	27(4)	-9(4)	0(4)	4(5)
F6	27(4)	39(5)	65(6)	0(5)	10(4)	-3(4)
F7	75(7)	41(5)	29(5)	-2(4)	17(5)	12(5)
F8	68(7)	31(5)	62(6)	12(5)	20(5)	1(5)
N1	27(6)	16(5)	23(6)	2(4)	3(5)	-4(4)
N2	25(6)	21(5)	22(5)	1(4)	4(4)	5(5)

N3	22(5)	15(5)	28(6)	0(4)	-1(5)	4(4)
N4	21(5)	18(5)	24(6)	0(4)	2(4)	0(4)
N5	17(5)	23(6)	18(5)	1(4)	5(4)	1(4)
N6	23(5)	21(5)	14(5)	4(4)	2(4)	4(4)
C1	18(6)	25(7)	20(6)	-2(5)	0(5)	4(5)
C2	30(7)	26(7)	22(7)	1(5)	-4(5)	8(6)
C3	34(7)	16(6)	19(6)	1(5)	8(5)	-1(5)
C4	25(7)	25(7)	25(7)	0(5)	8(5)	6(5)
C5	22(7)	26(7)	31(7)	0(6)	4(6)	0(5)
C6	23(7)	34(8)	29(7)	-4(6)	1(6)	-4(6)
C7	24(7)	29(7)	21(7)	2(6)	-7(5)	-8(6)
C8	32(7)	33(8)	15(6)	-1(5)	-3(5)	-2(6)
C9	41(8)	22(7)	22(7)	8(5)	5(6)	2(6)
C10	31(7)	18(6)	30(7)	0(5)	9(6)	-10(6)
C11	21(7)	30(7)	37(8)	1(6)	9(6)	-8(6)
C12	17(6)	37(8)	29(7)	2(6)	4(5)	-4(6)
C13	19(6)	21(6)	23(6)	-2(5)	6(5)	5(5)
C14	24(6)	15(6)	22(6)	-2(5)	6(5)	0(5)
C15	33(7)	18(6)	29(7)	-8(5)	4(6)	-2(6)
C16	26(7)	21(7)	33(7)	4(6)	8(6)	-5(5)
B2	19(7)	21(7)	26(8)	-1(6)	0(6)	4(6)
F1	91(9)	22(5)	111(10)	2(5)	62(8)	-2(5)
F2	45(5)	36(5)	42(5)	-4(4)	19(4)	12(4)
F3	32(4)	28(4)	58(6)	27(4)	23(4)	14(4)
F4	32(5)	140(12)	40(6)	-35(7)	6(4)	2(6)
B1	35(9)	25(8)	31(8)	3(7)	7(7)	1(7)

Table 4 Bond Lengths for SK3FeBF4_150K_0m_a.

Atom	**Atom**	**Length/Å**	**Atom**	**Atom**	**Length/Å**
Fe01	N1	2.002(11)	N4	C9	1.495(16)
Fe01	N2	1.980(11)	N4	C10	1.499(16)
Fe01	N3	2.033(11)	N5	C12	1.451(16)
Fe01	N4	2.008(10)	N5	C13	1.285(16)
Fe01	N5	1.988(10)	N6	C14	1.379(16)
Fe01	N6	1.987(10)	N6	C16	1.328(16)
S1	C1	1.710(13)	C2	C3	1.355(18)
S1	C2	1.715(14)	C3	C4	1.440(19)
S2	C15	1.700(14)	C5	C6	1.513(18)
S2	C16	1.698(13)	C6	C7	1.52(2)
F5	B2	1.372(17)	C8	C9	1.517(19)
F6	B2	1.393(17)	C10	C11	1.499(19)
F7	B2	1.390(17)	C11	C12	1.510(19)
F8	B2	1.394(17)	C13	C14	1.435(17)
N1	C1	1.306(16)	C14	C15	1.395(18)

N1	C3	1.349(17)	F1	B1	1.351(19)
N2	C4	1.293(17)	F2	B1	1.399(18)
N2	C5	1.460(16)	F3	B1	1.396(18)
N3	C7	1.477(16)	F4	B1	1.376(19)
N3	C8	1.463(17)			

Table 5 Bond Angles for SK3FeBF4_150K_0m_a.

Atom	**Atom**	**Atom**	**Angle/˚**	**Atom**	**Atom**	**Atom**	**Angle/˚**
N1	Fe01	N3	173.0(4)	C16	N6	C14	110.2(11)
N1	Fe01	N4	91.0(4)	N1	C1	S1	114.0(10)
N2	Fe01	N1	81.2(4)	C3	C2	S1	109.1(11)
N2	Fe01	N3	93.1(4)	N1	C3	C2	115.8(12)
N2	Fe01	N4	93.9(4)	N1	C3	C4	115.0(11)
N2	Fe01	N5	171.1(4)	C2	C3	C4	129.1(12)
N2	Fe01	N6	92.0(4)	N2	C4	C3	116.7(12)
N4	Fe01	N3	85.3(4)	N2	C5	C6	114.4(11)
N5	Fe01	N1	93.3(4)	C5	C6	C7	111.3(11)
N5	Fe01	N3	92.8(4)	N3	C7	C6	114.7(11)
N5	Fe01	N4	93.3(4)	N3	C8	C9	111.2(10)
N6	Fe01	N1	93.9(4)	N4	C9	C8	109.6(10)
N6	Fe01	N3	90.3(4)	N4	C10	C11	114.4(10)
N6	Fe01	N4	172.8(4)	C10	C11	C12	113.4(12)
N6	Fe01	N5	81.3(4)	N5	C12	C11	115.4(11)
C1	S1	C2	89.7(6)	N5	C13	C14	116.7(11)
C16	S2	C15	90.7(7)	N6	C14	C13	114.6(11)
C1	N1	Fe01	136.2(9)	N6	C14	C15	114.6(11)
C1	N1	C3	111.3(11)	C15	C14	C13	130.9(12)
C3	N1	Fe01	112.4(8)	C14	C15	S2	109.5(10)
C4	N2	Fe01	114.5(9)	N6	C16	S2	115.0(10)
C4	N2	C5	115.3(11)	F5	B2	F6	108.3(12)
C5	N2	Fe01	129.3(8)	F5	B2	F7	110.3(11)
C7	N3	Fe01	116.8(8)	F5	B2	F8	109.9(12)
C8	N3	Fe01	109.5(8)	F6	B2	F8	108.7(11)
C8	N3	C7	112.9(10)	F7	B2	F6	110.4(12)
C9	N4	Fe01	110.1(8)	F7	B2	F8	109.1(12)
C9	N4	C10	111.8(10)	F1	B1	F2	111.4(13)
C10	N4	Fe01	117.1(8)	F1	B1	F3	108.9(13)
C12	N5	Fe01	129.4(9)	F1	B1	F4	109.0(14)
C13	N5	Fe01	115.0(8)	F3	B1	F2	110.7(12)
C13	N5	C12	115.5(11)	F4	B1	F2	108.8(13)
C14	N6	Fe01	112.4(8)	F4	B1	F3	108.0(13)
C16	N6	Fe01	137.3(9)				

Table 6 Hydrogen Atom Coordinates (Å×10^4) and Isotropic Displacement Parameters (Å^2×10^3) for SK3FeBF4_150K_0m_a.

Atom	x	y	z	U(eq)
H3	6336	7372	1978	27
H4	6596	9650	3011	25
H1	9509	8763	5076	26
H2	6194	9529	6500	32
H4A	4233	9138	4826	29
H5A	2915	8889	3325	32
H5B	3181	8001	3559	32
H6A	3619	8758	1789	35
H6B	2414	8150	1857	35
H7A	4251	7219	2399	32
H7B	4039	7457	1253	32
H8A	5382	8327	694	33
H8B	7016	8219	1085	33
H9A	6705	9505	1192	35
H9B	5289	9406	1618	35
H10A	8938	9592	3397	31
H10B	8509	9951	2310	31
H11A	10264	9140	2193	34
H11B	8893	8711	1647	34
H12A	10229	7828	2625	33
H12B	10418	8379	3571	33
H13	9632	6891	3578	25
H15	8336	5705	4536	32
H16	4725	7099	4483	31

Crystal structure determination of [SK3FeBF4_150K_0m_a]

Crystal Data for $C_{16}H_{24}B_2F_8FeN_6S_2$ (*M* =594.00 g/mol): monoclinic, space group $P2_1/n$ (no. 14), *a* = 9.7734(7) Å, *b* = 17.4949(14) Å, *c* = 13.6597(11) Å, *β* = 100.286(2)°, *V* = 2298.1(3) Å^3, *Z* = 4, *T* = 150.01 K, μ(MoKα) = 0.922 mm^{-1}, *Dcalc* = 1.717 g/cm^3, 51435 reflections measured (3.822° ≤ 2Θ ≤ 50°), 4040 unique (R_{int} = 0.0589, R_{sigma} = 0.0260) which were used in all calculations. The final R_1 was 0.1175 (I > 2σ(I)) and wR_2 was 0.3225 (all data).

Refinement model description

Number of restraints - 0, number of constraints - unknown.

Details:

1. Fixed Uiso
 At 1.2 times of:
 All C(H) groups, All C(H,H) groups, All N(H) groups
2.a Ternary CH refined with riding coordinates:
 N3(H3), N4(H4)
2.b Secondary CH2 refined with riding coordinates:
 C5(H5A,H5B), C6(H6A,H6B), C7(H7A,H7B), C8(H8A,H8B), C9(H9A,H9B), C10(H10A, H10B), C11(H11A,H11B), C12(H12A,H12B)

2.c Aromatic/amide H refined with riding coordinates:
C1(H1), C2(H2), C4(H4A), C13(H13), C15(H15), C16(H16)

Crystal Refinement Data for Complex **1** [Fe**L**](BF_4) at 400 K

Table 1 Crystal data and structure refinement for VT_data_0m_a.

Identification code	VT_data_0m_a
Empirical formula	$C_{16}H_{22}B_2F_8FeN_6S_2$
Formula weight	591.98
Temperature/K	400.02
Crystal system	monoclinic
Space group	$P2_1/n$
a/Å	10.0590(13)
b/Å	17.415(2)
c/Å	14.2234(17)
α/°	90
β/°	98.737(4)
γ/°	90
Volume/Å^3	2462.7(5)
Z	4
ρ_{calc}g/cm^3	1.597
μ/mm^{-1}	0.860
F(000)	1200.0
Crystal size/mm^3	? × ? × ?
Radiation	MoKα (λ = 0.71073)
2Θ range for data collection/°	3.724 to 54.366
Index ranges	-11 ≤ h ≤ 12, -22 ≤ k ≤ 22, -18 ≤ l ≤ 18
Reflections collected	45318
Independent reflections	5471 [R_{int} = 0.0832, R_{sigma} = 0.0501]
Data/restraints/parameters	5471/0/338
Goodness-of-fit on F^2	1.055
Final R indexes [I>=2σ (I)]	R_1 = 0.0706, wR_2 = 0.1822
Final R indexes [all data]	R_1 = 0.1193, wR_2 = 0.2170
Largest diff. peak/hole / e Å^{-3}	0.89/-0.40

Table 2 Fractional Atomic Coordinates (×10^4) and Equivalent Isotropic Displacement Parameters (Å^2×10^3) for VT_data_0m_a. U_{eq} is defined as 1/3 of of the trace of the orthogonalised U_{IJ} tensor.

Atom	*x*	*y*	*z*	U(eq)
Fe01	6765.4(6)	3278.3(3)	3377.6(4)	49.4(2)
S1	6081(2)	973.1(10)	4849.3(15)	104.8(6)
S2	8390.4(19)	4241.9(11)	6356.1(11)	95.1(6)
N1	6528(4)	2211(2)	4012(3)	60.9(10)
N2	8605(4)	2777(3)	3313(3)	66.5(11)
N3	7259(5)	4250(2)	2640(3)	77.9(13)

N4	5795(5)	2926(3)	2036(3)	79.6(13)
N5	4968(4)	3635(2)	3762(3)	60.9(10)
N6	7426(4)	3771(2)	4703(3)	57.0(9)
C1	5616(6)	1851(4)	4383(5)	89.1(18)
C2	7598(7)	1078(3)	4518(4)	85.8(17)
C3	7673(5)	1768(3)	4067(4)	64.4(13)
C4	8763(5)	2111(3)	3667(4)	74.2(14)
C5	9787(6)	3135(5)	2982(6)	107(2)
C6	9591(9)	3844(6)	2516(8)	147(4)
C7	8645(9)	4404(5)	2564(9)	151(4)
C8	6411(9)	4231(4)	1694(6)	117(3)
C9	6222(9)	3427(4)	1331(4)	103(2)
C10	4357(10)	2816(7)	1912(7)	169(5)
C11	3507(8)	3210(7)	2337(7)	171(5)
C12	3588(6)	3509(4)	3250(5)	93.6(19)
C13	5054(5)	3920(3)	4587(4)	70.7(14)
C14	6360(5)	4003(3)	5147(3)	64.5(13)
C15	6699(7)	4257(4)	6045(4)	84.7(17)
C16	8545(6)	3879(4)	5263(4)	76.4(15)
F0AA	6551(14)	5772(10)	3536(16)	138(7)
F00E	8426(6)	6296(3)	3270(4)	153.0(19)
F00G	6960(30)	5562(9)	3945(18)	167(11)
F00P	6630(30)	6750(15)	3690(20)	216(15)
F00Q	6980(30)	6867(10)	4110(20)	179(13)
F00V	8216(19)	6421(17)	4722(13)	188(8)
F00W	8145(18)	5834(14)	4676(15)	164(8)
B00U	7548(9)	6215(5)	3907(6)	90(2)
B00V	7548(9)	6215(5)	3907(6)	90(2)
F00H	947(6)	573(4)	4206(5)	178(2)
F00I	2993(6)	793(5)	4676(4)	184(3)
F00L	2035(7)	1444(3)	3463(5)	194(3)
F00M	2507(8)	217(4)	3298(4)	191(3)
B00T	2056(9)	760(5)	3833(6)	93(2)

Table 3 Anisotropic Displacement Parameters ($Å^2×10^3$) for VT_data_0m_a. The Anisotropic displacement factor exponent takes the form: $-2\pi^2[h^2a^{*2}U_{11}+2hka^*b^*U_{12}+\ldots]$.

Atom	U_{11}	U_{22}	U_{33}	U_{23}	U_{13}	U_{12}
Fe01	44.3(4)	48.0(4)	57.0(4)	-0.6(3)	11.4(3)	4.6(3)
S1	110.0(14)	78.5(11)	121.4(14)	34.8(10)	3.0(11)	-14(1)
S2	107.9(13)	103.8(13)	68.5(9)	-13.7(8)	-2.9(8)	-11.8(10)
N1	54(2)	62(2)	66(2)	7(2)	6.2(18)	4.4(19)
N2	53(2)	76(3)	73(3)	-4(2)	16.9(19)	4(2)
N3	83(3)	57(3)	90(3)	2(2)	-1(3)	-3(2)
N4	91(3)	75(3)	77(3)	-22(2)	29(3)	-15(3)

N5	52(2)	64(2)	67(2)	-5(2)	8.7(19)	6.9(18)
N6	57(2)	60(2)	55(2)	-0.3(18)	11.5(18)	-0.3(18)
C1	71(4)	86(4)	108(5)	35(4)	8(3)	-2(3)
C2	100(5)	57(3)	92(4)	-4(3)	-10(3)	10(3)
C3	65(3)	53(3)	72(3)	-1(2)	1(2)	12(2)
C4	60(3)	74(4)	87(4)	-8(3)	7(3)	23(3)
C5	64(4)	129(6)	138(6)	16(5)	46(4)	6(4)
C6	105(6)	123(7)	234(11)	31(7)	93(7)	-9(5)
C7	99(6)	115(7)	234(11)	64(7)	6(7)	-30(5)
C8	132(7)	93(5)	116(5)	42(4)	-13(5)	-5(4)
C9	126(6)	114(6)	68(4)	-7(4)	11(4)	-19(5)
C10	119(7)	250(12)	140(7)	-121(8)	28(6)	-75(8)
C11	58(4)	281(14)	164(9)	-104(9)	-17(5)	8(6)
C12	51(3)	120(5)	106(5)	-19(4)	-1(3)	9(3)
C13	59(3)	76(3)	80(3)	-3(3)	22(3)	14(3)
C14	77(3)	60(3)	61(3)	-1(2)	23(2)	6(2)
C15	100(5)	90(4)	65(3)	-15(3)	18(3)	11(3)
C16	71(4)	90(4)	67(3)	2(3)	9(3)	-4(3)
F0AA	67(6)	147(18)	197(16)	-68(12)	14(7)	-26(8)
F00E	158(5)	157(5)	162(4)	28(4)	84(4)	-18(4)
F00G	230(30)	58(5)	250(20)	6(10)	170(20)	-9(10)
F00P	220(20)	190(30)	240(30)	90(20)	27(17)	97(19)
F00Q	250(30)	65(7)	250(30)	-21(12)	130(20)	-11(12)
F00V	137(12)	290(20)	126(11)	-73(15)	3(10)	14(19)
F00W	115(10)	201(16)	171(14)	106(14)	-1(10)	-9(12)
F00H	143(5)	182(6)	218(6)	-8(5)	58(4)	-56(4)
F00I	137(5)	264(8)	146(4)	-3(5)	8(4)	11(5)
F00L	235(7)	107(4)	255(7)	72(4)	81(6)	38(4)
F00M	304(8)	140(5)	142(4)	-10(4)	78(5)	62(5)
B00T	88(5)	92(6)	102(6)	32(5)	24(4)	20(4)

Table 4 Bond Lengths for VT_data_0m_a.

Atom	**Atom**	**Length/Å**	**Atom**	**Atom**	**Length/Å**
Fe01	N1	2.096(4)	C2	C3	1.370(8)
Fe01	N2	2.060(4)	C3	C4	1.440(8)
Fe01	N3	2.091(5)	C5	C6	1.401(11)
Fe01	N4	2.099(5)	C6	C7	1.371(12)
Fe01	N5	2.063(4)	C8	C9	1.496(10)
Fe01	N6	2.086(4)	C10	C11	1.314(12)
S1	C1	1.703(6)	C11	C12	1.390(11)
S1	C2	1.674(7)	C13	C14	1.436(8)
S2	C15	1.692(7)	C14	C15	1.346(7)
S2	C16	1.707(6)	F0AA	B00U	1.311(16)
N1	C1	1.289(7)	F00E	B00U	1.365(9)

N1	C3	1.379(6)	F00E	B00V	1.365(9)
N2	C4	1.264(7)	F00G	B00V	1.285(17)
N2	C5	1.481(7)	F00P	B00V	1.31(3)
N3	C7	1.439(9)	F00Q	B00U	1.32(2)
N3	C8	1.480(8)	F00V	B00V	1.299(17)
N4	C9	1.444(8)	F00W	B00U	1.340(16)
N4	C10	1.443(10)	F00H	B00T	1.347(9)
N5	C12	1.483(7)	F00I	B00T	1.409(10)
N5	C13	1.264(6)	F00L	B00T	1.300(9)
N6	C14	1.384(6)	F00M	B00T	1.335(10)
N6	C16	1.290(7)			

Table 5 Bond Angles for VT_data_0m_a.

Atom	**Atom**	**Atom**	**Angle/˚**	**Atom**	**Atom**	**Atom**	**Angle/˚**
N1	Fe01	N4	93.70(17)	N1	C3	C4	115.2(4)
N2	Fe01	N1	78.79(16)	C2	C3	N1	114.4(5)
N2	Fe01	N3	92.14(19)	C2	C3	C4	130.4(5)
N2	Fe01	N4	97.60(18)	N2	C4	C3	118.7(5)
N2	Fe01	N5	165.62(17)	C6	C5	N2	117.3(6)
N2	Fe01	N6	92.86(16)	C7	C6	C5	130.7(8)
N3	Fe01	N1	170.25(18)	C6	C7	N3	124.0(7)
N3	Fe01	N4	83.91(19)	N3	C8	C9	111.1(5)
N5	Fe01	N1	89.46(16)	N4	C9	C8	111.2(6)
N5	Fe01	N3	100.02(18)	C11	C10	N4	125.7(7)
N5	Fe01	N4	91.35(18)	C10	C11	C12	132.6(8)
N5	Fe01	N6	78.94(16)	C11	C12	N5	115.6(6)
N6	Fe01	N1	90.95(15)	N5	C13	C14	118.8(5)
N6	Fe01	N3	93.07(17)	N6	C14	C13	115.1(4)
N6	Fe01	N4	169.20(18)	C15	C14	N6	115.3(5)
C2	S1	C1	90.1(3)	C15	C14	C13	129.6(5)
C15	S2	C16	89.7(3)	C14	C15	S2	110.0(4)
C1	N1	Fe01	138.0(4)	N6	C16	S2	115.1(4)
C1	N1	C3	110.2(5)	F0AA	B00U	F00E	109.1(12)
C3	N1	Fe01	111.8(3)	F0AA	B00U	F00Q	105.4(16)
C4	N2	Fe01	115.5(4)	F0AA	B00U	F00W	105.0(13)
C4	N2	C5	117.0(5)	F00Q	B00U	F00E	113.6(12)
C5	N2	Fe01	127.3(4)	F00Q	B00U	F00W	113.5(17)
C7	N3	Fe01	119.6(4)	F00W	B00U	F00E	109.8(11)
C7	N3	C8	111.5(7)	F00G	B00V	F00E	117.7(11)
C8	N3	Fe01	106.9(4)	F00G	B00V	F00P	109.3(19)
C9	N4	Fe01	108.0(4)	F00G	B00V	F00V	112.6(16)
C10	N4	Fe01	118.0(4)	F00P	B00V	F00E	105.6(16)
C10	N4	C9	113.2(7)	F00V	B00V	F00E	105.4(12)
C12	N5	Fe01	128.2(4)	F00V	B00V	F00P	105.3(17)

C13	N5	Fe01	115.1(3)	F00H	B00T	F00I	99.3(7)
C13	N5	C12	116.2(5)	F00L	B00T	F00H	114.6(7)
C14	N6	Fe01	111.7(3)	F00L	B00T	F00I	106.0(8)
C16	N6	Fe01	138.3(4)	F00L	B00T	F00M	113.8(7)
C16	N6	C14	109.8(4)	F00M	B00T	F00H	115.3(8)
N1	C1	S1	115.2(5)	F00M	B00T	F00I	105.8(7)
C3	C2	S1	110.2(5)				

Table 6 Hydrogen Atom Coordinates (Å×10^4) and Isotropic Displacement Parameters (Å^2×10^3) for VT_data_0m_a.

Atom	***x***	***y***	***z***	**U(eq)**
H1	4764	2055	4395	107
H2	8290	719	4625	103
H4	9569	1849	3670	89
H5A	10480	3200	3530	129
H5B	10131	2777	2556	129
H6A	10447	4107	2672	177
H6B	9509	3719	1845	177
H7A	8637	4720	2001	182
H7B	8989	4724	3103	182
H8A	6832	4536	1249	140
H8B	5541	4456	1739	140
H9A	5554	3422	762	124
H9B	7062	3239	1161	124
H10A	4048	2869	1235	202
H10B	4220	2281	2065	202
H11A	2703	2895	2263	206
H11B	3281	3650	1925	206
H12A	3123	3163	3624	112
H12B	3113	3996	3210	112
H13	4286	4073	4827	85
H15	6092	4417	6437	102
H16	9375	3768	5084	92

Table 7 Atomic Occupancy for VT_data_0m_a.

Atom	***Occupancy***	**Atom**	***Occupancy***	**Atom**	***Occupancy***
F0AA	0.5	F00G	0.5	F00P	0.5
F00Q	0.5	F00V	0.5	F00W	0.5
B00U	0.5	B00V	0.5		

Crystal Data for $C_{16}H_{22}B_2F_8FeN_6S_2$ (*M* =591.98 g/mol): monoclinic, space group $P2_1/n$ (no. 14), *a* = 10.0590(13) Å, *b* = 17.415(2) Å, *c* = 14.2234(17) Å, *β* = 98.737(4)°, *V* = 2462.7(5) Å^3, *Z* = 4, *T* = 400.02 K, μ(MoKα) = 0.860 mm^{-1}, *Dcalc* = 1.597 g/cm^3, 45318 reflections measured (3.724° ≤ 2Θ ≤ 54.366°), 5471 unique (R_{int} = 0.0832, R_{sigma} = 0.0501) which were used in all calculations. The final R_1 was 0.0706 (I > 2σ(I)) and wR_2 was 0.2170 (all data).

Refinement model description

Number of restraints - 0, number of constraints - unknown.

Details:

1. Fixed Uiso
 At 1.2 times of:
  All C(H) groups, All C(H,H) groups
2. Shared sites
{B00V, B00U}
3. Uiso/Uaniso restraints and constraints
Uiso(B00V) = Uiso(B00U)
4. Rigid body (RIGU) restrains
 F0AA, F00E, F00G, F00P, F00Q, F00V, F00W, B00U, B00V
 with sigma for 1-2 distances of 0.004 and sigma for 1-3 distances of 0.004
5. Others
 Fixed Sof: F0AA(0.5) F00G(0.5) F00P(0.5) F00Q(0.5) F00V(0.5) F00W(0.5)
 B00U(0.5) B00V(0.5)
6.a Secondary CH2 refined with riding coordinates:
 C5(H5A,H5B), C6(H6A,H6B), C7(H7A,H7B), C8(H8A,H8B), C9(H9A,H9B), C10(H10A,
 H10B), C11(H11A,H11B), C12(H12A,H12B)
6.b Aromatic/amide H refined with riding coordinates:
 C1(H1), C2(H2), C4(H4), C13(H13), C15(H15), C16(H16)

Chapter 5 Appendices

Crystal Refinement Data for Complex **1** $[Fe\mathbf{L}_2](BF_4)_2$

Identification code	P1_a
Empirical formula	$C_{16}H_{12}B_2F_8FeN_8S_4$
Formula weight	674.05
Temperature/K	293(2)
Crystal system	triclinic
Space group	P1
a/Å	8.6440(17)
b/Å	8.8000(18)
c/Å	16.261(3)
α/°	89.91(3)
β/°	75.82(3)
γ/°	89.92(3)
Volume/Å^3	1199.2(4)
Z	2
ρ_{calc}g/cm^3	1.867
μ/mm^{-1}	1.066
F(000)	672.0
Radiation	MoKα (λ = 0.71073)
2Θ range for data collection/°	2.584 to 52.734
Index ranges	-10 ≤ h ≤ 10, -10 ≤ k ≤ 10, -20 ≤ l ≤ 20
Reflections collected	16965
Independent reflections	8547 [R_{int} = 0.0613, R_{sigma} = 0.0927]
Data/restraints/parameters	8547/3/623
Goodness-of-fit on F^2	1.059
Final R indexes [I>=2σ (I)]	R_1 = 0.0889, wR_2 = 0.2307
Final R indexes [all data]	R_1 = 0.0947, wR_2 = 0.2365
Largest diff. peak/hole / e Å^{-3}	2.37/-1.28
Flack parameter	0.036(13)

Table 2 Fractional Atomic Coordinates (×10^4) and Equivalent Isotropic Displacement Parameters (Å^2×10^3) for P1_a. U_{eq} is defined as 1/3 of of the trace of the orthogonalised U_{IJ} tensor.

Atom	*x*	*y*	*z*	U(eq)
Fe01	4733(2)	8156.5(19)	2391.8(12)	20.2(4)
Fe02	5269(2)	3173.2(19)	7625.3(12)	20.0(4)
S003	7022(4)	-1209(4)	8504(3)	28.7(8)
S004	3321(4)	7675(4)	7050(2)	26.4(7)
S005	6679(4)	12670(4)	2957(2)	26.4(7)
S006	9528(4)	6123(4)	2265(2)	29.0(8)
S007	-194(4)	10142(4)	2868(3)	29.8(8)
S008	2971(4)	3784(4)	1530(3)	29.1(8)
S009	479(4)	1146(4)	7757(2)	28.9(8)

S00A	10187(4)	5158(4)	7142(3)	29.2(8)
F00B	6942(10)	4171(10)	1279(6)	33(2)
F00C	3042(11)	-843(10)	8735(6)	33(2)
F00D	8772(13)	4565(11)	20(6)	41(2)
F00E	1204(13)	-436(11)	9988(6)	40(2)
F00F	7342(13)	2359(10)	253(6)	41(2)
F00G	764(13)	-2203(13)	9038(8)	49(3)
F00H	2646(13)	-2647(11)	9759(7)	43(2)
F00I	9228(12)	2810(13)	964(7)	45(3)
N00J	4475(15)	5073(13)	7248(7)	23(2)
N00K	5505(13)	10070(12)	2763(8)	21(2)
N00L	7352(15)	4114(13)	7519(8)	26(3)
N00M	3094(14)	2373(13)	7851(8)	24(2)
N00N	2628(16)	9089(14)	2500(8)	28(3)
N00O	6869(15)	7348(13)	2173(8)	25(2)
N00P	6119(16)	1199(14)	7880(9)	31(3)
C00Q	2745(18)	3820(16)	2611(8)	24(3)
F00R	1930(20)	3370(20)	5448(10)	92(6)
N00S	3886(15)	6174(14)	2155(9)	33(3)
C00T	7264(18)	-1143(16)	7424(9)	26(3)
F00U	1972(19)	1800(20)	4318(9)	74(4)
C00V	2077(18)	2501(16)	8646(9)	26(3)
F00W	8010(20)	6880(20)	5726(9)	81(5)
C00X	7594(19)	4756(16)	8254(9)	26(3)
C00Y	5427(17)	10192(15)	3603(9)	25(3)
C00Z	9064(17)	5396(16)	8159(10)	27(3)
C010	4517(18)	5207(15)	6393(9)	25(3)
C011	2395(17)	9735(16)	1756(10)	26(3)
C012	3281(19)	5181(17)	2828(11)	32(3)
N013	4270(20)	7749(19)	3604(10)	46(4)
N014	5014(17)	3857(17)	8768(9)	37(3)
C015	6136(17)	11322(16)	2333(10)	27(3)
F016	9810(20)	6649(18)	4471(13)	96(6)
F017	110(20)	1640(20)	5542(13)	106(7)
F018	8070(20)	8500(30)	4605(11)	107(7)
C019	7926(18)	7500(16)	1377(9)	25(3)
C01A	2416(17)	1652(15)	7313(10)	26(3)
C01B	6705(18)	221(16)	7196(11)	31(3)
C01C	6280(20)	4631(18)	8969(10)	32(3)
C01D	6222(17)	602(17)	8597(10)	29(3)
B01E	8074(19)	3472(17)	621(11)	25(3)
C01F	3771(16)	5595(16)	1438(10)	24(3)
C01G	1356(18)	9203(18)	3135(10)	30(3)
C01H	7430(20)	8185(19)	670(13)	39(4)
C01I	3720(19)	9626(19)	1036(13)	40(4)
N01J	3759(19)	3787(17)	9518(10)	41(3)
C01K	6093(19)	11530(17)	3811(9)	28(3)
C01L	910(18)	10386(17)	1852(10)	30(3)
C01M	576(17)	1916(16)	8700(11)	29(3)
N01N	5760(30)	2620(30)	6451(15)	75(6)

C01O	3892(17)	6557(15)	6184(8)	22(3)
C01P	3875(19)	6314(15)	7663(10)	28(3)
F01Q	2530(40)	850(40)	5493(13)	173(16)
C01S	7579(17)	6640(16)	2721(10)	26(3)
C01T	2520(20)	3198(19)	9366(10)	33(3)
B01U	1910(20)	-1526(16)	9382(10)	24(3)
C01V	5210(20)	3970(20)	5838(11)	40(4)
C01W	9394(19)	6906(18)	1330(10)	33(3)
N01X	5050(30)	8811(18)	1242(9)	53(5)
C01Y	8680(18)	4223(17)	6881(10)	29(3)
N020	6200(20)	8782(19)	511(11)	47(4)
C021	4770(20)	8935(17)	4146(14)	40(4)
F022	7260(30)	6110(40)	4603(13)	162(14)
C023	6660(30)	660(20)	6370(13)	52(5)
N025	6290(30)	1640(20)	5854(13)	69(6)
B026	1650(30)	1920(30)	5189(17)	58(7)
B028	8300(30)	7010(40)	4858(16)	63(8)
C1	3300(30)	5590(20)	3690(12)	47(4)
N2	3710(20)	6620(20)	4154(12)	55(4)

Table 3 Anisotropic Displacement Parameters ($Å^2×10^3$) for P1_a. The Anisotropic displacement factor exponent takes the form: $-2π^2[h^2a^{*2}U_{11}+2hka*b*U_{12}+…]$.

Atom	U_{11}	U_{22}	U_{33}	U_{23}	U_{13}	U_{12}
Fe01	11.9(9)	18.2(9)	30.3(10)	-0.7(7)	-4.4(7)	2.3(7)
Fe02	11.0(9)	18.0(9)	30.7(10)	-2.6(7)	-4.4(7)	3.5(7)
S003	18.2(18)	18.1(15)	51(2)	-0.6(13)	-10.8(15)	5.4(13)
S004	23.0(18)	18.6(15)	38.0(18)	0.4(12)	-8.1(14)	2.8(13)
S005	21.6(18)	19.9(15)	38.0(18)	-2.9(12)	-7.8(14)	1.3(13)
S006	15.6(17)	27.0(17)	44(2)	-2.3(14)	-6.2(14)	4.6(14)
S007	16.0(17)	25.3(17)	49(2)	-2.0(14)	-10.3(15)	5.6(14)
S008	21.0(18)	15.9(15)	50(2)	-2.8(13)	-9.3(15)	1.2(13)
S009	14.9(17)	26.3(17)	46(2)	-0.2(14)	-7.2(14)	2.9(14)
S00A	13.6(17)	27.8(17)	47(2)	-1.9(14)	-9.3(14)	-0.9(14)
F00B	19(4)	25(4)	53(5)	-6(4)	-3(4)	10(3)
F00C	27(5)	23(4)	45(5)	6(3)	-1(4)	-1(4)
F00D	47(6)	35(5)	40(5)	3(4)	-8(4)	-10(4)
F00E	46(6)	30(5)	41(5)	-7(4)	-7(4)	16(4)
F00F	42(6)	28(5)	48(6)	-4(4)	-1(4)	-10(4)
F00G	27(6)	51(6)	71(8)	-4(5)	-16(5)	-16(5)
F00H	43(6)	28(5)	54(6)	3(4)	-5(5)	22(4)
F00I	21(5)	53(6)	61(6)	6(5)	-7(4)	22(5)
N00K	9(5)	13(5)	43(6)	-4(4)	-8(5)	5(4)
N00L	19(6)	20(5)	40(7)	-1(5)	-12(5)	5(5)
N00M	18(6)	16(5)	39(7)	-1(4)	-6(5)	8(4)
N00N	24(7)	22(6)	42(7)	-1(5)	-15(5)	-1(5)
N00O	19(6)	20(5)	33(6)	-4(4)	-3(5)	-4(5)
N00P	19(7)	17(6)	58(8)	-6(5)	-10(6)	-6(5)
F00R	62(11)	145(16)	65(10)	-31(10)	-9(8)	-29(10)
N00S	19(7)	25(6)	49(8)	8(5)	1(5)	12(5)

F00U	67(9)	103(11)	54(7)	-21(7)	-17(6)	16(8)
F00W	67(10)	118(13)	58(8)	19(8)	-15(7)	-1(9)
C00Y	20(7)	15(6)	40(7)	-4(5)	-7(5)	14(5)
C00Z	15(7)	25(7)	40(8)	-5(5)	-4(6)	-6(5)
C010	19(7)	20(6)	37(7)	-3(5)	-7(5)	-2(5)
C011	15(7)	26(7)	39(8)	0(5)	-8(6)	4(6)
C012	20(8)	22(7)	54(9)	-5(6)	-7(7)	3(6)
N014	30(8)	39(8)	43(8)	3(6)	-10(6)	6(6)
C015	14(7)	25(7)	45(8)	-1(6)	-11(6)	10(6)
F016	64(9)	72(10)	125(14)	37(9)	28(9)	14(8)
F017	66(11)	93(12)	128(15)	-55(11)	33(10)	-12(9)
F018	98(14)	152(18)	64(10)	41(10)	-7(9)	53(13)
C01A	18(7)	18(6)	42(8)	4(5)	-6(6)	6(5)
C01B	16(7)	20(7)	57(10)	-3(6)	-8(7)	-2(6)
C01D	11(7)	27(7)	45(8)	-5(6)	-1(6)	5(6)
B01E	16(8)	15(7)	41(9)	1(6)	-3(6)	5(6)
C01F	8(6)	23(6)	44(8)	-3(5)	-11(5)	0(5)
C01G	17(7)	32(8)	45(8)	-5(6)	-14(6)	4(6)
C01H	25(8)	28(7)	72(12)	8(7)	-28(8)	1(7)
C01I	14(8)	34(8)	67(11)	-6(7)	-1(7)	-1(6)
N01J	34(8)	38(8)	48(8)	4(6)	-2(6)	4(6)
C01L	16(7)	26(7)	48(9)	-4(6)	-9(6)	9(6)
C01M	10(6)	19(6)	57(9)	-2(6)	-7(6)	2(5)
C01P	27(8)	17(6)	39(8)	2(5)	-7(6)	-1(6)
F01Q	190(30)	260(30)	94(14)	-95(18)	-99(17)	170(30)
C01S	14(7)	25(7)	40(8)	-3(5)	-11(6)	-4(6)
B01U	27(9)	8(6)	38(8)	1(5)	-10(7)	0(6)
C01W	25(8)	31(8)	41(8)	2(6)	-3(6)	11(6)
N01X	95(15)	38(8)	24(7)	-1(6)	-8(7)	-18(9)
C01Y	17(7)	27(7)	42(8)	-1(6)	-5(6)	1(6)
N020	39(10)	49(9)	51(9)	-10(7)	-9(7)	6(7)
C021	24(8)	18(7)	79(13)	4(7)	-16(8)	0(6)
F022	140(20)	280(30)	84(13)	89(18)	-68(14)	-140(20)
N025	88(16)	51(10)	66(12)	-9(8)	-15(10)	36(11)
B026	27(12)	86(18)	67(15)	-41(14)	-20(10)	9(12)
B028	26(11)	110(20)	52(13)	33(14)	-17(10)	-13(14)

Table 4 Bond Lengths for P1_a.

Atom	Atom	Length/Å	Atom	Atom	Length/Å
Fe01	N00K	1.962(12)	N00N	C011	1.395(19)
Fe01	N00N	1.963(13)	N00N	C01G	1.31(2)
Fe01	N00O	1.929(13)	N00O	C019	1.396(18)
Fe01	N00S	1.967(15)	N00O	C01S	1.35(2)
Fe01	N013	1.945(16)	N00P	C01B	1.40(2)
Fe01	N01X	1.910(14)	N00P	C01D	1.30(2)
Fe02	N00J	1.961(12)	C00Q	C012	1.36(2)
Fe02	N00L	1.952(14)	F00R	B026	1.39(3)
Fe02	N00M	1.956(13)	N00S	C012	1.40(2)

Fe02	N00P	1.968(13)	N00S	C01F	1.30(2)
Fe02	N014	1.914(15)	C00T	C01B	1.38(2)
Fe02	N01N	1.92(2)	F00U	B026	1.38(3)
S003	C00T	1.719(14)	C00V	C01M	1.38(2)
S003	C01D	1.728(14)	C00V	C01T	1.46(2)
S004	C01O	1.690(13)	F00W	B028	1.38(3)
S004	C01P	1.698(14)	C00X	C00Z	1.36(2)
S005	C015	1.701(16)	C00X	C01C	1.42(2)
S005	C01K	1.687(14)	C00Y	C01K	1.39(2)
S006	C01S	1.727(15)	C00Y	C021	1.44(2)
S006	C01W	1.698(17)	C010	C01O	1.381(19)
S007	C01G	1.717(15)	C010	C01V	1.45(2)
S007	C01L	1.707(16)	C011	C01I	1.43(2)
S008	C00Q	1.721(14)	C011	C01L	1.378(19)
S008	C01F	1.730(15)	C012	C1	1.45(3)
S009	C01A	1.713(15)	N013	C021	1.49(2)
S009	C01M	1.697(18)	N013	N2	1.34(2)
S00A	C00Z	1.713(15)	N014	C01C	1.39(2)
S00A	C01Y	1.682(17)	N014	N01J	1.42(2)
F00B	B01E	1.403(17)	F016	B028	1.34(3)
F00C	B01U	1.387(18)	F017	B026	1.34(3)
F00D	B01E	1.397(18)	F018	B028	1.40(4)
F00E	B01U	1.404(18)	C019	C01H	1.45(2)
F00F	B01E	1.38(2)	C019	C01W	1.36(2)
F00G	B01U	1.39(2)	C01B	C023	1.41(3)
F00H	B01U	1.393(18)	C01H	N020	1.27(2)
F00I	B01E	1.384(19)	C01I	N01X	1.46(3)
N00J	C010	1.386(19)	N01J	C01T	1.26(3)
N00J	C01P	1.321(19)	N01N	C01V	1.69(3)
N00K	C00Y	1.356(19)	N01N	N025	1.30(3)
N00K	C015	1.35(2)	F01Q	B026	1.38(4)
N00L	C00X	1.384(19)	N01X	N020	1.35(2)
N00L	C01Y	1.35(2)	F022	B028	1.34(4)
N00M	C00V	1.378(18)	C023	N025	1.29(3)
N00M	C01A	1.33(2)	C1	N2	1.28(3)

Table 5 Bond Angles for P1_a.

Atom	Atom	Atom	Angle/˚	Atom	Atom	Atom	Angle/˚
N00K	Fe01	N00N	89.5(5)	C01O	C010	N00J	113.7(12)
N00K	Fe01	N00S	173.6(5)	C01O	C010	C01V	128.4(14)
N00N	Fe01	N00S	90.4(5)	N00N	C011	C01I	115.3(14)
N00O	Fe01	N00K	89.4(5)	C01L	C011	N00N	113.5(13)
N00O	Fe01	N00N	174.0(5)	C01L	C011	C01I	131.2(15)
N00O	Fe01	N00S	91.3(5)	C00Q	C012	N00S	115.7(15)
N00O	Fe01	N013	93.9(6)	C00Q	C012	C1	123.8(16)
N013	Fe01	N00K	81.1(6)	N00S	C012	C1	120.5(16)
N013	Fe01	N00N	91.8(6)	C021	N013	Fe01	116.9(12)
N013	Fe01	N00S	92.5(7)	N2	N013	Fe01	139.5(14)

N01X	Fe01	N00K	93.7(6)
N01X	Fe01	N00N	82.7(8)
N01X	Fe01	N00O	91.6(8)
N01X	Fe01	N00S	92.7(6)
N01X	Fe01	N013	172.4(7)
N00J	Fe02	N00P	174.1(6)
N00L	Fe02	N00J	89.8(5)
N00L	Fe02	N00M	173.3(5)
N00L	Fe02	N00P	90.5(5)
N00M	Fe02	N00J	88.4(5)
N00M	Fe02	N00P	91.9(5)
N014	Fe02	N00J	93.9(5)
N014	Fe02	N00L	80.5(6)
N014	Fe02	N00M	93.2(6)
N014	Fe02	N00P	92.0(6)
N014	Fe02	N01N	173.3(9)
N01N	Fe02	N00J	85.1(8)
N01N	Fe02	N00L	92.8(9)
N01N	Fe02	N00M	93.5(9)
N01N	Fe02	N00P	89.0(8)
C00T	S003	C01D	90.3(7)
C01O	S004	C01P	90.6(7)
C01K	S005	C015	90.3(8)
C01W	S006	C01S	90.3(7)
C01L	S007	C01G	91.1(8)
C00Q	S008	C01F	90.7(7)
C01M	S009	C01A	91.0(8)
C01Y	S00A	C00Z	90.8(8)
C010	N00J	Fe02	117.3(9)
C01P	N00J	Fe02	131.9(10)
C01P	N00J	C010	110.7(12)
C00Y	N00K	Fe01	116.3(9)
C015	N00K	Fe01	132.0(11)
C015	N00K	C00Y	111.8(13)
C00X	N00L	Fe02	115.4(10)
C01Y	N00L	Fe02	133.7(12)
C01Y	N00L	C00X	110.8(14)
C00V	N00M	Fe02	120.6(10)
C01A	N00M	Fe02	127.4(10)
C01A	N00M	C00V	111.9(12)
C011	N00N	Fe01	114.8(10)
C01G	N00N	Fe01	132.9(11)
C01G	N00N	C011	112.3(13)
C019	N00O	Fe01	121.0(10)
C01S	N00O	Fe01	128.1(10)
C01S	N00O	C019	110.8(12)
C01B	N00P	Fe02	117.1(11)
C01D	N00P	Fe02	130.9(11)
C01D	N00P	C01B	111.9(13)
C012	C00Q	S008	108.7(11)
N2	N013	C021	103.4(15)
C01C	N014	Fe02	118.2(11)
C01C	N014	N01J	107.3(14)
N01J	N014	Fe02	134.5(13)
N00K	C015	S005	113.5(12)
N00O	C019	C01H	121.3(14)
C01W	C019	N00O	114.0(13)
C01W	C019	C01H	124.7(15)
N00M	C01A	S009	113.0(11)
N00P	C01B	C023	120.1(15)
C00T	C01B	N00P	113.9(15)
C00T	C01B	C023	126.0(16)
N014	C01C	C00X	111.3(14)
N00P	C01D	S003	114.0(11)
F00D	B01E	F00B	109.4(11)
F00F	B01E	F00B	109.6(12)
F00F	B01E	F00D	110.5(13)
F00F	B01E	F00I	109.2(12)
F00I	B01E	F00B	108.3(13)
F00I	B01E	F00D	109.8(13)
N00S	C01F	S008	113.7(11)
N00N	C01G	S007	113.1(12)
N020	C01H	C019	139.4(19)
C011	C01I	N01X	111.4(16)
C01T	N01J	N014	110.7(15)
C00Y	C01K	S005	111.2(11)
C011	C01L	S007	110.0(12)
C00V	C01M	S009	110.3(11)
C01V	N01N	Fe02	112.6(15)
N025	N01N	Fe02	150(2)
N025	N01N	C01V	97.2(18)
C010	C01O	S004	110.4(10)
N00J	C01P	S004	114.5(11)
N00O	C01S	S006	113.0(11)
N01J	C01T	C00V	137.2(16)
F00C	B01U	F00E	109.9(11)
F00C	B01U	F00H	109.0(13)
F00G	B01U	F00C	108.8(13)
F00G	B01U	F00E	110.4(13)
F00G	B01U	F00H	108.8(12)
F00H	B01U	F00E	109.9(13)
C010	C01V	N01N	107.0(15)
C019	C01W	S006	111.9(11)
C01I	N01X	Fe01	115.9(13)
N020	N01X	Fe01	139.2(17)
N020	N01X	C01I	104.9(14)
N00L	C01Y	S00A	114.0(12)
C01H	N020	N01X	107.4(18)
C00Y	C021	N013	107.6(16)
N025	C023	C01B	150(2)

C012	N00S	Fe01	119.1(11)	C023	N025	N01N	93(2)
C01F	N00S	Fe01	129.7(11)	F00U	B026	F00R	112(3)
C01F	N00S	C012	111.1(14)	F017	B026	F00R	105.5(18)
C01B	C00T	S003	109.9(11)	F017	B026	F00U	111(2)
N00M	C00V	C01M	113.8(13)	F017	B026	F01Q	108(3)
N00M	C00V	C01T	123.7(14)	F01Q	B026	F00R	111(2)
C01M	C00V	C01T	122.6(14)	F01Q	B026	F00U	109.1(19)
N00L	C00X	C01C	114.5(15)	F00W	B028	F018	112(3)
C00Z	C00X	N00L	113.9(13)	F016	B028	F00W	112(2)
C00Z	C00X	C01C	131.5(15)	F016	B028	F018	106.2(19)
N00K	C00Y	C01K	113.1(13)	F022	B028	F00W	107(2)
N00K	C00Y	C021	117.9(15)	F022	B028	F016	111(3)
C01K	C00Y	C021	128.9(15)	F022	B028	F018	108(2)
C00X	C00Z	S00A	110.5(11)	N2	C1	C012	145(2)
N00J	C010	C01V	117.9(13)	C1	N2	N013	103.7(17)

Table 6 Hydrogen Atom Coordinates (Å×10^4) and Isotropic Displacement Parameters (Å^2×10^3) for P1_a.

Atom	*x*	*y*	*z*	U(eq)
H00Q	2326.83	3039.23	2985.64	29
H00T	7706.58	-1913.56	7048.56	31
H00Z	9408.22	5891.1	8586.68	32
H015	6262.53	11439.4	1751.98	32
H01A	2939.77	1443.08	6753.31	32
H01C	6259.93	5015.17	9503.4	39
H01D	5894.41	1103.75	9113.71	34
H01F	4088.37	6106.89	923.18	29
H01G	1301.92	8814.81	3674.09	36
H01H	8267.07	8185.9	186.95	46
H01I	3734.59	10023.61	503.98	48
H01K	6201.69	11766.29	4351.51	33
H01L	561.53	10885.44	1426.03	36
H01M	-263.42	1940.84	9182.96	35
H01O	3798	6815.13	5643.83	27
H01P	3764.86	6431.56	8242.3	34
H01S	7071.93	6451.06	3285.56	31
H01T	1672.52	3213.49	9843.56	39
H01V	5328.11	3924.93	5254.44	48
H01W	10226.93	6924.76	843.45	40
H01Y	8755.48	3818.32	6344.43	35
H021	4663.01	8873.09	4727.54	48
H023	7124.04	-143.9	6027.1	63
H1	2847.9	4797.55	4043.72	57

Crystal structure determination of [P1_a]

Crystal Data for $C_{16}H_{12}B_2F_8FeN_8S_4$ (*M* =674.05 g/mol): triclinic, space group P1 (no. 1), *a* = 8.6440(17) Å, *b* = 8.8000(18) Å, *c* = 16.261(3) Å, *α* = 89.91(3)°, *β* = 75.82(3)°, *γ* = 89.92(3)°, *V* = 1199.2(4) Å^3, *Z* = 2, *T* = 293(2) K, μ(MoKα) = 1.066 mm^{-1}, *Dcalc* = 1.867 g/cm^3, 16965 reflections measured (2.584° ≤ 2Θ ≤ 52.734°), 8547 unique (R_{int} = 0.0613, R_{sigma} = 0.0927) which were used in all calculations. The final R_1 was 0.0889 (I > 2σ(I)) and wR_2 was 0.2365 (all data).

Refinement model description

Number of restraints - 3, number of constraints - unknown.

Details:

1. Fixed Uiso

At 1.2 times of:

All C(H) groups

2.a Aromatic/amide H refined with riding coordinates:

C00Q(H00Q), C00T(H00T), C00Z(H00Z), C015(H015), C01A(H01A), C01C(H01C), C01D(H01D), C01F(H01F), C01G(H01G), C01H(H01H), C01I(H01I), C01K(H01K), C01L(H01L), C01M(H01M), C01O(H01O), C01P(H01P), C01S(H01S), C01T(H01T), C01V(H01V), C01W(H01W), C01Y(H01Y), C021(H021), C023(H023), C1(H1)

Crystal Refinement Data for Complex **2** $[Fe\mathbf{L}_2](BPh_4)_2$

Identification code	p2onc_a
Empirical formula	$C_{64}H_{52}B_2FeN_8S_4$
Formula weight	1138.84
Temperature/K	293(2)
Crystal system	monoclinic
Space group	$P2_1/c$
a/Å	11.654(2)
b/Å	22.362(5)
c/Å	21.505(4)
α/°	90
β/°	98.16(3)
γ/°	90
Volume/Å^3	5548(2)
Z	4
ρ_{calc}g/cm^3	1.364
μ/mm^{-1}	0.473
F(000)	2368.0
Radiation	MoKα (λ = 0.71073)
2Θ range for data collection/°	2.642 to 56.566
Index ranges	-15 ≤ h ≤ 15, -28 ≤ k ≤ 29, -28 ≤ l ≤ 28
Reflections collected	88126
Independent reflections	13663 [R_{int} = 0.0270, R_{sigma} = 0.0154]
Data/restraints/parameters	13663/42/748
Goodness-of-fit on F^2	1.035
Final R indexes [I>=2σ (I)]	R_1 = 0.0386, wR_2 = 0.1029
Final R indexes [all data]	R_1 = 0.0393, wR_2 = 0.1036
Largest diff. peak/hole / e Å^{-3}	1.63/-0.47

Table 2 Fractional Atomic Coordinates (×10^4) and Equivalent Isotropic Displacement Parameters (Å^2×10^3) for p2onc_a. U_{eq} is defined as 1/3 of of the trace of the orthogonalised U_{IJ} tensor.

Atom	*x*	*y*	*z*	U(eq)
Fe01	7981.6(2)	6366.4(2)	1896.7(2)	23.02(6)
S002	8138.2(4)	4428.7(2)	2465.6(2)	32.87(9)
S003	10579.0(4)	6804.2(2)	3598.3(2)	34.67(9)
S004	5147.0(4)	5810.9(2)	373.8(2)	39.66(10)
S005	7943.2(4)	8241.6(2)	1123.0(2)	41.01(10)
N006	9205.4(11)	6572.1(5)	2591.1(5)	26.5(2)
N007	6922.5(11)	6110.1(5)	1153.8(5)	27.3(2)
N008	7854.5(11)	7203.8(6)	1608.6(6)	30.1(2)
N009	7932.6(11)	5546.7(6)	2223.9(5)	29.0(2)
N00A	9347.7(12)	6206.1(6)	1483.3(6)	32.0(3)
N00B	9484.9(12)	6075.7(6)	864.9(6)	34.2(3)
C00C	7319.2(13)	5967.1(6)	591.5(6)	28.1(3)
C00D	3642.9(13)	4272.3(6)	1559.0(6)	26.8(3)
C00E	1389.3(13)	4479.3(6)	1598.1(7)	29.0(3)
C00F	2981.8(13)	4638.1(6)	2643.3(6)	26.1(3)

C00G	10317.2(13)	6426.9(6)	2476.2(7)	27.2(3)
C00H	9228.4(14)	6782.7(7)	3162.2(7)	31.6(3)
C00I	7142.2(13)	5409.0(7)	2629.5(7)	29.6(3)
C00J	4740.3(13)	4480.5(7)	1460.1(6)	30.3(3)
C00K	2136.9(14)	4749.4(7)	3037.2(7)	31.8(3)
C00L	2954.9(12)	5409.5(6)	1703.6(7)	28.0(3)
C00M	3417.6(15)	3666.7(7)	1405.5(7)	32.3(3)
C00N	7641.0(14)	3287.5(6)	3695.2(7)	28.6(3)
C00O	6559.6(14)	3392.8(7)	3334.0(7)	32.3(3)
C00P	8512.1(14)	5066.2(7)	2102.6(7)	31.3(3)
C00Q	6941.5(14)	3410.3(7)	4862.7(7)	32.1(3)
C00R	9119.0(14)	3159.8(7)	4758.1(7)	31.4(3)
C00S	909.8(14)	3975.3(7)	1861.0(8)	35.1(3)
C00T	4388.2(14)	4557.3(7)	3609.7(7)	33.2(3)
C00U	8199.3(13)	4252.0(6)	4344.8(6)	29.4(3)
C00V	684.4(13)	4722.9(7)	1070.6(7)	32.2(3)
C00W	4107.8(13)	4537.5(6)	2954.9(7)	28.7(3)
C00X	6464.2(14)	5798.3(8)	121.2(7)	33.7(3)
C00Y	2803.2(14)	5631.5(7)	1082.3(7)	32.8(3)
C00Z	9013.6(16)	2538.2(7)	4847.8(7)	36.6(3)
C010	8357.3(14)	7506.7(7)	1200.5(7)	32.9(3)
C011	3314.5(14)	5838.5(6)	2169.4(7)	31.4(3)
C012	10210.7(15)	3399.7(7)	4972.1(7)	33.7(3)
C013	5794.2(14)	6041.2(7)	1101.4(7)	32.6(3)
C014	10386.9(14)	6245.4(7)	1840.7(7)	31.2(3)
C015	7431.3(15)	4696.6(7)	4501.6(7)	33.1(3)
C016	8538.9(14)	5983.4(7)	496.4(8)	33.9(3)
C017	8465.6(15)	3012.0(7)	3374.2(7)	32.3(3)
C018	2400.3(15)	4758.0(8)	3693.7(7)	37.2(3)
C019	7086.1(14)	7564.0(7)	1880.0(8)	34.7(3)
N01A	6755(2)	6673.1(12)	2360.0(11)	26.3(5)
C01B	5555.2(14)	4117.9(8)	1222.1(7)	36.5(3)
C01C	6999.9(16)	3698.3(7)	5453.2(7)	35.2(3)
C01D	11161.2(14)	6517.7(7)	2975.9(7)	32.1(3)
C01E	3527.7(16)	4665.9(7)	3981.0(7)	37.1(3)
C01F	3451.1(15)	6445.1(7)	2034.2(9)	38.0(3)
C01G	9924.3(18)	2185.0(8)	5131.1(8)	41.4(4)
C01H	7149.8(14)	4821.4(7)	2805.9(7)	31.9(3)
C01I	9130.8(14)	4462.2(7)	4053.9(7)	34.2(3)
C01J	8229.6(17)	2846.9(7)	2741.7(7)	38.0(4)
C01K	11138.1(16)	3049.1(8)	5260.0(7)	38.2(3)
C01L	4224.6(16)	3299.7(8)	1166.3(7)	38.3(4)
C01M	7579.0(17)	5303.2(7)	4382.9(7)	39.2(4)
C01N	8520.0(17)	5487.5(7)	4100.0(8)	40.5(4)
C01O	5291.1(16)	3524.5(8)	1071.7(7)	39.8(4)
C01P	6311.3(16)	3232.4(7)	2700.6(8)	38.2(3)
C01Q	9300.6(15)	5067.8(8)	3938.4(8)	38.4(3)
C01R	10993.8(17)	2440.5(8)	5343.0(7)	42.0(4)
C01S	-382.8(15)	4475.8(8)	814.0(8)	39.2(4)
C01T	2894.9(15)	6239.6(8)	944.6(9)	40.3(4)

C01U	7147.2(18)	2954.0(7)	2403.3(7)	40.3(4)
C01V	6164.5(17)	3615.8(8)	5850.8(8)	41.3(4)
C01W	3208.4(16)	6651.0(7)	1423.5(10)	42.9(4)
C01X	-157.8(16)	3726.1(8)	1610.3(9)	42.0(4)
C01Y	5996.2(17)	3021.9(8)	4713.6(8)	40.6(4)
C01Z	-806.8(15)	3973.8(8)	1083.9(9)	43.1(4)
C020	7038.5(17)	8141.8(7)	1671.9(8)	40.8(4)
B021	2718.6(14)	4702.1(7)	1871.6(7)	25.5(3)
C022	6353(3)	5836.5(17)	2911.9(18)	28.9(7)
C023	5239.5(18)	3232.9(9)	5682.6(9)	47.0(4)
C024	5158.9(19)	2931.2(9)	5111.9(10)	48.8(4)
B025	7969.4(16)	3529.4(7)	4424.2(7)	28.9(3)
C026	6408(6)	7401(3)	2414(3)	35.7(12)
N027	6158.2(19)	6398.7(10)	2810.3(10)	30.5(4)
N1	6232(3)	6898.5(17)	2675.9(16)	37.5(7)
N2	6813(3)	6408(2)	2464.4(16)	30.4(7)
C0	6476(4)	7230.8(17)	2281(2)	32.5(8)
C1	6573(5)	5909(3)	2745(3)	33.1(12)

Table 3 Anisotropic Displacement Parameters ($Å^2×10^3$) for p2onc_a. The Anisotropic displacement factor exponent takes the form: $-2π^2[h^2a^{*2}U_{11}+2hka*b*U_{12}+…]$.

Atom	U_{11}	U_{22}	U_{33}	U_{23}	U_{13}	U_{12}
Fe01	30.8(1)	21.88(10)	17.89(9)	-1.15(6)	8.69(7)	1.21(7)
S002	45.1(2)	24.99(17)	29.86(17)	1.89(13)	9.91(15)	-3.20(14)
S003	43.7(2)	39.4(2)	20.95(16)	-1.58(13)	4.62(14)	-3.23(16)
S004	37.08(19)	59.8(3)	22.75(17)	-4.47(16)	6.56(14)	-6.17(17)
S005	58.8(3)	24.28(18)	42.4(2)	2.66(15)	15.51(19)	4.30(16)
N006	34.0(6)	22.3(5)	24.2(5)	0.7(4)	7.4(4)	0.0(4)
N007	39.7(6)	23.4(6)	19.6(5)	0.7(4)	7.2(4)	0.7(5)
N008	36.7(6)	23.2(6)	29.9(6)	-4.7(4)	3.1(5)	4.3(5)
N009	37.6(6)	28.9(6)	20.3(5)	3.1(4)	3.6(4)	-7.2(5)
N00A	44.8(7)	22.1(6)	32.9(6)	1.1(5)	18.5(5)	2.8(5)
N00B	42.9(7)	33.8(7)	28.1(6)	-0.9(5)	12.6(5)	3.6(5)
C00C	38.8(7)	26.7(7)	19.6(6)	0.1(5)	6.5(5)	1.6(5)
C00D	36.1(7)	25.9(7)	18.8(6)	0.4(5)	5.5(5)	4.6(5)
C00E	34.4(7)	24.0(6)	30.3(7)	-4.5(5)	10.4(5)	1.9(5)
C00F	37.4(7)	17.2(6)	25.5(6)	-0.3(5)	10.4(5)	-0.3(5)
C00G	32.5(7)	24.0(6)	26.0(6)	0.3(5)	6.9(5)	-1.1(5)
C00H	39.1(8)	31.8(7)	24.9(6)	0.5(5)	8.2(5)	0.7(6)
C00I	33.2(7)	31.4(7)	24.4(6)	4.9(5)	4.2(5)	-2.4(6)
C00J	35.0(7)	34.7(7)	21.6(6)	-0.5(5)	5.7(5)	3.8(6)
C00K	38.4(7)	28.1(7)	30.9(7)	-1.1(5)	11.8(6)	2.5(6)
C00L	32.2(7)	22.8(6)	30.7(7)	2.4(5)	10.7(5)	3.2(5)
C00M	43.4(8)	26.8(7)	27.9(7)	-1.8(5)	8.8(6)	4.9(6)
C00N	42.9(8)	18.7(6)	24.8(6)	1.5(5)	6.5(5)	-1.6(5)
C00O	42.4(8)	23.4(7)	31.2(7)	1.6(5)	5.2(6)	-0.2(6)
C00P	41.9(8)	29.6(7)	23.5(6)	-0.2(5)	8.3(5)	-8.9(6)
C00Q	45.7(8)	23.5(7)	28.6(7)	1.4(5)	10.9(6)	0.8(6)
C00R	47.2(8)	26.5(7)	21.0(6)	0.6(5)	6.9(6)	2.0(6)

C00S	40.7(8)	28.1(7)	38.2(8)	-2.1(6)	11.7(6)	-1.5(6)
C00T	41.6(8)	30.6(7)	27.5(7)	-2.8(5)	5.8(6)	-0.8(6)
C00U	40.6(7)	24.5(7)	22.2(6)	0.1(5)	2.0(5)	-2.2(5)
C00V	36.7(7)	30.7(7)	30.2(7)	-5.5(5)	8.3(6)	2.4(6)
C00W	37.7(7)	24.6(6)	25.5(6)	-1.8(5)	9.8(5)	-1.2(5)
C00X	38.0(8)	43.5(9)	20.7(6)	-2.5(6)	7.5(5)	-0.9(6)
C00Y	36.7(7)	30.9(7)	32.7(7)	6.3(6)	11.7(6)	4.5(6)
C00Z	53.8(9)	28.4(7)	27.9(7)	1.3(6)	7.0(6)	1.2(6)
C010	43.8(8)	25.9(7)	29.3(7)	-3.1(5)	6.1(6)	5.5(6)
C011	38.2(7)	22.3(7)	35.5(7)	1.0(5)	11.5(6)	1.8(5)
C012	47.3(9)	29.4(7)	24.6(6)	-0.6(5)	5.7(6)	2.4(6)
C013	42.6(8)	36.0(8)	20.2(6)	-0.2(5)	7.9(5)	-1.2(6)
C014	41.4(8)	26.6(7)	25.9(7)	-0.2(5)	6.1(6)	5.1(6)
C015	48.2(8)	26.8(7)	24.9(6)	-0.8(5)	6.8(6)	0.2(6)
C016	38.6(8)	28.7(7)	34.4(7)	1.4(6)	4.5(6)	1.9(6)
C017	46.2(8)	24.5(7)	26.9(7)	2.8(5)	7.9(6)	2.4(6)
C018	48.5(9)	35.6(8)	31.2(7)	-3.3(6)	18.9(7)	2.0(7)
C019	41.0(8)	27.3(7)	36.9(8)	-2.2(6)	9.7(6)	7.2(6)
N01A	28.8(8)	27.1(8)	24.1(8)	-0.2(7)	7.6(6)	1.3(7)
C01B	34.0(7)	53.2(10)	22.6(6)	-0.4(6)	5.3(5)	9.6(7)
C01C	48.5(9)	30.3(7)	27.4(7)	0.6(6)	8.3(6)	0.1(6)
C01D	37.3(7)	35.1(8)	24.6(6)	0.5(5)	6.3(5)	-2.5(6)
C01E	54.7(9)	34.3(8)	23.9(7)	-3.2(6)	11.3(6)	-0.3(7)
C01F	42.2(8)	22.4(7)	52.7(10)	-2.5(6)	18.1(7)	-0.8(6)
C01G	67.8(11)	28.2(8)	29.8(7)	4.0(6)	12.6(7)	7.9(7)
C01H	37.2(7)	31.8(7)	27.9(7)	4.5(5)	8.8(6)	-3.5(6)
C01I	40.5(8)	30.7(8)	31.0(7)	4.0(6)	4.0(6)	-1.0(6)
C01J	65.0(11)	22.9(7)	28.5(7)	0.9(5)	15.0(7)	3.8(7)
C01K	47.3(9)	41.2(9)	25.9(7)	-3.5(6)	4.5(6)	6.3(7)
C01L	54.6(10)	30.8(8)	29.9(7)	-4.6(6)	7.7(7)	12.0(7)
C01M	61.6(10)	25.9(7)	29.9(7)	-2.1(6)	6.0(7)	4.3(7)
C01N	62.3(11)	24.3(7)	32.7(8)	1.1(6)	-1.0(7)	-8.1(7)
C01O	47.9(9)	47.5(9)	24.2(7)	-2.5(6)	5.7(6)	21.1(7)
C01P	51.3(9)	28.0(7)	32.7(8)	3.5(6)	-2.5(7)	-5.6(6)
C01Q	43.8(8)	36.0(8)	34.2(8)	7.7(6)	1.0(6)	-9.5(7)
C01R	60.5(10)	40.5(9)	25.7(7)	4.0(6)	8.5(7)	17.5(8)
C01S	38.0(8)	44.1(9)	35.2(8)	-11.9(7)	4.0(6)	5.2(7)
C01T	44.3(9)	35.5(8)	44.4(9)	16.7(7)	17.8(7)	9.1(7)
C01U	72.4(12)	24.0(7)	23.7(7)	0.2(5)	4.1(7)	-4.7(7)
C01V	58.7(10)	37.4(9)	30.6(8)	0.8(6)	15.9(7)	3.7(7)
C01W	47.6(9)	23.4(7)	62.5(11)	11.5(7)	23.8(8)	5.0(6)
C01X	44.8(9)	31.3(8)	53.1(10)	-9.8(7)	18.5(8)	-8.0(7)
C01Y	57.1(10)	29.8(8)	37.9(8)	-3.8(6)	16.6(7)	-8.0(7)
C01Z	37.3(8)	42.8(9)	50.2(10)	-19.5(8)	10.0(7)	-4.3(7)
C020	55(1)	27.3(8)	42.8(9)	-1.8(6)	16.3(7)	9.6(7)
B021	33.4(7)	20.3(7)	23.9(7)	-0.3(5)	8.5(5)	1.2(5)
C022	33.5(17)	31.7(15)	24.0(18)	3.6(12)	12.6(12)	2.1(11)
C023	59.4(11)	42.4(10)	44.6(10)	4.0(7)	26.2(8)	-3.5(8)
C024	61.3(11)	37.4(9)	51.8(11)	-1.8(8)	22.8(9)	-13.6(8)
B025	41.6(8)	22.3(7)	23.7(7)	-0.3(5)	7.4(6)	-0.4(6)

C026	41(2)	35(3)	32(3)	-7(2)	10(2)	9(2)
N027	36.4(10)	32.7(11)	25.3(9)	2.2(8)	14.3(8)	3.4(8)
N1	41.8(18)	43.9(19)	29.4(15)	-8.2(13)	14.2(13)	10.6(14)
N2	32.0(16)	39(2)	20.8(15)	-5.7(14)	6.8(12)	3.9(15)
C0	40.4(16)	29.0(18)	29.9(18)	-4.7(13)	11.0(13)	7.4(15)
C1	32(3)	47(3)	22(3)	4.2(19)	10.3(18)	-1.5(19)

Table 4 Bond Lengths for p2onc_a.

Atom	Atom	Length/Å	Atom	Atom	Length/Å
Fe01	N006	1.9675(14)	C00N	C017	1.403(2)
Fe01	N007	1.9607(14)	C00N	B025	1.651(2)
Fe01	N008	1.9714(13)	C00O	C01P	1.399(2)
Fe01	N009	1.9672(13)	C00Q	C01C	1.417(2)
Fe01	N00A	1.9634(14)	C00Q	C01Y	1.404(2)
Fe01	N01A	1.978(2)	C00Q	B025	1.648(2)
Fe01	N2	1.956(4)	C00R	C00Z	1.411(2)
S002	C00P	1.7112(15)	C00R	C012	1.397(2)
S002	C01H	1.6951(17)	C00R	B025	1.649(2)
S003	C00H	1.7147(17)	C00S	C01X	1.400(2)
S003	C01D	1.7090(16)	C00T	C00W	1.400(2)
S004	C00X	1.6997(17)	C00T	C01E	1.389(2)
S004	C013	1.7169(16)	C00U	C015	1.410(2)
S005	C010	1.7142(16)	C00U	C01I	1.408(2)
S005	C020	1.7053(19)	C00U	B025	1.651(2)
N006	C00G	1.3916(19)	C00V	C01S	1.401(2)
N006	C00H	1.3119(18)	C00Y	C01T	1.399(2)
N007	C00C	1.3918(17)	C00Z	C01G	1.392(2)
N007	C013	1.313(2)	C011	C01F	1.401(2)
N008	C010	1.311(2)	C012	C01K	1.406(2)
N008	C019	1.3928(19)	C015	C01M	1.396(2)
N009	C00I	1.3901(19)	C017	C01J	1.399(2)
N009	C00P	1.315(2)	C018	C01E	1.386(3)
N00A	N00B	1.3926(17)	C019	C020	1.366(2)
N00A	C014	1.342(2)	C019	C026	1.527(7)
N00B	C016	1.280(2)	C019	C0	1.407(5)
C00C	C00X	1.368(2)	N01A	N027	1.410(3)
C00C	C016	1.465(2)	N01A	C0	1.294(5)
C00D	C00J	1.405(2)	C01B	C01O	1.390(3)
C00D	C00M	1.410(2)	C01C	C01V	1.396(2)
C00D	B021	1.656(2)	C01F	C01W	1.383(3)
C00E	C00S	1.411(2)	C01G	C01R	1.388(3)
C00E	C00V	1.412(2)	C01I	C01Q	1.396(2)
C00E	B021	1.654(2)	C01J	C01U	1.385(3)
C00F	C00K	1.409(2)	C01K	C01R	1.386(3)
C00F	C00W	1.404(2)	C01L	C01O	1.382(3)
C00F	B021	1.650(2)	C01M	C01N	1.390(3)
C00G	C014	1.439(2)	C01N	C01Q	1.385(3)
C00G	C01D	1.365(2)	C01P	C01U	1.386(3)

C00I	C01H	1.367(2)	C01S	C01Z	1.386(3)
C00I	C022	1.512(4)	C01T	C01W	1.390(3)
C00I	C1	1.342(7)	C01V	C023	1.384(3)
C00J	C01B	1.400(2)	C01X	C01Z	1.385(3)
C00K	C018	1.402(2)	C01Y	C024	1.402(3)
C00L	C00Y	1.413(2)	C022	N027	1.291(4)
C00L	C011	1.407(2)	C023	C024	1.392(3)
C00L	B021	1.654(2)	C026	N1	1.287(8)
C00M	C01L	1.400(2)	N1	N2	1.399(5)
C00N	C00O	1.403(2)	N2	C1	1.317(7)

Table 5 Bond Angles for p2onc_a.

Atom	Atom	Atom	Angle/˚	Atom	Atom	Atom	Angle/˚
N006	Fe01	N008	91.75(5)	C012	C00R	B025	126.62(14)
N006	Fe01	N01A	91.98(8)	C01X	C00S	C00E	123.00(16)
N007	Fe01	N006	172.50(5)	C01E	C00T	C00W	119.94(15)
N007	Fe01	N008	90.63(5)	C015	C00U	B025	123.19(14)
N007	Fe01	N009	88.40(5)	C01I	C00U	C015	115.23(14)
N007	Fe01	N00A	92.00(6)	C01I	C00U	B025	121.29(13)
N007	Fe01	N01A	95.47(8)	C01S	C00V	C00E	123.16(16)
N008	Fe01	N01A	78.55(9)	C00T	C00W	C00F	122.93(14)
N009	Fe01	N006	90.07(5)	C00C	C00X	S004	110.81(11)
N009	Fe01	N008	173.13(6)	C01T	C00Y	C00L	122.60(16)
N009	Fe01	N01A	94.77(9)	C01G	C00Z	C00R	122.88(17)
N00A	Fe01	N006	80.76(6)	N008	C010	S005	114.46(12)
N00A	Fe01	N008	93.48(5)	C01F	C011	C00L	122.92(15)
N00A	Fe01	N009	93.35(5)	C00R	C012	C01K	122.56(16)
N00A	Fe01	N01A	169.11(9)	N007	C013	S004	114.74(11)
N2	Fe01	N006	90.51(11)	N00A	C014	C00G	113.22(14)
N2	Fe01	N007	96.25(11)	C01M	C015	C00U	122.86(16)
N2	Fe01	N008	97.08(14)	N00B	C016	C00C	133.25(15)
N2	Fe01	N009	76.27(14)	C01J	C017	C00N	122.73(16)
N2	Fe01	N00A	166.50(13)	C01E	C018	C00K	120.35(14)
C01H	S002	C00P	89.88(8)	N008	C019	C026	127.5(3)
C01D	S003	C00H	89.81(8)	N008	C019	C0	111.2(2)
C00X	S004	C013	89.79(8)	C020	C019	N008	114.10(15)
C020	S005	C010	90.02(8)	C020	C019	C026	118.1(3)
C00G	N006	Fe01	113.79(9)	C020	C019	C0	134.5(2)
C00H	N006	Fe01	135.29(11)	N027	N01A	Fe01	131.1(2)
C00H	N006	C00G	110.75(13)	C0	N01A	Fe01	117.0(2)
C00C	N007	Fe01	121.79(10)	C0	N01A	N027	111.7(3)
C013	N007	Fe01	127.68(10)	C01O	C01B	C00J	119.92(16)
C013	N007	C00C	110.53(12)	C01V	C01C	C00Q	122.68(16)
C010	N008	Fe01	132.88(11)	C00G	C01D	S003	110.52(12)
C010	N008	C019	110.90(13)	C018	C01E	C00T	119.07(14)
C019	N008	Fe01	116.22(11)	C01W	C01F	C011	120.37(16)
C00I	N009	Fe01	119.10(10)	C01R	C01G	C00Z	120.24(16)
C00P	N009	Fe01	130.45(10)	C00I	C01H	S002	110.86(11)

C00P	N009	C00I	110.38(12)	C01Q	C01I	C00U	122.72(16)
N00B	N00A	Fe01	132.92(11)	C01U	C01J	C017	120.28(16)
C014	N00A	Fe01	116.91(10)	C01R	C01K	C012	120.30(17)
C014	N00A	N00B	110.11(13)	C01O	C01L	C00M	120.39(16)
C016	N00B	N00A	114.80(14)	C01N	C01M	C015	119.59(16)
N007	C00C	C016	124.35(13)	C01Q	C01N	C01M	119.74(15)
C00X	C00C	N007	114.13(14)	C01L	C01O	C01B	119.14(15)
C00X	C00C	C016	121.52(13)	C01U	C01P	C00O	120.16(16)
C00J	C00D	C00M	115.23(13)	C01N	C01Q	C01I	119.86(16)
C00J	C00D	B021	121.84(13)	C01K	C01R	C01G	118.79(16)
C00M	C00D	B021	122.85(13)	C01Z	C01S	C00V	120.25(17)
C00S	C00E	C00V	114.31(14)	C01W	C01T	C00Y	120.41(16)
C00S	C00E	B021	120.15(13)	C01J	C01U	C01P	118.86(15)
C00V	C00E	B021	125.32(13)	C023	C01V	C01C	120.44(16)
C00K	C00F	B021	122.89(13)	C01F	C01W	C01T	118.68(15)
C00W	C00F	C00K	115.27(13)	C01Z	C01X	C00S	120.53(17)
C00W	C00F	B021	121.42(12)	C024	C01Y	C00Q	122.81(16)
N006	C00G	C014	114.46(13)	C01X	C01Z	C01S	118.71(16)
C01D	C00G	N006	114.23(13)	C019	C020	S005	110.51(12)
C01D	C00G	C014	131.16(14)	C00E	B021	C00D	108.13(11)
N006	C00H	S003	114.66(12)	C00E	B021	C00L	112.77(12)
N009	C00I	C022	127.35(18)	C00F	B021	C00D	108.61(11)
C01H	C00I	N009	114.09(14)	C00F	B021	C00E	111.25(12)
C01H	C00I	C022	118.46(18)	C00F	B021	C00L	106.84(11)
C1	C00I	N009	108.7(3)	C00L	B021	C00D	109.16(11)
C1	C00I	C01H	137.2(3)	N027	C022	C00I	130.6(3)
C01B	C00J	C00D	122.86(15)	C01V	C023	C024	118.87(17)
C018	C00K	C00F	122.41(15)	C023	C024	C01Y	120.20(18)
C00Y	C00L	B021	122.71(13)	C00Q	B025	C00N	113.64(13)
C011	C00L	C00Y	114.72(14)	C00Q	B025	C00R	106.35(12)
C011	C00L	B021	122.57(13)	C00Q	B025	C00U	111.05(12)
C01L	C00M	C00D	122.45(16)	C00R	B025	C00N	108.28(12)
C00O	C00N	B025	122.65(14)	C00R	B025	C00U	113.69(13)
C017	C00N	C00O	115.18(14)	C00U	B025	C00N	103.98(11)
C017	C00N	B025	121.90(14)	N1	C026	C019	132.0(5)
C01P	C00O	C00N	122.79(16)	C022	N027	N01A	116.6(2)
N009	C00P	S002	114.78(11)	C026	N1	N2	115.4(4)
C01C	C00Q	B025	119.55(14)	N1	N2	Fe01	130.7(3)
C01Y	C00Q	C01C	114.98(15)	C1	N2	Fe01	117.3(4)
C01Y	C00Q	B025	125.44(14)	C1	N2	N1	111.8(4)
C00Z	C00R	B025	118.17(14)	N01A	C0	C019	116.8(3)
C012	C00R	C00Z	115.21(15)	N2	C1	C00I	118.5(4)

Table 6 Hydrogen Atom Coordinates (Å×10^4) and Isotropic Displacement Parameters (Å^2×10^3) for p2onc_a.

Atom	*x*	*y*	*z*	U(eq)
H00H	8565	6910	3318	38
H00J	4934	4876	1557	36
H00K	1377	4820	2855	38

H00M	2706	3505	1465	39
H00O	5984	3577	3524	39
H00P	9081	5072	1840	38
H00S	1322	3801	2217	42
H00T	5150	4498	3796	40
H00V	941	5064	885	39
H00W	4693	4454	2716	34
H00X	6587	5691	-282	40
H00Y	2636	5363	752	39
H00Z	8305	2357	4712	44
H010	8894	7337	972	40
H011	3468	5714	2585	38
H012	10328	3807	4922	40
H013	5378	6112	1433	39
H014	11082	6164	1692	37
H015	6799	4580	4693	40
H016	8648	5912	83	41
H017	9200	2936	3591	39
H018	1815	4826	3938	45
H01B	6272	4274	1165	44
H01C	7620	3953	5581	42
H01D	11944	6435	2977	39
H01E	3706	4677	4416	44
H01F	3706	6711	2357	46
H01G	9816	1776	5178	50
H01H	6676	4659	3076	38
H01I	9654	4186	3934	41
H01J	8802	2664	2548	46
H01K	11852	3226	5395	46
H01L	4042	2902	1070	46
H01M	7051	5582	4492	47
H01N	8625	5891	4020	49
H01O	5825	3282	910	48
H01P	5584	3313	2478	46
H01Q	9936	5189	3753	46
H01R	11603	2207	5537	50
H01S	-808	4649	461	47
H01T	2745	6369	530	48
H01U	6984	2841	1984	48
H01V	6230	3819	6231	50
H01W	3254	7057	1335	52
H01X	-434	3391	1799	50
H01Y	5922	2816	4334	49
H01Z	-1513	3807	915	52
H020	6577	8439	1810	49
H022	5941	5667	3207	35
H023	4681	3178	5946	56
H024	4548	2669	4994	59
H026	6056	7726	2580	43
H0	5899	7403	2480	39

H1	6021	5904	3018	40

Table 7 Atomic Occupancy for p2onc_a.

Atom	*Occupancy*	Atom	*Occupancy*	Atom	*Occupancy*
N01A	0.6	C022	0.6	H022	0.6
C026	0.4	H026	0.4	N027	0.6
N1	0.4	N2	0.4	C0	0.6
H0	0.6	C1	0.4	H1	0.4

Crystal structure determination of [p2onc_a]

Crystal Data for $C_{64}H_{52}B_2FeN_8S_4$ (M =1138.84 g/mol): monoclinic, space group $P2_1/c$ (no. 14), a = 11.654(2) Å, b = 22.362(5) Å, c = 21.505(4) Å, β = 98.16(3)°, V = 5548(2) Å^3, Z = 4, T = 293(2) K, μ(MoKα) = 0.473 mm^{-1}, *Dcalc* = 1.364 g/cm^3, 88126 reflections measured (2.642° ≤ 2Θ ≤ 56.566°), 13663 unique (R_{int} = 0.0270, R_{sigma} = 0.0154) which were used in all calculations. The final R_1 was 0.0386 (I > 2σ(I)) and wR_2 was 0.1036 (all data).

Refinement model description

Number of restraints - 42, number of constraints - unknown.
Details:
1. Fixed Uiso
At 1.2 times of:
All C(H) groups
2. Restrained distances
C022-C00I
1.46 with sigma of 0.02
C1-C00I
1.44 with sigma of 0.02
C019-C0
1.44 with sigma of 0.02
C026-C019
1.46 with sigma of 0.02
N1-C026
1.34 with sigma of 0.02
N027-C022
1.34 with sigma of 0.02
3. Uiso/Uaniso restraints and constraints
Uanis(N01A) ≈ Ueq: with sigma of 0.001 and sigma for terminal atoms of
0.0005
4. Rigid body (RIGU) restrains
C022, C1, N027, N2, N01A, N1, C026, C0
with sigma for 1-2 distances of 0.004 and sigma for 1-3 distances of 0.004
5. Others
Fixed Sof: N01A(0.6) C022(0.6) H022(0.6) C026(0.4) H026(0.4) N027(0.6)
N1(0.4) N2(0.4) C0(0.6) H0(0.6) C1(0.4) H1(0.4)
6.a Aromatic/amide H refined with riding coordinates:
C00H(H00H), C00J(H00J), C00K(H00K), C00M(H00M), C00O(H00O), C00P(H00P),
C00S(H00S), C00T(H00T), C00V(H00V), C00W(H00W), C00X(H00X), C00Y(H00Y),
C00Z(H00Z), C010(H010), C011(H011), C012(H012), C013(H013), C014(H014),
C015(H015), C016(H016), C017(H017), C018(H018), C01B(H01B), C01C(H01C),
C01D(H01D), C01E(H01E), C01F(H01F), C01G(H01G), C01H(H01H), C01I(H01I),
C01J(H01J), C01K(H01K), C01L(H01L), C01M(H01M), C01N(H01N), C01O(H01O),
C01P(H01P), C01Q(H01Q), C01R(H01R), C01S(H01S), C01T(H01T), C01U(H01U),
C01V(H01V), C01W(H01W), C01X(H01X), C01Y(H01Y), C01Z(H01Z), C020(H020),
C022(H022), C023(H023), C024(H024), C026(H026), C0(H0), C1(H1)

Crystal Refinement Data for Complex **4** [Fe**L**$_2$](Br)$_2$

Identification code	Mono
Empirical formula	$C_{18}H_{20}Br_2FeN_8O_2S_4$
Formula weight	724.33
Temperature/K	293(2)
Crystal system	monoclinic
Space group	$P2_1/n$
a/Å	8.6690(17)
b/Å	17.524(4)
c/Å	19.320(4)
α/°	90
β/°	101.98(3)
γ/°	90
Volume/Å^3	2871.0(10)
Z	4
ρ_{calc}g/cm^3	1.676
μ/mm^{-1}	3.631
F(000)	1440.0
Radiation	MoKα (λ = 0.71073)
2Θ range for data collection/°	3.17 to 56.56
Index ranges	-10 ≤ h ≤ 10, -23 ≤ k ≤ 23, -25 ≤ l ≤ 25
Reflections collected	47743
Independent reflections	6568 [R_{int} = 0.1722, R_{sigma} = 0.0771]
Data/restraints/parameters	6568/3/333
Goodness-of-fit on F^2	1.081
Final R indexes [I>=2σ (I)]	R_1 = 0.1322, wR_2 = 0.3732
Final R indexes [all data]	R_1 = 0.1656, wR_2 = 0.3993
Largest diff. peak/hole / e Å^{-3}	2.92/-2.18

Table 2 Fractional Atomic Coordinates (×10^4) and Equivalent Isotropic Displacement Parameters (Å^2×10^3) for Mono. U_{eq} is defined as 1/3 of of the trace of the orthogonalised U_{IJ} tensor.

Atom	*x*	*y*	*z*	U(eq)
Br01	-1834.3(17)	5949.6(8)	3555.1(9)	45.8(4)
Br02	1262(2)	1080.5(9)	4329.3(10)	57.7(5)
Fe03	4430(2)	3194.6(10)	2982.1(11)	34.6(5)
S004	3331(5)	3075(2)	5157(2)	48.7(9)
S005	5429(5)	3056(2)	799(2)	49.0(9)
S006	9380(5)	3955(3)	3847(3)	58.1(11)
S007	-600(5)	2629(3)	2003(3)	56.7(11)
N008	4781(15)	3274(7)	2027(7)	44(3)
N009	3955(15)	3256(8)	3927(7)	49(3)
N00A	6684(13)	3377(6)	3381(6)	39(2)
N00B	2255(13)	2886(6)	2581(7)	39(3)
N00C	4741(18)	2084(7)	3050(8)	54(3)
O00D	1627(16)	5642(8)	4584(10)	80(4)

N00E	3920(20)	4258(10)	3080(12)	24(4)
C00F	5241(15)	2739(8)	1607(9)	44(3)
C00G	2027(19)	2086(8)	2541(9)	47(4)
C00H	4620(17)	3969(9)	1676(8)	44(3)
C00I	3170(19)	3963(9)	4801(8)	49(4)
C00J	3904(17)	2733(9)	4428(9)	47(3)
C00K	3521(17)	3971(8)	4156(8)	43(3)
C00L	4951(18)	3959(9)	1011(8)	45(3)
C00M	7714(16)	2756(8)	3588(8)	44(3)
C00N	4191(18)	4624(10)	2029(9)	51(4)
C00O	538(19)	1859(10)	2238(10)	55(4)
C00P	979(19)	3251(10)	2321(8)	50(4)
C00Q	9253(19)	2997(12)	3867(9)	60(4)
C00R	3450(20)	1614(11)	2812(10)	57(4)
N00S	5970(20)	1610(9)	3323(12)	80(5)
C00T	7440(18)	4016(10)	3497(8)	48(3)
C00U	2400(20)	6380(11)	4596(12)	69(5)
C00V	3480(20)	4583(14)	3671(9)	65(5)
C00W	7260(20)	1987(10)	3548(11)	62(5)
C00X	-1530(30)	4784(14)	1917(13)	33(5)
O00Y	4310(30)	1430(13)	5520(11)	51(5)
O00Z	-200(30)	4926(13)	2335(12)	52(5)
N010	3840(30)	4879(14)	2586(12)	38(5)
N011	3650(40)	4930(15)	3095(18)	55(7)
C012	5610(60)	1100(30)	5370(20)	76(11)
N00F	4030(40)	4302(18)	2727(17)	51(8)

Table 3 Anisotropic Displacement Parameters ($Å^2×10^3$) for Mono. The Anisotropic displacement factor exponent takes the form: $-2π^2[h^2a^{*2}U_{11}+2hka*b*U_{12}+…]$.

Atom	U_{11}	U_{22}	U_{33}	U_{23}	U_{13}	U_{12}
Br01	28.3(7)	36.5(7)	71.5(10)	0.3(6)	8.0(6)	-1.8(5)
Br02	45.9(10)	45.5(9)	82.6(12)	5.0(7)	15.4(8)	-1.0(7)
Fe03	17.7(9)	25.5(8)	60.5(12)	-3.0(7)	7.7(7)	-0.6(6)
S004	33(2)	48(2)	67(2)	-2.2(16)	12.6(16)	-1.7(14)
S005	29(2)	51(2)	69(3)	-5.6(17)	15.8(16)	3.6(15)
S006	22.8(19)	69(3)	80(3)	-5(2)	5.1(17)	-7.9(16)
S007	29(2)	68(3)	71(3)	-1(2)	4.9(17)	-8.4(17)
N008	37(7)	33(6)	60(8)	4(5)	6(5)	10(5)
N009	33(7)	50(7)	62(8)	-17(6)	6(5)	-7(5)
N00A	22(6)	33(5)	61(7)	-2(5)	7(5)	-4(4)
N00B	23(6)	27(5)	67(8)	-6(5)	11(5)	-4(4)
N00C	63(9)	32(6)	67(9)	2(5)	14(7)	11(6)
O00D	41(7)	66(8)	126(13)	16(8)	-2(7)	0(6)
N00E	19(10)	20(8)	33(11)	3(7)	2(7)	1(6)
C00F	15(6)	43(7)	75(10)	8(6)	15(6)	2(5)
C00G	40(9)	42(8)	63(9)	-8(6)	20(7)	-19(6)
C00H	29(7)	48(8)	54(8)	7(6)	6(6)	0(6)
C00I	38(9)	55(9)	51(8)	-7(6)	3(6)	5(6)
C00J	28(7)	42(8)	73(10)	-10(7)	13(6)	1(5)

C00K	27(7)	41(7)	60(9)	-9(6)	8(6)	5(5)
C00L	31(8)	52(8)	54(8)	1(6)	10(6)	5(6)
C00M	18(7)	46(8)	67(9)	2(6)	10(6)	7(5)
C00N	31(8)	52(9)	72(10)	-12(7)	16(7)	8(6)
C00O	28(8)	50(9)	89(12)	-14(8)	21(7)	-9(6)
C00P	35(8)	58(9)	56(9)	-1(7)	8(6)	4(6)
C00Q	25(8)	87(13)	64(10)	-1(9)	2(7)	13(8)
C00R	42(10)	57(10)	76(12)	4(8)	20(8)	-5(7)
N00S	48(10)	44(8)	145(17)	1(9)	11(10)	-2(7)
C00T	29(8)	62(9)	54(9)	-7(7)	7(6)	-9(6)
C00U	39(9)	66(9)	94(14)	-1(9)	-2(9)	-3(7)
C00V	33(9)	111(16)	52(9)	18(9)	7(7)	-8(9)
C00W	31(9)	47(9)	116(16)	-8(9)	31(9)	-6(6)
N010	39(14)	47(13)	27(11)	11(9)	4(9)	6(10)
N011	45(17)	40(14)	80(20)	3(13)	13(14)	4(11)

Table 4 Bond Lengths for Mono.

Atom	Atom	Length/Å	Atom	Atom	Length/Å
Fe03	N008	1.936(13)	N00B	C00P	1.286(19)
Fe03	N009	1.956(14)	N00C	C00R	1.39(2)
Fe03	N00A	1.972(11)	N00C	N00S	1.37(2)
Fe03	N00B	1.960(11)	O00D	C00U	1.46(2)
Fe03	N00C	1.965(12)	N00E	C00V	1.40(3)
Fe03	N00E	1.934(18)	N00E	N010	1.44(3)
Fe03	N00F	2.01(3)	C00G	C00O	1.36(2)
S004	C00I	1.696(17)	C00G	C00R	1.49(2)
S004	C00J	1.699(17)	C00H	C00L	1.37(2)
S005	C00F	1.698(16)	C00H	C00N	1.42(2)
S005	C00L	1.708(16)	C00I	C00K	1.34(2)
S006	C00Q	1.68(2)	C00K	C00V	1.42(2)
S006	C00T	1.681(16)	C00M	C00Q	1.40(2)
S007	C00O	1.678(18)	C00M	C00W	1.40(2)
S007	C00P	1.757(17)	C00N	N010	1.26(3)
N008	C00F	1.353(19)	C00N	N00F	1.50(4)
N008	C00H	1.386(18)	N00S	C00W	1.29(2)
N009	C00J	1.34(2)	C00V	N011	1.30(4)
N009	C00K	1.405(18)	C00X	O00Z	1.29(3)
N00A	C00M	1.412(17)	O00Y	C012	1.35(5)
N00A	C00T	1.294(18)	N011	N00F	1.39(4)
N00B	C00G	1.415(17)			

Table 5 Bond Angles for Mono.

Atom	Atom	Atom	Angle/˚	Atom	Atom	Atom	Angle/˚
N008	Fe03	N009	172.1(5)	N00S	N00C	Fe03	135.4(12)
N008	Fe03	N00A	91.2(5)	N00S	N00C	C00R	106.1(14)
N008	Fe03	N00B	88.4(5)	C00V	N00E	Fe03	125.4(16)
N008	Fe03	N00C	95.1(5)	C00V	N00E	N010	104.4(18)

N008	Fe03	N00F	75.6(10)	N010	N00E	Fe03	130.1(18)
N009	Fe03	N00A	90.6(5)	N008	C00F	S005	114.9(11)
N009	Fe03	N00B	90.7(5)	N00B	C00G	C00R	115.8(13)
N009	Fe03	N00C	92.6(6)	C00O	C00G	N00B	115.0(15)
N009	Fe03	N00F	96.7(10)	C00O	C00G	C00R	129.1(15)
N00A	Fe03	N00F	92.7(10)	N008	C00H	C00N	118.9(15)
N00B	Fe03	N00A	173.3(5)	C00L	C00H	N008	115.3(14)
N00B	Fe03	N00C	82.0(6)	C00L	C00H	C00N	125.7(15)
N00B	Fe03	N00F	93.7(10)	C00K	C00I	S004	111.8(12)
N00C	Fe03	N00A	91.3(6)	N009	C00J	S004	114.6(11)
N00C	Fe03	N00F	169.9(10)	N009	C00K	C00V	115.9(16)
N00E	Fe03	N008	96.2(8)	C00I	C00K	N009	114.3(14)
N00E	Fe03	N009	76.0(8)	C00I	C00K	C00V	129.8(15)
N00E	Fe03	N00A	91.9(7)	C00H	C00L	S005	110.1(12)
N00E	Fe03	N00B	94.8(6)	C00Q	C00M	N00A	111.9(14)
N00E	Fe03	N00C	168.2(8)	C00Q	C00M	C00W	123.2(15)
C00I	S004	C00J	90.0(8)	C00W	C00M	N00A	124.8(14)
C00F	S005	C00L	90.4(8)	C00H	C00N	N00F	102.1(18)
C00T	S006	C00Q	90.5(8)	N010	C00N	C00H	146(2)
C00O	S007	C00P	91.9(8)	C00G	C00O	S007	109.4(12)
C00F	N008	Fe03	130.2(10)	N00B	C00P	S007	111.8(12)
C00F	N008	C00H	109.1(13)	C00M	C00Q	S006	110.8(12)
C00H	N008	Fe03	120.7(10)	N00C	C00R	C00G	109.8(14)
C00J	N009	Fe03	132.9(11)	C00W	N00S	N00C	111.6(16)
C00J	N009	C00K	109.3(14)	N00A	C00T	S006	116.2(13)
C00K	N009	Fe03	117.8(11)	N00E	C00V	C00K	104.9(19)
C00M	N00A	Fe03	120.2(9)	N011	C00V	C00K	158(2)
C00T	N00A	Fe03	129.3(11)	N00S	C00W	C00M	136.4(18)
C00T	N00A	C00M	110.6(13)	C00N	N010	N00E	108(2)
C00G	N00B	Fe03	114.0(9)	C00V	N011	N00F	99(3)
C00P	N00B	Fe03	134.1(11)	C00N	N00F	Fe03	122.8(19)
C00P	N00B	C00G	111.8(13)	N011	N00F	Fe03	133(3)
C00R	N00C	Fe03	118.4(12)	N011	N00F	C00N	104(3)

Table 6 Hydrogen Atom Coordinates (Å×10^4) and Isotropic Displacement Parameters (Å^2×10^3) for Mono.

Atom	*x*	*y*	*z*	U(eq)
H00D	758.52	5662	4317.37	121
H00F	5437.79	2235.45	1750.73	52
H00I	2875.06	4392.35	5025.1	59
H00J	4162.44	2222.99	4379.47	57
H00L	4919.17	4383.46	719.1	54
H00A	4159.28	5034.59	1721.04	61
H00N	4049.11	5124.62	1867.47	61
H00O	203.24	1354.72	2172.12	66
H00P	901.56	3780.4	2302.54	60
H00Q	10093.93	2672.75	4039.92	72
H00R	3473.69	1083.5	2820.21	69
H00T	6938.64	4484.02	3391.73	58

H00C	2523.4	6508.41	4127.45	103
H00E	3419.49	6357.07	4907.27	103
H00G	1771.94	6762.73	4762	103
H00B	3222.52	5089.86	3733.58	79
H00V	3116.72	4978.9	3914.83	79
H00W	8099.27	1666.12	3729.93	75
H00H	-1450.65	4879.52	1437.23	50
H00K	-2332.31	5106.48	2037.93	50
H00M	-1809.51	4258.72	1966.4	50
H00Y	3840.27	1657.43	5169.43	77
H00Z	-353.6	5102.98	2707.11	79
H01A	5517.28	1075.33	4869.21	114
H01B	5704.97	586.98	5561.54	114
H01C	6525.74	1386.18	5582.02	114

Table 7 Atomic Occupancy for Mono.

Atom	***Occupancy***	**Atom**	***Occupancy***	**Atom**	***Occupancy***
N00E	0.5	H00A	0.5	H00N	0.5
H00B	0.5	H00V	0.5	C00X	0.5
H00H	0.5	H00K	0.5	H00M	0.5
O00Y	0.5	H00Y	0.5	O00Z	0.5
H00Z	0.5	N010	0.5	N011	0.5
C012	0.5	H01A	0.5	H01B	0.5
H01C	0.5	N00F	0.5		

Experimental

Crystal structure determination of $[FeL_2](Br)_2$

Crystal Data for $C_{18}H_{20}Br_2FeN_8O_2S_4$ (M =724.33 g/mol): monoclinic, space group $P2_1/n$ (no. 14), a = 8.6690(17) Å, b = 17.524(4) Å, c = 19.320(4) Å, β = 101.98(3)°, V = 2871.0(10) Å^3, Z = 4, T = 293(2) K, μ(MoKα) = 3.631 mm^{-1}, *Dcalc* = 1.676 g/cm^3, 47743 reflections measured (3.17° ≤ 2Θ ≤ 56.56°), 6568 unique (R_{int} = 0.1722, R_{sigma} = 0.0771) which were used in all calculations. The final R_1 was 0.1322 (I > 2σ(I)) and wR_2 was 0.3993 (all data).

Refinement model description

Number of restraints - 3, number of constraints - unknown.
Details:
1. Fixed Uiso
At 1.2 times of:
All C(H) groups, All C(H,H) groups
At 1.5 times of:
All C(H,H,H) groups, All O(H) groups
2. Rigid body (RIGU) restrains
C00U, O00D
with sigma for 1-2 distances of 0.004 and sigma for 1-3 distances of 0.004
3. Others
Fixed Sof: N00E(0.5) H00A(0.5) H00N(0.5) H00B(0.5) H00V(0.5) C00X(0.5)
H00H(0.5) H00K(0.5) H00M(0.5) O00Y(0.5) H00Y(0.5) O00Z(0.5) H00Z(0.5)
N010(0.5) N011(0.5) C012(0.5) H01A(0.5) H01B(0.5) H01C(0.5) N00F(0.5)
4.a Aromatic/amide H refined with riding coordinates:
C00F(H00F), C00I(H00I), C00J(H00J), C00L(H00L), C00N(H00A), C00N(H00N),
C00O(H00O), C00P(H00P), C00Q(H00Q), C00R(H00R), C00T(H00T), C00V(H00B),
C00V(H00V), C00W(H00W)

4.b Idealised Me refined as rotating group:
C00U(H00C,H00E,H00G), C00X(H00H,H00K,H00M), C012(H01A,H01B,H01C)
4.c Idealised tetrahedral OH refined as rotating group:
O00D(H00D), O00Y(H00Y), O00Z(H00Z)

Crystal Refinement Data for Complex **5** [Fe**L**$_2$](I)2

Table 1 Crystal data and structure refinement for P21n_a.

Identification code	P21n_a
Empirical formula	$C_{18}H_{14}FeI_4N_9S_4$
Formula weight	1048.07
Temperature/K	293(2)
Crystal system	monoclinic
Space group	$P2_1/n$
a/Å	8.7710(18)
b/Å	30.380(6)
c/Å	11.331(2)
α/°	90
β/°	101.47(3)
γ/°	90
Volume/Å^3	2959.0(11)
Z	4
ρ_{calc}g/cm^3	2.353
μ/mm^{-1}	4.992
F(000)	1948.0
Radiation	MoKα (λ = 0.71073)
2Θ range for data collection/°	2.682 to 56.564
Index ranges	-11 ≤ h ≤ 11, -40 ≤ k ≤ 40, -14 ≤ l ≤ 14
Reflections collected	49217
Independent reflections	7259 [R_{int} = 0.0270, R_{sigma} = 0.0143]
Data/restraints/parameters	7259/21/344
Goodness-of-fit on F^2	1.073
Final R indexes [I>=2σ (I)]	R_1 = 0.0432, wR_2 = 0.0975
Final R indexes [all data]	R_1 = 0.0461, wR_2 = 0.0990
Largest diff. peak/hole / e Å^{-3}	1.99/-2.04

Table 2 Fractional Atomic Coordinates (×10^4) and Equivalent Isotropic Displacement Parameters (Å^2×10^3) for P21n_a. U_{eq} is defined as 1/3 of of the trace of the orthogonalised U_{IJ} tensor.

Atom	*x*	*y*	*z*	U(eq)
I001	9171.6(4)	5547.9(2)	7076.8(3)	26.40(8)
I02	-1503.1(4)	7316.2(2)	850.7(4)	43.63(12)
I03	-1311.4(5)	6588.3(2)	-737.6(5)	50.71(13)
I04	-1470.3(7)	8079.6(2)	2516.2(5)	58.74(15)
Fe05	4491.6(7)	6244.4(2)	3291.6(5)	14.52(12)
S006	7541.7(15)	7068.0(4)	6113.5(11)	25.5(2)
S007	1737.8(15)	5277.1(4)	717.5(13)	29.3(3)
S008	8888.6(15)	5810.7(5)	2161.0(13)	30.4(3)
S009	143.2(16)	6816.2(5)	4141.3(15)	35.9(3)
N00A	6426(4)	6020.1(12)	2880(3)	16.9(7)
N00B	3261(4)	5873.5(14)	2032(4)	21.9(8)
N00C	2603(5)	6423.0(14)	3831(4)	22.2(8)

N00D	5745(5)	6656.1(13)	4421(4)	21.7(8)
N00E	4873(5)	5757.3(14)	4434(4)	26.3(9)
C00F	7073(5)	5666.3(14)	3580(4)	20.3(9)
C00G	2820(6)	6053.7(18)	886(4)	25.4(10)
N00H	4063(6)	5590.2(16)	5270(4)	33.8(10)
C00I	6171(6)	5514.3(17)	4440(5)	26.3(10)
C00J	6046(5)	7065.7(14)	3966(5)	20.1(9)
C00K	1987(6)	5768.2(18)	62(5)	28.4(11)
C00L	2055(6)	6190.4(18)	4711(5)	25.8(10)
C00M	6460(6)	6617.5(16)	5545(5)	25.4(10)
C00N	2765(5)	5470.2(17)	2064(5)	25.1(10)
C00O	7262(5)	6127.3(16)	2096(5)	23.5(9)
C00P	7002(6)	7327.6(15)	4765(5)	22.8(9)
C00Q	1690(6)	6757.8(18)	3450(5)	27.7(10)
N00R	4526(10)	6772(3)	2310(8)	13.6(16)
C00S	8423(6)	5513.1(17)	3323(5)	29.0(11)
C00T	727(6)	6363(2)	4994(5)	33.1(12)
C00U	5336(6)	7177(3)	2750(6)	44.2(17)
C00V	2819(7)	5805(2)	5328(6)	35.3(12)
C00W	3195(8)	6503(2)	673(7)	44.5(16)
N00X	5958(10)	5058(3)	1437(8)	83(3)
N00Z	3839(9)	6845(3)	1094(7)	20.2(15)
C010	4591(13)	4304(3)	1306(11)	85(3)
N011	4465(10)	7085(3)	1785(8)	24.1(17)
N0AA	4094(11)	6644(3)	1900(9)	19.5(17)
C1	5349(9)	4703(3)	1411(8)	63(2)

Table 3 Anisotropic Displacement Parameters ($Å^2×10^3$) for P21n_a. The Anisotropic displacement factor exponent takes the form: $-2π^2[h^2a^{*2}U_{11}+2hka^*b^*U_{12}+…]$.

Atom	U_{11}	U_{22}	U_{33}	U_{23}	U_{13}	U_{12}
I001	27.91(17)	29.61(16)	20.27(15)	0.31(12)	1.38(11)	2.24(12)
I02	27.41(19)	55.2(3)	51.8(2)	32.2(2)	16.35(16)	3.98(16)
I03	44.0(2)	59.6(3)	54.8(3)	26.1(2)	24.9(2)	18.0(2)
I04	77.3(4)	54.7(3)	48.8(3)	13.9(2)	23.8(2)	-18.4(3)
Fe05	13.0(3)	14.2(3)	16.8(3)	1.1(2)	4.2(2)	-0.8(2)
S006	23.3(6)	27.8(6)	25.9(6)	-7.1(5)	6.0(5)	-5.0(5)
S007	20.7(6)	29.8(6)	34.8(7)	-11.8(5)	-0.6(5)	-0.6(5)
S008	19.5(6)	38.1(7)	35.7(7)	-1.0(5)	10.6(5)	6.5(5)
S009	22.0(6)	43.9(8)	46.1(8)	-2.2(6)	17.2(6)	5.5(6)
N00A	15.3(17)	13.9(16)	20.2(17)	-1.1(13)	0.5(13)	0.0(13)
N00B	12.8(17)	32(2)	20.3(18)	-4.4(16)	1.4(14)	3.5(15)
N00C	15.6(18)	27(2)	26(2)	-5.1(16)	8.2(15)	-4.3(15)
N00D	17.2(18)	18.5(18)	32(2)	-7.1(16)	12.1(16)	-3.5(14)
N00E	35(2)	22.6(19)	19.8(19)	1.3(15)	2.3(17)	-9.6(17)
C00F	19(2)	14.1(19)	26(2)	-1.6(16)	0.4(17)	3.0(16)
C00G	21(2)	32(3)	20(2)	-2.4(19)	-2.6(17)	2.4(19)
N00H	38(3)	33(2)	32(2)	8.2(19)	11(2)	-5(2)
C00I	26(2)	25(2)	26(2)	-0.1(19)	-0.4(19)	-3.5(19)
C00J	16(2)	14.8(19)	32(2)	-7.5(17)	12.0(18)	-4.0(16)

C00K	26(3)	34(3)	22(2)	-7(2)	-3.2(19)	3(2)
C00L	20(2)	35(3)	25(2)	-3.4(19)	10.2(18)	-5.9(19)
C00M	21(2)	21(2)	35(3)	-2.5(19)	8.8(19)	-2.8(18)
C00N	16(2)	32(3)	27(2)	-3.9(19)	2.7(17)	0.7(18)
C00O	18(2)	26(2)	27(2)	1.6(18)	5.1(17)	3.2(17)
C00P	21(2)	18(2)	31(2)	-6.3(18)	10.2(18)	-3.2(17)
C00Q	19(2)	33(3)	34(3)	-1(2)	11.7(19)	0.3(19)
N00R	13(4)	14(4)	13(4)	-4(3)	2(3)	-4(3)
C00S	25(2)	25(2)	36(3)	0(2)	3(2)	8.3(19)
C00T	24(3)	49(3)	30(3)	-2(2)	14(2)	-4(2)
C00U	12(2)	90(5)	31(3)	-13(3)	7(2)	-1(3)
C00V	27(3)	41(3)	37(3)	-2(2)	4(2)	-3(2)
C00W	35(3)	35(3)	69(5)	-17(3)	25(3)	-5(3)
N00X	61(5)	93(6)	92(6)	-46(5)	12(4)	-15(4)
N00Z	17(4)	21(4)	21(4)	7(3)	1(3)	2(3)
C010	88(7)	65(6)	121(9)	12(6)	68(7)	28(5)
N011	24(4)	22(4)	25(4)	9(3)	3(3)	6(3)
N0AA	21(5)	16(4)	22(5)	0(4)	8(4)	6(3)
C1	39(4)	84(6)	65(5)	-31(5)	11(3)	11(4)

Table 4 Bond Lengths for P21n_a.

Atom	Atom	Length/Å	Atom	Atom	Length/Å
I02	I03	2.8771(9)	N00C	C00Q	1.313(7)
I02	I04	2.9865(9)	N00D	C00J	1.392(6)
Fe05	N00A	1.969(4)	N00D	C00M	1.309(7)
Fe05	N00B	1.964(4)	N00E	N00H	1.388(6)
Fe05	N00C	1.954(4)	N00E	C00I	1.356(7)
Fe05	N00D	1.962(4)	C00F	C00I	1.448(7)
Fe05	N00E	1.951(4)	C00F	C00S	1.356(7)
Fe05	N00R	1.955(8)	C00G	C00K	1.373(7)
Fe05	N0AA	1.964(9)	C00G	C00W	1.434(8)
S006	C00M	1.716(5)	N00H	C00V	1.284(8)
S006	C00P	1.701(5)	C00J	C00P	1.361(6)
S007	C00K	1.700(6)	C00J	C00U	1.435(8)
S007	C00N	1.714(5)	C00L	C00T	1.372(7)
S008	C00O	1.710(5)	C00L	C00V	1.458(8)
S008	C00S	1.712(6)	N00R	C00U	1.459(11)
S009	C00Q	1.706(5)	N00R	N00Z	1.406(11)
S009	C00T	1.702(6)	C00U	N011	1.235(10)
N00A	C00F	1.388(6)	C00W	N00Z	1.233(10)
N00A	C00O	1.301(6)	C00W	N0AA	1.518(13)
N00B	C00G	1.392(6)	N00X	C1	1.201(13)
N00B	C00N	1.303(7)	C010	C1	1.374(14)
N00C	C00L	1.383(6)	N011	N0AA	1.392(12)

Table 5 Bond Angles for P21n_a.

Atom	Atom	Atom	Angle/˚	Atom	Atom	Atom	Angle/˚

I03	I02	I04	176.13(2)	C00I	N00E	Fe05	116.7(4)
N00B	Fe05	N00A	90.24(16)	C00I	N00E	N00H	109.9(4)
N00B	Fe05	N0AA	77.7(4)	N00A	C00F	C00I	114.6(4)
N00C	Fe05	N00A	174.20(17)	C00S	C00F	N00A	114.7(4)
N00C	Fe05	N00B	90.51(17)	C00S	C00F	C00I	130.7(5)
N00C	Fe05	N00D	91.09(16)	N00B	C00G	C00W	120.0(5)
N00C	Fe05	N00R	93.5(3)	C00K	C00G	N00B	113.4(5)
N00C	Fe05	N0AA	93.1(3)	C00K	C00G	C00W	126.5(5)
N00D	Fe05	N00A	88.73(16)	C00V	N00H	N00E	113.9(5)
N00D	Fe05	N00B	174.26(18)	N00E	C00I	C00F	113.2(4)
N00D	Fe05	N0AA	96.7(4)	N00D	C00J	C00U	119.2(5)
N00E	Fe05	N00A	81.52(18)	C00P	C00J	N00D	114.4(5)
N00E	Fe05	N00B	92.51(18)	C00P	C00J	C00U	126.3(5)
N00E	Fe05	N00C	92.70(19)	C00G	C00K	S007	110.8(4)
N00E	Fe05	N00D	92.92(18)	N00C	C00L	C00V	124.3(5)
N00E	Fe05	N00R	168.4(3)	C00T	C00L	N00C	113.9(5)
N00E	Fe05	N0AA	168.7(3)	C00T	C00L	C00V	121.7(5)
N00R	Fe05	N00A	92.1(3)	N00D	C00M	S006	114.6(4)
N00R	Fe05	N00B	97.2(3)	N00B	C00N	S007	114.6(4)
N00R	Fe05	N00D	77.2(3)	N00A	C00O	S008	114.1(4)
N0AA	Fe05	N00A	92.7(3)	C00J	C00P	S006	110.5(4)
C00P	S006	C00M	89.9(2)	N00C	C00Q	S009	114.7(4)
C00K	S007	C00N	89.9(3)	C00U	N00R	Fe05	124.0(6)
C00O	S008	C00S	90.3(2)	N00Z	N00R	Fe05	129.3(7)
C00T	S009	C00Q	90.0(3)	N00Z	N00R	C00U	106.7(7)
C00F	N00A	Fe05	114.0(3)	C00F	C00S	S008	109.6(4)
C00O	N00A	Fe05	134.8(3)	C00L	C00T	S009	110.5(4)
C00O	N00A	C00F	111.2(4)	C00J	C00U	N00R	102.6(6)
C00G	N00B	Fe05	117.6(3)	N011	C00U	C00J	150.5(8)
C00N	N00B	Fe05	131.1(4)	N00H	C00V	C00L	134.2(6)
C00N	N00B	C00G	111.3(4)	C00G	C00W	N0AA	102.1(6)
C00L	N00C	Fe05	121.4(3)	N00Z	C00W	C00G	147.0(8)
C00Q	N00C	Fe05	127.7(4)	C00W	N00Z	N00R	108.7(8)
C00Q	N00C	C00L	110.9(4)	C00U	N011	N0AA	104.5(8)
C00J	N00D	Fe05	116.8(3)	C00W	N0AA	Fe05	122.5(7)
C00M	N00D	Fe05	132.5(3)	N011	N0AA	Fe05	131.5(8)
C00M	N00D	C00J	110.6(4)	N011	N0AA	C00W	106.0(7)
N00H	N00E	Fe05	133.4(4)	N00X	C1	C010	176.0(11)

Table 6 Hydrogen Atom Coordinates (Å×10^4) and Isotropic Displacement Parameters (Å^2×10^3) for P21n_a.

Atom	*x*	*y*	*z*	U(eq)
H00I	6453.72	5274.24	4945.62	32
H00K	1611.48	5834.45	-744.85	34
H00M	6386.9	6366.29	5999.72	30
H00N	2952.37	5300.79	2761.82	30
H00O	6998.95	6356.13	1547.69	28
H00P	7315.17	7609.29	4596.63	27
H00Q	1873.58	6948.04	2850.85	33

H00S	9005.81	5281.67	3717.38	35
H00T	216.77	6248.09	5570.69	40
H00U	5380.18	7441.6	2344.93	53
H00V	2287.43	5688.11	5889.24	42
H00W	2766.85	6560.72	-130.28	53
H01A	4171.59	4245.58	472.73	127
H01B	3761.83	4313.49	1745.45	127
H01C	5311.23	4075.9	1627.86	127

Table 7 Atomic Occupancy for P21n_a.

Atom	***Occupancy***	**Atom**	***Occupancy***	**Atom**	***Occupancy***
N00R	0.5	H00U	0.5	H00W	0.5
N00Z	0.5	N011	0.5	N0AA	0.5

Crystal structure determination of [P21n_a]

Crystal Data for $C_{18}H_{14}FeI_4N_9S_4$ (*M* =1048.07 g/mol): monoclinic, space group $P2_1/n$ (no. 14), *a* = 8.7710(18) Å, *b* = 30.380(6) Å, *c* = 11.331(2) Å, *β* = 101.47(3)°, *V* = 2959.0(11) Å^3, *Z* = 4, *T* = 293(2) K, μ(MoKα) = 4.992 mm^{-1}, *Dcalc* = 2.353 g/cm^3, 49217 reflections measured (2.682° ≤ 2Θ ≤ 56.564°), 7259 unique (R_{int} = 0.0270, R_{sigma} = 0.0143) which were used in all calculations. The final R_1 was 0.0432 (I > 2σ(I)) and wR_2 was 0.0990 (all data).

Refinement model description

Number of restraints - 21, number of constraints - unknown.

Details:

1. Fixed Uiso
 At 1.2 times of:
  All C(H) groups
 At 1.5 times of:
  All C(H,H,H) groups
2. Uiso/Uaniso restraints and constraints
N00X ≈ C1 ≈ C010: within 1.7A with sigma of 0.04 and sigma for terminal
atoms of 0.08
3. Rigid body (RIGU) restrains
 I03, I02, I04
 with sigma for 1-2 distances of 0.004 and sigma for 1-3 distances of 0.004
4. Others
 Fixed Sof: N00R(0.5) H00U(0.5) H00W(0.5) N00Z(0.5) N011(0.5) N0AA(0.5)
5.a Aromatic/amide H refined with riding coordinates:
 C00I(H00I), C00K(H00K), C00M(H00M), C00N(H00N), C00O(H00O), C00P(H00P),
 C00Q(H00Q), C00S(H00S), C00T(H00T), C00U(H00U), C00V(H00V), C00W(H00W)
5.b Idealised Me refined as rotating group:
 C010(H01A,H01B,H01C)